National Library
of Canada

Acquisitions and
Bibliographic Services Branch

395 Wellington Street
Ottawa, Ontario
K1A 0N4

Bibliothèque nationale
du Canada

Direction des acquisitions et
des services bibliographiques

395, rue Wellington
Ottawa (Ontario)
K1A 0N4

Your file Votre référence

Our file Notre référence

NOTICE

The quality of this microform is heavily dependent upon the quality of the original thesis submitted for microfilming. Every effort has been made to ensure the highest quality of reproduction possible.

If pages are missing, contact the university which granted the degree.

Some pages may have indistinct print especially if the original pages were typed with a poor typewriter ribbon or if the university sent us an inferior photocopy.

AVIS

La qualité de cette microforme dépend grandement de la qualité de la thèse soumise au microfilmage. Nous avons tout fait pour assurer une qualité supérieure de reproduction.

S'il manque des pages, veuillez communiquer avec l'université qui a conféré le grade.

La qualité d'impression de certaines pages peut laisser à désirer, surtout si les pages originales ont été dactylographiées à l'aide d'un ruban usé ou si l'université nous a fait parvenir une photocopie de qualité inférieure.

Canada

ON THE FLOW MECHANICS OF MINE BACKFILL SLURRIES IN PIPELINES

by

Riadh Bouzaiene

A thesis submitted to the Faculty of Graduate Studies and Research
in partial fulfillment of the requirement for the degree of
Doctor of Philosophy

Department of Mining and Metallurgical Engineering,
McGill University,
Montreal, Canada
April, 1995

ISBN 0-612-08082-X

Canada

To My Father Ali and Mother Jamila

To My Brothers Anis, Jamel and Fadhel

ABSTRACT

This thesis deals with the flow mechanics of hydraulic and high density mine backfill slurries in pipelines. Various empirical, rheological and mechanistic approaches are presented and analysed along with some aspects pertinent to experimental testing of backfill slurries.

The main contribution of this work is, particularly, in the development of an analytical model to describe the flow and predict the pressure gradient of a class of high density backfill whose motion in pipelines follows the Plug Flow Model (PFM). The development of the model called for investigating the conditions required for establishing Plug Flow. It was found that mix proportioning procedures, similar to those found in the concrete industry, are key factors in obtaining Plug Flow.

Pressure drop was found to be a function of the thickness of the Bingham plastic annular layer surrounding the cylindrical core of aggregates. Analytical equations were proposed to solve for the thickness of this layer by considering the rheology of the mixture. Alternatively, the thickness of the annular layer may be estimated by considering the relative proportions of the mixture with respect to aggregates void content. The model offered pressure drop predictions in good agreement with published data. The proposed model may also serve as an alternative to Mooney's method, when dealing with the annular lubricating layer effect characterising mixtures in Plug Flow.

RÉSUMÉ

Cette thèse traite des mécanismes d'écoulement, hydrauliques et à haute densité, des boues de remblais miniers dans les pipelines. Diverses approches empiriques, rhéologiques et mécaniques sont présentées et analysées ainsi que certains aspects pertinents à l'étude expérimentale des boues de remblais minier.

L'apport principal de cet ouvrage réside particulièrement dans l'élaboration d'un modèle analytique pour décrire l'écoulement et calculer la perte de charge d'une catégorie de remblais minier à haute densité dont le flux, dans les pipelines, suit le modèle d'écoulement-bouchon. Le développement de ce modèle a appelé à l'examen des conditions nécessaires à l'établissement de ce type d'écoulement. On a trouvé que des procédures de dosage, comparables à celles de l'industrie du béton, sont des facteurs clefs à l'obtention de ce genre d'écoulement.

On a ainsi démontré que la perte de charge est fonction de l'épaisseur de la couche annulaire, du type Bingham plastique, entourant le noyau cylindrique d'agrégats. Des équations analytiques, basées sur des données rhéologiques du mélange, sont proposées pour calculer l'épaisseur de cette couche. Alternativement, cette épaisseur pourrait être éstimée en considérant le dosage des composantes du mélange par rapport à l'indice de vide des agrégats. Les résultats de perte de charge obtenues par ce modèle sont en accord avec des données expérimentales publiées. On a enfin démontré que le modèle d'écoulement-bouchon proposé, pourrait être substitué à la méthode de Mooney pour l'analyse de l'effet de la couche annulaire lubrifiante, typique à ce genre de boues de remblais.

ACKNOWLEDGMENTS

I would like to thank:

Prof. Hassani and Prof. Scoble for their financial support and supervision throughout the course of this study.

Prof. Mujumdar, Prof. Finch, Prof. Mitri of McGill University, and Prof. Farah of Laurentian University for their helpful comments and suggestions regarding this thesis.

Prof. Sellgren of Luleå University of Technology, Sweden, for his cooperation and advice.

Prof. Dealy and Prof. Van de Ven, of the Department of Chemical Engineering, McGill University, for their helpful discussion on some aspects of the Plug Flow Model.

Mr. Knoepfel and his group of technicians.

The staff of PSE Library.

All the colleagues of the Mining and Metallurgical Engineering Department for their friendship.

This work was partly supported by grants from NSERC for which the author is grateful.

TABLE OF CONTENTS

LIST OF FIGURES

CHAPTER FOUR

CHAPTER FIVE

CHAPTER SIX

CHAPTER SEVEN

APPENDIX ONE

Case study: Pipeline Conveying of High Density Fill at Kidd Creek Mine

LIST OF TABLES

LIST OF SYMBOLS

Most of the symbols used in this thesis are defined in the text. The following list is given as a general reference and for symbols whose definition in the text might have been omitted.

A	cross sectional area of pipe [L^2]
A_1	area of upper layer [L^2]
A_2	area of lower layer [L^2]
C, C_v	volumetric solids concentration
C_w	solids concentration by weight
C_1	volume fraction solids in upper layer
C_2	volume fraction solids in lower layer
Cb	concentration of loose-packed bed
C_d, C_D	drag coefficient
d	particle diameter [L]
D	pipe diameter [L]
f	fanning friction factor
g	acceleration of gravity [LT^{-2}]
i, J	pressure gradient [L (of water)/L (of pipe))
$k = \frac{R_1}{R_2}$	core to pipe radius ratio
L	pipe length [L]
ΔP	pressure differential [$L^{-1}MT^{-2}$]
Q	volumetric flow rate [L^3T^{-1}]
R	pipe radius [L]
r	radial distance [L]
Re	Reynolds number
S_m	specific gravity of slurry
S, S_s, s	specific gravity of solid particles
V	average flow velocity [$L\,T^{-1}$]
V_c	volume of dry coarse solid particles [L^3]

V_f volume of dry fine solid particles [L^3]

V_w volume of water [L^3]

Greek letters

τ shear stress [$L^{-1}MT^{-2}$]

μ dynamic viscosity [$L^{-1}MT^{-1}$]

υ kinematic viscosity [L^2T^{-1}]

ρ density [ML^{-3}]

β angle subtended by lower layer

η_s coefficient of static friction

ϕ angle of internal friction

CHAPTER ONE

INTRODUCTION

The large scale mining operations underway nowadays generate large amounts of ore which, after processing, becomes the source of a waste by-product for disposal. The most common form of waste products are flotation tailings; which are the residue from ground ore after washing and milling. Tailing ponds have been used as disposal sites but this option has been the target of increasing criticism because of its negative environmental impact and the risks of contamination of land and ground water by acid and other industrial pollutants.

The need to dispose of the waste material is usually coupled with the necessity to fill the void formed by mining. These two objectives are met by using a combination of tailings, aggregates and binders as backfill material. In addition to being a means of waste disposal, backfilling is also intended to ensure safety and continuity of the mining operation by providing adequate ground support and control.

Backfill systems usually include facilities for classifying, comminution, dewatering, mixing, transportation and storage as shown in Figure 1.1 (Chen and Hassani, 1992) . After preparation, the fill is distributed through pipelines having horizontal and vertical sections. The flow is maintained either under the action of gravity or with the aid of a pump. A typical backfill system is shown in Figure 1.2. The seven stages that describe the process are (Barret, et al.1988) :

1. Transport of total tailing from the mineral processing plant
2. Backfill plant where total tailings are classified by hydrocyclones
3. Pipe transport of classified tailings to storage tanks or silos at each shaft
4. Storage and supply of classified tailings (slurry is agitated in the process)
5. Borehole/pipe range transport
6. Underground pipe transport (gravity-fed using the potential energy in the borehole/pipe range)
7. Stope filling (3 stages: deposition of slurry, movement of solids, and movement and removal of excess water)

Figure 1.1 Flow chart of a typical backfill system
(adapted from Chen and Hassani, 1992)

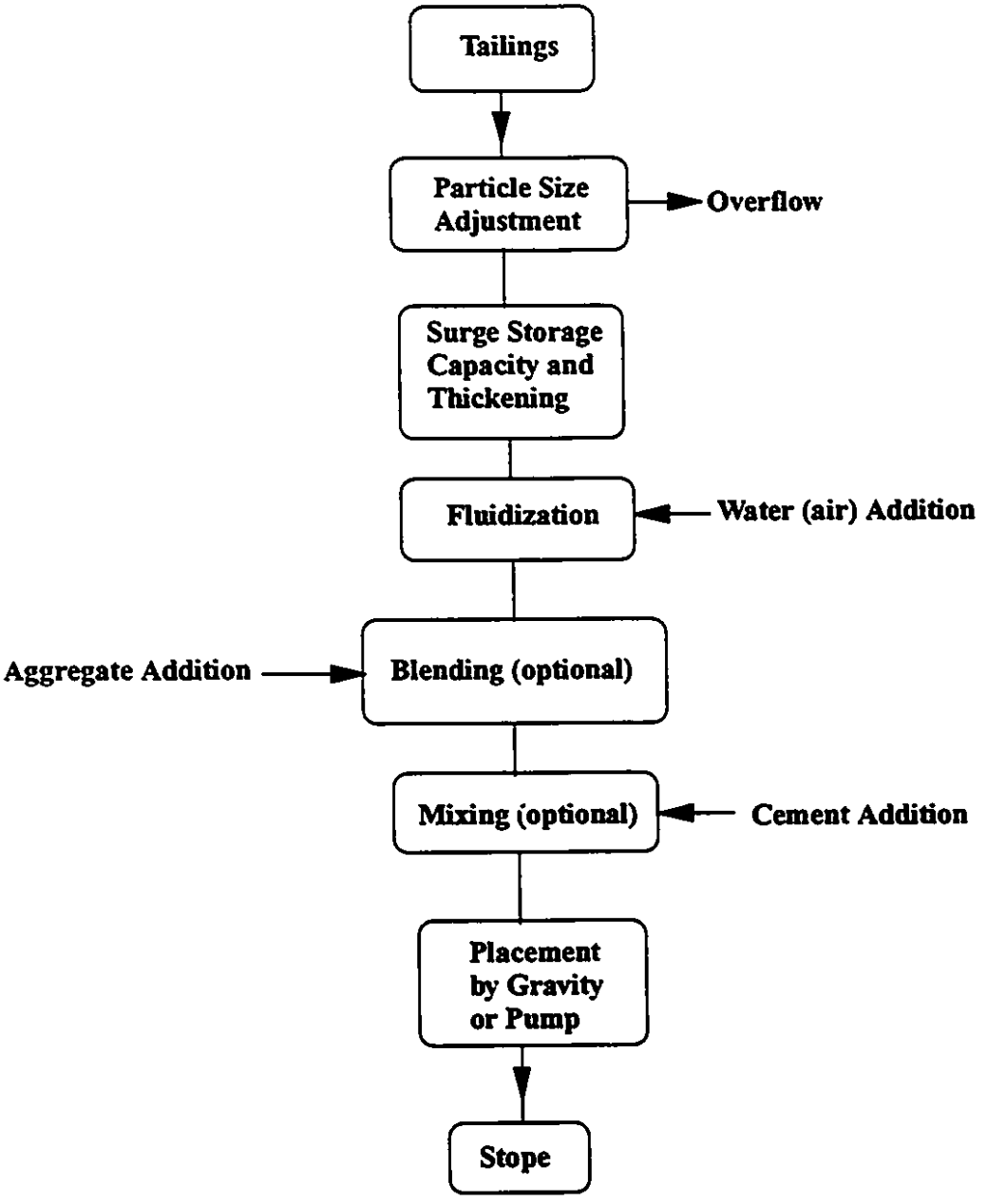

Figure 1.2 Schematic layout of a typical backfill system

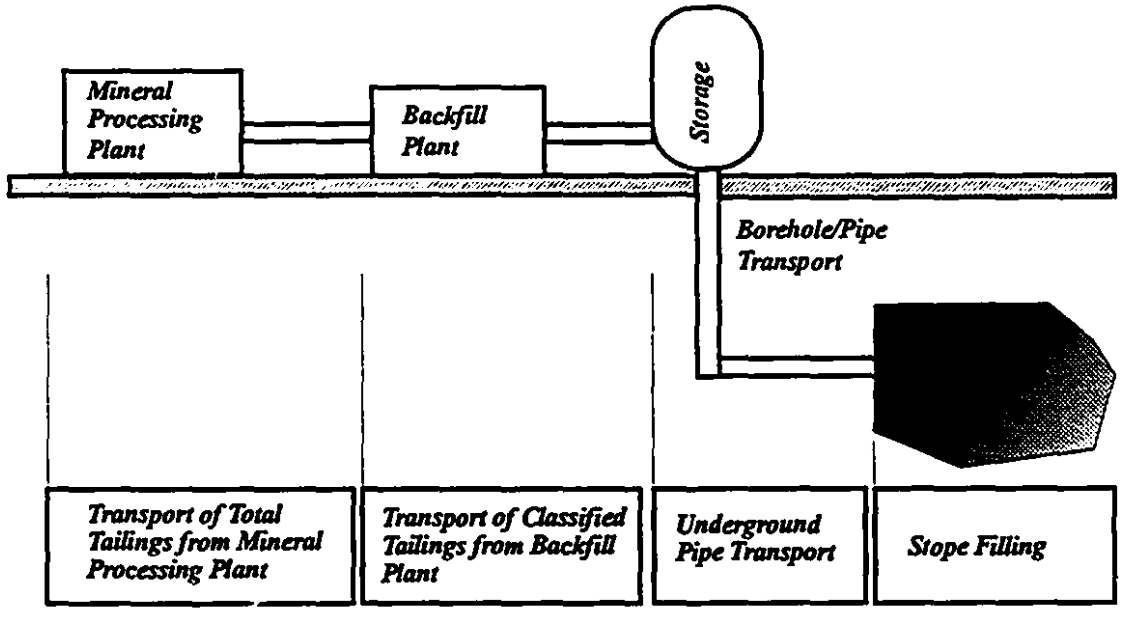

Four out of seven stages making up a backfill system involve pipeline transport. The contribution of the transport related costs to the overall costs for a typical 50,000 tons/month classified tailing system is in the order of 50 per cent (Kramers et al. ,1989). Therefore improvement in the operating efficiency of hydraulic transport systems, in terms of higher solids flow rate and lower energy consumption, will result in a substantial economy for the mining industry.

The composition of the mixture in the pipeline, its concentration, and its flow mechanics vary from one stage to another. Designing such conveying systems requires full understanding of the parameters influencing it at each stage. Whereas, the mixture may be transported with relatively low concentration and high velocity in the first stage, it is usually placed in the stopes at a high solids concentration and relatively low flow velocity.

The design of a backfill system must adequately meet requirements for fill with sufficient strength properties and minimum liquefaction potential. Coarse grained , well graded backfill for example is known (Clark, 1988) to yield better placement characteristics in terms of minimum porosity and optimum water/solids ratio. Hydraulic fill with fine-grained solids is also common, although the current tendency is toward pumpable highly concentrated mixtures, known as high density stabilized backfill.

In addition to tailings, other components may be added to form backfill mixtures which are designed to flow in pipelines with reasonable pressure losses under the action of gravity or pumps. These additional components are:

- Coarse and fine aggregates
- Binding agents, usually cement and/or pozzolanic materials, such as fly ash or smelter slag.
- Water and possibly other additives to improve flow characteristics or drainage after placement.

Typical size distributions of full and classified plant tailings representative of practice in several countries and a broad range of ore types (Thomas et al., 1979) are shown in Figure 1.3a and 1.3b. Grading limits for pumpable highly

concentrated mixtures, and mix proportioning procedures are presented in Chapter Five in connection with the Plug Flow Mechanism. The physical, chemical and hydraulic characteristics of some backfill slurries common to mines in Canada is given in Scoble and Piciaccha (1991).

The flow of backfill slurries in pipelines belongs to the general class of flow of solid-liquid mixtures. This is a physically complex phenomenon involving multi-phase flow and interactions. Many monographs such as Bain & Bonnington (1970), Wasp et al. (1977), Govier & Aziz (1987), and Wilson et al. (1992), and Conference proceedings such as the Hydrotransport series sponsored by the British Hydrodynamic Research Association (BHRA) in Europe and the Coal and Slurry Technology Association in North America, just to name a few, have been in the forefront of developing this science since the middle of this century.

Although initial hydrotransport applications were in the field of long distance coal pipelining, the technology quickly gained grounds in other areas such as the pipelining of ore material to processing plants and that of plant tailings and other aggregates back to the mines as backfill. The latter went through two stages. The first involved the transport of low concentration hydraulic fill underground and the second and more recent stage dealt with the transport of high density fill.

1.1 Hydraulic Fill

Hydraulic fill is characterized by relatively low solids concentration (less than 49% by volume, (Stewart, 1959)). It is prepared from plant tailings by classification in hydrocyclones followed by filtration or thickening. It is usually transported in the turbulent flow regime (as described in Chapter Three) by gravity or centrifugal pumps . Hydraulic fill produces excess water after placement due to its low solids concentration and high permeability. For cemented fill, the particle size distribution of hydraulic fill may not be optimum for strength and cement economy. Furthermore, this type of fill requires bulkheads which add to the inconvenience and cost of this backfill procedure. However, one of the advantages of hydraulic fill is its capacity to tightly fill the voids due to its high flowability.

Figure 1.3a Cumulative particle size distributions of full plant tailings
(adapted from Thomas et al., 1979)

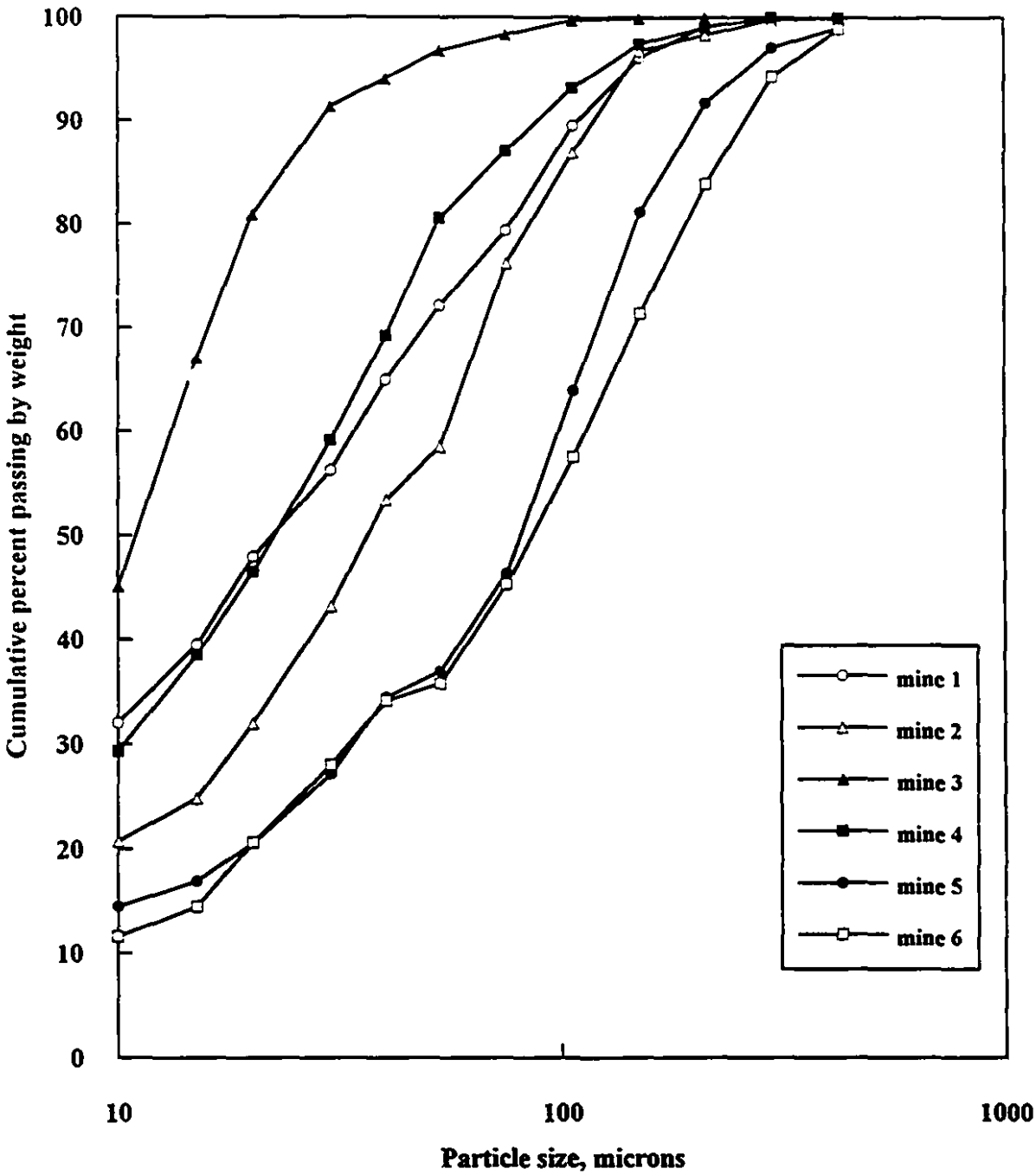

Figure 1.3b Particle size distributions of classified plant tailings (adapted from Thomas et al., 1979)

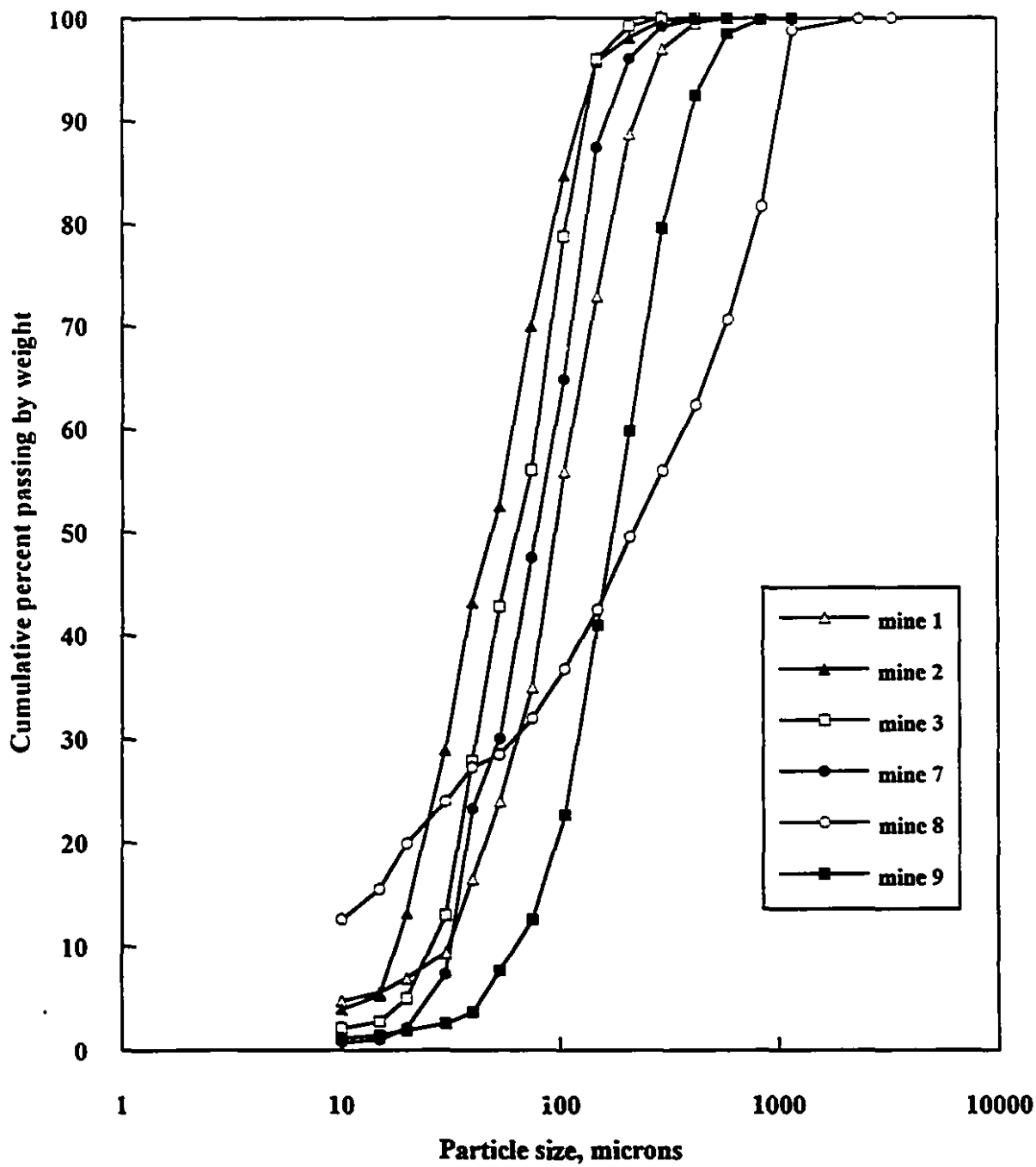

1.2 High Density Fill

High density fills have a higher solids concentration compared to hydraulic fill. They require thickening in silos or by using filters. They are usually transported in the turbulent flow regime by gravity, centrifugal or positive displacement pumps. Some excess water is produced after placement but this is not as critical as for hydraulic fill. The size distribution of high density fills contains a larger fines fraction than that of conventional fill. This explains the better strength properties and cement economy associated with high density fill. However, bulkheads may still be required, and the risk of liquefaction may be present.

Another type of high density backfill may be obtained by adjusting the size distribution and concentration of the material by means of proper mix design (as shown in Chapter Five). The velocity of the flow at which solids fall out of suspension may be greatly reduced to the point that it is no longer a limiting factor in the hydraulic design. The carrying medium made up of the base liquid and the fine fraction may be regarded for design purposes as pseudo-homogeneous with non-Newtonian rheology. Whether this carrying medium (which may be referred to as paste) acts as a vehicle for coarser particles (Chapter Three, Wasp's method) or as an annular layer (Chapter Five, Plug Flow), the outcome is beneficial due to higher flow rates of solids at lower water content, and to substantial saving in pumping energy. Positive displacement pumps are usually used in addition to any potential energy available in the system. This type of high density fill offers high strength properties with minimum cement requirements and no excess water. Bulkheads are not required as there is no risk of liquefaction.

The technology of high density backfill has been the focus of a great deal of attention by the mining industry worldwide due to its advantages. Some of the main contributors and/or users of this technology are :

1. Preussag-Bad Grund mine, Germany
2. Chamber of Mines and the University of Witwatersrand, South Africa
3. Lucky Friday mine, Hecla Mining Co., and the U.S. Bureau of Mines, USA
4. Elura Mine, Australia
5. Dome Mine, Canada
6. INCO -- Mines Research Department, Canada

Details about fill preparation facilities and the delivery methods of some of the above mines are found in Hartman et al. (1992).

1.3 THESIS OBJECTIVES AND CONTRIBUTIONS

The objective of this thesis is to select, evaluate and contribute to some of the methods of analysing pipe flow of solid-liquid mixtures in the context of mine backfill pipeline transportation. This task is required to enable those involved in the design and implementation of pipeline transportation systems in the mining industry to make more informed decisions regarding the flow conditions required to establish reliable and cost effective backfill operations. Incidence of blockages, burst pipes, and operational difficulties are still common in many mines, although, progress has been reported in the technical literature (Bouzaiene and Hassani, 1992) on methods that may be useful in solving such problems. However, the details of these methods are often scattered over a number of sources, which do not always address slurry flow problems in the particular context of the mine backfill industry.

Thus, this research sets out to investigate the flow mechanics of mine backfill slurries in pipelines with particular attention to high density fill, which has become the preferred material for stope filling, due to its advantages over hydraulic fill. Various empirical, rheological and mechanistic approaches are identified and analysed along with some aspects pertinent to experimental testing of backfill slurries. Figure 1.4 shows typical distributions of solid particles in a pipe cross-section for each flow condition investigated and the corresponding method of analysis.

The original contribution of this work is, particularly, in the development of an analytical model for high density backfill wherein Plug Flow with a Bingham plastic annular layer is assumed to be the flow mechanism. This model offered pressure loss predictions in good agreement with published data. It may also be used as an analytical alternative to Mooney's method for analyzing the annular layer effect in pipelines for mixtures in Plug Flow.

Although the Plug Flow Mechanism has been known qualitatively for many years to describe the flow of many types of highly concentrated mixtures (such as fresh

concrete), the proposed approach may be the first attempt at formulating a comprehensive predictive model for describing it within the framework of the mining industry. The contribution of this model is also in finding the link between mix-proportioning, aggregates void content, and the resulting pressure gradient via the introduction of a parameter k (equal to R1/R2, the ratio of the core to pipe diameter) for which two predictive methods are proposed:

1) Using a rheological approach
2) Using a volume balance of the Plug Flow Model components

In contrast to the current trial-and-error practice, this approach may be considered a more systematic basis for designing mixtures capable of Plug Flow (as defined in Chapter Five), and predicting their behaviour.

Since not all backfill mixtures can be transported in Plug Flow, other flow models are considered: empirical for settling slurries, rheological for non-settling suspensions, and mechanistic for mixed regimes flows. The most relevant of these methods are selected and analysed.

The remainder of the thesis is laid out as follows:

Chapter Two deals with the fundamental concepts common to the study of solid-liquid mixtures in pipes. Reference to these concepts is made throughout this study.

In **Chapter Three**, selected empirical approaches used for analysing the flow characteristics and predicting the pressure drop and critical velocity of settling slurries are presented. Special attention is given to Wasp's method, which is unique among semi-empirical approaches in its ability to handle slurries with wide particle size distributions similar to that of some hydraulic backfill mixtures.

Chapter Four focuses on non-settling slurries and the rheological approaches for the analysis of their flow behavior. A numerical method is proposed for calculating parameters associated with the Metzner & Reed (1955) approach to obviate the need for graphical methods for estimating rheological parameters K' and n' for the case of a Power Law model.

Chapter Five deals with mixtures at relatively high concentration moving in Plug Flow with a Bingham plastic annular lubricating layer. An original approach for designing such mixtures, and explaining their flow behaviour in terms of the annular layer effect is presented.

In **Chapter Six**, a detailed analysis of an updated version of the two-layer model is presented, where the holdup effect in the lower layer is taken into account, and the concentration distribution in the upper layer is described by a second order diffusion equation. A fast converging root finding algorithm is implemented to solve the model equations .

Chapter Seven gives a description of the miscellaneous aspects of experimental testing of backfill slurries. A special section on a new device for measuring the concentration distribution in a settling column is presented.

This study is concluded in **Chapter Eight** by summarizing the results and making recommendations for future investigations.

Figure 1.4 Schematic slurry flow models and corresponding methods of analysis

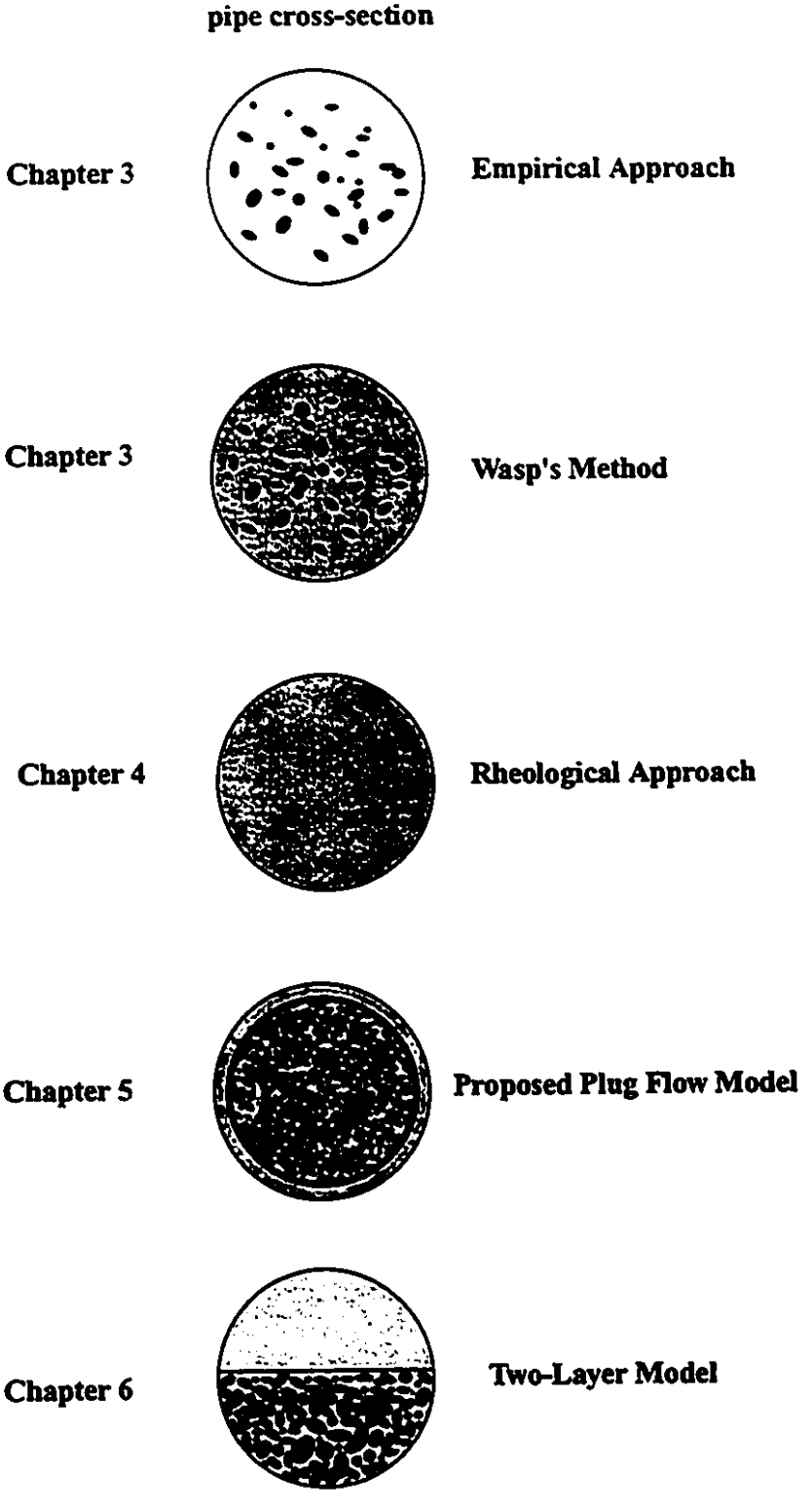

CHAPTER TWO

FUNDAMENTAL CONCEPTS

In developing and discussing flow models of backfill slurries and solid-liquid mixtures in general, the definition of a number of key concepts and their underlying assumptions is required. A basic understanding of these concepts is a prerequisite to using them in any modeling procedure. It is proposed in this chapter to present the most relevant parameters used in the modeling of backfill slurry flow and to discuss the scope of their usefulness and their limitations.

2.1 Characteristics of Backfill Distribution Systems

There are fundamental differences between hydraulic fill distribution and conventional slurry transportation. In addition to lateral fill movement, backfill systems are characterized by extensive vertical or near vertical downward flow at relatively high solids concentrations . Making use of this available potential energy in the system for fill placement may obviate the need for any additional pumping equipment and its associated cost. However, gravity-flow backfill systems are subjected to unsteady flow conditions resulting from free fall in the vertical drops.

According to Thomas et al. (1979), the emphasis with fill distribution systems should be on engineering for reliability rather than the conventional minimum friction loss approach. This is due to the fact that costs incurred from interrupting the mining/backfill cycle far exceed potential cost savings in a tightly designed fill distribution system. With a well designed fill distribution system; blockages, pipe bursts and accelerated wear must be prevented even at some extra costs resulting from higher safety factors.

Another important difference between hydraulic fill transportation and conventional slurry conveying is the fact that the particle size distribution of solids is usually determined by the milling process (for maximizing mineral recovery) and mine specifications (for highest strength and stability properties) rather than

by the transportation requirements (for flowability and minimum pressure loss). The task of the backfill system designer is to modify the run-of-the mill particle size distribution to give the fill material acceptable flow characteristics in the pipelines and adequate support properties in the stopes.

Backfill practice requires the fill to be placed in the stopes at the highest possible solids concentration. It was determined experimentally that the maximum flowable solids concentration for classified mill tailings fill slurry is about 49.5 per cent. by volume (Stewart, 1959).

2.1.1 Basic Configurations For Fill Distribution

There are three possible configurations for moving the fill material from a point on the surface to the stope underground as shown in Figure 2.1.

Configuration A has the advantage of being totally contained underground, thus causing no disruption to surface activities. Furthermore, the ratio of the vertical to horizontal distance is usually so favorable that little or no pumping energy is required ; in fact, measures to restrict the flow velocity are sometimes taken to control the wear rate of the pipeline system.

The disadvantages of such a circuit become apparent when the ratio of the vertical to horizontal distance is relatively large or small. The first case is encountered in deep mines where the stope to be filled is close to the vertical drop section of the pipeline. This results in very high pressure at take-off point, and a burst line may disrupt the shaft level or main level operations. In the second case, a pump may be needed to convey the fill in the horizontal section of the pipeline with the incurred additional energy and maintenance costs.

Configuration B has the advantage of making the conversion from vertical head to horizontal pressure progressive, thus shorter and lighter pipes can be used. The pressure at take-off points are moderate and line failures, if any, do not disrupt the main shaft or main level of operation. The circuit can be developed progressively as the mine expands. The disadvantages of this configuration are in terms increased maintenance costs resulting from the stepwise pipeline paths.

Figure 2.1 Three basic fill distribution circuits

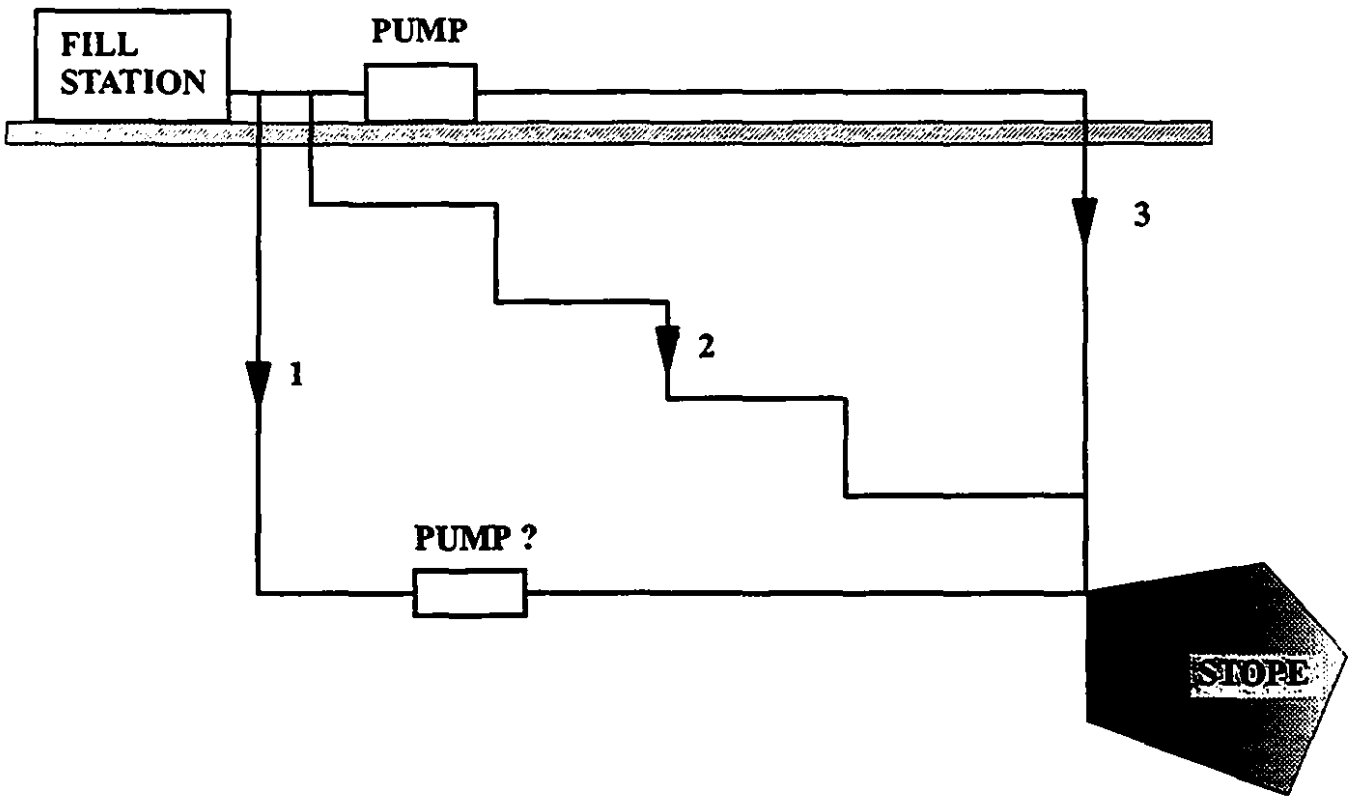

Configuration C has the advantage of easy installation, inspection and maintenance, with no special underground level and no disruption of the main shaft. However, such a system makes the filling operation dependent upon a pumping operation and requires a long borehole to place fill underground which results in high pressure take-off point. Furthermore some disruption to surface activities is possible, and in very cold weather, freezing may be a problem.

2.2 Energy Equation For a Backfill System

The hydraulic design of mining backfill transportation systems is based on head loss analysis, line velocities and flow regimes. Analysis usually starts by the Bernoulli equation for the conservation of energy. As applied to continuous incompressible fill flow in pipeline, this equation may be stated as follows:

$$\frac{P_2-P_1}{\rho} + \left(\frac{V^2}{2\alpha}\right)_2 - \left(\frac{V^2}{2\alpha}\right)_1 + g(h_2-h_1) - g(E_A - E_L) = 0 \qquad (2.1)$$

The terms of this equation are all expressed in energy per unit mass of fluid. They represent from left to right : pressure differential, kinetic energy change, potential energy change, and the difference between pump energy input and energy lost to friction. α is a kinetic energy correction factor that depends on the velocity profile. α ranges between 0.5 for a parabolic velocity profile to 1.0 for a flat one.

The hydraulic (or piezometric) head is defined as :

$$H_H = h + \frac{P}{\rho g} \qquad (2.2)$$

and total (or stagnation) head is defined as:

$$H_T = h + \frac{P}{\rho g} + \frac{V^2}{2g} \qquad (2.3)$$

The hydraulic grade is the slope of the straight line drawn through the hydraulic heads along the pipe and represent the rate at which the hydraulic head decreases

Figure 2.2 Definition of the terms in the Bernoulli equation

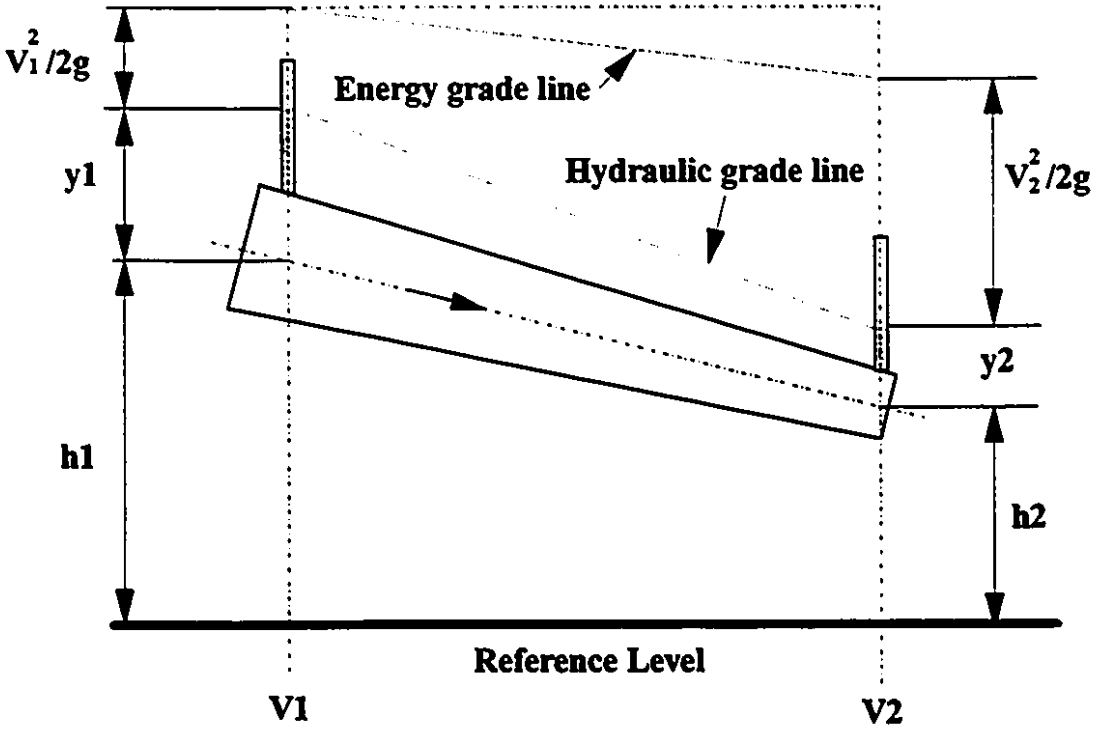

as a result of the pipe friction along the pipeline. The hydraulic grade line and the energy line (representing the total head) are shown in Figure 2.2.

The hydraulic grade line is a very useful graphical design tool for checking the pressure magnitude in the pipeline. For example, if the hydraulic grade line falls below ground level, a negative pressure is indicated. This would result in *cavitation*, a wear- accelerating phenomenon manifested by periodic vaporization and recondensation of the fluid, and with the solid particles present, this could cause a sand-blasting effect capable of eroding the pipe wall.

Slack flow is also a phenomenon associated with a negative hydraulic grade line. It is manifested by the pipe operating partially full with the open portion above the fluid filled with vapor as a result of the negative pressure. This uneven load can cause an accelerated wear rate which shortens the life span of the pipeline.

Thus to avoid slack flow and cavitation, it is required to design the pipeline system such that the hydraulic grade line never intersect or fall below the ground profile. It is also recommended that at the pipeline outlet, the hydraulic grade line ends with a positive (non-zero) magnitude as a safety factor. These principles are illustrated in Figure 2.3.

In the case of a gravity-fed backfill pipeline system, the energy balance occurs between the driving hydrostatic head on one side, and the kinetic energy and the energy losses due to friction on the other. It is assumed that the system is under full flow and steady state conditions, that inlet and outlet pressures are atmospheric, and that the rate of change of level in the storage tank is negligible.

The energy balance is thus expressed by the following equation:

$$\Delta H = \Sigma H_{f_i} + \Sigma K_i \frac{U_i^2}{2g} + \frac{U_d^2}{2g} \qquad (2.4)$$

where:

ΔH = total hydrostatic head (potential energy available)
H_{f_i} = energy loss caused by friction in a pipe segment
U_i = velocity through a bend, fitting or valve
U_d = velocity at the discharge end of the pipeline
K_i = flow resistance coefficient

The assumption of the incompressibility of the fluid is usually valid; however, the continuity condition may not always be satisfied, especially in the free fall sections of the vertical pipes or boreholes. Free fall should be avoided as it can cause inlet static pressure below atmospheric and hence drawing air into the fill line. Furthermore, pipe hammer resulting from impact, as the flow joins the full flow section of the pipe, may cause accelerated wear of the pipeline.

In practice, it is important to know the location and the magnitude of the points of maximum pressure developed in the system in order to select pipe materials and fittings capable of accommodating such operating conditions. Knowledge of whether the system is operating under full flow or free fall conditions is also required.

Maximum pressure is developed at the lowest point of the vertical section of a pipe or borehole. In such analysis, It is common to assume that kinetic energy is negligible compared to other terms in the Bernoulli equation. Furthermore, if the energy equation is written between two points in the system at atmospheric pressure such as the inlet and exit points for example, then this energy equation becomes merely a balance between the potential energy available in the system and the frictional energy losses.

The potential energy of the system is that of the equivalent vertical length of slurry between the inlet and the outlet of the pipe system. Frictional energy losses, on the other hand, depend on the flow velocity, specific gravity, particle size distribution and concentration of the fill slurries.

Figure 2.3 Hydraulic grade lines

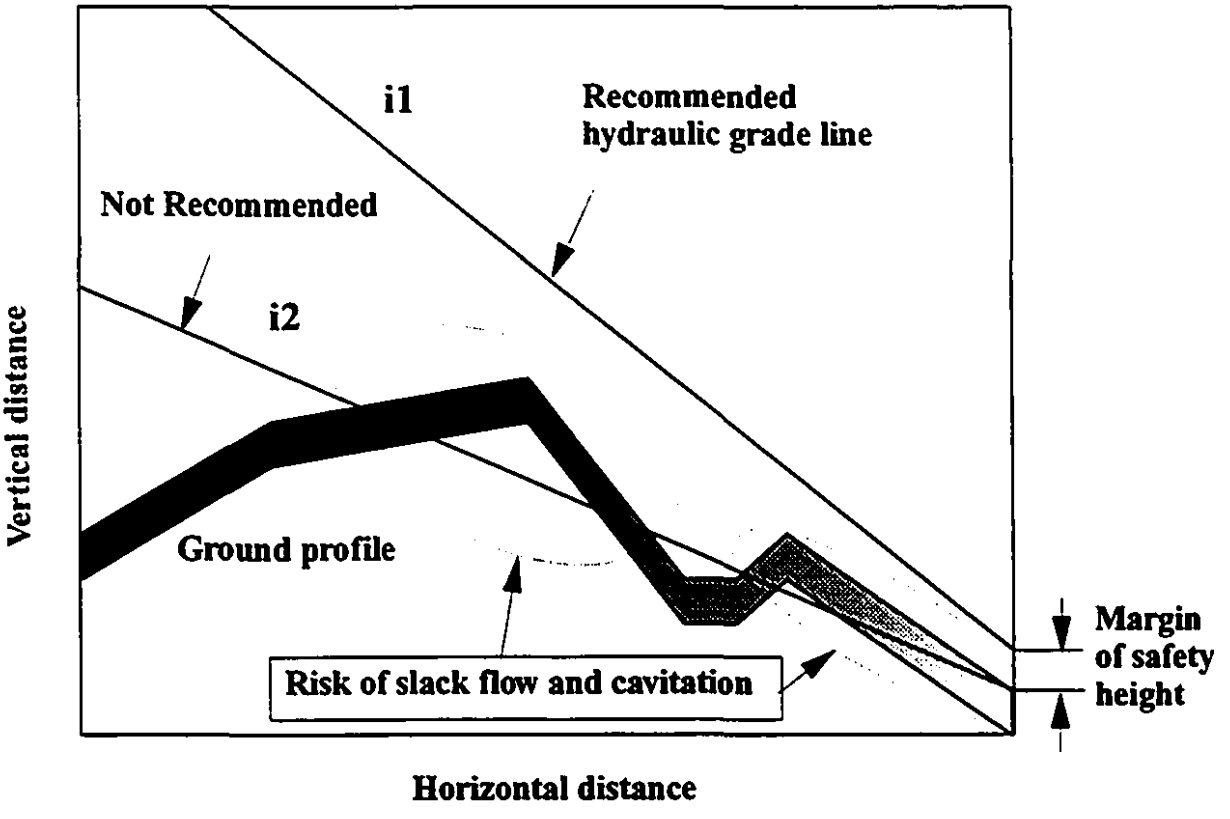

The Darcy-Weisbach equation has been a standard method for estimating such frictional pressure losses. This equation requires knowledge of the friction factor. If no previous data are available about a particular slurry, flow tests over a wide range of Reynolds numbers may be required to determine such friction factors. If the slurry is designed to flow in the laminar regime, rheological experiments have to be conducted to determine the rheological parameters. Depending on each case, appropriate methods as described in the following chapters should be applied to predict frictional energy losses.

2.3 Backfill Distribution System Design Principles

When designing an hydraulic fill system, it is recommended to use as high a solids concentration as possible in order to minimize the volume of water for fill transportation. The operating flow velocity should be as low as possible to minimize pipe wear, but high enough to keep coarser particles in suspension.

Critical velocity is usually introduced as a lower bound for the operating velocity below which deposition of solid particles forms a stationary bed indicating imminent plugging of the pipeline. As solids concentration increases, critical velocity becomes less relevant due to the hindered settling tendency of the particles.

In order to reduce the effect of free fall on the flow behavior of the slurry, pipe diameter in the free fall region may be reduced or some method of restricting the flow should be provided. Reducing pipe diameter may offer a suitable and economical solution. However, restricting flow velocity at the slurry inlet and/or exit, in order to reduce pressure losses, may result in a free fall situation if the entry velocity becomes less than the natural flow velocity of the system. Practical examples to illustrate this point are found in Thomas et al (1979).

The basic data required for the design of a backfill transportation systems are defined as follows:

1) The volume of the void to be filled per day V, (m^3/day):

It can be estimated from the average production output M (Tons/day) and the unit weight of ore γ (T/m^3) as given by:

$$V = \frac{M}{\gamma} \tag{2.5}$$

2) The fill delivery rate Q_p (m^3/hr) is given by:

$$Q_p = \frac{V}{T} \tag{2.6}$$

where T, (hr/day) is the fill delivery time per day of operation.

3) The slurry discharge rate Q_s(m^3/hr) is given by:

$$Q_s = K\frac{Q_p}{C_v} \tag{2.7}$$

where:

K is a coefficient that accounts for a percentage loss of solids during placement (e.g. K=1.05), and C_v is the solids concentration by volume.

4) The slurry operating flow velocity V_{op} (m/sec) is given by:

$$V_{op} = \frac{Q_s}{900\,\pi D^2} \tag{2.8}$$

where D is the pipe diameter in meter.

2.4 Particle Size Distribution

Particle size distribution is one of the primary properties used to characterize a mixture of solid particles. Along with the specific gravity of solids and their concentration, it has a strong influence on the flow behavior of the mixture. There are many ways of presenting a particle size distribution. The most common in the field of hydrotransport is the cumulative distribution by weight (oversize or undersize) often obtained by sieve analysis using the Tyler mesh scale. To detect the presence of more than one mode in the distribution, a "unit-interval" distribution curve or a histogram may be used, which is made up of the various bars corresponding to different screen sizes and having heights equal to the individual percent retained values.

For mono-modal finely powdered materials many empirical models are available in the literature that could be used for curve fitting. More than one distribution may fit well a set of measurements. The Gates-Gaudin-Schumann has the advantage of being the simplest. Table 2.1 lists the most common two-parameter models of these distributions. $P_S(d)$ is the cumulative fraction finer than screen size d. The parameter are d_{50} (median size) and m (dimensionless parameter) or the standard deviation σ .

2.4.1 The Black Mesa Particle Size Distribution

The success of the Black Mesa pipeline project was in part due to the extensive laboratory investigation on the optimal size distribution for minimal pumping energy required for transporting coal in pipelines over a long distance. This particle size distribution became an industry standard often used for comparison (Hanks et al., 1982). The cumulative particle size distribution and the corresponding histogram are shown in Figure 2.4 and 2.5 respectively.

Table 2.1

Two-parameter Particle Size Distribution Functions
(after Shook and Roco 1991)

Distribution	**$P_S(d)$**
Rosin-Rammler	$1-\exp\left(-\ln 2\left(\frac{d}{d_{50}}\right)^m\right)$
Gates-Gaudin-Schumann	$0.5\left(\frac{d}{d_{50}}\right)^m$
Gaudin-Meloy	$1-\left(1-\left(\frac{d}{d_{50}}\right)\left(1-\sqrt[m]{0.5}\right)\right)^m$
Log normal	$\left(\frac{1}{\sqrt{2\pi}}\right)\int_{-\infty}^{x}\exp\left(-\frac{t^2}{2}\right)dt$ where $x=\frac{\ln(d/d_{50})}{\ln\sigma}$

Figure 2.4 Cumulative particle size distribution of Black Mesa Coal
(adapted from Hanks et al., 1982)

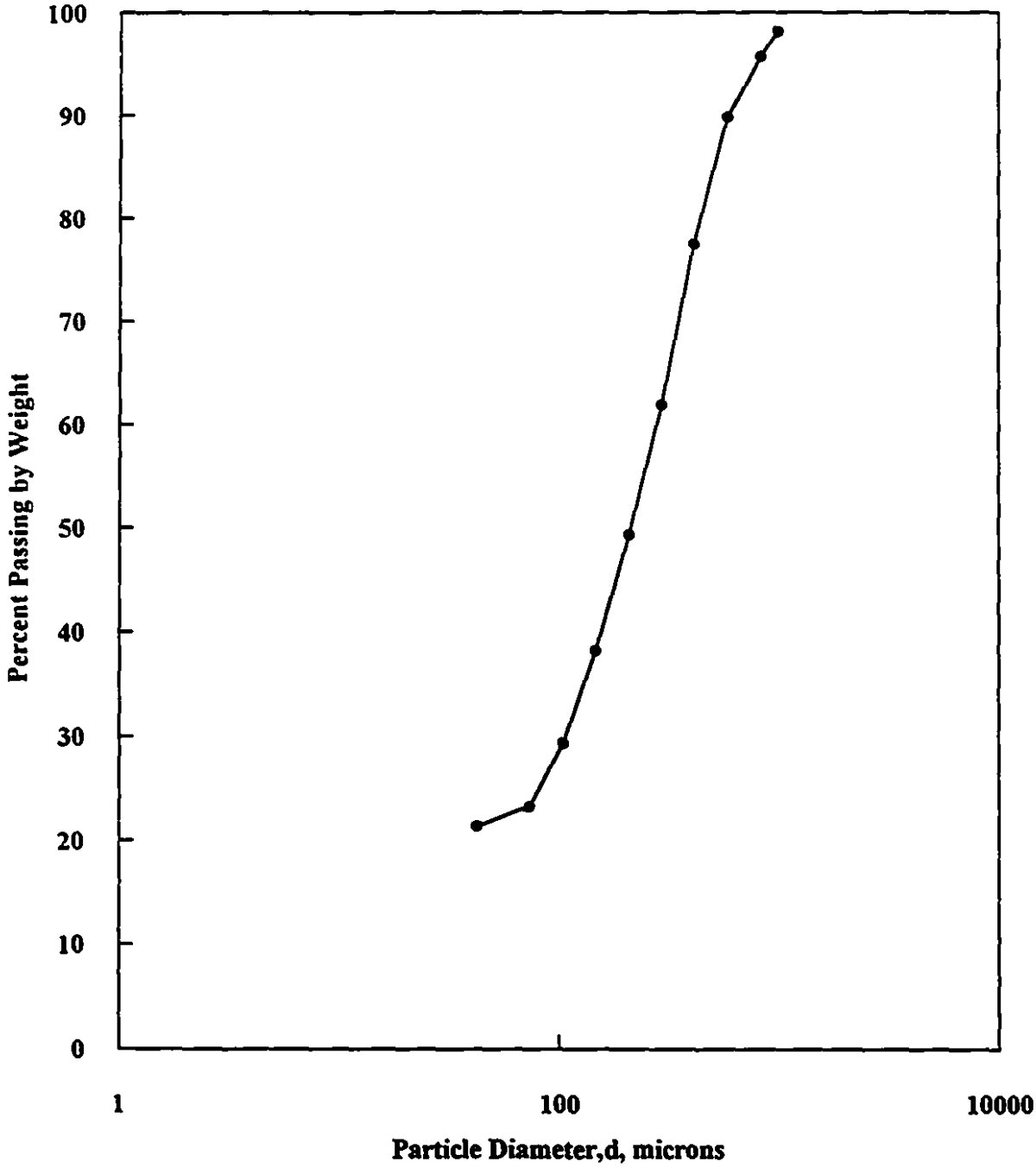

Figure 2.5 Histogram of Black Mesa Coal (adapted from Hanks et al., 1982)

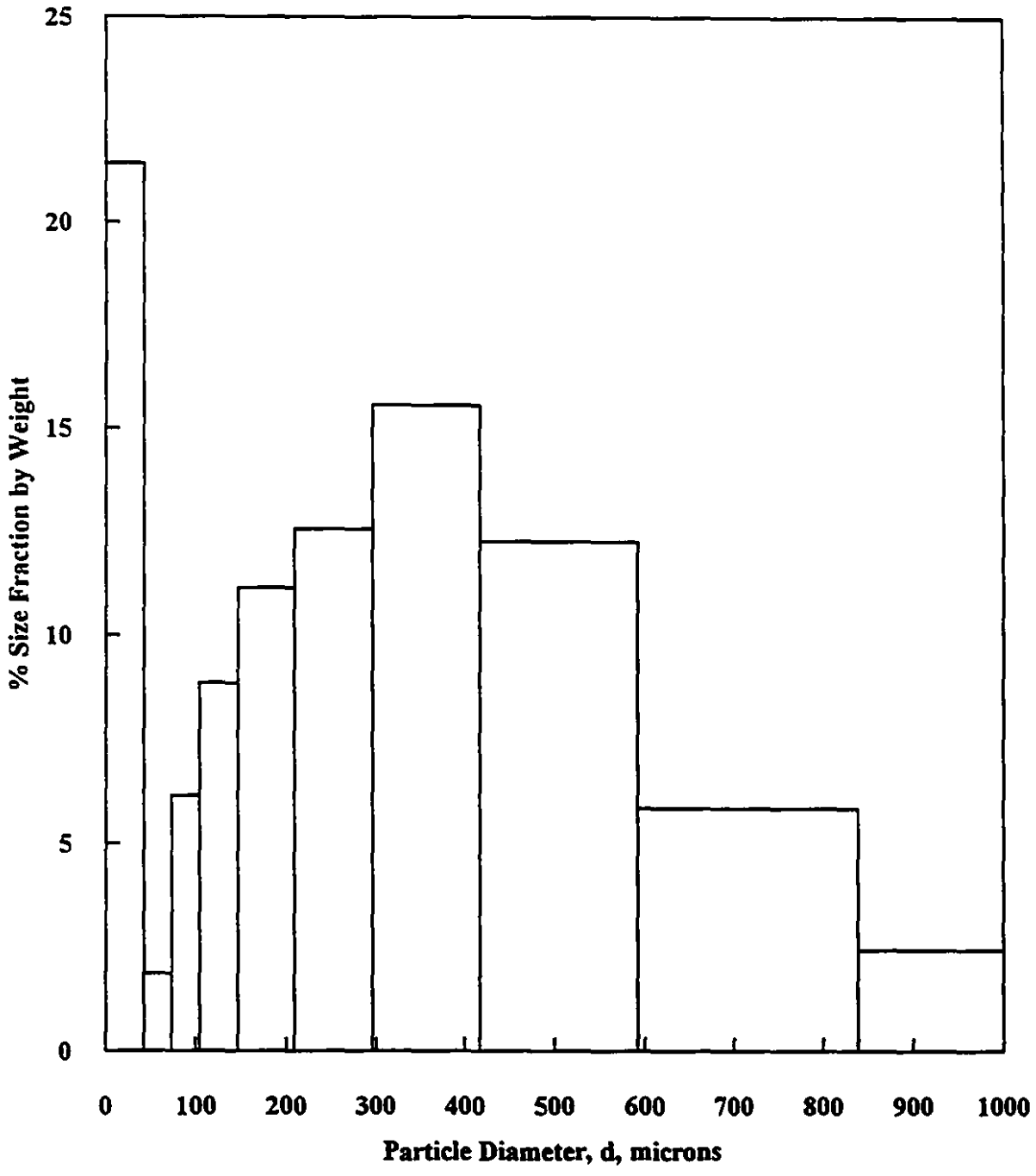

2.5 Particle Size Classification

When the particle size distribution is made up of several size fractions ranging from fine to coarse, it is necessary for the purpose of some hydraulic design methods to delineate the fine fraction from the coarse one. An important criterion for such delineation is the terminal settling velocity of solid particles. For a spherical particle, the terminal settling velocity in still water is expressed by:

$$V_o = \sqrt{\frac{4gd(S_s-1)}{3C_d}} \qquad (2.9)$$

The fine fraction of a suspension which remains symmetrically suspended during flow, may be defined by an upper limit on the particle size whose maximum terminal settling velocity lies in the laminar zone. According to Stoke's law, the drag coefficient for a sphere in the laminar zone is given by :

$$C_d = \frac{24}{Re} \qquad (2.10)$$

where the Reynolds number is given by:

$$Re = \frac{V_o d\rho}{\mu} \qquad (2.11)$$

Substituting Equation (2.10) in (2.9) reduces the terminal settling velocity to:

$$V_o = \frac{gd^2(S_s-1)}{18\,\mu} \qquad (2.12)$$

The limiting Reynolds number in the laminar zone may be taken as Re*=1. Substituting Equation (2.10) in (2.9), and solving for the maximum particle size dmax in water, falling in the laminar zone :

$$d_{max} = \sqrt[3]{\frac{18\,\nu^2\,Re^*}{g\,(S_S-1)}} \qquad (2.13)$$

If the terminal settling velocity is in the turbulent zone, i.e. for $Re = \frac{V_o d\rho}{\mu} > 800$, then Newton's law gives (Govier and Aziz, 1987):

$$V_o = 1.7408\sqrt{dg(S_S-1)} \qquad (2.14)$$

from which the minimum diameter falling in the turbulent zone is given by:

$$d_{min} = \left(\left(\frac{\nu Re^{**}}{1.7408}\right)^2 \cdot \frac{1}{g(S_S-1)}\right)^{\frac{1}{3}} \qquad (2.15)$$

with $Re^{**} = 800$

If water is the suspending fluid with $\nu = 10\text{-}6\,\frac{m^2}{Sec}$, then the ratio of *coarse* to *fine* particle diameter is given by::

$$\frac{dmin}{dmax} = 22.72 \qquad (2.16)$$

For given specific gravity of solids, a particle is defined as *coarse* if its diameter equals or exceeds dmin. Similarly a particle is defined as *fine* if its diameter is smaller than dmax. This classification is shown in Figure 2.6

2.6 Hanks's Method for Particle Size Classification (Hanks et al.1982)

According to this method, the key concept in classifying a particle as coarse or fine depends on its rheological behavior.

Figure 2.6 Boundary for coarse and fine particles as a function of specific gravity of solids

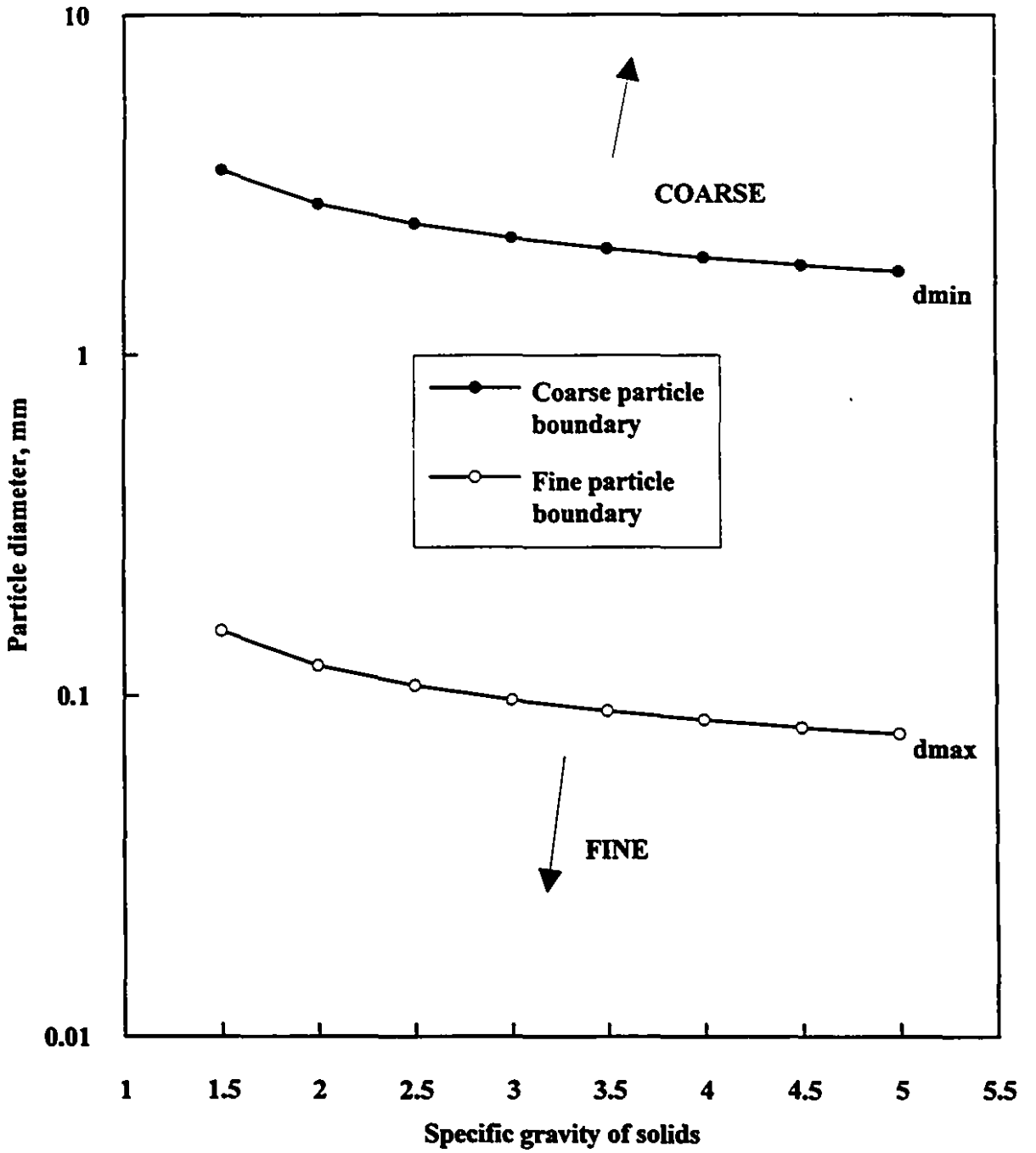

2.6.1 Fine Fraction Definition

The fine fraction of the slurry making up the suspending medium, or vehicle, is that portion of total solids present in a slurry which, when combined with all the free liquid carrier fluid, creates a new homogeneous carrier medium in which the remainder of the solid particles (and any absorbed fluid) are heterogeneously or pseudo-homogeneously suspended.

2.6.2 Coarse Fraction Definition

A coarse fraction is defined as one which does not contribute to the rheology of the *vehicle*, although it does contribute to total slurry hydraulic resistance.

2.6.3 Method for Determining the Rheologically Active Fines

1. The particle size distribution is divided in size fractions as obtained from sieve analysis.

2. Starting with the finest fraction, one determines its shear stress versus shear rate dependence as a function of solids concentration over a wide range. Yield stress (if present) should be determined.

3. A new set of slurries consisting of the original fraction plus the next one in order are prepared in the proportions called for by the particle size distribution; and the rheological measurements are repeated as a function of total solids concentration.

4. Plot the parameters of the rheological model used to describe the behavior of the above suspensions as a function of the "equivalent" total solids concentration (defined below) for each of the slurries.

5. If the addition of the next higher fraction does not effect the magnitude of the rheological parameters determined for the previous size fraction alone, then the limit of particle size influence on rheology is determined.

The *equivalent* total solids concentration (i.e. the saturated solid volume fraction in the slurry) is given by:

$$\phi_{ss} = \frac{\rho_S - W_{ss}(\rho_S - \rho_L)}{\rho_S - W_{ts}(\rho_S - \rho_L)} \left(\frac{W_{ts}}{W_{ss}}\right) \qquad (2.17)$$

where:

W_{ss}= weight fraction of dry solid in the saturated solid material
W_{ts} = dry weight fraction of total solids in the slurry
ρ_S = density of dry solids
ρ_L = density of the liquid

In such a slurry, the vehicle portion consists of the fraction (β) of rheologically active fines plus the water which is absorbed in these solids plus all the free water. By a volume balance, the volume fraction of saturated solids in the vehicle portion is related to the volume fraction of saturated solids in the total slurry by the relation:

$$\phi_{sv} = \frac{\beta\, \phi_{ss}}{1 - (1-\beta)\, \phi_{ss}} \qquad (2.18)$$

where:

β= fraction of the particle size distribution determined to be rheologically active

Thus given ϕ_{sv}, the corresponding *equivalent* total slurry concentration is given by:

$$\phi_{ss} = \frac{\phi_{sv}}{\beta + (1-\beta)\, \phi_{sv}} \qquad (2.19)$$

In Hanks et al. (1982) experiments with coal having a Black Mesa distribution, only particles finer than 44 microns were found to be rheologically active. The

remaining particles were considered *coarse* , i.e. they contribute to the overall hydraulic resistance of the slurry through heterogeneous flow phenomenon only (not rheological phenomena).

2.7 Mean Particle Diameter

The best way to represent particle size characteristics of a mixture of solid particles is to display its particle size distribution. If it is required to have a single measure of central tendency of the distribution, then various mean particle diameters are available depending on the intended application.

Among the common ways of describing a representative size of backfill material of graded particles is the d_{50} size, i.e. the size corresponding to 50 percent passed of the total sample by mass. Other sizes such as d_{85} have been used to characterize the average particle size of the coarse fraction of the slurry. Other mean diameters sometimes used to represent the distribution are: the volume mean d_{vm}, specific surface mean d_{ssm}, and mass mean diameter d_{mm}, as given by (Hanks 1981):

$$d_{vm} = \left(\frac{\Sigma_j \Delta Y_j}{\Sigma_k \Delta Y_k d_k^{-3}} \right)^{\frac{1}{3}} = \left(\frac{1}{\Sigma_k w_k / d_k^3} \right)^{\frac{1}{3}} \qquad (2.20)$$

$$d_{ssm} = \left(\frac{\Sigma_j \Delta Y_j}{\Sigma_k \Delta Y_k d_k^{-1}} \right) = \frac{1}{\Sigma_j w_j / d_j} \qquad (2.21)$$

$$d_{mm} = \frac{\Sigma_k \Delta Y_k d_k}{\Sigma_j \Delta_j Y_j} = \Sigma_j w_j d_j \qquad (2.22)$$

where $\Delta Y_j = Y_j - Y_{j-1}$ is the j-th increment in percent undersize and w_j is the weight fraction of the j-th increment.

2.8 Solids Concentration

Solids concentration is defined either on a volume or weight basis. Most equations include the solids concentration by volume :

$$C_v = \frac{S_m - 1}{S_s - 1} \tag{2.23}$$

The solids concentration by weight is given by:

$$C_w = \frac{(S_m - 1)S_s}{(S_s - 1)S_m} \tag{2.24}$$

The relation between the two concentrations is expressed by:

$$C_w = \frac{C_v S_s}{S_m} \tag{2.25}$$

The expressions relating the specific gravity of the mixture to the concentration by volume and by weight are respectively given by:

$$S_m = 1 + C_v (S_s - 1) \tag{2.26}$$

$$S_m = \frac{S_s}{S_s - C_w (S_s - 1)} \tag{2.27}$$

The mass flow rate of solids--a parameter of practical interest, is given by:

$$M_s = Q\, C_v\, \rho_s \tag{2.28}$$

Where the volumetric flow rate Q is expressed as:

$$Q = \frac{\pi D^2}{4} V \qquad (2.29)$$

2.9 Holdup Phenomena

The holdup effect is measured by the holdup ratio H, defined as the ratio of average in-situ concentration to the mean discharge concentration. When solid particles are suspended and transported by a moving fluid, the fluid phase tends to have a higher in-situ average velocity than the solid one. This may explain the so-called "slip" of one phase past another or "holdup" of one phase relative to another. This slip velocity may be predicted by the Ergun's equation as shown in Chapter Six on the two layer model.

Holdup is a significant parameter when dealing with saltation or moving bed flow regimes, for which transport is by asymmetric suspension. This may account for the error in many empirical correlations corresponding to such regimes in predicting pressure losses. For symmetric flow regimes, such as homogeneous or pseudo-homogeneous, it is common to assume that holdup is negligible.

2.10 Terminal Settling Velocity

The terminal settling velocity is defined as the velocity reached by a particle (with density ρ_p) falling in a still fluid (with density ρ) when the gravitational force F_g just balances the drag force F_d, respectively given by:

$$F_g = \frac{\pi d^3}{6} (\rho_p - \rho) g \qquad (2.30)$$

$$F_d = C_d \frac{\rho V_o^2}{2} \frac{\pi d^2}{4} \qquad (2.31)$$

Which yields the terminal settling velocity:

$$V_o = \sqrt{\frac{4gd(\rho_p - \rho)}{3C_d \rho}} \qquad (2.32)$$

The drag coefficient C_d is a function of the Reynolds number. By substituting the values of C_d corresponding to laminar, intermediate and turbulent flow, the terminal settling velocity may be calculated as follows (Govier and Aziz, 1977):

Laminar region, $\frac{d V_o \rho}{m} < 1$

$$C_d = \frac{24 \mu}{d V_o \rho} \qquad (2.33)$$

$$V_o = \frac{g(\rho_p - \rho)d^2}{18 \mu} \qquad (2.34)$$

Transition region, $1 < \frac{d V_o \rho}{\mu} < 1000$

$$C_d = \left(\frac{d\, Vo\, R}{m}\right)^{-0.625} \qquad (2.35)$$

$$V_o = 0.2 \left(\frac{(\rho_p - \rho)}{g\, r}\right)^{0.72} d^{1.18} \left(\frac{\rho}{\mu}\right)^{-0.45} \qquad (2.36)$$

Turbulent region, $\frac{d V_o \rho}{\mu} > 800$

$$C_d = 0.44 \qquad (2.37)$$

$$V_o = 1.74 \left(\frac{g(\rho_p - \rho)}{\rho}\right)^{0.5} d^{0.5} \qquad (2.38)$$

For irregularly shaped particles common in practice, the terminal settling velocity is lower than that of spherical particles of comparable size due to the higher drag coefficient of irregular particles. It is common to correct for this error in settling velocity by multiplying the terminal settling velocity for a spherical particle by a shape factor k, which is a function of the sphericity defined as:

$$\psi = \frac{d_{av}}{n\, d_s} \qquad (2.39)$$

where:

d_{av}= average screen size of the particle
d_s= diameter of a sphere having the same volume as the particle
n = ratio of the surface area per unit mass of the particles to that of spheres of diameter d_{av}

2.11 Drag Coefficient

The drag coefficient C_D is defined by:

$$C_D = \frac{F_D}{0.5\, A_p\, \rho_L\, v_r\, |v_r|} \qquad (2.40)$$

where F_D is the drag force in the direction of the velocity v_r of the fluid relative of a particle with projected cross sectional area A_p. The drag coefficient C_D depends on the shape of the particle and its characteristic Reynolds number $Rep = \frac{d\,|v_r|\rho_L}{\mu}$, where d is the characteristic dimension of the particle, and ρ_L is the density of the liquid. C_D also depends on the particle surface roughness, the degree of turbulence in the fluid, and the acceleration of the fluid relative to the particle.

The drag force on a solid immersed in a moving fluid consists of two components: the viscous drag force (skin friction) and the form drag. For steady Newtonian flows past spherical particles, C_D may be given by the following relations:

• Stoke's law where drag force is entirely due to skin friction:

$$C_D = \frac{24}{Rep}, \text{ for } Rep < 0.2 \qquad (2.41)$$

• Intermediate law where both viscous and form drag are present:

$$C_D = \frac{24}{Rep}\cdot(1+0.15\, R_{ep}^{0.687}), \text{ for } 0.2 < Rep < 1000 \qquad (2.42)$$

• Newton's law where only form drag is present:

$$C_D = 0.44, \text{ for } 1000 < Rep < 2\cdot 10^5 \qquad (2.43)$$

Alternatively C_D may be expressed by the single equation:

$$C_D = \frac{24}{Rep} + \frac{3.5}{R_{ep}^{0.3}} + 0.23\, k \log_{10}\left(\frac{Rep}{1500}\right), \text{ for } Rep < 7\cdot 10^4 \qquad (2.44)$$

where $k = 0$ for $Rep < 7\cdot 10^4$, and 1 otherwise.

For particles with broad size distribution, an estimate for a mean drag coefficient may be obtained from:

$$\sqrt{\frac{1}{C_{Dm}}} = \Sigma_i\left(\frac{x_i}{\sqrt{C_{Di}}}\right) \qquad (2.45)$$

where x_i is the fraction of particles in screen interval i with median diameter d_i.

In practice it is preferable to measure drag coefficient of particles, thus taking their actual shape and surface characteristics into account. This is achieved by measuring the terminal settling velocity V_s of a single particle falling unhindered in a settling column of diameter D. A force balance between the drag and buoyancy forces gives an estimate of the drag coefficient as given by:

$$C_D = \frac{4gd(S - 1)}{3V_\infty^2} \qquad (2.46)$$

where $V\infty$ is given approximately by :

$$V_\infty = V_s \left(\frac{(1 - 0.475d/D)}{(1 - d/D)} \right)^4 \text{ for } Rep < 1 \qquad (2.47)$$

For hindered settling, Equations (2.41) to (2.43) may be used with a modified Reynolds number for multi-particle systems at volumetric concentration (c), as given by (Shook, 1991):

$$Res = \frac{d\,(1 - c)\,|v_L - v_s|\,\rho_L}{\mu_L} \qquad (2.48)$$

Figure 2.7 illustrates qualitatively the influence of particle size on concentration distribution, drag coefficient and settling velocity.

2.12 Transition Velocity

In homogeneous fluids, it is the velocity at which transition from laminar to turbulent flow occurs. This velocity is important because a significant increase in flow resistance is observed once the flow becomes turbulent. The transition
ɔcity depends on the Reynolds number, which is defined as the ratio of inertial
es to viscous forces, expressed by :

$$Re = \frac{D\,V\,\rho}{\mu} = \frac{DV}{\nu} \qquad (2.49)$$

where:
D = diameter of pipe
V = mean flow velocity
ρ= density of fluid
μ = absolute (dynamic) viscosity
ν = kinematic viscosity

Figure 2.7 Effect of particle size on concentration distribution, drag coefficient and settling velocity (adapted from Lazarus, 1989)

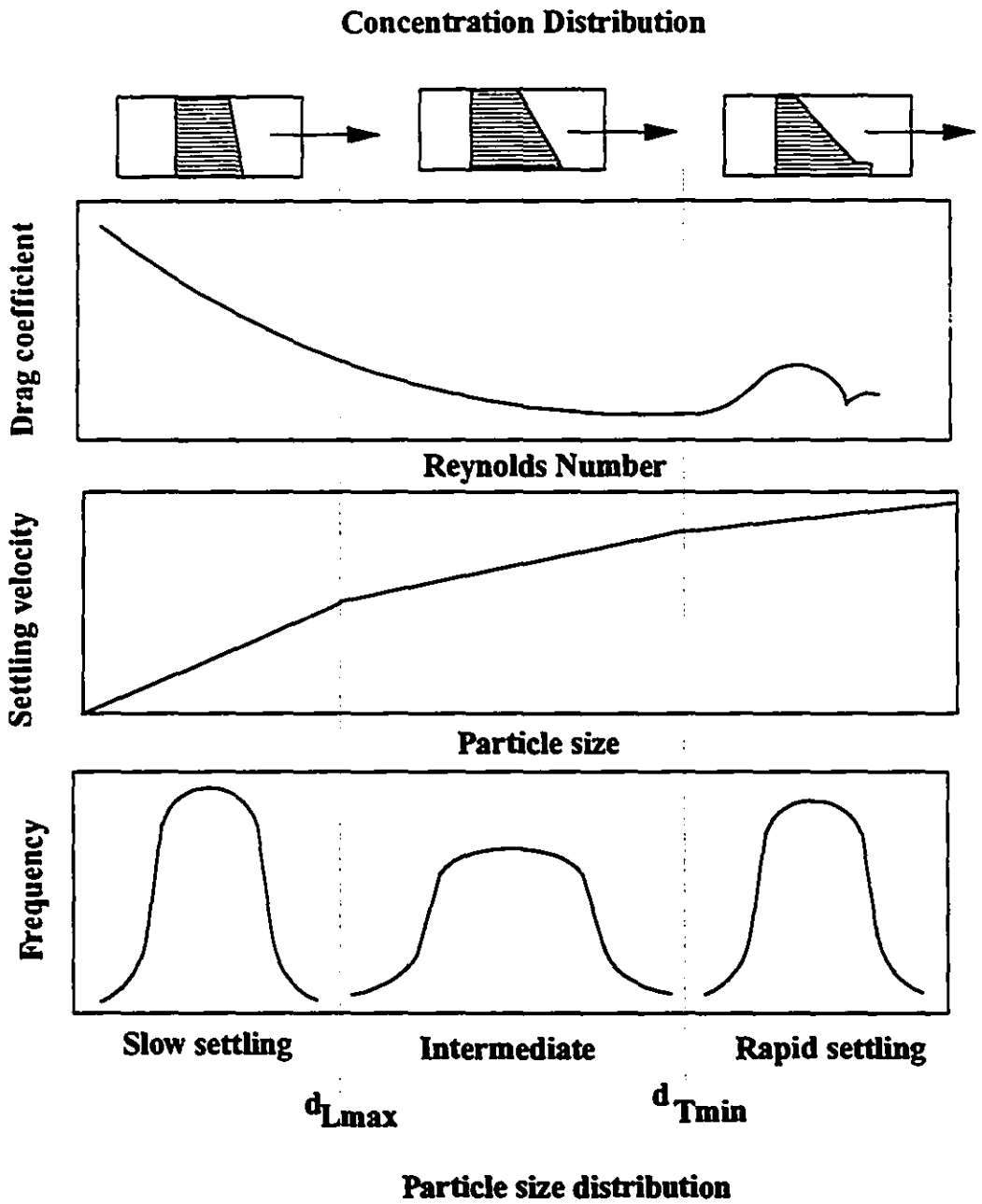

For Newtonian fluids, the absolute viscosity is a constant parameter readily obtained from the slope of a shear stress-shear rate curve. However, when the fluid is non-Newtonian, an *effective viscosity* equivalent to the absolute viscosity in the Newtonian case has to be defined.

2.13 Critical Flow Velocity

Turian et al. (1977) defined the critical velocity as *the minimum velocity demarcating flows in which the solids form a bed at the bottom of the pipe from fully suspended flow*. This velocity is also referred to as the minimum carrying or the limiting deposit velocity, and it is one of the most important design parameters in slurry transport. It is the transition velocity between heterogeneous flow and moving bed flow.

Other authors defined the critical velocity as the transition velocity between moving bed flow and stationary bed. A more systematically defined critical velocity that usually falls between the aforementioned velocities is the one corresponding to the minimum in the pressure-velocity curve.

2.14 Velocity Distribution

For a homogeneous fluid in turbulent flow, an expression for the velocity profile may be obtained by making use of the mixing length theory developed by Prandtl. This velocity is given by:

$$\frac{U}{U^*} = \frac{1}{\kappa} \ln\left(\frac{y}{y_o}\right) \qquad (2.50)$$

where:

U= instantaneous velocity in x-direction

$U^* = \sqrt{\frac{\tau_w}{\rho}}$ = friction velocity

κ = Von Karman constant (= 0.4)

y = distance from the bottom of the pipe

y_o = constant

The above equation is based on the assumption that the mixing length is proportional to the distance away from the pipe wall, i.e.:

$$L_m = \kappa y \tag{2.51}$$

The mixing length is defined as the mean distance traveled by the fluid element over which it retained its original properties (such as velocity); at greater distances than the mixing length, the fluid element mixes with its surroundings.

It is found experimentally (Wasp et al., 1977) that the above equation is valid only near the pipe wall. An approximate solution for the velocity profile is obtained by assuming that Equation (2.51) is valid over the whole boundary layer, and is given by:

$$\frac{U_{max} - U}{U^*} = 5.75 \log_{10} \left(\frac{r}{y}\right) \tag{2.52}$$

which is valid only in the region away from the wall. A general form for the expression of the velocity profile that covers the whole boundary layer may be expressed by:

$$\frac{U_{max} - U}{U^*} = f\left(\frac{r}{y}\right) \tag{2.53}$$

where r is the radial distance from the pipe axis. The exact form of this functional relationship is not known.

For the asymmetric suspension mode of solid liquid mixtures, Newitts et al. (1962) have developed an empirical expression for predicting the velocity in the case of water mixture of coarse and sand gravel. They correlated the displacement of the maximum velocity with the equation:

$$y' - \frac{D}{2} = 15.2\left(C\sqrt{\frac{\tau_w g_c}{\rho_w}} \right)^{1.81} \qquad (2.54)$$

where y' is the distance from the bottom of the pipe to the point of the maximum fluid velocity. The velocity profile below the maximum point is given by:

$$(1-R^*)\frac{\tau_w g_c}{\rho_w} = (0.1176 - 0.0538 \log C)\left(1 - \frac{y}{y'}\right) \qquad (2.55)$$

where R* is the ratio of the velocity at a point to the maximum velocity in the presence of solids, divided by the corresponding ratio for water alone at the same hydraulic gradient, and y is the distance from the bottom of the pipe. Above the point of maximum velocity, they found the velocity profile to be described by the simple 1/7 power law (Govier and Aziz, 1987).

Experimental investigations of solid-liquid flow have shown that there may be significant asymmetry of the velocity curves, especially in the case of large particle suspensions.

2.15 Viscosity

By definition viscosity is a property for continuous media having homogeneous and isotropic properties. It applies to fluids and to colloidal (non-settling) suspensions with fluid-like behavior. It is a rheological property defined as the ratio of shear stress to the rate of shear , i.e. :

$$\mu = \frac{\tau}{-dV/dy} \qquad (2.56)$$

The above equation describes the absolute viscosity. The kinematic viscosity is the ratio of absolute (dynamic) viscosity to density of the fluid, i.e.:

$$\upsilon = \frac{\mu}{\rho} \qquad (2.57)$$

Newtonian fluids are those for which the shear stress is directly proportional to the rate of shear. Fluids which do not satisfy this condition are called non-Newtonian. For such class of fluids, there are several models each describing a specific shear stress-shear rate relationship, which will be discussed further in Chapter Four.

For solid-liquid suspensions, the concept of viscosity is a rather "sticky" subject. The difficulty arises from the fact that a suspension is inherently a discontinuous medium; whereas the attribution of rheological properties to a material assumes it to be a continuum. For non-colloidal suspensions made up of large fraction of settling coarse particles, the concept of viscosity becomes inapplicable. On the other hand, when the solid fraction is sufficiently fine and forms a colloidal suspension capable of meaningful rheological characterization, the rheological approach acquires great practical significance.

In practice, when dealing with a slurry with a wide particle size distribution, the concept of *apparent* viscosity is introduced to characterize the rheology of the suspension. It is defined as the ratio of wall shear stress to the rate of shearing strain as given by:

$$\mu_a = \frac{\tau_w}{\left(\frac{-dV}{dy}\right)} \qquad (2.58)$$

Apparent viscosity is very sensitive to solids concentration. Several analytical and empirical models are found in the literature describing this dependence. Sellgren (1989) proposed a semi-empirical expression given by:

$$\frac{\mu_a}{\mu_o} = \left(1 - \frac{C}{\alpha}\right)^{-\beta} \qquad (2.59)$$

where α and β are coefficients determined from rheological measurements. In case of non-Newtonian fluids, it is common to define an *effective* viscosity as the ratio of shear stress to average shear rate at the boundary. For pipes, the effective viscosity is given by:

$$\mu_e = \frac{\tau_w}{\left(\frac{8V}{D}\right)} \qquad (2.60)$$

where D is the pipe diameter and V is the mean flow velocity.

For Bingham plastics and pseudo-plastics, the effective viscosities are respectively given by :

$$\mu_e(\text{Bingham}) = \eta\left(1+\frac{\tau_y D}{3\eta V}\right), \text{ for } \frac{\tau_y}{\tau_y} < 0.4 \qquad (2.61)$$

$$\mu_e \text{ (Pseudo-plastic)} = K\left(\frac{3n+1}{4n}\right)\left(\frac{8V}{D}\right)^{n-1} \qquad (2.62)$$

2.16 Pressure Gradient

Once the pipe diameter and the operating velocity are selected, the pressure drop down the pipeline has to be estimated so that pumping power requirement can be determined, and the proper pump capacity selected. For water flow in pipes, the Darcy-Weisbach equation is usually used to compute the head loss due to friction, as given by:

$$h_f = \frac{\Delta P}{\rho g} = \frac{2fL}{D}\frac{V^2}{g} \qquad (2.63)$$

where:

h_f = head loss due to friction
f = friction factor
L = length of pipe
V = flow velocity
g = acceleration of gravity
ρ= density of fluid

Sometimes, the head loss equation is given by:

$$h_f = \frac{\lambda L}{D}\frac{V^2}{2g} \qquad (2.64)$$

In this case, it should be understood that the corresponding friction factor (λ) (sometimes designated by f in the literature) is 4 times the friction factor f defined by equation (2.63). For consistency, only the friction factor f as defined by equation (2.63) will be used henceforth.

Most of the empirical equations used to predict the pressure loss in the transport of solid-liquid suspension are of the form:

$$\frac{J - J_w}{C\,J_w} = K\left(\frac{V^2\sqrt{Cd}}{g\,D\,(S_S-1)}\right)^n \qquad (2.65)$$

where K and n are empirical constants determined from data collected by loop tests. J_w is the pressure loss incurred from the fluid phase, and is usually computed using Equation (2.63). In this equation, the effects of solids concentration C, specific gravity S_S, and drag coefficient C_d are taken into account . Various correlations based on this model are presented and discussed in Chapter Three. Figure 2.8 summarizes the various parameters influencing the pressure gradient.

Figure 2.8 Main variables affecting pressure gradient in pipeline slurry flow

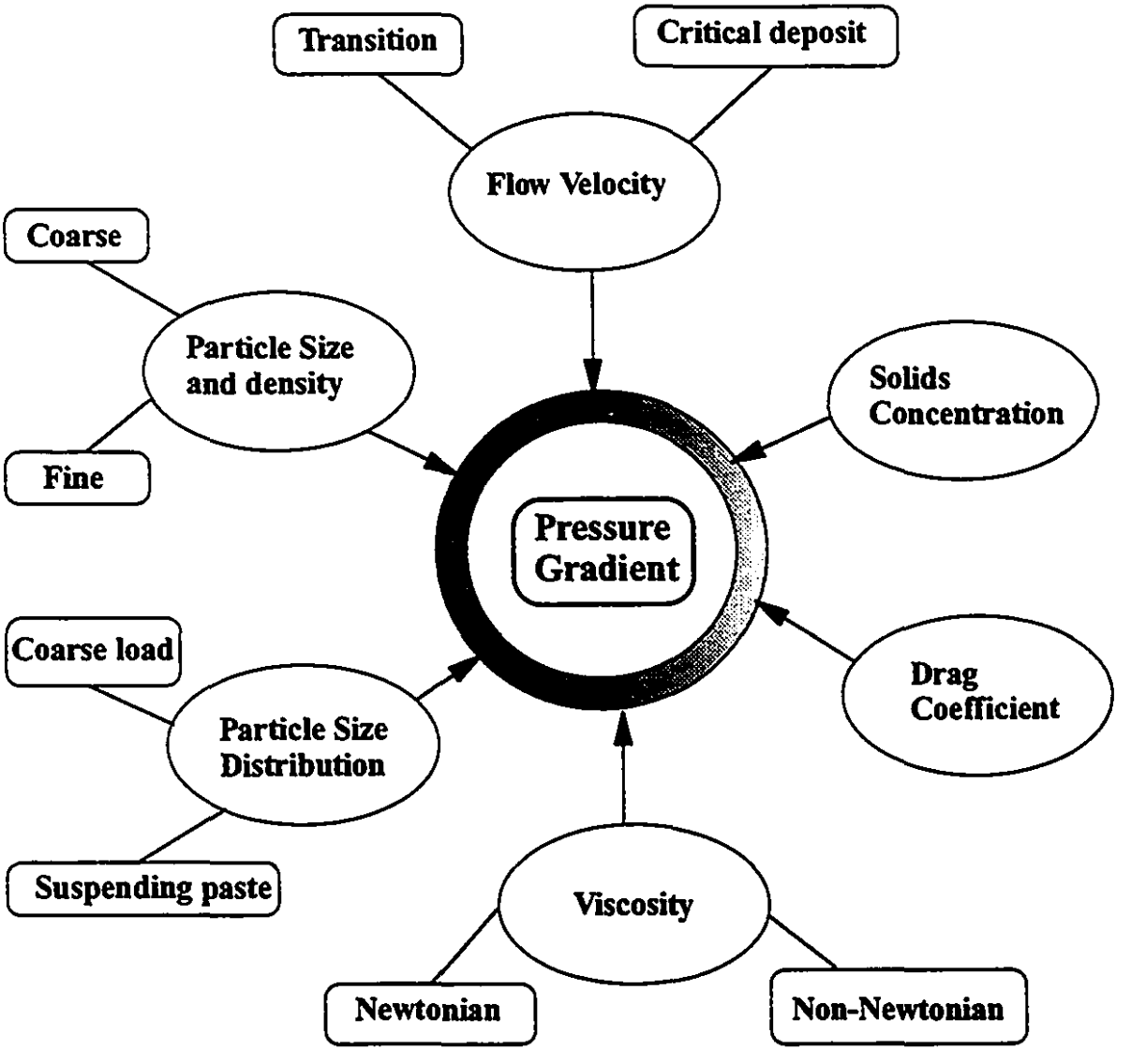

CHAPTER THREE

TRANSPORT OF SETTLING SLURRIES

EMPIRICAL APPROACH

The objective of this chapter is to present and compare some selected empirical approaches used for analysing the flow characteristics and predicting the pressure drop and critical velocity of settling slurries. Special attention will be given to Wasp's method, which is unique among semi-empirical approaches in its ability to handle slurries with wide particle size distributions similar to that of some hydraulic backfill mixtures.

3.1 Flow Regime Classification

To characterize the slurry and the flow conditions, and to match them with an adequate pressure loss prediction method, three fundamental parameters will be used, namely: flow velocity, solids concentration and particle size (for solid particles with a given density). For each combination of flow velocity, solids concentration and particle size, a description of the most likely prevalent flow conditions and some known methods of dealing with them will be presented. Qualitative definitions of *high* and *low* magnitudes of the aforementioned parameters will be given as a general guide to this classification scheme.

Slurries are usually classified as settling or non-settling. Settling slurries can be transported in one of the following flow regimes:

- Pseudo-homogeneous
- Heterogeneous
- Saltation
- Moving bed

Figure 3.1. Schematic plot of pressure drop vs. flow velocity (adapted from Govier and Aziz , 1987)

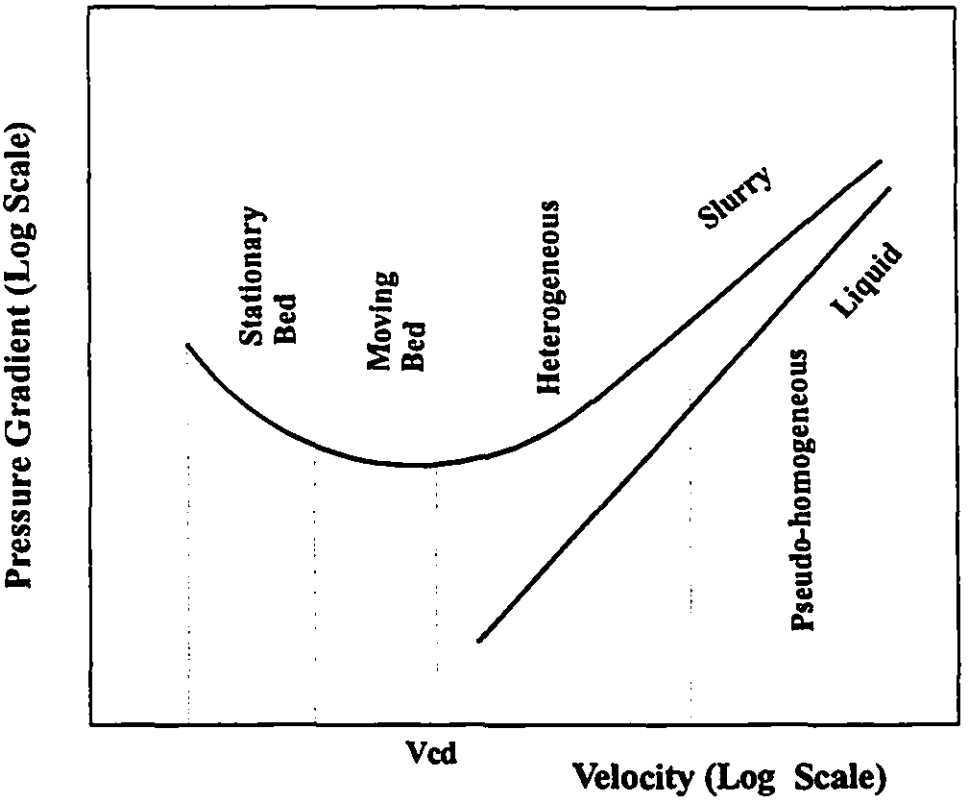

Such slurries have a characteristic pressure drop-velocity curve as shown in Figure 3.1. Except for sliding bed flow; turbulence and buoyancy are the main suspension mechanisms for these regimes. Flow velocity is usually controlled by the pressure available upstream of the flow. The main factor that controls the settling behavior are the specific gravity of solid particles, their size and shape, the volumetric concentration of the slurry and the degree of turbulence in the flow.

Attempts to classify flow regimes as a function of particle size have been made. For example Durand and Condolios (1952) concluded that for the hydraulic transport of sand with a specific gravity of 2.65, such classification is given by:

- $d < 40\ \mu m$ ..... (non-settling) homogeneous suspension
- $40\ \mu m < d < .015$ mm .... heterogeneous flow
- $0.015 < d < 1.5$ mm ..... Saltation flow
- $d > 1.5$ mm ..... moving bed flow

Wilson (1982) found that the boundary between fine particle and coarse particle behavior can be shown graphically as the locus on a plot of pipe and particle diameter based on water as a carrier fluid. He pointed out that a particle may shift from fine particle to coarse particle behaviour and vice versa depending on pipe diameter and to a lesser extent on the specific gravity of the solid particles.

3.2 Definition of *Coarse* and *Fine* Particles

As shown in Chapter Two, the maximum particle size in water falling in the laminar zone for non-interacting spherical particles, as found from Stokes law, is given by:

$$dmax = \left(\frac{18\ \nu^2\ Re^*}{g\ (S-1)} \right)^{1/3} \qquad (3.1)$$

with $Re^* = 1$ as an upper limit criterion for laminar flow.

Similarly, the minimum diameter falling in the turbulent zone is given by:

$$d_{min} = \left(\left(\frac{\nu Re^{**}}{1.7408} \right)^2 \cdot \frac{1}{g(S_s-1)} \right)^{1/3} \qquad (3.2)$$

with $Re^{**} = 800$

Since settling velocity is hindered in most slurries due to particle interaction, dmax may be considered as an approximate upper limit for the top size of what would be defined as a *fine particle*. Similarly dmin may be considered an approximate lower limit of what would be defined as a *coarse particle*. Alternatively, a fine particle may be defined as one which is rheologically active, otherwise it is considered coarse. Chapter Two outlined a method for determining this property. Figure 3.2 illustrates the combined effect of particle size and specific gravity on the flow regime, and Figure 3.3 shows the combined effect of particle size and flow velocity.

3.3 Definition of *High* and *Low* Solids Concentration

Low solids concentration is defined as one in which particle interaction is not significant and may not change the Newtonian character of the carrying fluid. Conversely, *High solids concentration* may be defined when the aforementioned conditions are not met.

3.4 Definition of *High* and *Low* Flow Velocity

High flow velocity is defined as the velocity range inducing a degree of turbulence sufficient to suspend a coarse particle in the flow. *Low flow velocity* is assumed to be large enough to induce laminar flow of the slurry or to sustain a stable laminar annular layer around a core of solid particles in plug flow (as described in Chapter Five). Figure 3.4 illustrate the combined effect of solids concentration and velocity on the flow regime.

Figure 3.2 Combined effect of particle size and specific gravity on the flow regimes (adapted from Chem. Eng., June, 1971)

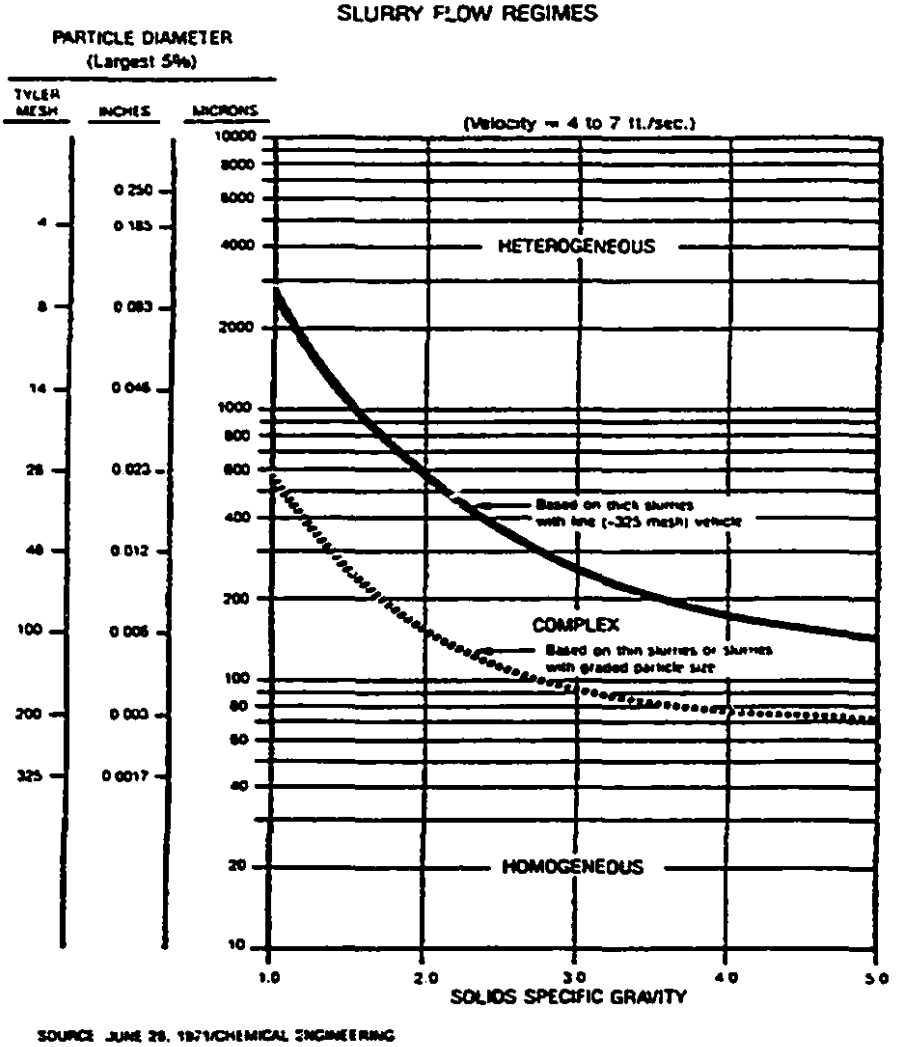

SOURCE: JUNE 28, 1971/CHEMICAL ENGINEERING

Figure 3.3 Combined effect of particle and flow velocity on flow regime (adapted from Raudkivi, 1990)

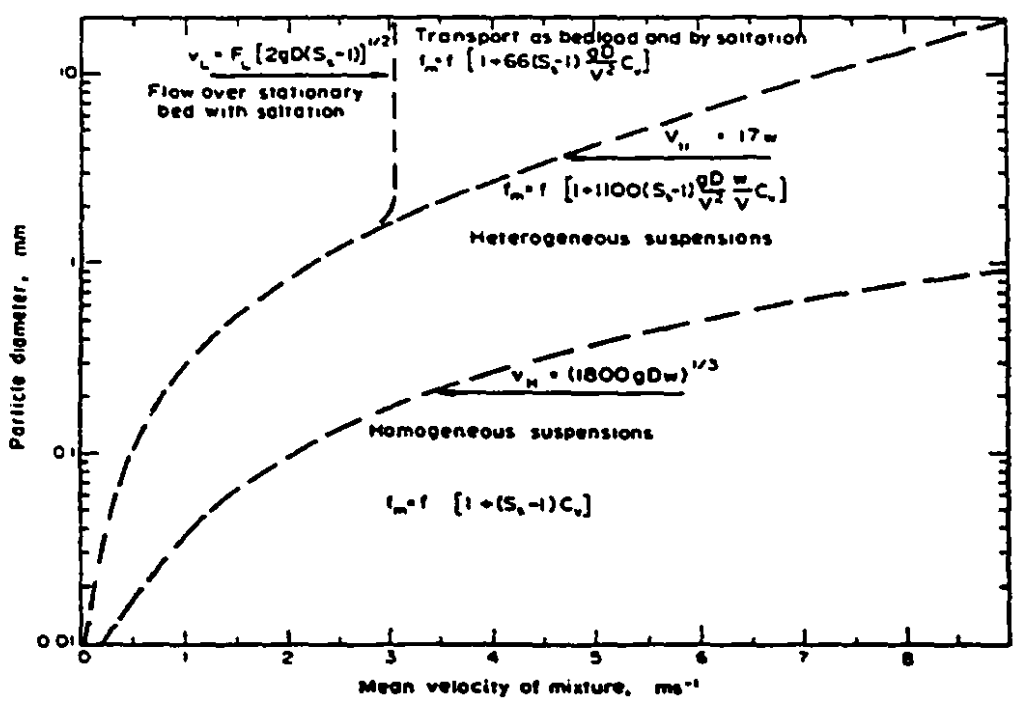

Figure 3.4 Flow regimes as a function of concentration and flow velocity (adapted from Raudkivi, 1990)

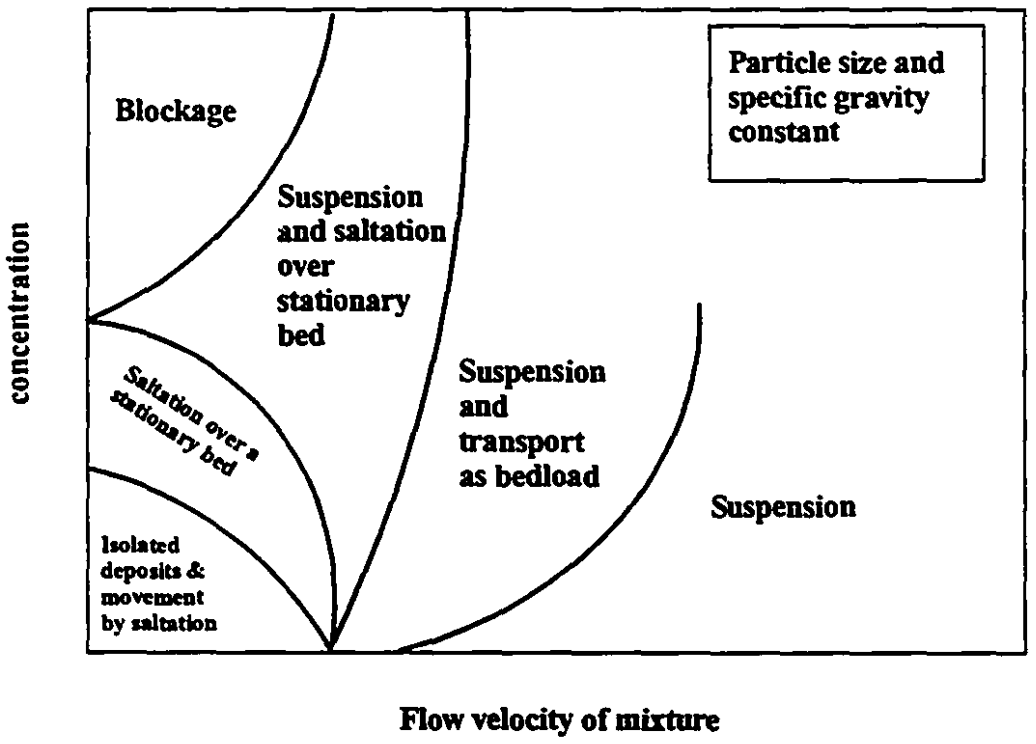

3.5 Case #1: Low flow velocity - Low solids concentration - Coarse particles

This combination would most likely result in a **sliding bed** along the bottom of the pipe or saltation flow condition where particles are alternatively picked up by the liquid and deposited further along the pipe.

Saltation flow is an unsteady flow condition which occurs at lower flow velocity compared to turbulent heterogeneous suspension, and at higher flow velocity compared to sliding bed flow. Zandi and Govatos (1967) proposed a flow regime delineation criterion given by:

$$N_i = \frac{V^2 \sqrt{C_d}}{C\, D\, g\, (S\text{-}1)} < 40 \qquad (3.4)$$

If satisfied, this criterion indicates that the flow regime is either saltation or sliding bed but not heterogeneous. Turian and Yuan (1977) used an empirical method for flow regime delineation, where they curve-fitted 2848 data points belonging to various flow regimes. They defined regime number configurations giving a more systematic way of delineating flow regimes. They also defined the friction factor for slurry (f) and for water (f_w) flowing at the same velocity as given by:

$$f = \frac{-\Delta P\, D}{2\, \rho\, V^2\, L} \qquad (3.5)$$

By curve fitting 1230 data points belonging to saltation regime, they found that :

$$f - f_w = 0.9857\, \zeta_1 \qquad (3.6)$$

where:

$$\zeta_1 = C^{1.018}\, f_w^{1.046}\, C_d^{-0.4213} \left(\frac{V^2}{Dg(S\text{-}1)} \right)^{1.354} \qquad (3.7)$$

Once the slurry friction factor is determined, the pressure loss can be readily obtained. For sliding bed flow, a simple equation was derived by Newitt et al. (1955), which related the flow resistance to the friction between the solid particles and the bottom of the pipe wall. They assumed that the magnitude of the flow resistance is proportional to the coefficient of friction and the apparent weight of solids in unit length of pipes. The pressure loss equation they proposed is given by:

$$\frac{i - i_w}{C\, i_w} = K\,(S - 1)\,\frac{g\,D}{V^2} \qquad (3.8)$$

Where K is an empirical constant proportional to the coefficient of friction. An Upper limit for the incremental head loss in the case of a sliding bed flow may be obtained with K=60.

3.6 Case #2: Low flow velocity - High solids concentration - Coarse particles

This combination would most likely lead to a stationary bed condition which would eventually result in a plugged line. Therefore this situation is to be avoided. Preventive measures to avoid pipe blockage are discussed by Takaoka et al.(1980).

3.7 Case #3: High flow velocity - Low solids concentration - Coarse particles

This situation is common in practice. The flow in this case would most likely be heterogeneous, where solid particles are held in suspensions by turbulent eddies. The best known empirical approach to predicting pressure loss in such condition is that of Durand and Condolios (1952). Their work dealt with the hydraulic transport of sand in water with particles size up to 1 inch in diameter and volumetric concentration up to 22 percent for pipe diameters ranging from 1.5 to 22 inches. Their empirical equation is given by:

$$\phi = K\,(\psi)^{-m} \qquad (3.9)$$

where ϕ, the dimensionless excess headloss function is given by:

$$\phi = \frac{i_m - i_f}{C_v\, i_f} \qquad (3.10)$$

i_m = slurry mixture frictional headloss (meters of fluid per meter of pipe)
i_L = fluid frictional headloss in the same pipe at the same flow velocity

$$\psi = \frac{V^2 \sqrt{C_d}}{g\, D(S\text{-}1)} \qquad (3.11)$$

A value of m = 1.5 was originally used by Durand and Condolios(1952). A value of K=150 has been used to fit a wide range of experimental data (Hanks, 1981). Variations of the Durand equation abound in the literature; which confirms the credibility of the form of the basic original equation without precluding the possibility of some parameter adjustments required to fit particular data.

After analyzing a large number of data, Zandi and Govatos (1967) concluded that the Durand equation would be valid only if the criterion for heterogeneous flow is satisfied, as given by:

$$N_i = \frac{V^2 \sqrt{C_d}}{C\, D\, g\, (S\text{-}1)} > 40 \qquad (3.12)$$

3.8 Case #4: High flow velocity - High solids concentration - Coarse particles

Most empirical equations in connection with coarse-particle hydraulic transport deal with relatively low concentrations. Therefore, extending such equations to cases where concentration is high may lead to unreliable results. Instead, Wilson's model for dense- phase flow (Wilson, 1982) could be used as a method of analysis.

It is expected that with high concentration of coarse particles and high flow velocity; mechanical friction between solid particles and pipe wall will be excessively high, leading to accelerated pipe wear. Dewatering (or desaturation) of the mixture due to the slip of the fluid phase past solid particles may lead to a plugged pipe.Therefore this mode of solid particles transport is not recommended.

3.9 Case # 5: Mixed Flow Systems

Some of the main contributions to the analysis of mixed flow systems may be attributed to two sources. The first source is Wasp et al. (1977), who introduced the concept of two- phase *vehicle*, which was subsequently extended by Hanks (1981) to cover the effect of a non-Newtonian carrier fluid medium. The second source is Wilson (1976) who introduced a mechanistic stratified flow model made up of a sliding bed portion and a suspended portion (described in Chapter Five) . This method was later extended and applied by Lazarus (1989) to include wide particle size distribution systems.

The most noticeable difference between the two approaches is that the Wasp-Hanks method still relies on Durand's empirical equation for the prediction of the pressure loss of the suspended coarse particles. Furthermore, Hanks makes use of rheological techniques to predict the effect of the non-Newtonian behaviour of the carrier fluid on the overall pressure loss; whereas the Wilson-Lazarus approach develops its predictions of the pressure gradient from mechanistic first principles.

Both approaches have their merits and their limitations. The Wasp-Hanks method seems to be suitable for relatively high flow velocity and low solids concentration in the presence of a sufficient amount of fines to act as a vehicle for transporting the coarser particles. Lazarus (1989) concluded, after experimentally evaluating his method, that his correlations predict better at low and intermediate concentration than at high concentration. Wilson's dense-phase approach could be suitable for high concentration, although a systematic evaluation of this method for the case of a wide particle size distribution remains to be done.

3.10 Critical Deposit Velocity

Most suspensions exhibit some degree of settling which depends on the relative density of the suspended solid particles with respect to the carrying fluid as well as on their size and shape. Critical deposit velocity may be defined as the velocity at or below which the solids start to form a sliding bed. This velocity usually falls close to the minimum point in the pressure - velocity curve for single sized particles. For multi-sized particles, this minimum point is much less pronounced.

In practice, this flow regime is usually detected by visual inspection of a transparent section of the pipeline.

Although no single formula claims to predict the critical velocity for all slurries, the equation developed by Durand (1957) is usually used as a first approximation for slurries at low solids concentration. This equation is given by:

$$V_c = F_L \sqrt{2\, g\, D\, (S_s - 1)} \qquad (3.16)$$

Where:
D = pipe diameter
S_s = specific gravity of solids
F_L = coefficient depending on the particle size and volumetric concentration

For uniformly sized particles, the factor F_L may be read from Figure 3.5 for concentration up to 15 per cent. by volume.

Durand's equation has been modified by Wasp et al. (1977) and later by Hanks (1981) to include the effect of relative particle size with respect to pipe diameter. The modified equation, referred to as the Durand-Wasp-Hanks or DWH correlation is given by :

$$V_c = 3.116\, \phi_s^{0.186} \sqrt{2gD(s-1)} \left(\frac{d_p}{D}\right)^{\frac{1}{6}} \qquad (3.17)$$

where particle diameter d_p is usually taken to be d_{85}.

Newitt et al. (1955) proposed a relation which is based on the assumption that Newton's law apply for the calculation of the terminal settling velocity of the particle ; i.e. that C_D=0.44, and is given by:

$$V_c = 19.63 \sqrt{\frac{gD(s-1)}{C_D}} \qquad (3.18)$$

Figure 3.5 FL value vs. particle diameter, for the evaluation of critical transport velocity (adapted from Durand, 1952)

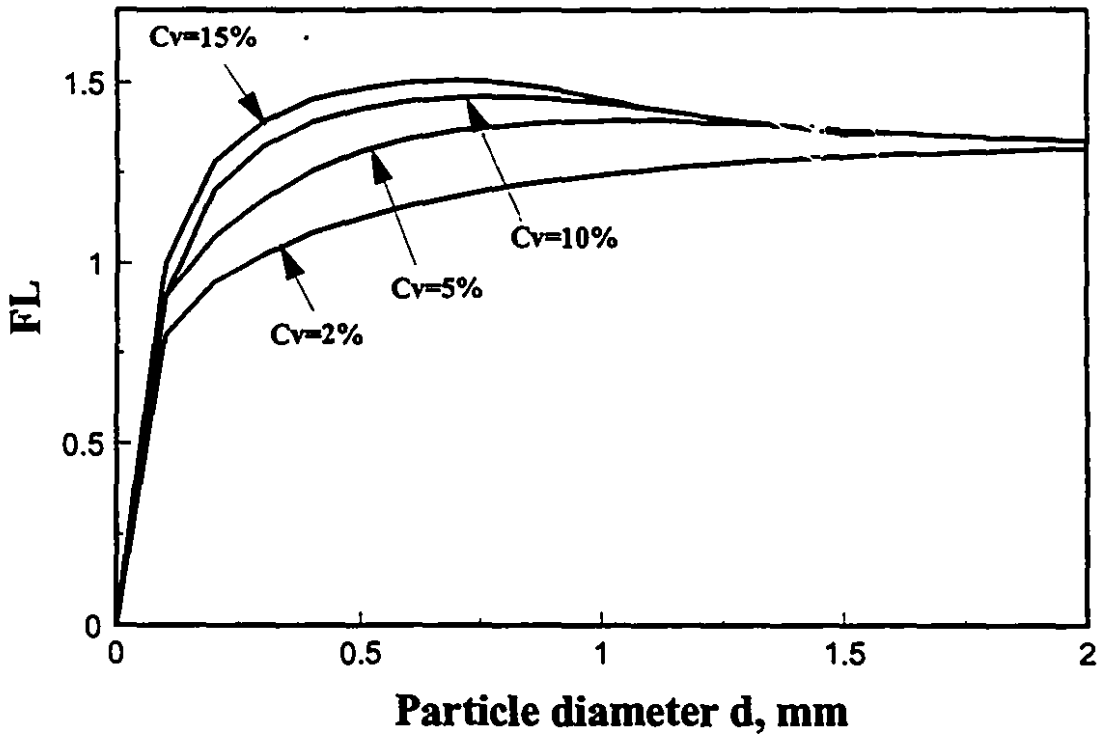

For uniformly sized spherical particles of diameter (d) flowing in smooth pipes, critical velocity is usually assumed to be a function of three dimensionless parameters as given by:

$$V_c = \text{function}\left(\left(\frac{d}{D}\right), \frac{D\rho_o\sqrt{gd(s-1)}}{\mu_o}, C_v\right) \qquad (3.19)$$

Other correlations in graphical form (Wilson, 1979) or in algebraic form with various degrees of complexity have been proposed (Oroskar and Turian (1980), Wani (1986), Turian et al. (1987) , Gillies and Shook (1991), Shah and Lord's (1991), Etc. Some of these are presented below.

3.11 Oroskar and Turian's (1980) correlation

This correlation is best used for particle diameters less than 0.5 mm. It is given by:

$$\frac{V_c}{\sqrt{gd(s-1)}} = 1.85C^{0.1536}(1-C)^{0.3564}\left(\frac{D}{d}\right)^{0.378}Re_p^{0.09}X^{0.30} \qquad (3.20)$$

where:

$$Re_p = \frac{D\rho_f\sqrt{gd(s-1)}}{\mu_L}$$

$$X = \frac{2}{\sqrt{\pi}}\left(\frac{2}{\sqrt{\pi}}\gamma\exp\left(-\frac{4\gamma^2}{\pi}\right) + \int_{\gamma}^{\infty}\exp\left(-\frac{4\gamma^2}{\pi}\right)d\gamma\right), \; s = \frac{\rho_s}{\rho_f}, \text{ and } \gamma = \frac{V_s}{V_c}$$

Vs is the hindered settling velocity of the particles as given by the expression:

$$V_s = V_\infty (1 - C)^2 \qquad (3.21)$$

Iterations are required to determine V_c. For the case where $\gamma = \frac{V_s}{V_c} < 0.5$, X is between 0.9 and 1.0. Thus the factor $X^{0.3}$ approaches unity, and may be neglected, hence giving an explicit formula for the critical deposit velocity V_c. According to Shook and Roco (1980), this correlation is less reliable for large particles in large pipes for which Gillies's (1991) correlation is more suitable.

3.12 Gillies and Shook's (1991) correlation

The critical deposit velocity is given by:

$$V_c = F \sqrt{gD \frac{\rho_s - \rho_f}{\rho_f}} \qquad (3.22)$$

which is similar in form to Durand's equation except that the equivalent fluid density ρ_f and a factor F are computed by:

$$\rho_f = \frac{\rho_s C_f + \rho_L (1 - C_T)}{1 - C_T + C_f} \qquad (3.23)$$

where C_f is the concentration of the -74μm fraction of solid particles, and C_T is the mean in-situ total solids concentration ($C_f = C_T \frac{\text{volume of -74μm solids}}{\text{Total volume of solids}}$), and

$$F = \exp(0.51 - 0.0073 C_D - 12.5 K_2) \qquad (3.24)$$

where:

$$K_2 = \left(\left(\frac{\mu_L^2}{g \rho_L d_{50}^3} \right)^{1/3} - 0.14 \right)^2$$

d_{50} is the median diameter of the +74μm fraction, settling in a fluid of density ρ_f and viscosity μ_f made up of the -74μm fraction of solid particles at concentration C_f. This correlation is derived from data obtained with pipes up to 0.5 m in diameter and slurries with viscosities between 0.5 and 5 centipoise. It covers coarser particles and larger pipe diameters than that of Oroskar and Turian (1980). It is not applicable, however, to slurries with high viscosities, a case which may be better handled by the Shah and Lord's (1991) method.

3.13 Shah and Lord's (1991) Correlation

Most of the methods outlined above assume the carrier fluid to be Newtonian. For mixtures with a particle size distribution containing a large fines fraction capable of forming a new suspending non-Newtonian medium, no information was available for estimating the critical deposit velocity before the work of Shah and Lord (1991). In their laboratory investigation, they attempted to quantify the solids transport capabilities of various non-Newtonian fluids by estimating the critical deposition (V_c) or resuspension (V_s) velocities in horizontal pipes. In their analysis, they modified the equation of Oroskar and Turian (1980), and generalized it to the case of non-Newtonian fluids as given by:

$$\frac{[V_c] \text{ or } [V_s]}{\sqrt{gd(s-1)}} = Y\, C^{0.1536}\,(1-C)^{0.3564}\left(\frac{d}{D}\right)^{-w}\left(\frac{D\rho_f\sqrt{gd(s-1)}}{\mu_a}\right)^{z} \qquad (3.25)$$

Where coefficient Y, and exponents w and z are adjustable constants that can be evaluated by regression analysis for particular critical velocity data sets.The non-Newtonian character of the fluid is taken into account by the inclusion of apparent viscosity (μ_a) in the equation above.

Predictions from these correlations often do not agree with each other. According to Hanks (1981), this is expected, as most of these correlations are developed for a particular set of experimental data, and are based primarily on dimensional arguments or on overall macroscopic pressure loss flow rate data. The fundamental problem is that none of these methods considers in their analysis the dynamic behaviour of a particle suspended in a turbulent shear field.This dynamic behaviour was analyzed by Hanks and Sloan (1981) who proposed a rheology-

based model for critical deposition velocities. It is claimed that their method was successful in correlating all types of critical velocity data where other correlations disagree. However, this model uses four adjustable empirical parameters obtained from two sets of sand data for its predictions of other solid-liquid mixtures.

3.14 Computer Program For Comparing Various Methods of Predicting Pressure Loss and Critical Flow Velocity in Horizontal Flow of Slurries in Pipelines.

The equations and correlations used in this program are listed below. Comparison of pressure drop predictions from Turian & Yuan , Durand, Zandi, Worster, and Newitt are given in Figure 3.6, which shows that most of these correlations tend to give fairly close results in the pseudo-homogeneous and heterogeneous flow regimes, but as flow velocity decreases, some discrepancies become apparent.

3.14.1 Pressure Loss Correlations

- **Durand and Condolios (1957)**

$$\frac{J - J_w}{C\, J_w} = K\left(\frac{V^2\, C_d^{0.5}}{g\, D\, (S_s-1)}\right)^n \qquad (3.26)$$

with K=150, and n=-1.5

For coarse particles (greater than 1mm) , the drag coefficient may be ignored, and the Durand and Condolios correlation may be expressed by:

$$\frac{J - J_w}{C\, J_w} = 135\left(\frac{V^2}{gD(s-1)}\right)^{-1.35} \qquad (3.27)$$

- **Zandi and Govatos (1967)**

Heterogeneous flow if :

$$\Psi = \frac{V^2\sqrt{C_D}}{gD(s-1)} > 10$$

$$\frac{J - J_w}{C\,Jw} = 6.3\ \Psi^{-0.354} \qquad (3.28)$$

Saltation flow if :

$\Psi < 10$

$$\frac{J - J_w}{C\,Jw} = 6.3\ \Psi^{-0.354} \qquad (3.29)$$

- **Worster and Denny (1955)**

Correlation derived from experimental data of large coal particles in water:

$$\frac{J - J_w}{C\,Jw} = 120\left(\frac{V^2}{gD(s-1)}\right)^{-1.5} \qquad (3.30)$$

- **Newitt et al. (1953)**

For coarse particles in heterogeneous flow:

$$\frac{J - J_w}{C\,Jw} = \frac{1100(s-1)gdV_s}{V^3} \qquad (3.31)$$

For coarse particles in sliding bed or saltation flow:

$$\frac{J - J_w}{C\,Jw} = \frac{66(s-1)gd}{V^2} \qquad (3.32)$$

Figure 3.6 Pressure gradient vs flow velocity --Empirical correlations

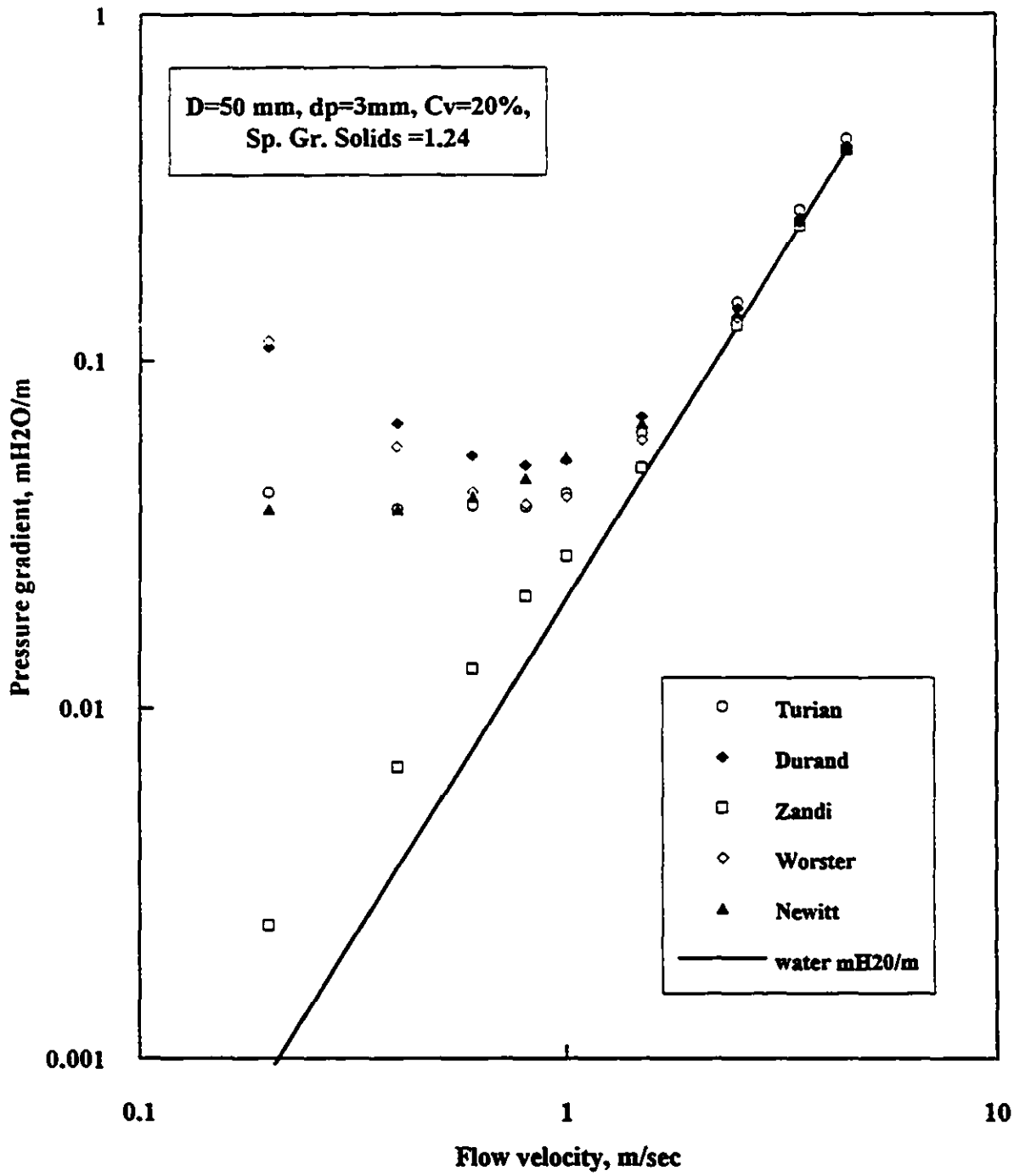

3.14.2 Critical Velocity Correlations

- **Bain and Bonnington (1970)**

$$V_c=3.43\ C^{0.33}\left(gD(s-1)/C_D^{0.5}\right)^{0.5} \qquad (3.33)$$

This equation was derived for a pipeline operating at constant concentration of solids by differentiating Durand's equation (with K=85) relating velocity and pressure drop and equating it to zero. This approach assumes the critical velocity to be the minimum in the pressure drop-velocity curve. It is considered conservative as its predictions exceed in some cases the observed critical deposit velocity.

- **Durand and Condolios (1952) for Coarse Particles**

For coarse particles exceeding 1mm in diameter, the parameter F_L in Durand's correlation described above for predicting critical velocity is no longer dependent on solids concentration and may be assigned the approximate value of 1.34, thus this correlation may be condensed to the following equation:

$$V_L = 5.935\sqrt{D(s-1)} \qquad (3.34)$$

- **Newitt et al. (1953)**

$$V_c = 17\ V_s = 19.63\sqrt{\frac{gD(s-1)}{C_D}} \qquad (3.35)$$

- **Zandi and Govatos (1967)**

$$V_c = \sqrt{\frac{40\ C\ D\ g\ (s-1)}{\sqrt{C_D}}} \qquad (3.36)$$

- **Scale-up for Critical Velocity**

If data for critical velocity V_{exp} is available for a given pipe diameter D_{exp}, and provided slurry properties (concentration, solids density, particle size) remain constant, it is possible to estimate the critical velocity for another pipe of diameter D, as given by:

$$V_c = V_{exp}\sqrt{\frac{D}{D_{exp}}} \qquad (3.37)$$

3.14.3 Turian and Yuan's Method (1977) for Estimating the Pressure Gradients and Type of Flow Regimes

Turian and Yuan (1977) used correlations based on curve-fitting 2848 data points belonging to various flow regimes for a range of pipe diameters up to D=0.160m. They defined regime number configurations which enables flow regime delineation. They expressed pressure drop in terms of the carrier liquid density ρ_L and a friction factor f as given by:

$$i\,\rho_L\,g = \frac{2f\,V^2\rho_L}{D} \qquad (3.38)$$

Flow regimes were coded as shown in Table 3.1

Table 3.1
Flow regimes and their codes

Regime	Stationary bed	Saltation	Heterogeneous	Homogeneous
Code	0	1	2	3

The friction factor f is related to the carrier fluid friction factor for the same pipe diameter and at the same velocity by the correlation:

$$f - f_L = K\,C_v^{\alpha}\,f_L^{\beta}\,C_D^{\gamma}\left(\frac{V^2}{gD(S_s-1)}\right)^{\delta} \qquad (3.39)$$

Where the coefficients are given in Table 3.2

Table 3.2
Coefficients for computing Turian and Yuan's correlation

Code	K	α	β	γ	δ
0	0.4036	0.7389	0.7717	-0.4054	-1.096
1	0.9857	1.018	1.046	-0.4213	-1.354
2	0.5513	0.8687	1.200	-0.1677	-0.6938
3	0.8444	0.5024	1.428	-0.1516	-0.3531

Flow regime selection starts by computing a set of regime numbers defined by:

$$R_{ij} = \frac{V^2}{K1\, C_v^{\alpha 1}\, f_L^{\beta 1}\, C_D^{\gamma 1}\, g\, D\, (S_s - 1)} \qquad (3.40)$$

where regime number coefficients are given in Table 3.3. The drag coefficients are computed from correlations given in terms $C_D^{0.5}$Re, but if available, measured ones are preferred.

Table 3.3
Coefficient for computing Regime Numbers

Regime Number	K1	α1	β1	γ1
R01	31.93	1.083	1.064	-0.0616
R12	2.411	0.2263	-0.2334	-0.3840
R23	0.2859	1.075	-0.67	-0.9375
R13	1.167	0.5153	-0.382	-0.5724
R02	0.4608	-0.3225	-1.065	-0.5906
R03	0.3703	0.3183	-0.8837	-0.7496

The flow regime is then determined by computing (R_{01}-1), (R_{12}-1), (R_{23}-1), and inspecting Table 3.4. Uncertainty is removed by computing (R_{13}-1), (R_{02}-1), (R_{03}-1).

Table 3.4
Criteria for flow regime selection

R01 - 1	R12 - 1	R23 - 1	R02 - 1	R03 - 1	R13 - 1	Regime Code
neg	neg	neg				0
pos	neg	neg				1
pos	pos	neg				2
pos	pos	pos				3
neg	neg	pos		neg		0
neg	neg	pos		pos		3
neg	pos	pos		neg		0
neg	pos	pos		pos		3
neg	pos	neg	neg			0
neg	pos	neg	pos			2
pos	neg	pos			neg	1
pos	neg	pos			pos	3

Uncertainty in the results of Turian and Yuan's correlation increases for flow in larger pipes (D> 0.160m) and for mixtures with a significant fines fraction (Shook, 1991).

3.14.4 The Method of Wasp et al. (1977) –The Two-Phase *Vehicle* Concept

This method applies to compound flow systems where the slurry is made up of a wide size distribution of solid particles in a liquid. The coarse fraction of this distribution, is assumed to be suspended in a homogeneous medium called the *vehicle* made up of the fine fraction of the distribution, and assumed to be Newtonian . The total friction loss is considered to be the sum of that due to the homogeneous *vehicle* alone, plus that of the heterogeneous fraction.

To determine this homogeneous fraction, Wasp et al. (1977) used the concentration distribution equation of Ismail (1952) to identify the fraction of solids which were symmetrically distributed. This equation was derived from the equation of continuity for the solids in slurry form. It gives the relative local fraction of solids $\frac{\phi}{\phi_r}$ as a function of $\zeta = \frac{y}{y_m}$, with y being a radial distance and y_m the location of maximum fluid velocity in the channel:

$$\frac{\phi}{\phi_r} = \left(\frac{\zeta_r(1-\zeta)}{\zeta(1-\zeta_r)}\right)^Z, \qquad (3.41)$$

with $\phi = \phi_r$ for $\zeta = \zeta_r$

and, $Z = \frac{V_t}{\kappa \beta V^*}$, where:

V_t = terminal settling velocity

$V^* = V\sqrt{\frac{f}{2}}$

β = constant of proportionality (=1 for a conservative estimate)

κ = Von Karman constant (= 0.4)

Equation (3.41) gives only the relative value of ϕ with respect to ϕ_r; the latter must be known from another source. It also predicts a value of ϕ=0 for ζ=1, a value which is not correct. Thus Ismail (1952) observed that in the vicinity of ζ=1, one should assume the mass transfer coefficient E_S equal to some constant E_S^*, for which case the continuity equation may be directly integrated to give the concentration distribution equation:

$$\ln\left(\frac{\phi}{\phi_r}\right) = -\frac{\beta'}{\alpha'} Z (\zeta - \zeta_r) \qquad (3.42)$$

with $\alpha' = \zeta_S^*(1-\zeta_S^*)$; ζ_S^* is the location at which $E_S = E_S^*$

Thus if it is assumed that Equation (3.41) and Equation (3.42) give the same value for ϕ at point ζ_s^*, then, $\zeta_s^* = \zeta_r$. Equation (3.42) was used by Wasp to describe the concentration distribution in the vertical plane of the pipe with $y_m = \frac{D}{2}$. Using the concentration profile data of Ismail (1952), Wasp determined that at the location ζ=0.08, Equation (3.42) could be reduced to the empirical concentration distribution equation :

$$\log_{10}\left(\frac{\phi_{0.08}}{\phi_r}\right) = -1.8\,Z \qquad (3.43)$$

The choice of the value ζ=0.08, was dictated by equipment considerations in the experimental work of Wasp. According to Hanks (1981), in the light of the new research findings, the simple equation of Ismail (1952) on which Wasp's method is based may not be fully correct, however it is a reasonable approximation and works well in Wasp's method for computing the pressure loss. Wasp's method has a two-part procedure:

1) The vehicle and its properties must be determined by a trial and error method.
2) Durand's equation is applied to each asymmetrically suspended segment of the particle size distribution independently and the result is added up to obtain an integrated average of the entire mixture.

3.14.4.1 Vehicle Determination

The particle size distribution is divided into size fractions as determined for example by sieve analysis. All particles on an individual screen are assumed to have a uniform diameter equal to the geometric mean of the screen and the next larger screen size. The mean diameter of the jth cut of the particle size distribution is given by:

$$\bar{d}_{pj} = \sqrt{d_{pj}\, d_{pj-1}} \qquad (3.44)$$

For each fraction of the particle size distribution, the corresponding input volume fraction ϕ_{sj} is determined from:

$$\phi_{sj} = \frac{w_j w_m \rho_m}{\rho_s} \qquad (3.45)$$

where:

w_j = the weight fraction of the jth cut in the particle size distribution
w_m = the weight fraction of solids in the total mixture
ρ_m = the density of the total mixture
ρ_s = the density of solids

Calculation is started by assuming an initial value for $\phi_{0.08}$, for example all material with $d_d < 0.074$ microns (200 mesh), and then computing the density and the viscosity of the vehicle as given by:

$$\rho_v = \phi_{0.08}\rho_s - (1 - \phi_{0.08})\rho_L \qquad (3.46)$$

and

$$\mu_v = \mu_L\left(1 + 2.5\phi_{0.08} + 10.05\phi_{0.08}^2 + 0.00273\exp(16.6\phi_{0.08})\right) \qquad (3.47)$$

The Reynolds number is then computed:

$$R_e = \frac{DV\rho_v}{\mu_v}$$

and the fanning fraction factor f_v is determined from standard Newtonian fraction factor correlation such as Churchill's equation (Churchill, 1977) :

$$f = 2\left(\left(\frac{8}{Re}\right)^{12} + \left(\frac{1}{A+B}\right)^{1.5}\right)^{0.0833} \qquad (3.48)$$

where:

$$A = \left(2.457 \ln \left(\frac{1}{\left(\frac{7}{Re}\right)^{0.9} + 0.27\frac{k}{D}} \right) \right)^{16}$$

$$B = \left(\frac{37530}{Re} \right)^{16}$$

This value is then used in Equation (3.43) :

$$\log_{10}\left(\frac{\phi_{0.08,j}}{\phi_{sj}}\right) = -5.143\frac{V_{tj}}{V_m\sqrt{\frac{f_v}{2}}} \qquad (3.49)$$

The terminal settling velocity of the particles of size d_{pj} is expressed in terms of the drag coefficient C_{Dj} by :

$$V_{tj} = \sqrt{\frac{4g(\rho_s - \rho_v)\, d_{pj}}{3\rho_v C_{Dj}}} \qquad (3.50)$$

Drag coefficients can be computed from the following set of empirical curve-fit equations (Hanks, 1981). By rearranging Equation (3.50), and defining $Y_j = C_{Dj}R_{pj}^2$, one obtains:

$$Y_j = \frac{4g(\rho_s - \rho_v)\,\rho_v d_{pj}^3}{3\mu_v^2} \qquad (3.51)$$

C_{Dj} is then computed from one of the following equations:

a) if $0 < Y_j \leq 2.4$,

$$C_{Dj} = \frac{576}{Y_j} \tag{3.52}$$

b) if $2.4 < Y_j \leq 5(10)^5$) Re_{pj}

$$C_{Dj} = \frac{Y_j}{Re_{pj}^2} \tag{3.53}$$

where:

$$Re_{pj} = 0.139 Y_j \left(1+\sqrt{1+0.06111 Y_j^{0.575}}\right)^{-1.739}$$

c) if $5(10)^5 < Y_j \leq 5(10)^7$

$$C_{Dj} = 0.40 \tag{3.54}$$

d) if $Y_j > 5(10)^5$

$$C_{Dj} = 0.44 \tag{3.55}$$

Once C_{Dj} is known, V_{tj} is computed and used in Equation(3.49) to compute $\phi_{0.08,j}$. This calculation is repeated for each size fraction in the particle size distribution. From these results, one then computes:

$$\phi_{0.08} = \Sigma_j \phi_{0.08,j} \tag{3.56}$$

This value is compared with the value initially assumed. If there is agreement to four significant figures, the homogeneous vehicle volumetric concentration is determined, along with the corresponding density, viscosity, and the individual size fractions in the particle size distribution which are symmetrically suspended. If not, then the new value of $\phi_{0.08}$ is used to start computation for another iteration. This iterative procedure is repeated until the four significant-figure convergence criterion is met.

• **Alternative direct method of computing settling velocity and drag coefficient**

For each size fraction of average diameter d_{pj}, the unhindered free terminal settling velocity in the vehicle can be calculated directly from (Darby, 1986):

$$V_{tj} = \frac{\mu_v N_{Rej}}{d_j \rho_v} \qquad (3.57)$$

where:

$$N_{Rej} = \left(\sqrt{14.42 + 1.827\, N_{Arj}^{0.5}} - 3.798 \right)^2$$

and

$$N_{Arj} = \frac{d_i^3 \rho_v^2 (s-1)}{\mu_v^2}$$

The drag coefficient required by Durand's equation for computing the excess pressure loss of each heterogeneously suspended coarse fraction is obtained from the terminal settling velocity as given by:

$$C_{Dj} = \frac{4(s-1)g d_j}{3V_{tj}^2} \qquad (3.58)$$

3.14.4.2 Total Pressure Loss Calculation

Having determined the properties of the vehicle, the next step is to calculate the excess pressure loss due to the asymmetrically suspended fraction of the particle size distribution. The portion of the jth cut of the particle size distribution which is asymmetrically suspended is given by:

$$\phi_{a,j} = \phi_{sj} - \phi_{0.08,j} \qquad (3.59)$$

These values are computed for each cut. The Durand's equation in the form:

$$\Phi_{Hj} = 150\ \phi_{a,j} \left(\frac{gD(s-1)}{V_m^2 \sqrt{C_{dj}}} \right)^{\frac{3}{2}} \qquad (3.60)$$

is used to compute the excess pressure loss function for each size cut. These are then summed up to obtain the total excess pressure loss for the mixture, i.e.:

$$\Phi_{Hm} = \Sigma_j \Phi_{Hj} \qquad (3.61)$$

The overall pressure loss is calculated from:

$$J_T = J_V\ (1+\Phi_{Hm}) \qquad (3.62)$$

where J_V is calculated from the vehicle friction factor determined in the first part of the calculation.

Hanks (1981) points out that Wasp (1977) used Durand's equation with the erroneous K=82 coefficient rather than the correct one K=150. However, Wasp also adjusted the constant in Ismail's concentration profile equation to 1.8 in order to make the combined effect produce accurate values for J_T when comparing his predictions with experimental results for coal slurry data. The above system of equations with a value of 1.8 in Ismail's equation and K=150 in Durand's correlation will result in a conservatively high estimate of J_T.

Results From Program Wasp.m

The flow chart of Wasp's method is shown in Figure 3.7 .

- **Input Parameters**

Pipe diameter, D = 0.2 m
Mean flow velocity, V = 1.5 m/sec
Solids volumetric concentration, Cv = 0.50

Specific gravity of solids, S = 1.4
Relative pipe roughness, k/D = 0.00022
Liquid (water) viscosity = 100.2 x 10 ^(-5) Pa.sec at 20 C
Liquid (water) density = 1000 kg/m^3
Particle size distribution (see Table 3.5)

Figure 3.7 Flowchart of Wasp's method

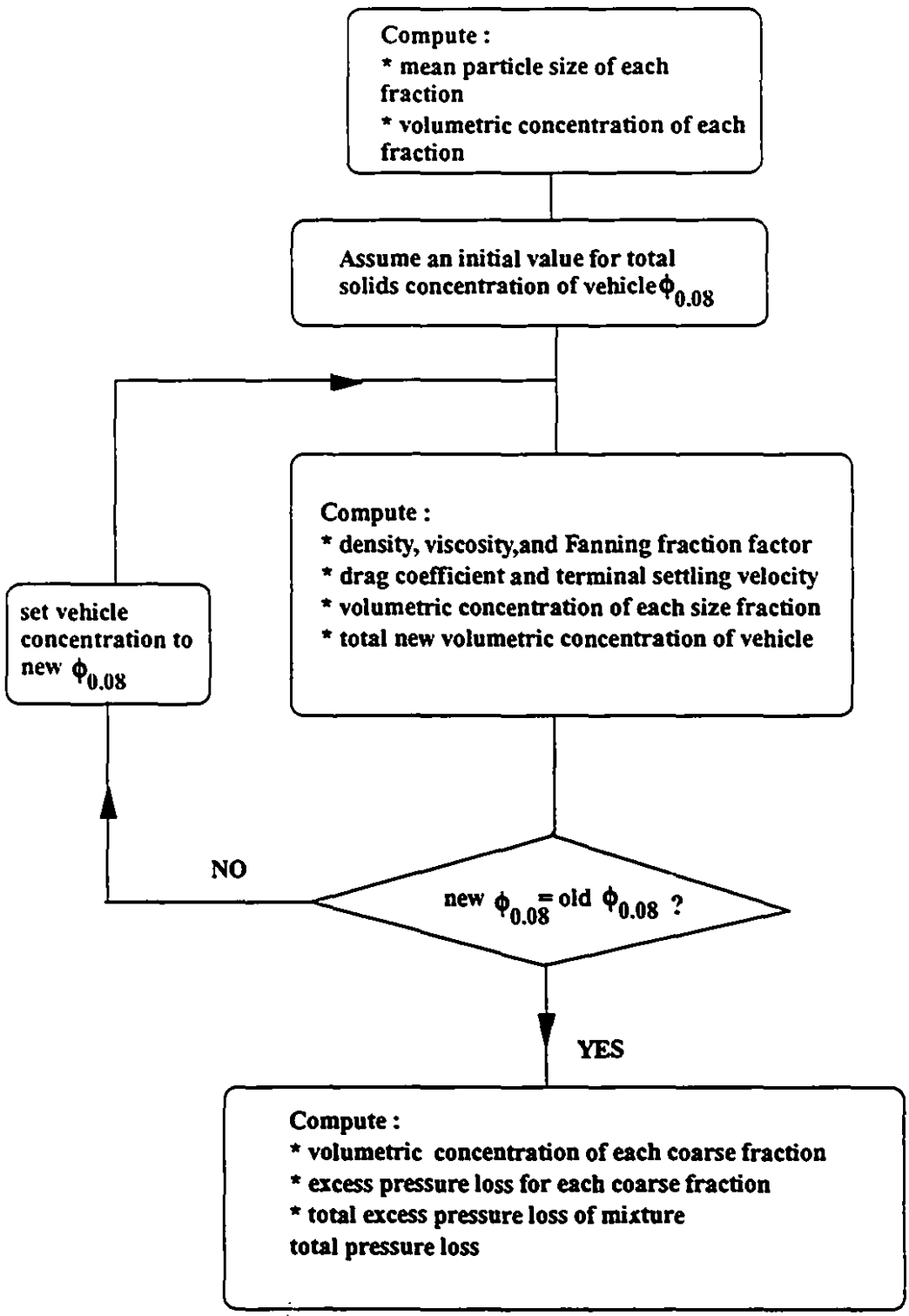

• **Results After Convergence in 7 Iterations:**

Table 3.5
Sample Results from Program Wasp.m

Size fraction	dm, microns	Cw	$\phi_{s,j}$	$\phi_{0.08,j}$	C_{Dj}	$\phi_{a,j}$	$\phi_{H,j}$
1	841	0.074	0.0317	0.0023	6	0.0295	0.0989
2	594	0.183	0.0784	0.0169	13	0.0615	0.1186
3	297	0.212	0.0909	0.0578	73	0.0331	0.0172
4	148.5	0.160	0.0686	0.0606	490	0.008	0.001
5	68	0.144	0.0489	0.0476	5107	0.0013	0
6	35	0.257	0.1101	0.1094	37454	0.0008	0

Carrier suspension (vehicle) properties:

Density, ρ_v = 1117.8 kg/m^3

Viscosity, μ_v = 0.0034 Pa.sec

Reynolds Number, Rev = 1.32x10^(5)

$\phi_{0.08} = \Sigma_j \phi_{0.08,j} = 0.2945$

Pressure gradient results

Pressure drop contribution of vehicle, Jv = 0.0187 m water/m

Pressure drop contribution of coarse fraction, Jv Φ_{Hm} = Jv $\Sigma_j \Phi_{Hj}$ = .0044 m water/m

Total pressure drop, $J_T = J_{v(}\ 1+\Phi_{Hm)}$ = 0.0231 m water/m

Critical deposit velocity

Vcd =1.25 m/sec, with d85=470.6 microns (Equation 3.17)

CHAPTER FOUR

TRANSPORT OF HOMOGENEOUS NON-SETTLING SLURRIES: RHEOLOGICAL APPROACH

4.1 Introduction

The main characteristic of homogeneous non-settling slurries is that the mixture of finely divided solid particles and carrying fluid forms a viscous colloidal medium with new physical properties different from the original fluid phase in the mixture.

The purpose of rheological studies is to determine, from small samples, representative flow properties of slurries and to extrapolate these properties to larger pipe diameters. Rotary and capillary viscometers are the instruments used for such studies . Their convenience, however carries with it design and operating limitations, such as end effects and/or slip , which require that the data obtained be corrected before any subsequent analysis.

In the following, basic theory underlying the behavior of Newtonian and non-Newtonian fluids in fully developed flow will be presented. A survey of rheological models will be presented with emphasis on the merits and limitations of each model.

4.2 The Shear Stress-Shear Rate Relationship in Pipe Flow:

Figure 4.1 shows the parameters used in analyzing flow in a pipe. The rheology of most slurries is time-independent and may be expressed by the functional relationship:

$$-\frac{dV}{dr} = f(\tau) \qquad (4.1)$$

where $-\frac{dV}{dr}$ is the shear rate and τ is the shear stress in the pipe.

Figure 4.1 Definition of flow parameters in a circular pipe

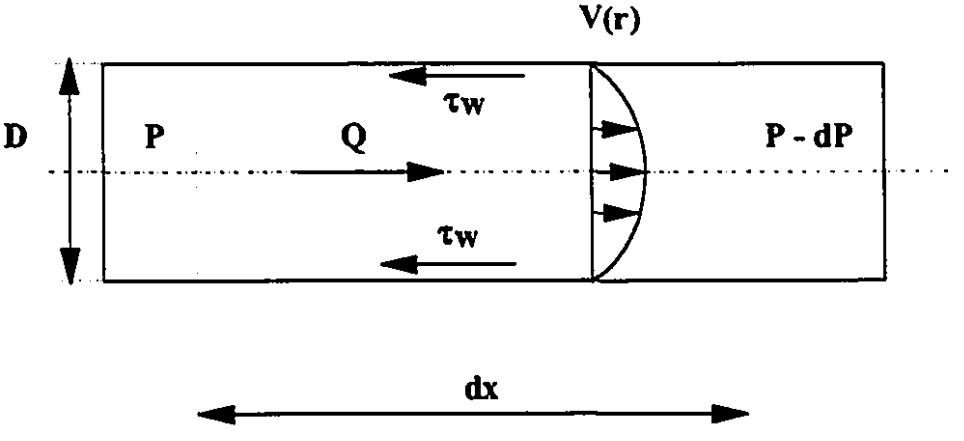

4.2.1 Wall Shear Stress

An expression for the shear stress in pipe flow may be found from a balance of forces on a cylindrical element as expressed by:

$$- \pi r^2 \Delta P = 2\pi r \Delta x \, \tau \qquad (4.2)$$

which is equivalent to:

$$\tau = - \frac{r}{2} \frac{\Delta P}{\Delta x} \qquad (4.3)$$

where ΔP is the static pressure difference between x and $x+\Delta x$. At the pipe wall, $r = \frac{D}{2}$ and $\tau = \tau_w$, and the above equation becomes:

$$\tau_w = - \frac{D}{4} \frac{\Delta P}{\Delta x} \qquad (4.4)$$

4.2.2 Wall Shear Rate

Shear rate is the gradient of the velocity profile. It is identical to the nominal shear rate 8V/D only in the case of a Newtonian fluid. Thus 8V/D is also referred to as the Newtonian wall shear rate.

Assuming non-slip condition at the wall, the relation between the true shear rate and the nominal one is estimated from the equation (Skelland, 1967):

$$\frac{8V}{D} = \frac{4}{\tau_w^3} \int_0^{\tau_w} \tau^2 f(\tau) d\tau \qquad (4.5)$$

which shows that the wall shear stress is a unique function of the nominal shear rate, hence of the true shear rate.

4.3 Newtonian Flow

For flow in a pipe, a fluid is said to be Newtonian when the shear stress is directly proportional to the rate of shear as expressed by:

$$\tau = \mu\left(-\frac{dV}{dr}\right) \qquad (4.6)$$

where:

τ	=	shear stress
μ	=	dynamic viscosity
r	=	radial distance from the center of the pipe
V	=	velocity perpendicular to r

For Newtonian flow, the Reynolds number is defined as:

$$Re = \frac{VD\rho m}{\mu} \qquad (4.7)$$

The laminar flow regime is delineated by the critical Reynolds number for the transition to turbulent flow as given by: $Re < 2300$. In this case the friction factor is given by:

$$f = \frac{16}{Re} \qquad (4.8)$$

Figure 4.2 shows the friction factor design chart for Newtonian fluids (Moody diagram). Any other shear stress-shear rate relationship indicates that the fluid is non-Newtonian. This deviation from the Newtonian behaviour may be attributed to one or more of the following factors: particle size and shape, flexibility and tendency to flocculate or disperse in the carrying fluid, surface-chemical characteristics, concentration, and temperature.

Figure 4.2 Moody diagram (adapted from Govier and Aziz, 1987)

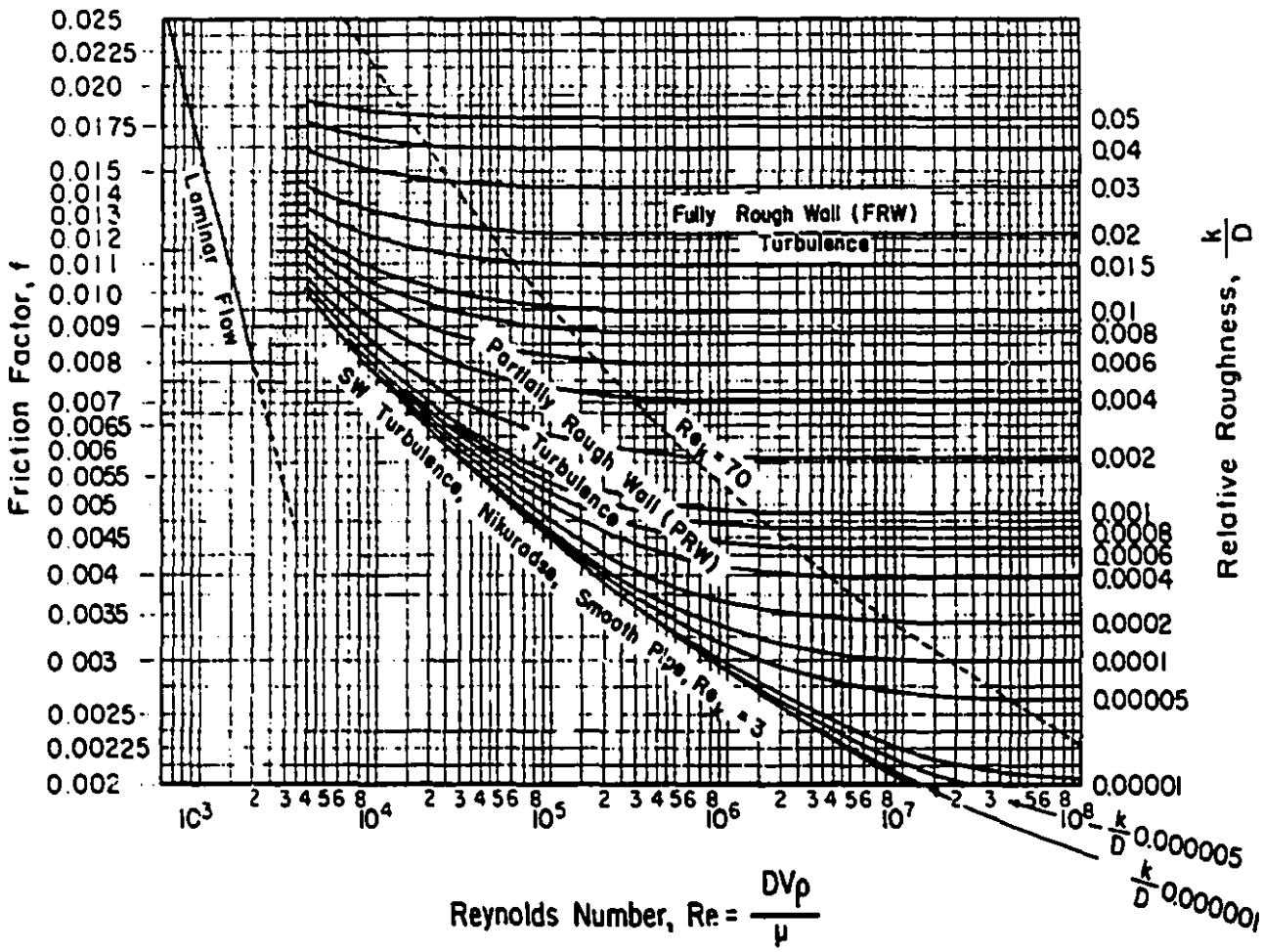

4.4 Non-Newtonian Flow

For non-Newtonian fluids, viscosity is shear rate dependent. This is true whether viscosity at a particular shear rate is defined as the tangent to the curve at that point or as the apparent viscosity which would apply if the material were regarded as Newtonian.

Interpretation of the average measurements of flow properties require rheological models capable of predicting the flow behaviour outside the conditions used for their initial development such as pipe diameter, flow velocity, and density and concentration of the suspension under investigation.

Non-Newtonian fluids are identified by their non-linear shear stress-shear rate relationship. The nature of this non-linearity may include some time-dependent or visco-elastic properties. However, such properties are negligible in the context of pipe flow as the fluid is assumed to be under constant shear rate throughout the pipeline. It is important, however, to guard against errors arising from such phenomena in laboratory viscometer or small scale loop tests.

The most common rheological models encountered in the literature are shown in Figure 4.3 and can be described by the generalized yield power law (Slatter and Lazarus, 1988):

$$\tau = \tau_y + K\left(-\frac{dV}{dr}\right)^n \qquad (4.9)$$

Depending on the value of (τ_y) and (n) the following rheological models are obtained:

a) Yield-pseudo-plastic ($n<1$, $\tau_y>0$)
b) Bingham plastic ($n=1$, $\tau_y>0$)
c) Yield dilatant ($n>1$, $\tau_y>0$)
d) Pseudo-plastic ($n<1$, $\tau_y=0$)
e) Dilatant ($n>1$, $\tau_y=0$)
f) Newtonian ($n=1$, $\tau_y=0$)

Figure 4.3 Rheological models of time-independent fluids

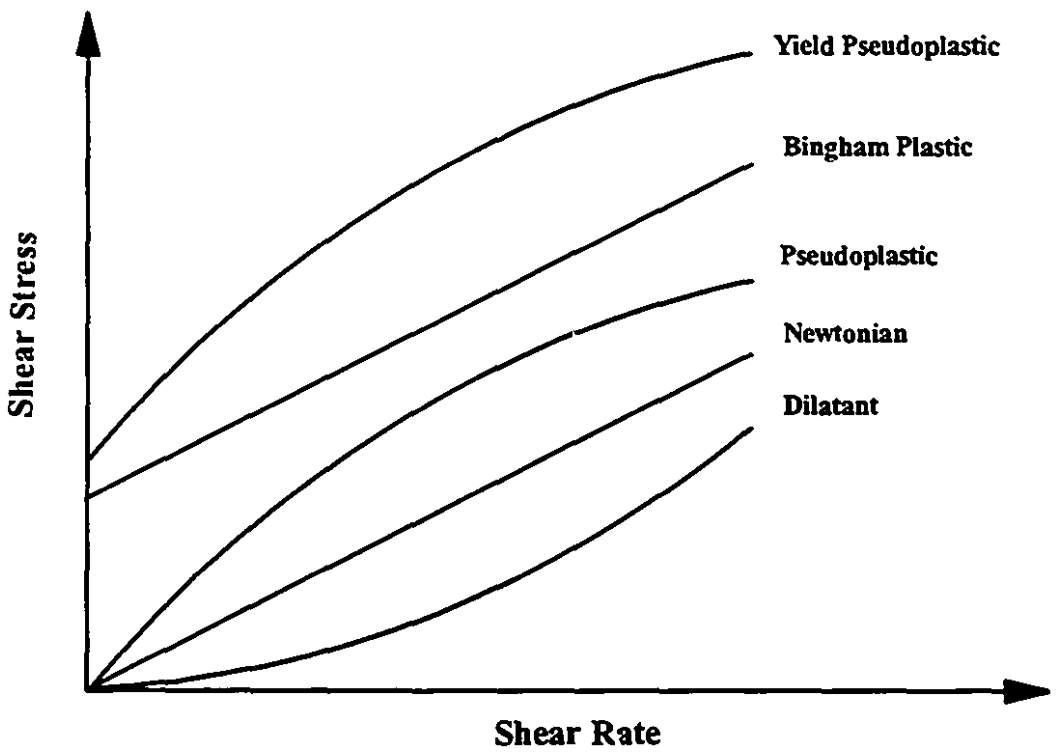

The Bingham plastic and the power law (or pseudo-plastic) models are of particular interest because of their simplicity and the wide range of fluids they can describe.The power law model may be simpler to use in the laminar flow regime, since it gives a single correlation when the generalized method of Dodge and Metzner (1959) is used as will be shown in the following sections.

Conversely, the Bingham plastic model may have an advantage in the turbulent flow regime since a single correlation is used in connection with the Hedstrom method. Furthermore, the Bingham plastic model makes use of physically meaningful parameters such as the yield stress (τ_y) and the coefficient of rigidity (η), compared to the somewhat ambiguous fluid consistency index (n) and the flow behaviour index (K) of the power law model. The Yield pseudo-plastic model is less used because it requires the determination of three empirical parameters compared to just two for the previous models.

4. 5 True Shear Rate: The Rabinowitsch-Mooney Relation

The true shear rate may be obtained from the nominal one by applying the Rabinowitsch-Mooney transformation. This transformation stipulates that the true shear rate at the wall is related to the nominal one by the relation (Govier and Aziz, 1987):

$$\left(-\frac{dV}{dr}\right)_w = \frac{8V}{D}\left(\frac{1+3n'}{4n'}\right) \qquad (4.10)$$

where:

$$n' = \frac{d\ln\left(\frac{D\Delta P}{4L}\right)}{d\ln\left(\frac{8V}{D}\right)} \qquad (4.11)$$

For a Newtonian fluid n'=1, and $-\frac{dV}{dr} = \frac{8V}{D}$, however for a non-Newtonian fluid n' is not constant. In general the true shear rate is a linear function of the nominal rate of shear. At a particular rate of shear, the constant of proportionality $\left(\frac{1+3n'}{4n'}\right)$ is

determined once n' is obtained as the slope of $\ln\left(\frac{D\Delta P}{4L}\right)$ versus $\ln\left(\frac{8V}{D}\right)$ curve.

Generating a rheogram involves finding (n') for all the nominal shear rates used in the data and computing the corresponding true shear rates. For a continuous pseudo-shear rate curve, this amounts to evaluation of the derivative of this curve at each nominal shear rate.

Alternatively, if a rheogram is available and it is desired to find the pseudo-shear diagram (or the flow rate-pressure drop relationship), then the following equation may be used (Govier and Aziz, 1987):

$$\frac{8Q}{\pi D^3} = \frac{2V}{D} = \frac{1}{\tau_w^3}\int_0^{\tau_w} \tau^2 f(\tau)d\tau \qquad (4.12)$$

The differentiability of a function presumes its continuity, and for the case of experimental data, least square fit continuous curves are usually used. Thus the accuracy of this procedure depends on the accuracy of the model with which the data is fitted. Lazarus and Slatter (1988) show that for the case of fitting data generated from the Buckingham equation for a Bingham plastic model with a third order polynomial, the error for plastic viscosity is 12.68% and that of yield stress is 0.5%. For lower order polynomials, these errors are much larger.

4.6 Metzner and Reed (1955) Generalized Reynolds Number Technique

When the rheological behaviour of a fluid does not conform to any known constitutive rheological equation, or when it is preferred to directly scale-up from data taken from a small diameter pipe, the generalized Reynolds Number technique of Metzner and Reed (1955), may be applied. This method is applicable to all time-independent fluids in laminar pipe flow.

Given a flow curve (pseudo shear stress-shear rate diagram), it is possible to find two parameters K' and n' for each data point such that :

$$\frac{D\Delta P}{4L} = K'\left(\frac{8V}{D}\right)^{n'} \qquad (4.13)$$

This equation represents the tangent to the plot of $\ln\left(\frac{D\Delta P}{4L}\right)$ versus $\ln\left(\frac{8V}{D}\right)$ curve at a given point. In the general case K' and n' are not constant but vary with the nominal shear rate. This method makes it possible to scale up the results without having to select a rheological model for the suspension. Results, thus obtained, may be considered as preliminary estimates of the full scale pressure loss-velocity curves. This method should be supported by experimental evidence that the data used indeed falls in the laminar flow regime. This is achieved by plotting it in the dimensionless form of friction coefficient and verifying that indeed:

$$f = \frac{16}{Re_{MR}} = \frac{D\Delta P}{2\rho V^2 L} \qquad (4.14)$$

with Re_{MR}, the generalized Reynolds number as defined by:

$$Re_{MR} = \frac{D^{n'} V^{2-n'}}{K' 8^{n'-1}}$$

Thus knowledge of K' and n' is sufficient to solving for the Fanning friction factor, hence for the pressure gradient.

4.6.1 Numerical Method for Finding K' and n' From Shear Stress-Nominal Shear Rate Data For a Power Law Model :

In this case, K' and n' are constant, thus starting from the relation:

$$\frac{D\Delta P}{4L} = \tau_w = K' \left(\frac{8V}{D}\right)^{n'} \qquad (4.15)$$

For a set of N data points two equations are constructed as follows:

$$\Sigma_i \ln \tau_{w,i} = N \ln K' + n' \Sigma_i \ln\left(\frac{8V_i}{D}\right) \qquad (4.16)$$

$$\Sigma_i V_i \ln \tau_{w,i} = \ln K' \Sigma_i V_i + n' \Sigma_i V_i \ln\left(\frac{8V_i}{D}\right) \qquad (4.17)$$

These are two linear equations which may be solved simultaneously for ln(K') and n'.

4.7 The Power Law Model (Pseudo-Plastic Fluids)

This flow model is expressed by a shear stress-shear rate relationship given by:

$$\tau = K\left(-\frac{dV}{dr}\right)^n \qquad (4.18)$$

where K is fluid consistency, and n is flow behaviour index. If n<1, the fluid is known as "shear thinning", otherwise, if n>1, the fluid is known as "shear thickening" or dilatent.

The wall shear stress is given by:

$$\tau_w = \frac{DP}{4L} = K\left(\frac{4n}{3n+1}\right)^n\left(\frac{8V}{D}\right)^n \qquad (4.19)$$

The relation between the true wall shear rate and the nominal one is found from substituting $f(\tau) = \left(\frac{\tau}{K}\right)^{1/n}$ in Equation (4.5). This give:

$$\left(-\frac{dV}{dr}\right)_w = \frac{8V}{D}\left(\frac{3n+1}{4n}\right) \qquad (4.20)$$

Figure 4.4 shows the deviation of the nominal shear rate from the true shear rate at the wall as a function of $\zeta = \frac{\tau_y}{\tau_w}$ for a Power law fluid.

Once the Metzner and Reed parameter K' is obtained as shown in the previous section, the Power law parameter K may be obtained from:

$$K = \frac{K'}{(3n+1/4n)^n} \qquad (4.21)$$

The power law parameter (n) is the same as (n').

Example 1

Table 4.1
Hypothetical Flow Data for Example 1

Mean flow velocity, V, m/sec	Wall shear stress, τ_w, Pa	Nominal shear rate, 8V/D, 1/sec
0.006	1.31	1.51
0.086	2.31	21.75
0.256	2.92	64.76
0.504	3.37	127.49
0.824	3.74	208.44
1.208	4.06	305.58
1.649	4.34	417.14
2.144	4.59	542.35
2.686	4.81	679.46
3.271	5.02	827.45

		Actual	Estimated
Bingham Plastic	Yield stress (Pa)	-	1.79
	Viscosity (Pa sec)	-	0.0042
Power Law	K	1.38	1.38
	n	0.213	0.213

Figure 4.5 shows Power law flow data fitted with estimated Power law and Bingham plastic models for comparison.

Figure 4.4 Deviation of true to nominal shear rate ratio as a function of the Power law parameter n

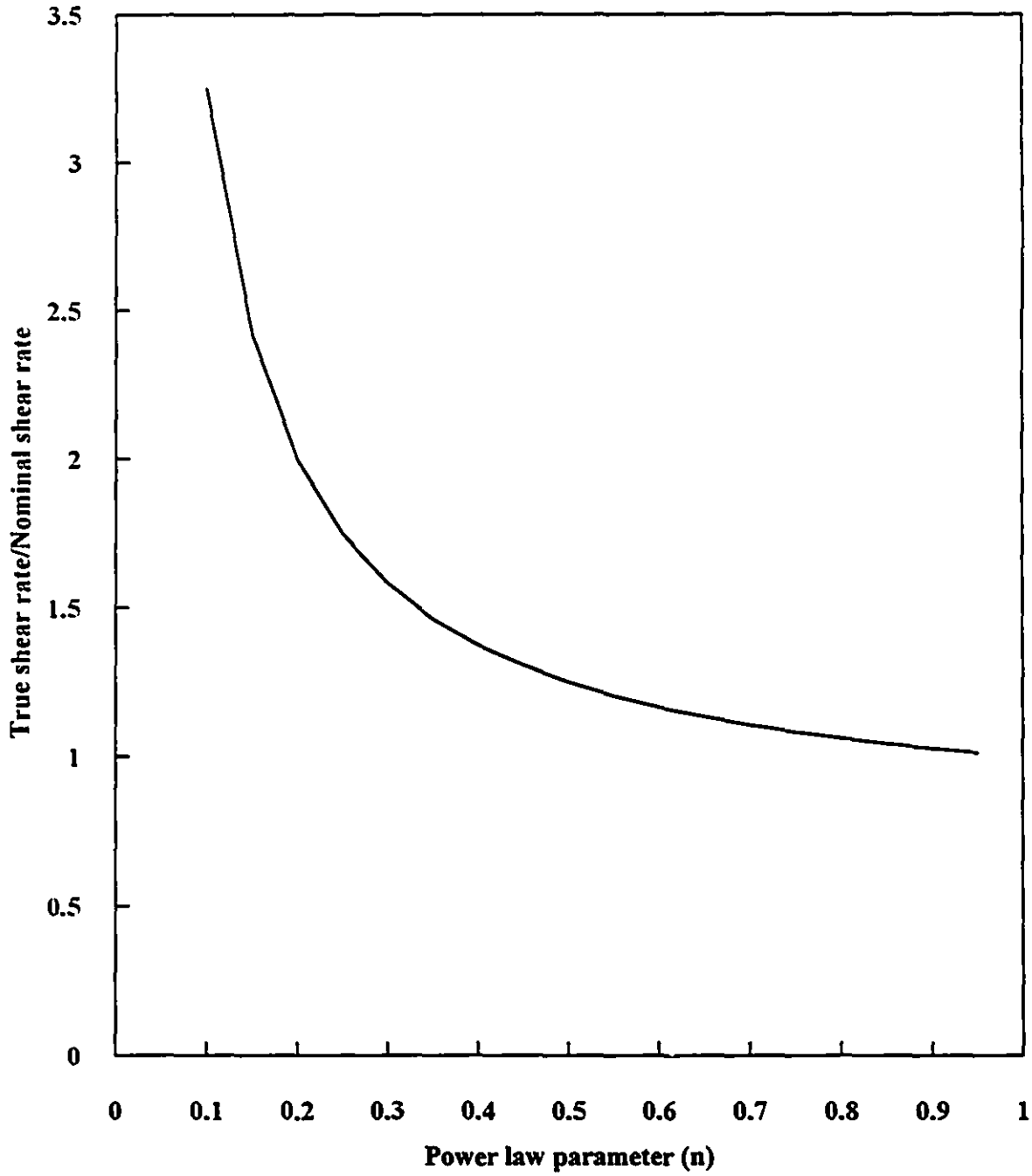

Figure 4.5 Example1: Power law data fitted with estimated Power law and Bingham plastic models

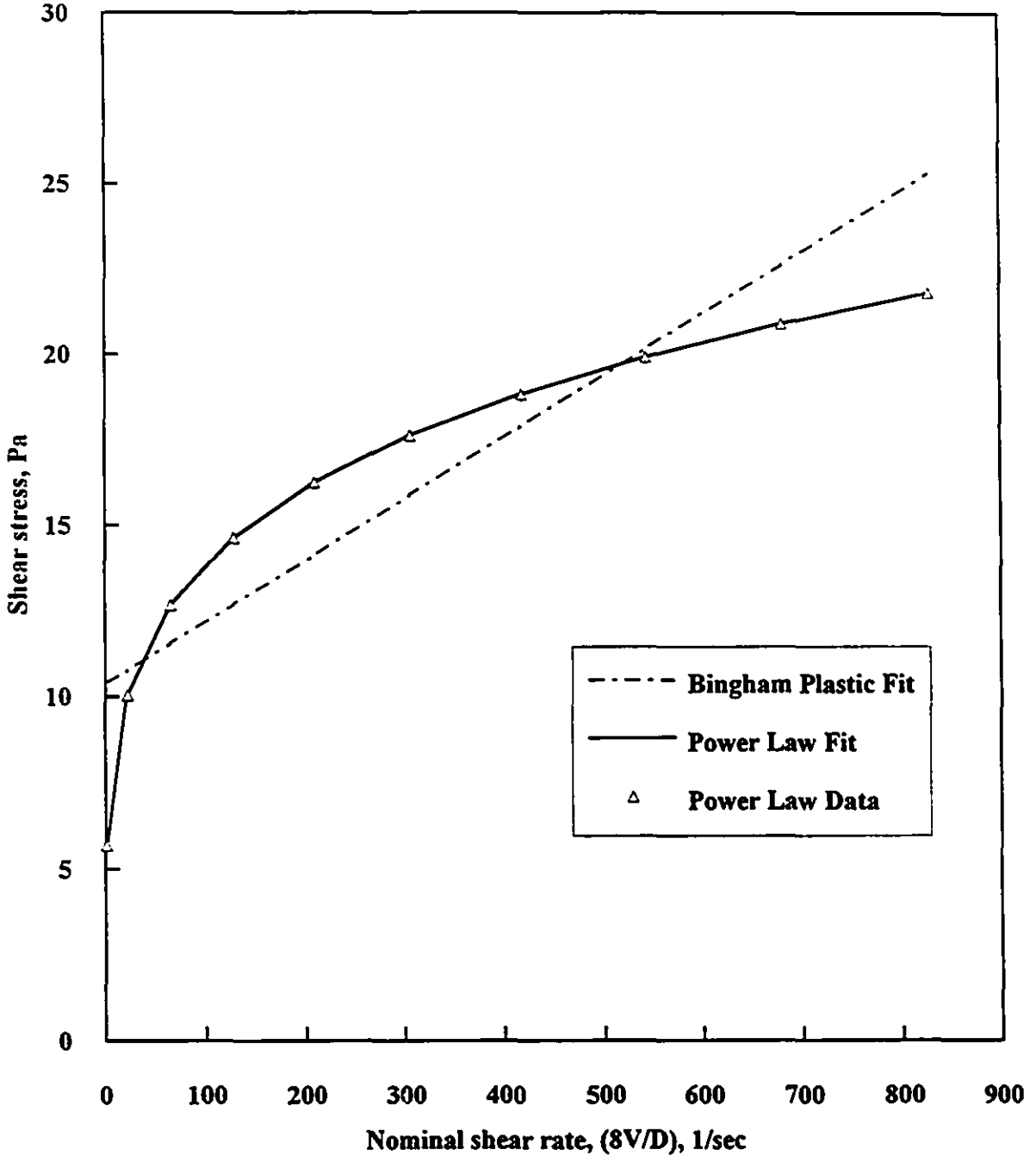

The Fanning friction factor for a power law fluid is given by:

$$f = \frac{16}{R'_c} \tag{4.22}$$

Where the Reynolds number is defined as (Govier and Aziz, 1987):

$$R'_e = \frac{8\, D^n\, V^{2-n}\, \rho_m}{K}\left(\frac{n}{2(3n+1)}\right)^n \tag{4.23}$$

Figure 4.6 is a friction factor design chart for Power law fluids. A possible explanation for the shear thinning behaviour (n <1) characteristic of Power Law fluids is the possibility of realignment of asymmetric particles in the direction of the flow, thus offering less resistance to shear.

Shear thickening (dilatant behaviour) (n >1), on the other hand, may be the result of a change in the void ratio caused by an increase in the shearing action (Bain and Bonnington, 1977) . The ability of the original amount of fluid to act as a lubricant to the solid particles is decreased because of inability of the available quantity of fluid to fill the voids created by the shearing action. This in turn, causes a sharp increase in the shear stress. This situation may be encountered with some slurries or pastes at very high solids concentration. Depending on the particle size distribution and other physico-chemical factors, the optimum solids concentration may range between 50 to 70 per cent. by mass (Verkerk, 1988).

Other factors of surface-chemical nature, such as pH or zeta potential, may also play a significant role in the mode of rheological behavior of the suspension. The use of chemical additives such as flocculents or dispersents may help in designing mixtures pumpable over longer distances at high solids concentration and relatively low energy cost.

Figure 4.6 Friction factor design chart for Power law fluids
(adapted from Dodge and Metzner, 1959)

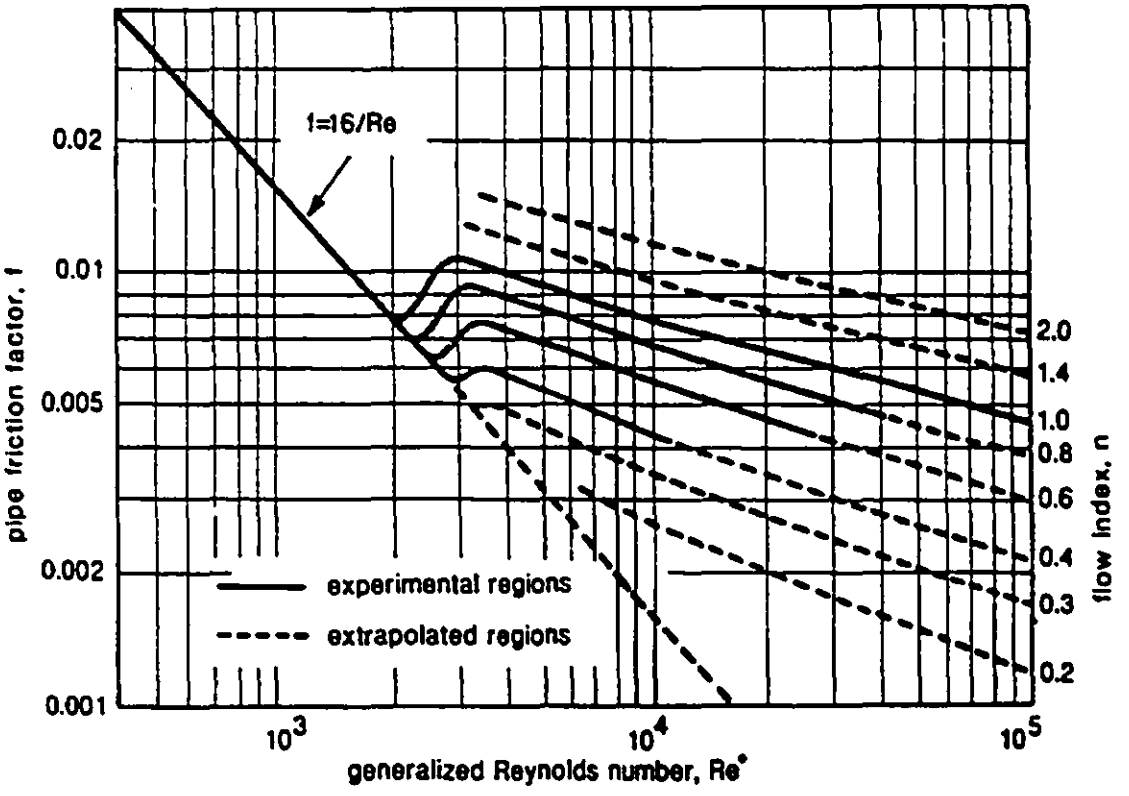

4.8 The Bingham Plastic Model

The shear stress-shear strain defining the Bingham plastic model is given by:

$$\tau = \tau_y + \eta\left(-\frac{dV}{dr}\right), \text{ for } \left(-\frac{dV}{dr}\right) > \tau_y \qquad (4.24)$$

$$\left(-\frac{dV}{dr}\right) = 0, \text{ for } \tau \le \tau_y$$

where τ_y is the yield stress required to initiate flow, and η is the plastic viscosity (also known as the coefficient of rigidity) which is identical to that of a Newtonian fluid. Slurries with narrow particle size distribution or high surface-chemical forces usually behave as Bingham plastics. Drilling mud, sewage sludge and slurries of limestone are common examples.

Because of the discontinuity in the velocity profile of a Bingham plastic, the wall shear stress $\frac{D\Delta P}{4L}$ cannot be directly expressed in terms of the shearing rate at the pipe wall. Instead, It is expressed by the Buckingham equation given by:

$$\tau_w = \frac{D\Delta P}{4L} = \eta\frac{8V}{D}\left(1 - \frac{4}{3}\frac{\tau_y}{\tau_w} + \frac{1}{3}\left(\frac{\tau_y}{\tau_w}\right)^4\right)^{-1} \qquad (4.25)$$

For $\frac{\tau_y}{\tau_w} < 0.4$, neglecting the fourth power term leads to results of sufficient accuracy (less than 1.8 % error) and allows the simplification of the above equation.Taking this simplification into account, the wall shear stress for a Bingham plastic material may be expressed by:

$$\tau_w = \eta\left(\frac{8V}{D}\right) + \frac{4}{3}\tau_y \qquad (4.26)$$

The relation between the true wall shear rate and the nominal one is found from substituting $f(\tau) = \frac{1}{\eta}(\tau - \tau_y)$ in Equation (4.5). This gives:

$$\left(-\frac{dV}{dr}\right)_w = \frac{8V}{D}\frac{1-\zeta}{1-\frac{4}{3}\zeta+\frac{1}{3}\zeta^4} \qquad (4.27)$$

where $\zeta = \frac{\tau_y}{\tau_w}$

Figure 4.7 shows the deviation of the nominal shear rate from the true shear rate at the wall as a function of $\zeta = \frac{\tau_y}{\tau_w}$ for a Bingham plastic fluid. A series of laminar flow curves may be obtained from :

$$f = \frac{16}{Re_B}\left(1+\frac{He}{6Re_B}-\frac{He^4}{3f^3Re_B^7}\right) \qquad (4.28)$$

where the dimensionless Hedstrom number is defined as $He = \frac{\tau_y D^2 \rho_m}{\eta^2}$, and the Bingham Reynolds number as $Re_B = \frac{VD\rho_m}{\eta}$

Figure 4.8 shows the friction factor design chart for Bingham plastic fluids. For a fluid with a given yield stress, the position of the laminar flow curve depends on the pipe diameter. It is reported by Bain and Bonnington(1970) that for all concentrations of chalk slurries tested by British Hydrodynamic Research Association, laminar flow persisted down to a friction factor around f = 0.02, after which the friction factor remained constant.

Figure 4.7 Deviation of true to nominal shear rate ratio as a funtion of yield to wall shear stress ratio for the Bingham plastic model

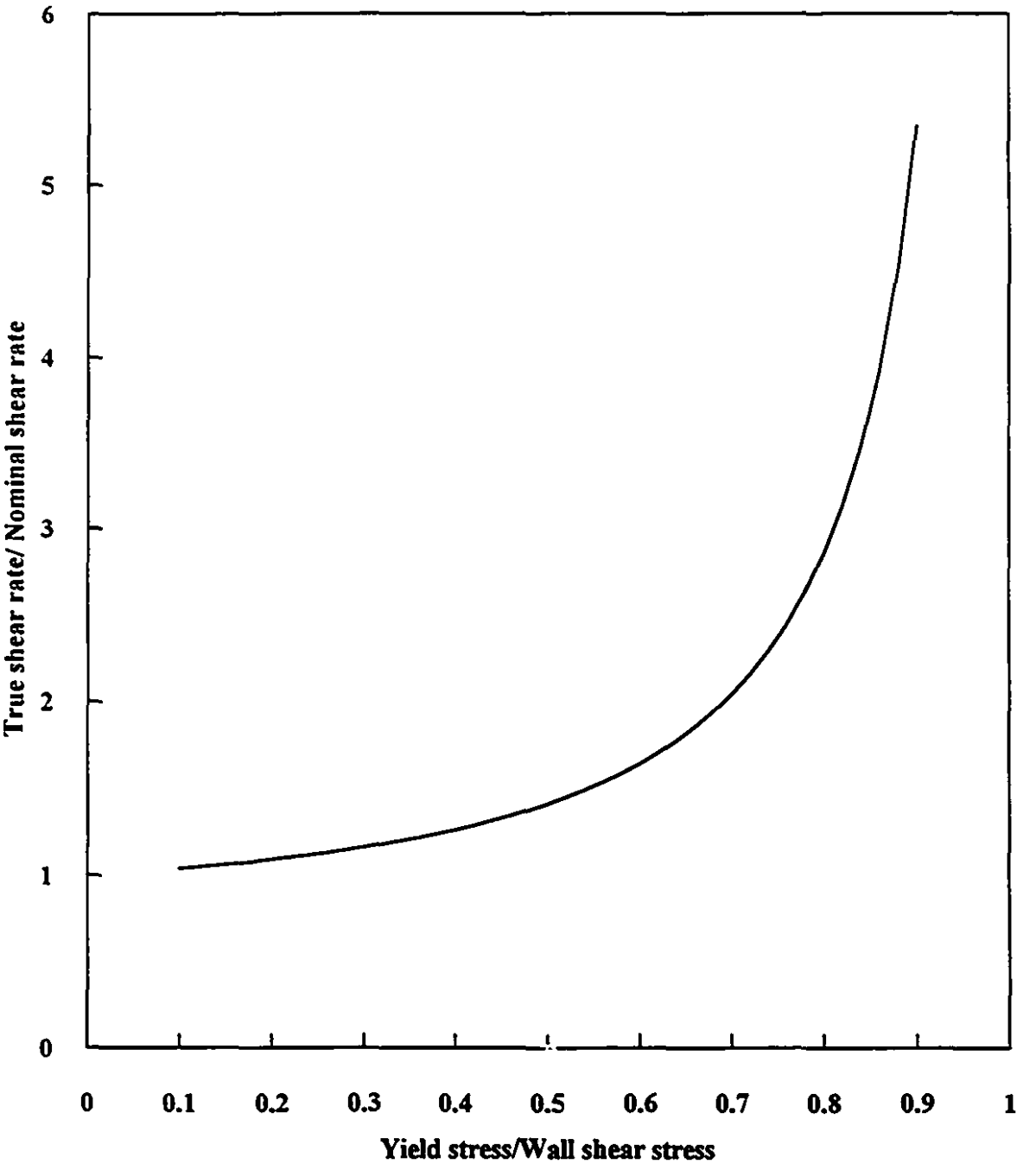

Figure 4.8 Friction factor design chart for Bingham plastic fluids (adapted from Woodcock and Mason, 1987)

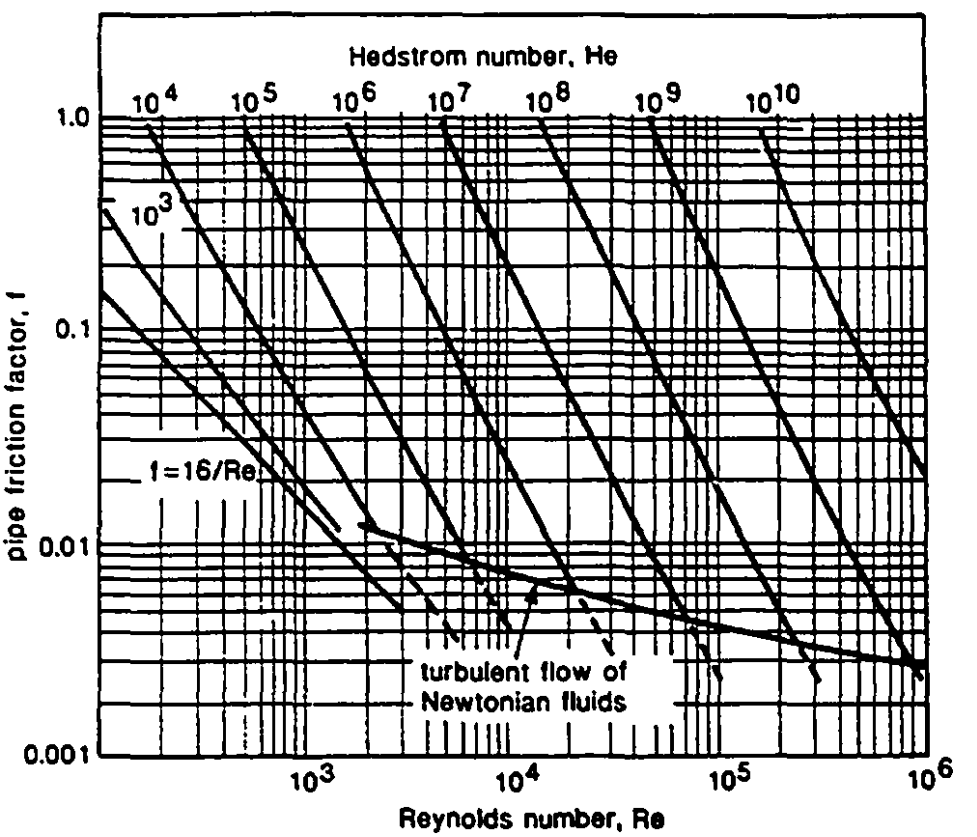

4.8.1 Rheological Parameters From Shear Stress-Nominal Shear Rate Data: Numerical Method

Starting from the Buckingham equation in the form:

$$\frac{8V}{D} = \frac{\tau_w}{\eta}\left(1 - \frac{4}{3}\left(\frac{\tau_y}{\tau_w}\right) + \frac{1}{3}\left(\frac{\tau_y}{\tau_w}\right)^4\right) \qquad (4.29)$$

Two equations are constructed as follow (Shook, 1991):

$$\eta \, \Sigma_i \frac{8V_i}{D} = \Sigma_i \, \tau_{w,i} - \frac{4}{3} N \, \tau_y + \frac{1}{3} \tau_y^4 \, \Sigma_i \, \tau_{w,i}^{-3} \qquad (4.30)$$

$$\eta \, \Sigma_i \, \tau_{w,i} \frac{8V_i}{D} = \Sigma_i \, \tau_{w,i}^2 - \frac{4}{3} \tau_y \, \Sigma_i \, \tau_{w,i} + \frac{1}{3} \tau_y^4 \, \Sigma_i \, \tau_{w,i}^{-2} \qquad (4.31)$$

where N is the number of data points.

Eliminating η between the two equations, one obtains a fourth degree equation in τ_y :

$$(a4a5 - a1a8)\,\tau_y^4 + (a1a7 - a3a5)\tau_y + (a2a5 - a6a1) = 0 \qquad (4.32)$$

where:

$$a1 = \Sigma_i \frac{8V_i}{D}, \quad a2 = \Sigma_i \, \tau_{w,i}, \; a3 = \frac{4}{3}N, \; a4 = \frac{1}{3}\Sigma_i \, \tau_{w,i}^{-3}$$

$$a5 = \Sigma_i \, \tau_w\left(\frac{8V_i}{D}\right), \; a6 = \Sigma_i \, \tau_{w,i}^2, \; a7 = \frac{4}{3}\Sigma_i \, \tau_{w,i}, \; a8 = \frac{1}{3}\Sigma_i \, \tau_{w,i}^{-2}$$

The following example illustrates this procedure.

Example 2

Table 4.2
Hypothetical flow data for Example 2

Mean flow velocity, V, m/sec	Wall shear stress, τ_w, Pa	Nominal shear rate, 8V/D, 1/sec
0.006	136.7	1.51
0.086	181.2	21.75
0.256	275.8	64.76
0.504	413.8	127.49
0.824	591.9	208.44
1.208	805.6	305.58
1.649	1051.0	417.14
2.144	1326.5	542.35
2.686	1628.2	679.46
3.271	1953.7	827.45

		Actual	Estimated
Bingham Plastic	Yield stress (Pa)	100	104.2
	Viscosity (Pa sec)	2.2	2.19
Power Law	$K=K'(4n/3n+1)^{-n}$	-	40.88
	n	-	0.567

Figure 4.9 shows Bingham palstic flow data fitted with estimated Power law and Bingham plastic models for comparison.

Figure 4.9 Example 2: Bingham plastic Data fitted with an estimated Bingham plastic and Power law models

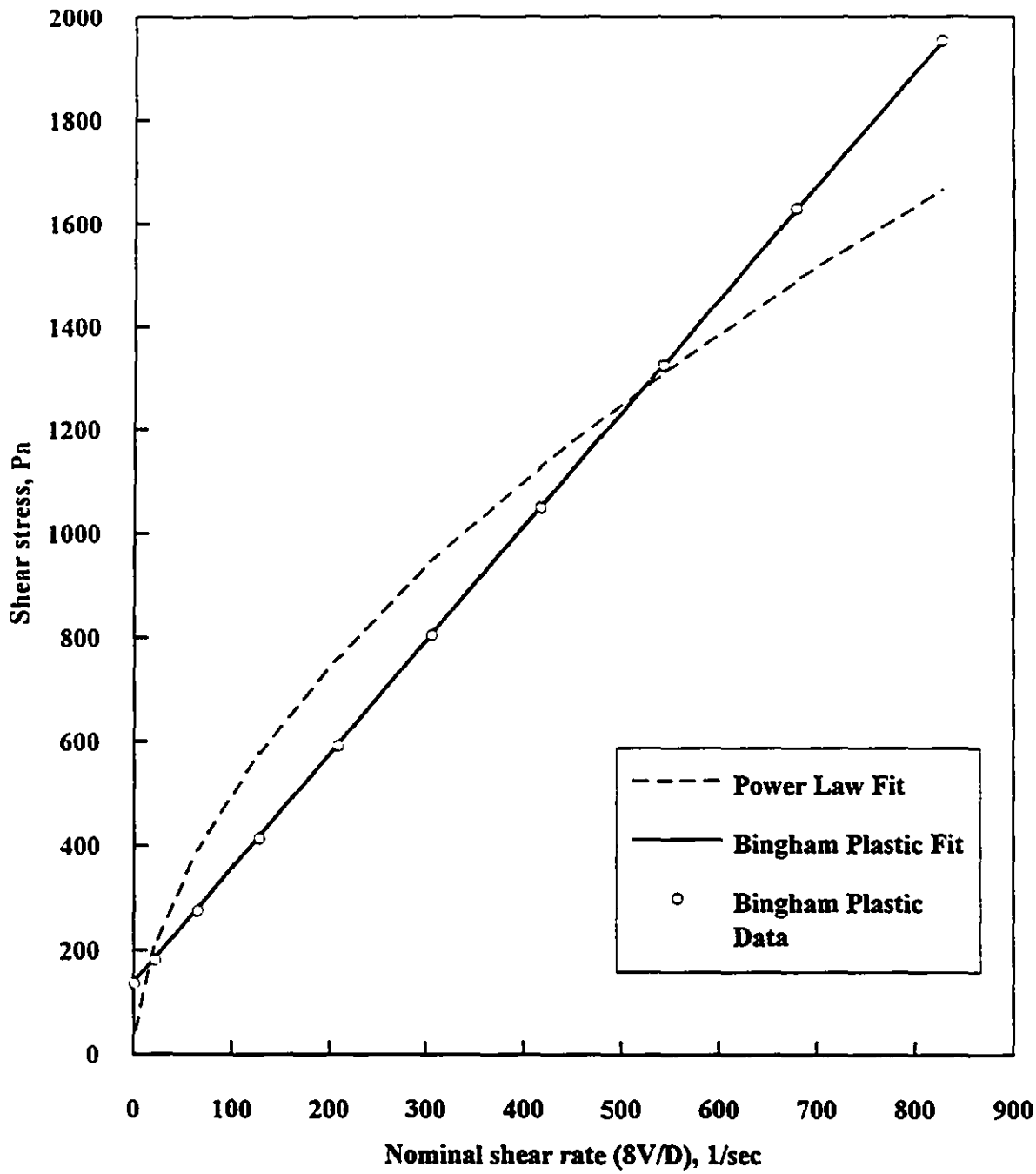

4.9 The Casson Model

The relation between the shear stress and the shear rate for this model is expressed by:

$$\sqrt{\tau} = \sqrt{\tau_c} + \sqrt{\mu_c\left(\frac{dV}{dr}\right)}, \text{ for } \tau > \tau_c \qquad (4.33)$$

$$-\frac{dV}{dr} = 0, \text{ for } \tau \le \tau_c$$

Where τ_c is the casson model equivalent to the yield stress.

The wall shear stress is related to the nominal shear rate by (Darby, 1986):

$$\tau_w = \mu_c\left(\frac{8V}{D}\right) - \frac{4}{3}\tau_c + \frac{16}{7}\sqrt{\tau_w\tau_c} + \frac{\tau_c^4}{21\,\tau_w^3} \qquad (4.34)$$

The Fanning friction factor is calculated from:

$$f = \frac{16}{Rec}\left(1 - \frac{16\sqrt{2}}{7}\frac{\sqrt{Ca}}{\sqrt{fRec}} + \frac{8}{3}\frac{Ca}{fRec^2} - \frac{16}{21}\frac{Ca^4}{f^4\,Rec^8}\right)^{-1} \qquad (4.35)$$

where:

$$Ca = \frac{D^2\tau_c\rho_m}{\mu_c^2} \qquad (4.36)$$

$$Rec = \frac{DV\rho_m}{\mu_c} \qquad (4.37)$$

4.10 Yield pseudo-plastic (Herschel-Bulkley)

The relation between the shear stress and the shear rate for this model is expressed by:

$$\tau = \tau_y + K\left(-\frac{dV}{dr}\right)^n, \text{ for } \tau > \tau_y \tag{4.38}$$

$$-\frac{dV}{dr} = 0, \text{ for } \tau \leq \tau_c$$

The wall shear stress is related to the nominal shear rate by (Darby, 1986):

$$\tau_w = \tau_y + K\left(\left(\frac{8V}{D}\right)\left(\frac{3n+1}{4n}\right)\right)^n [A]^{-n} \tag{4.39}$$

The Fanning friction factor is calculated from:

$$f = \frac{2He_{HB}}{Re_{HB}^2} + \frac{16}{Re_{HB}}[A]^{-n} \tag{4.40}$$

where:

$$[A] = \left(\left(1-\frac{\tau_y}{\tau_w}\right)^3 + \frac{2(3n+1)}{(2n+1)}\left(\frac{\tau_y}{\tau_w}\right)\left(1-\frac{\tau_y}{\tau_w}\right)^2 + \frac{(3n+1)}{(n+1)}\left(\frac{\tau_y}{\tau_w}\right)^2\left(1-\frac{\tau_y}{\tau_w}\right)\right)$$

$$He_{HB} = Re_{HB}^2 \frac{\tau_y}{\rho_m V^2}$$

$$Re_{HB} = \frac{8D^n V^{2-n}\rho_m}{K\left(\frac{2(3n+1)}{n}\right)^n}$$

4.10.1 Numerical Method for Finding Rheological Parameters (τ_y,K,n) From Shear Stress-Nominal Shear Rate Data:

The yield-pseudoplastic shear stress-nominal shear rate relation may be expressed by (Paterson, 1991):

$$\frac{8V}{D} = \frac{4n}{\sqrt[n]{K}\,\tau_w^3}(\tau_w - \tau_y)^{(n+1/n)}\left(\frac{(\tau_w - \tau_y)^2}{3n+1} + \frac{2\tau_y(\tau_w - \tau_y)}{2n+1} + \frac{\tau_y^2}{n+1}\right) \qquad (4.41)$$

The rheological parameters may be obtained using an optimization program described by Paterson (1991), which for a given yield stress (determined independently by the vane method or estimated from the pseudo-shear diagram), values of K and n are selected which minimize the error in the nominal shear rate $\frac{8V}{D}$ on a τ_w versus $\frac{8V}{D}$ diagram.

4.11 Laminar-Turbulent Transition Velocity

For Newtonian fluids, transition to turbulent flow is recognized by a distinct change of curvature or slope of the shear stress-shear rate curve or a discontinuity in the f-Re curve. For non-Newtonian fluids, no such discontinuity is observed in the f-Re or head loss versus velocity curves , although the transition is clearly defined especially with Bingham fluids (Shook and Roco, 1991). This transition can be expressed in terms of the Hedstrom number $He = \frac{\rho D^2 \tau_y}{\eta^2}$, as:

$$\left(\frac{DV\rho}{\eta}\right)_{trans} = 2100\left(1 - \frac{4}{3}\alpha_c + \frac{1}{3}\alpha_c^3\right)(1 - \alpha_c)^{-3} \qquad (4.42)$$

where:

$$\frac{\alpha_c}{(1-\alpha_c)^3} = \frac{He}{16800}$$

with α_c being the ratio of the yield stress to the pipe wall shear stress at transition.

D.G. Thomas (1963) proposed the following implicit equation for the transition velocity of a Bingham fluid:

$$\frac{VD\rho}{\eta} = 2100\left(1 + \frac{\tau_y D}{6\eta V}\right) \qquad (4.43)$$

For other non-Newtonian fluids, the Metzner & Reed Reynolds number $Re_{n'}$ was defined so that in laminar flow $f = \frac{16}{Re_{n'}}$. Experiments indicate that the transition region occurs for $Re_{n'}$ between 2100 and 3000 (Shook and Roco, 1991) .

4.12 Turbulent Flow

According to Bain & Bonnington (1970), a conservative approach for finding the friction factor f for non-Newtonian turbulent fluids consists in assuming that the onset of turbulent flow occurs when the f-Re curve for laminar flow intersects the smooth pipe turbulent flow curve for Newtonian fluids, and then using the fully developed turbulent flow a friction coefficient for Newtonian flow at the same Reynolds number.

Lower friction coefficient could be used if better understanding of the effect of turbulence on the pipeline resistance to flow is achieved. For a Bingham plastic fluid, there are cases where each slurry concentration has shown a different curve in the turbulent regime. A downward trend in the f-Re curves is observed in all cases. For a pseudo-plastic fluid, each slurry concentration may yield a different value of the slurry behaviour index n, which gives a separate curve in the friction coefficient versus generalized Reynolds number graph.

4.12.1 Newtonian Fluids

(k/D) of the pipe. In the transition region it is dependent on both the Reynolds number and the relative roughness. These observations are based on the Moody Diagram from which the Fanning friction factor can be read (Figure 4.2)

Among empirical equations for Newtonian fluids found in the literature giving the friction factor, four are given below:

1) Iterative method (Colebrook-White formula)

$$\frac{1}{\sqrt{f}} = -4 \log\left(\frac{k}{3.7D} + \frac{1.26}{Re\sqrt{f}}\right) \qquad (4.44)$$

2) Direct method (Churchill, W., 1977)

$$f = 2\left(\left(\frac{8}{Re}\right)^{12} + (A+B)^{-1.5}\right)^{0.0833} \qquad (4.45)$$

where :

$$A = 2.457 \ln\left(\left(\frac{7}{Re}\right)^{0.9} + \frac{0.27\,k}{D}\right)$$

$$B = \left(\frac{37530}{Re}\right)^{16}$$

4) Direct method (Zigrang and Sylvester, 1982)

- For rough pipes:

$$\frac{1}{\sqrt{f}} = -4 \log\left(\frac{k/D}{3.7} - \frac{5.2}{Re}\log\left(\frac{k/D}{3.7} - \frac{5.02}{Re}\log\left(\frac{k/D}{3.7} - \frac{13}{Re}\right)\right)\right) \qquad (4.46)$$

- For smooth pipes:

$$f = \frac{0.0791}{Re^{0.25}} \qquad (4.47)$$

4) Direct method (Halland, S. E., 1983)

$$\frac{1}{\sqrt{f}} = -3.6 \log\left(\left(\frac{k}{3.71D}\right)^{1.11} + \frac{6.9}{Re}\right) \qquad (4.48)$$

4.12.2 Bingham Plastic Fluids

Darby (1986) presented empirical equations based on graphs proposed by Hanks and Dadia(1971) of the friction factor f versus Reb for parametric values of Heb, giving generalized relations between f, Reb and Heb. For Heb≥1000:

$$f = (f_L^m + f_T^m)^{1/m} \qquad (4.49)$$

where:

$$f_T = \frac{10^a}{Reb^{0.193}}$$

$$a = -1.378(1 + 0.14\exp(-2.9\times10^{-5}Reb))$$

$$m = 1.7 + \frac{40\,000}{Reb}$$

F_L is the laminar friction factor.

4.12.3 Power Law Fluids

Dodge and Metzner (1959) derived an equivalent to the Von Karman equation as given by:

$$\frac{1}{\sqrt{f}} = \frac{4}{n^{0.75}} \log(Re' f^{1-n/2}) - \frac{0.4}{n^{1.2}} \qquad (4.50)$$

Hanks and Ricks (1975) presented graphical results, approximated by the following empirical equations (Darby, 1986) for all Reynolds numbers (laminar through turbulent) up to 10^5:

$$f = \frac{16(1-\alpha)}{Re'} + \alpha \left(f_T^8 + f_{TR}^8 \right)^{-0.125} \qquad (4.51)$$

where:

$$f_T = 0.0682\left(\sqrt{n}\, R_{e'}^{(1.87+2.39n)^{-1}}\right)^{-1}$$

$$f_{TR} = 1.79 \cdot 10^{-4} \exp(-5.24n) R_{e'}^{(0.414+0.757n)}$$

$$\alpha = \frac{1}{1+4^{-\Delta}} \quad \text{with} \quad \Delta = Re' - Re^*, \text{ and } Re^* = 2100 + 875(1-n)$$

f_T is the friction factor in turbulent flow for $4000<Re'<10^5$, and f_{TR} is the friction factor for the transition region from Re* to 4000, where Re* is the critical transition number from laminar to turbulent flow.

Experimental confirmation of these correlations over a large portion of the dimensionless relations remains a subject of investigation because of lack of sufficient data in the literature.

4.12.4 Bowen's Approach For Non-Newtonian Fluids in Turbulent Flow

Most flow models are valid over a range of shear rates beyond which their reliability becomes questionable. This is mainly due to the fact that, by definition, rheological models are based on the assumption of laminar flow behaviour. Therefore, such flow models cannot be expected to give reliable data in the turbulent flow regime.

When designing hydraulic transport systems operating around the transition to turbulent flow, it is highly recommended to simulate the expected flow behaviour in a small scale loop test or in a capillary viscometer and to extend the flow range to the turbulent region. Bowen (1961) proposed a simple method for handling data from turbulent flow tests. Assuming the viscosity to be constant, the Blasius law representing the turbulent flow in smooth pipes given by:

$$f = \frac{0.316}{R_e^{0.25}} \qquad (4.52)$$

was interpreted, as:

$$D^{1.25}\frac{\Delta P}{L} = k\,V^{1.75} \qquad (4.53)$$

For a Bingham plastic, a graph of $\frac{D^{1+b}\,\Delta P}{4L}$ versus V is plotted on a log scale. Extrapolation to full scale is considered valid only if this graph conforms to a straight line for all diameters used. The coefficient (b) is determined from the straight line on a logarithmic scale of the graph $\frac{D\Delta P}{4L}$ versus $\frac{8V}{D}$ with a slope equal to (2-b) .

Similarly, for a pseudo-plastic material, all results should correlate when plotted as $\frac{D^{(1+bn)}\,\Delta P}{4L}$ versus V, where (n), the flow-behaviour index, is determined from the laminar regime and (b) is the slope of the turbulent flow curve .

CHAPTER FIVE

A PLUG FLOW MODEL (PFM) FOR HIGH DENSITY MINE BACKFILL

5.1 Introduction

Plug Flow is the mechanism by which highly concentrated mixtures (such as concrete and high density mine backfill) are transported. It is established when the bulk material flows as a core of inter-locked and water-saturated solid particles surrounded by a thin annular layer of a homogeneous mixture made up of water and very fine particles. The plug-forming ability of high density backfill for example is a result of a careful mix design governed by the -325 mesh fines and the grading of the coarser aggregates. The -325 mesh fines should form a stable and homogeneous dense fluid medium with a shear yield stress capable of maintaining the coarse particles in suspension under laminar flow condition.

The apparent slip phenomenon in tube viscometers takes place according to two possible mechanisms. The first is when actual slip at the pipe wall occurs; and the second is when an annular layer is formed around a core of interlocked particles moving in Plug Flow. This flow mechanism occurs when concrete or highly concentrated mine backfill are transported in pipelines. A similar phenomenon also occurs with fibrous materials such as paper pulp . In such applications the apparent "slip" or more accurately the annular lubricating layer effect is rather beneficial as it reduces frictional energy losses and wear rate of the pipeline.

In this chapter, a general equation for the flow of a moving core surrounded by a Bingham plastic annular layer is derived. Based on this equation, an analytical interpretation of slip effects in tube viscometers for the case of highly concentrated suspensions in Plug Flow is presented. An assessment of the suitability of Mooney's method to correct for slip of highly concentrated suspensions in Plug Flow is proposed along with new methods of estimating the annular layer thickness. Comparison with experimental results from the literature (Duckworth et al. (1986)) are made to evaluate theoretical findings.

5.2 The Flow of Highly Concentrated Suspensions in Pipes --A Literature Review

Laird (1957) presented an analytical solution to the laminar flow of a Bingham plastic fluid in an annular conduit. This mode of flow is widely observed in various industries dealing with the pipeline conveying of wastes , slurries and suspensions of all kinds. Laird's solution is of particular interest to the oil industry where flow of the cutting fluids takes place in the annulus formed by the drill pipe and the borehole.

Ede (1957) investigated the basic mechanics of concrete pumping and found that unsaturated materials pass stresses by inter-particle contact . As a result, frictional pressure losses tend to rise exponentially with distance pumped. For saturated suspensions, frictional pressure losses are appreciably lower and the resistance to flow is linear with distance pumped.

Elliot and Gliddon (1970) performed rheological experiments to validate the concept that optimum flow properties of a solid-water mixture can be obtained by adjusting the size distribution of the solid to give the greatest packing density. They found that the ideal mixture for low pumping power is bi-modal with high proportions of fines mixed with a larger proportion of coarser particles . Such particle size distribution cannot be obtained by a single stage crushing operation. They found that with concentrations above 55% by weight, these mixtures behave like Bingham plastics with laminar flow over a very wide range of velocities. Such mixtures were found to be stable as they can be allowed to remain stationary in pipelines for long periods without segregation. They showed that the pH of a mixture had a remarkable but completely reversible effect on the flow properties. This was attributed to the presence of clay in the suspension.

Browne and Bamforth (1977) presented a qualitative model for relating the state of concrete in the pipeline to the concrete mix components and pumping system. They described test methods for assessing the pumpability of concrete. Impermeability of concrete material to the fluid medium in the mixture was found to play an important role in minimizing pipe blockages. A special device was designed to test for pumpability by measuring the rate of bleeding of the mixture

under pressure. Pumping trials were performed to check the validity of the bleeding test apparatus and to measure the effect of variations in mix proportions on the pressure versus time traces. The void meter test and its value as a mix proportioning tool were described in relation to the optimization of the cement content.

Cheng (1977) presented a review on the rheology of solid-liquid mixtures at very high solids concentration including unsaturated systems. He explained their behaviour in terms of the granular and viscous characteristics of the particulate solids and the fluid medium respectively, which he called the *granulo-viscous* behaviour. This phenomena is manifested by several characteristic features including: stick-slip, changes in flow curves, packing density variation, wall effect, etc.

In a later publication, Cheng (1984) presented further observations on the rheological behaviour of dense suspensions. He concluded that the steady shear properties of a dense suspension may not be characterized by an unique flow curve, but rather by a wide shear stress versus shear rate flow band with a mean and a standard deviation which are a function of solids concentration, particle size distribution and the geometry of the viscometer and its dimensions. It was observed that an increase in data spread (as measured by the standard deviation) is caused by an increase in the solids concentration and the decrease in viscometer gap to particulate diameter ratio. This property is attributed to poor sample reproducibility with respect to solids concentration and particle size distribution. Furthermore, the inherent two-phase nature of the suspension results in particle migration and non-uniform packing density in a sample. Therefore the viscosity distribution or flow band depends on viscometer geometry and dimensions. It is concluded that because of the complex and poorly reproduced behaviour which is inevitable with dense suspension, it is necessary to resort to full scale testing if one wishes to have reliable results for industrial applications . Laboratory viscometers are deemed useful only for providing qualitative results.

Best and Lane (1980) conducted a testing and evaluation program to determine the effect of significant parameters on the pumping characteristics of concrete. Such parameters included water-cement ratio, mortar volume, air content, slump, sand and aggregate proportions , and the addition of fly ash. Two laboratory scale rigs

were designed, one for pumping paste and mortar and a larger one for concrete. Both tests are said to have produced good correlation of results between laboratory and field tests using full scale concrete pumps.

Tattersall and Banfill (1983) presented three mechanisms that may be used to describe the flow of concrete in pipes. In the first one, concrete is assumed to flow as a Bingham plastic material, and analysis yields the standard Buckingham-Reiner equation relating the flow rate to the pressure gradient. In the second approach, it is assumed that a Newtonian layer of a given viscosity and thickness surrounds the Bingham plastic concrete core. The third approach generalized the latter concept to a Bingham plastic annular layer.

Manheimer (1985) showed that with many slurries, particularly at stresses near the yield value, flow is entirely due to slip. A simple model was proposed that defines slip in terms of a thin film of fluid that lubricates the walls of the viscometer. This model was reported to predict many of the observed effects of slip and accounts for the anomalous results that are often observed when rheological measurements of slurries are correctly analyzed. The fact that the primary mechanism of flow at low shear stresses is slip rather than shear is taken as an indirect evidence that these slurries have a yield stress. The author cautions against using data reported in the literature unless it is known that appropriate measures were taken to correct for slip effects.

Duffy et al. (1984, 1985, 1987) introduced the concept of a new suspending medium for the pipeline transport of coarse, high density and dense phase particles and capsules. This concept is based on the properties of a suspension of flexible elastic fibers to mechanically entangle to form an interlocking structure which supports solid particles. In this way, particles do not settle or collide while flowing and remain in suspension when flow is momentarily stopped. Various flow mechanisms were described and emphasis was placed on the central core flow with an annular suspension of fibers. This mechanism is perceived to be very favorable, not only because of the resulting stabilization of the suspension but also because of the appreciable reduction in frictional pressure losses, and the minimization of the main causes of pipe wear i.e. solid particle contact with the pipe wall and high flow velocities.

Assuming plug flow, Gandhi (1987) showed that adding coarse particles to a high density mixture increases the core diameter hence reducing the annular layer thickness. This rationale, supported by flow equations, accounted for the observed increase in pressure gradient and the substantial decrease in flow velocity.

Tatsis et al. (1988a) described a comprehensive study of pipe flow prediction for high concentration slurries containing coarse particles. Their goal was to establish reliable design techniques for using "pump packing" (i.e pumped backfill) in underground coal mine. A number of stabilized backfill slurries made up of crushed colliery shale/tailing/water at 60/20/20 per cent concentration by weight were prepared and pumped. Viscometer methods were also used to predict pipe pressure gradients. Data were collected using the pseudo-plastic equation and the slip model correlation. Provided the variations in slurry properties due to batching were taken into account, laboratory predictions were reported to be in good agreement with actual full scale pumping test results.

Tatsis et al. (1988b) described the design of a new probe for sensing a phase boundary in pipe flow of a solid-liquid suspension. The device was initially used for detecting the location of the dense phase in stratified flow but was modified subsequently to test its applicability to high concentration colliery waste. Tatsis et al. (1990) used this modified version of the probe to measure the annular thickness associated with plug flow of high concentration slurries . They developed a mathematical model based on a mechanistic approach to describe the case of eccentric plug flow. Their experimental data was compared with independent theoretical predictions and "excellent" agreement was reported to have been obtained. Their study suggests that minimum pressure loss requirements are satisfied under plug flow conditions. However, to ensure that plug flow occurs, they suggest further research work to establish the relationship between particle size distribution, core porosity and coarse and fines ratio with the size of rigid core. They also suggest making improvements to the design of the probe to make it re-usable.

Soszynski (1991) analyzed published experimental results concerning the plug flow of paper pulp suspensions with clear water annulus. He presented an exact solution to the Navier-Stokes equation which yielded the annulus thickness, the shear stress at the plug surface and the ratio of the plug to bulk velocity.

Paterson et al. (1992, 1993) attributed the pipe diameter dependency on the rheogram of some highly concentrated slurries to their "granulo-viscous" behaviour (Cheng 1977), which they described as "anomalous". The total shear stress, in this case, is a combination of both viscous shear stress and solid shear stress due to particle-pipe wall interaction. A method for subtracting out the viscous shear stress component from the total shear stress using experimental data for the pseudo-shear diagram was proposed. The remaining shear stress is taken to be a function of the coefficient of sliding friction between the particles and the pipe wall and the lateral dispersive stress.

Kalyon et al.(1993) presented a comprehensive study of the rheology of highly concentrated suspensions (Cv=76.5 %) using both capillary and torsional viscometers. Significant slip at the wall was observed in both the Poiseuille (capillary) and Couette (torsional) flow. A flow visualization technique was applied for the first time to determine the slip velocities in torsional flow directly and also to provide the true deformation rate and the feedback on yielding. The contribution of the slip of the suspension at the wall to the volumetric flow rate in capillary flow was found to increase with decreasing shear stress giving rise to plug flow at sufficiently low shear stress values. The observed plug flow is related to the shear thinning behaviour of the suspension (over the apparent shear rate range of 30-300 s^{-1}), and differs from the behaviour of shear thickening suspensions, which may exhibit plug flow at high wall shear stress values i.e. above a critical wall shear stress in capillary flow. Flow instabilities were observed at concentrations close to the maximum packing fraction, and there was clear evidence of the slip layer effect manifested by diameter dependence of the shear stress versus shear rate curve. The study is concluded by pointing out to the need for more research on the mechanics of plug flow and its dependence on the shear rate sensitivity of the suspension as well as on the modes of development of the apparent slip layer and its dependence on the geometry and the deformation field.

Among the above methods, some were based on simplifying assumptions reducing the suspension to a homogeneous medium which could be characterized by a standard rheological model (Elliot and Gliddon (1970), Sakuta et al.(1979), Duckworth et al. (1987)). Others adopted simplified versions of the Plug Flow

model (Menheimer (1985), Soszynski (1991)) or resorted to semi-empirical approaches for analyzing such flow behavior (Ede (1957), Browne and Bamforth (1977), Paterson et al. (1992, 1993)).

Whenever the rheogram of a concentrated suspension showed pipe diameter dependency, slip effect is often assumed to be the cause and Mooney's method or a variation thereof is usually used to correct for such "anomalous" behavior. It is well established that rheological data must be corrected for slip effect --whenever applicable, otherwise they are deemed of questionable validity.

Although several authors recognized the peculiar nature of slip in highly concentrated suspensions as being a result of Plug Flow with a annular layer (Cheng, (1975) , Ferguson and Kemblowski, (1991)), no theoretical analysis was made to date to substantiate such observations. Except for Soszynski (1991), who analyzed the special case of Plug Flow with a Newtonian annular layer, no attempt was made (to the authors' knowledge) to predict analytically the thickness of this layer in the case of a non-Newtonian fluid layer.

5.3 Proposed Model: Plug Flow With a Bingham Plastic Annular Layer

A schematic of the Plug Flow Model (PFM) with its velocity distribution are shown in Figure 5.1.

Laird (1957) derived an analytical equation for the flow of a Bingham plastic material in an annulus. Our derivation follows his analysis except that we assign a non-zero velocity boundary conditions at the core interface (i.e. $V(R_1)= V_c$).

The Bingham plastic equation is given by:

$$\tau = \tau_y + \mu \left|\frac{dV}{dr}\right| \qquad (5.1)$$

To allow the two shear stress terms to be additive , this equation may be written as:

$$\tau = \tau_y - \mu \frac{dV}{dr} \qquad (5.2)$$

Figure 5.1 Plug flow and velocity profile

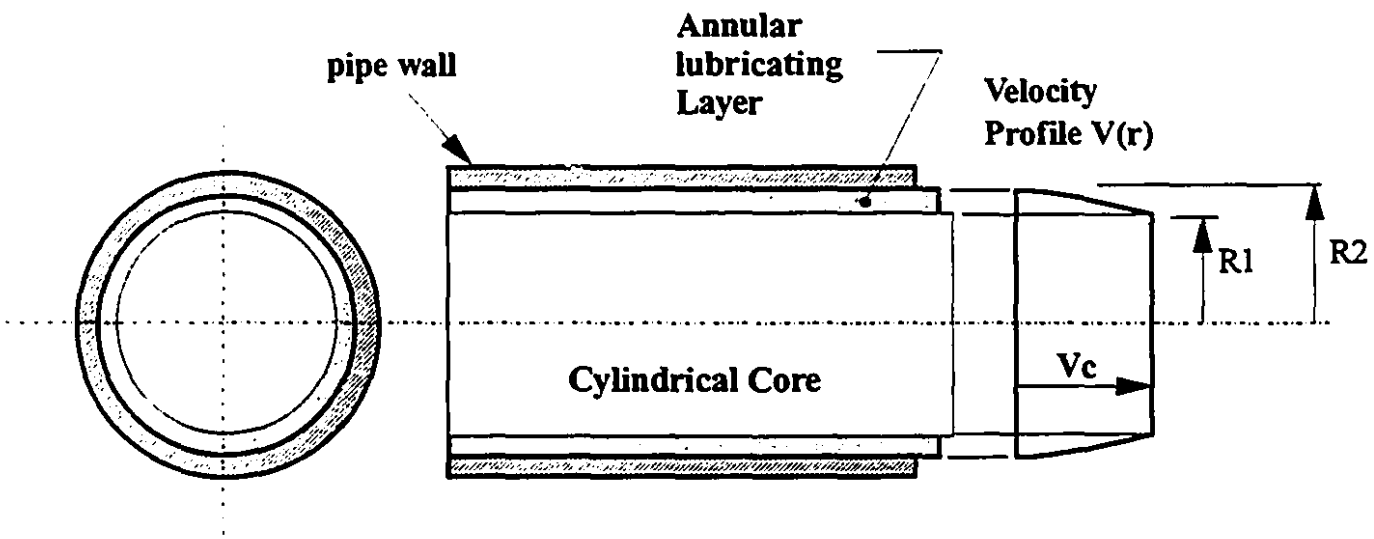

The shear force acting on the lateral surface of the core is given by:

$$A\cdot\tau = 2\pi rL\cdot(\tau_y - \mu\frac{dV}{dr}) \qquad (5.3)$$

Equating differential shear force and differential pressure force as r is increased to r+dr:

$$d\left(2\pi rL\cdot(\tau_y - \mu\frac{dV}{dr})\right) = d\,(\Delta P\pi r^2) \qquad (5.4)$$

Integration yields the velocity distribution equation:

$$V(r) = \frac{1}{\mu}\left(-\frac{\Delta P r^2}{4L} + B\cdot\ln(r) + \tau_y r + C\right) \qquad (5.5)$$

To obtain B and C, Apply the boundary conditions: $V(R_1)=V_c$ and $V(R_2)=0$:

$$B = \frac{1}{\ln(k)}\left(\mu V_c - \frac{\Delta P}{4L}(R_2^2 - R_1^2) + \tau_y(R_2 - R_1)\right) \qquad (5.6)$$

$$C = \frac{\Delta P R_2^2}{4L} - B\ln(R_2) - \tau_y R_2 \qquad (5.7)$$

Substituting B and C into the velocity distribution equation and rearranging, we obtain:

$$V(r) = V_c\left(\frac{\ln\left(\frac{r}{R_2}\right)}{\ln(k)}\right) + \frac{\Delta P}{4\mu L}\left((R_2^2 - r^2) - (R_2^2 - R_1^2)\frac{\ln\left(\frac{r}{R_2}\right)}{\ln(k)}\right) - \frac{\tau_y}{\mu}\left((R_2 - r) - (R_2 - R_1)\frac{\ln\left(\frac{r}{R_2}\right)}{\ln(k)}\right) \qquad (5.8)$$

Which is the velocity distribution for a fully developed laminar shear flow of a Bingham plastic fluid in an annulus (i.e. for R1<r<R2) with a non-zero velocity boundary condition at the core interface.

This Analytical solution reduces to that of Gandhi (1987) when the core is assumed to be free flowing and to that of Epstein (1963) and Charles (1963) when the annulus layer fluid is assumed to be Newtonian. Our model is also consistent with that of Tattersal and Banfill (1983), wherein shear flow takes place only in the annular region, while the rest of the material move as a solid plug.

A force balance on a control volume of a core section involving the pressure gradient acting on its cross-sectional area and the resisting fluid shear stress acting on its lateral surface yields:

$$\left(\frac{\Delta P}{L}\right)\cdot\pi R_1^2 L = (\tau_y - \mu\frac{dV}{dr})\cdot 2\pi R_1 L \qquad (5.9)$$

Differentiating Equation (5.8) with respect to (r) and substituting in Equation (5.9) yields the core velocity:

$$V_c = \frac{1}{\mu}\left(\frac{\Delta P}{4L}(R_2^2 - R_1^2) - \tau_y(R_2 - R_1)\right) \qquad (5.10)$$

Substituting Equation (5.10) in Equation (5.8) reduces the latter to the equation derived by Gandhi (1987) who assumed that the shear stress distribution is linear within the annular layer , i.e. $\tau(r) = \tau_w \frac{r}{R_2}$, for $R1 \le r \le R2$

to obtain:

$$V(r) = \frac{1}{\mu}\left(\frac{\Delta P}{4L}(R_2^2 - r^2) - \tau_y(R_2 - r)\right) \qquad (5.11)$$

Total flow rate is the sum of annulus and core flow rates, i.e.:

$$Q = Q_a + Q_c = \frac{\pi}{\mu}\left(\frac{\Delta P}{8L}\left(R_2^4 - R_1^4\right) - \frac{\tau_y}{3}\left(R_2^3 - R_1^3\right)\right) \qquad (5.12)$$

where:

$$Q_a = \int_{R_1}^{R_2} 2\pi r V(r) dr = \frac{2\pi}{\mu}\left(\frac{\Delta P}{16L}(R_2^2 - R_1^2)^2 - \frac{\tau_y}{6}(R_2^3 + 2R_1^3 - 3R_2R_1^2)\right) \quad (5.13)$$

$$Qc = \pi R_1^2 V_c = \frac{\pi R_1^2}{\mu}\left(\frac{\Delta P}{4L}(R_2^2 - R_1^2) - \tau_y(R_2 - R_1)\right) \quad (5.14)$$

Average flow velocity and average annular layer velocity are given respectively by:

$$V = \frac{Q}{\pi R_2^2} \quad (5.15)$$

$$V_a = \frac{Q_a}{\pi(R_2^2 - R_1^2)} \quad (5.16)$$

From the above equations, it is found that the pressure gradient increases as the average flow velocity increases for a constant k. This result is confirmed by the experimental findings of Duckworth et al. (1986) as will be discussed later.

The pressure gradient also increases as k increases for a constant flow velocity. Figure 5.2 shows a family of curves of pressure gradients versus k for different values of flow velocity.

5.4 Annular Layer Thickness Estimation

Considering the relation between the shear stress at the wall $\frac{D\Delta P}{4L}$ with the apparent shear rate $\frac{8V}{D}$, as described by Equations 5.12 and 5.15, the wall shear stress-shear rate relation for a Bingham plastic fluid in the annulus is given by:

$$\frac{D\Delta P}{4L} = \frac{4}{3}\tau_y\left(\frac{1-k^3}{1-k^4}\right) + \left(\frac{\mu}{(1-k^4)}\right)\frac{8V}{D} \quad (5.17a)$$

Figure 5.2 Variation of pressure gradient with k for increasing values of average flow velocity

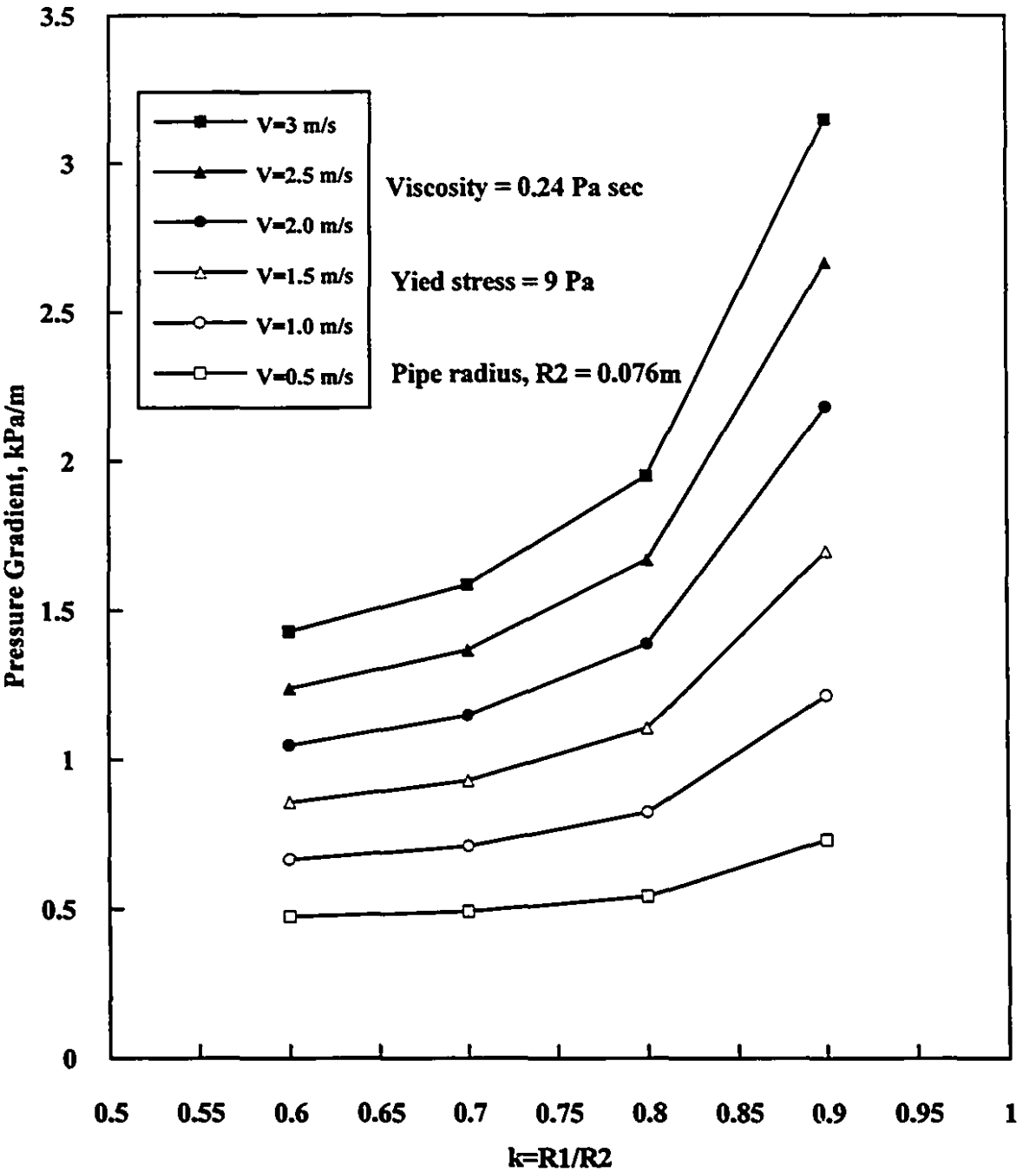

Equation (5.17a) may be related to the data of Duckworth et al. (1986) by equating it with the approximate Buckingham equation :

$$\frac{D\Delta P}{4L} = \frac{4}{3}\tau_{y_a} + \mu_a \frac{8V}{D} \qquad (5.17b)$$

From which, the apparent to actual viscosity ratio is found as:

$$\frac{\mu_a}{\mu} = \frac{1}{1-k^4} \qquad (5.18)$$

If the core radius is taken to be zero, i.e. the flow is entirely made up of the fluid suspension, then, as expected, the apparent viscosity and the actual one are identical.

The apparent to actual yield stress is given by:

$$\frac{\tau_{y_a}}{\tau_y} = \left(\frac{1-k^3}{1-k^4}\right) \qquad (5.19)$$

which correctly reduces to the Bingham plastic approximation when k=0. As the annulus layer thickness decreases (i.e as k approaches unity), the ratio of apparent to actual viscosity increases, whereas the ratio of apparent to actual yield stress decrease as shown in Figure 5.3

Assuming that Plug Flow with an annular layer is the transport mechanism, it is shown by Equations (5.18) and (5.19) that the measured (i.e. apparent) yield stress and viscosity of the material are a function of the core to pipe radius ratio k. To determine an estimate of the annular layer thickness, it is necessary to solve for the ratio k and to determine via independent measurements the actual viscosity and yield stress of the fluid material using methods described by Nguyen and Boger (1992).

Figure 5.3 Variation of apparent to actual yield stress and viscosity ratios with k

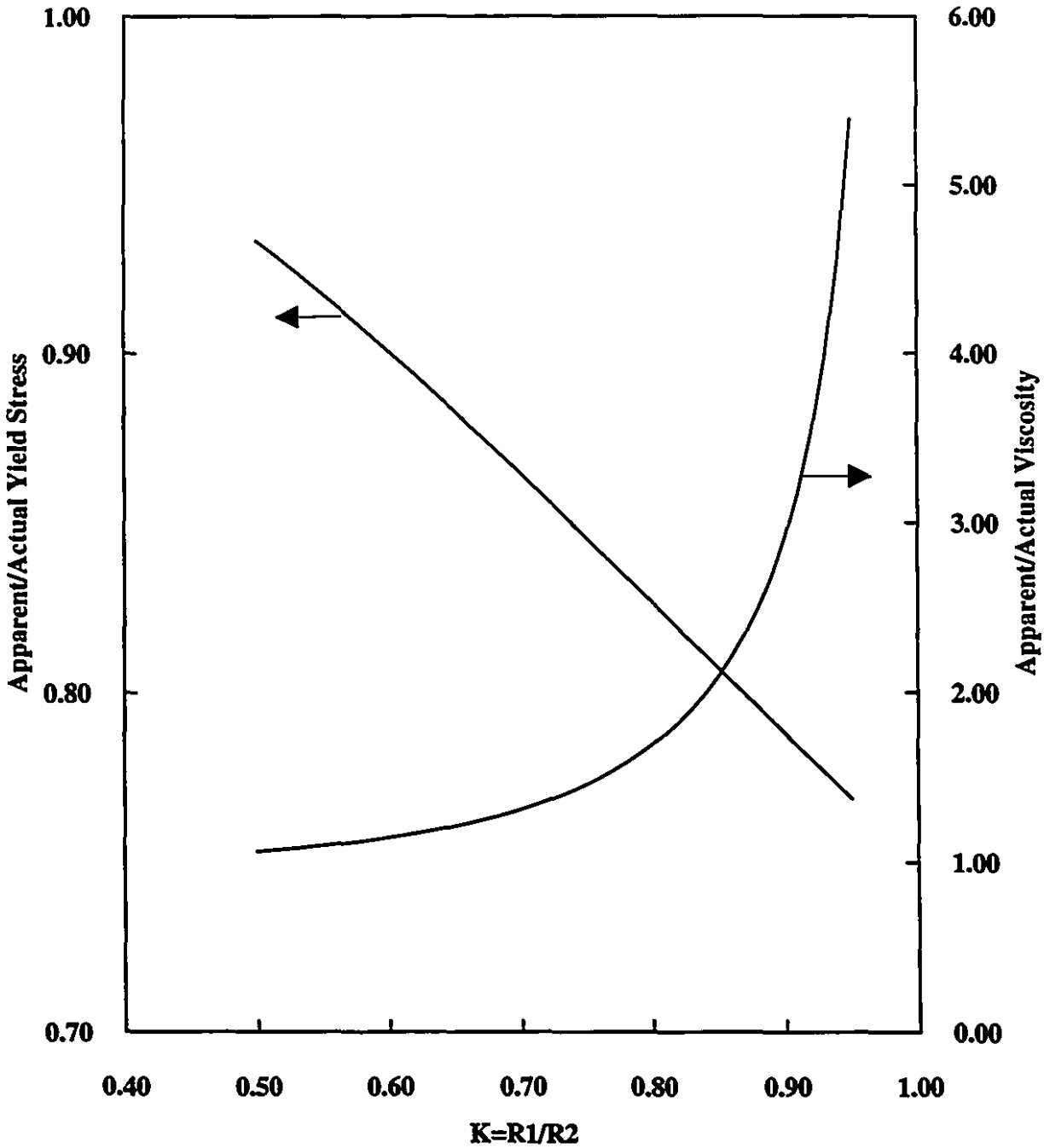

Hence, the thickness of the annular layer is given by:

$$\delta = R_2 (1 - k) \tag{5.20}$$

Using Equation (5.18), k can be obtained as:

$$k = \left(1 - \frac{\mu}{\mu_a}\right)^{0.25} \tag{5.21}$$

Similarly, k can also be obtained numerically from Equation (5.19)

5.5 Alternative Approach of Estimating Annular Layer Thickness

For a selected particle size distribution of coarse aggregates, the thickness of the annular layer is taken to be a function of the void content for loosely packed aggregates and the amount of rheologically active fines (-325 mesh). Minimum saturation state in the mixture is reached when the volume of the paste making up the annular layer is exactly equal to the void content. Any excess of paste volume (V_{paste}) beyond the voids volume (V_{voids}) is assumed to go toward increasing the annular layer thickness. This is expressed by :

$$V_{pipe} - V_{core} = \pi \cdot L (R_2^2 - R_1^2) = V_{paste} - V_{voids} \tag{5.22}$$

From which an estimate of the annular layer thickness is obtained as:

$$\delta = R_2 - \sqrt{R_2^2 - \frac{1}{\pi \cdot L}(V_{paste} - V_{voids})} \tag{5.23}$$

From which the ratio k is obtained as:

$$k = \sqrt{1 - \left(\frac{V_{paste} - V_{voids}}{V_{pipe}}\right)} \tag{5.24}$$

From the volume balance equation:

$$V_c + V_f + V_w = V_{pipe} \tag{5.25}$$

where V_c and V_f are the volumes of dry coarse and fine particles and V_w is the volume of water added.

Given the volume ratio of coarse to fine fractions as:

$$\frac{V_c}{V_f} = \alpha = \left(\frac{W_c}{W_f}\right)\left(\frac{S_f}{S_c}\right) \tag{5.26}$$

S_c and S_f being the specific gravity of coarse and fine solid particles respectively, and W_c and W_f the weight fractions of the coarse and fine particles respectively.

One, then obtains:

$$k = \sqrt{1 - \left(\frac{1+\alpha(1 - C_v)}{1+\alpha} - \frac{V_{voids}}{V_{pipe}}\right)} \tag{5.27}$$

The voids to pipe volume ratio can be estimated from a simple measurement by the voidmeter (described in section 5.8).The container of a representative sample of aggregates should have the same diameter as the pipe in question. Thus given the coarse to fine fractions ratio, and the volumetric concentration of solids, it becomes possible to predict the core to pipe diameter ratio k. This result is illustrated in Figure 5.4

Plug flow requires that no segregation occurs within the moving core of particles. To satisfy this condition, the particle size distribution should have the maximum amount of coarse aggregate possible which should be continuously graded down to give the minimum void content and fines. This would result in a high internal friction to the passage of the fluid phase but a low surface area of aggregate presented to the walls of the pipe. It is known in the literature (German, 1989) that a variety of multi-modal distribution could be designed to answer this requirement. Section 5.6 elaborates on this subject.

Figure 5.4 Variation of k with the voids to pipe volume ratio, Vv/Vp

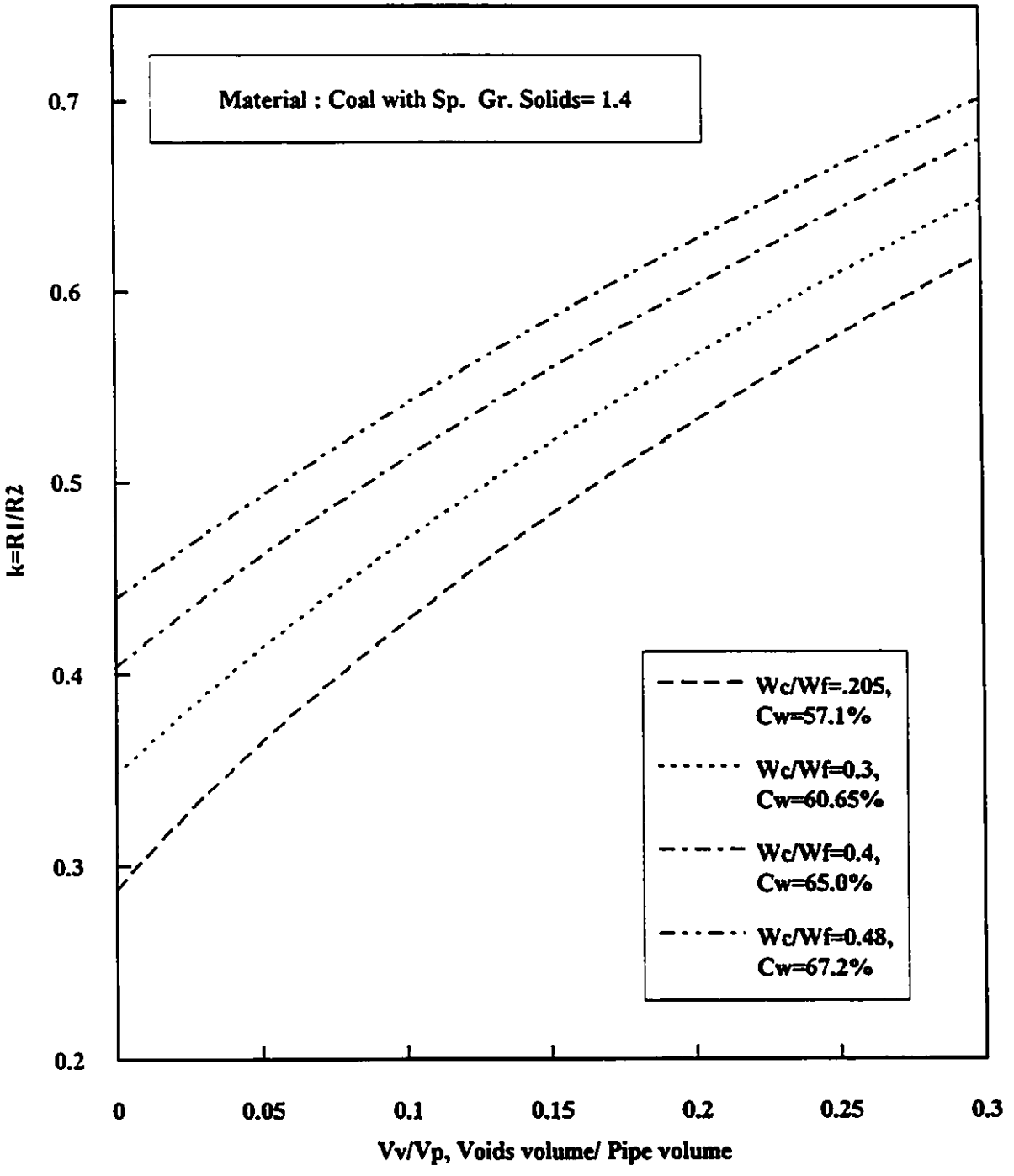

5.6 Particle Size Distribution of a Plug Flow Mixture: Case of Fresh Concrete

The concrete industry uses standard grading envelopes for preparing concrete mixtures known to give good workability and pumping characteristics. Figure 5.5 , 5.6, 5.7, 5.8 show the ASTM C33 specification limits for the grading of fine and coarse aggregates and the desired combined size distribution. The combined grading is recommended on the basis of experience gained in pumping mixes with different proportions (Popovics, (1982), ACI Committee 304, (1971-72), Powers,(1968)).

5.7 Mix Proportioning for Pumping: A Graphical Approach to Optimum Gradation (Wilson, F., 1974)

The pumpability and the workability of a mixture are influenced by variations in the properties of mix ingredients. Good gradation is the prime condition for pumpability. In general, pumpability is influenced by three factors:

- Gradation in all sizes
- Quantity, grind fineness, particle shape, and voids in the aggregate
- Sand size by quantity, Fineness Modulus (FM)

To ensure trouble free pumping, constant repeated uniformity of aggregate production , handling and mixing is required.

Some principles of early proportioning methods:

- **The Box method**: Available ingredients are combined in a variety of trial proportions until the trial volume (box) attains the heaviest weight.

- **The maximum density method**: Maximum density at the least total voids is sought through different trial mixes.

- **Minimum voids method**: The objective in this case is to seek the particle size distribution of coarse aggregates which offer the least voids so as to minimize the paste volume required to fill these voids. The Voidmeter described in section 5.8 is usually used for this method.

Figure 5.5 Coarse, fine and recommended combined particle size distribution for dmax=38.1mm(11/2 in)

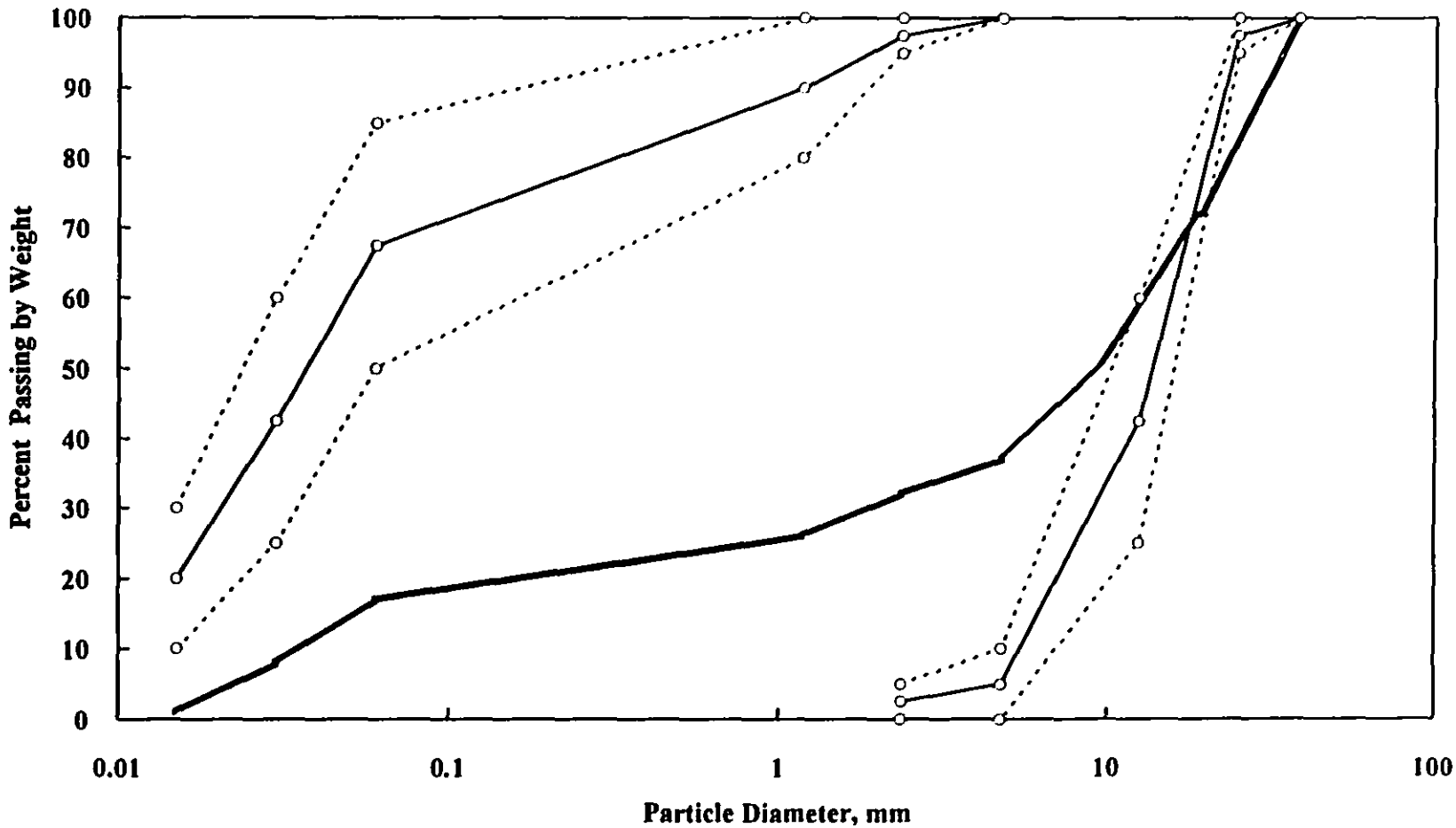

Figure 5.6 Grading of coarse, fine and combined aggregates for dmax=25.4mm (1in.)

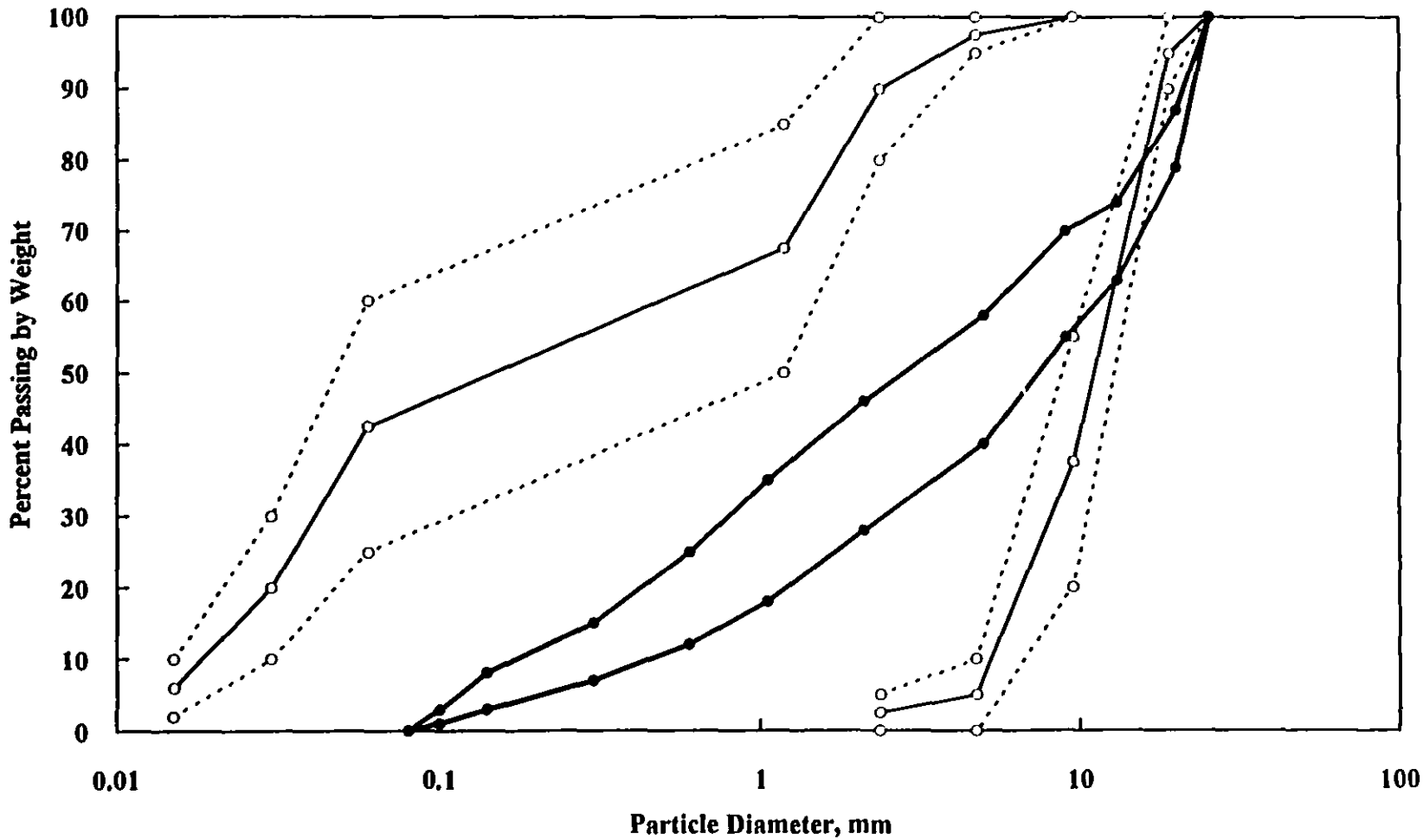

Figure 5.7 Grading of coarse, fine and combined aggregates for dmax=19.1mm (3/4 in.)

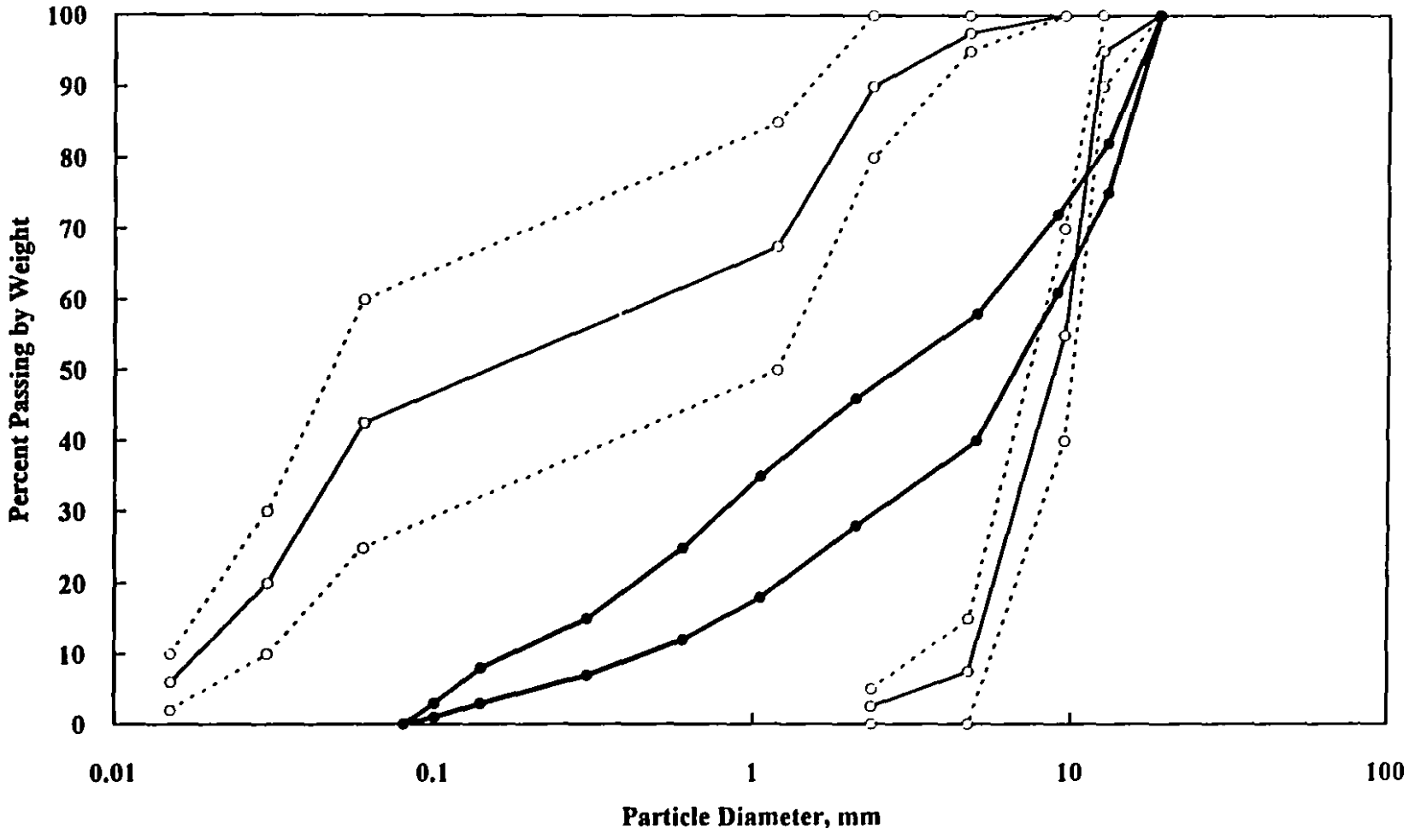

Figure 5.8 Grading of coarse and fine aggregates for dmax=12.5mm

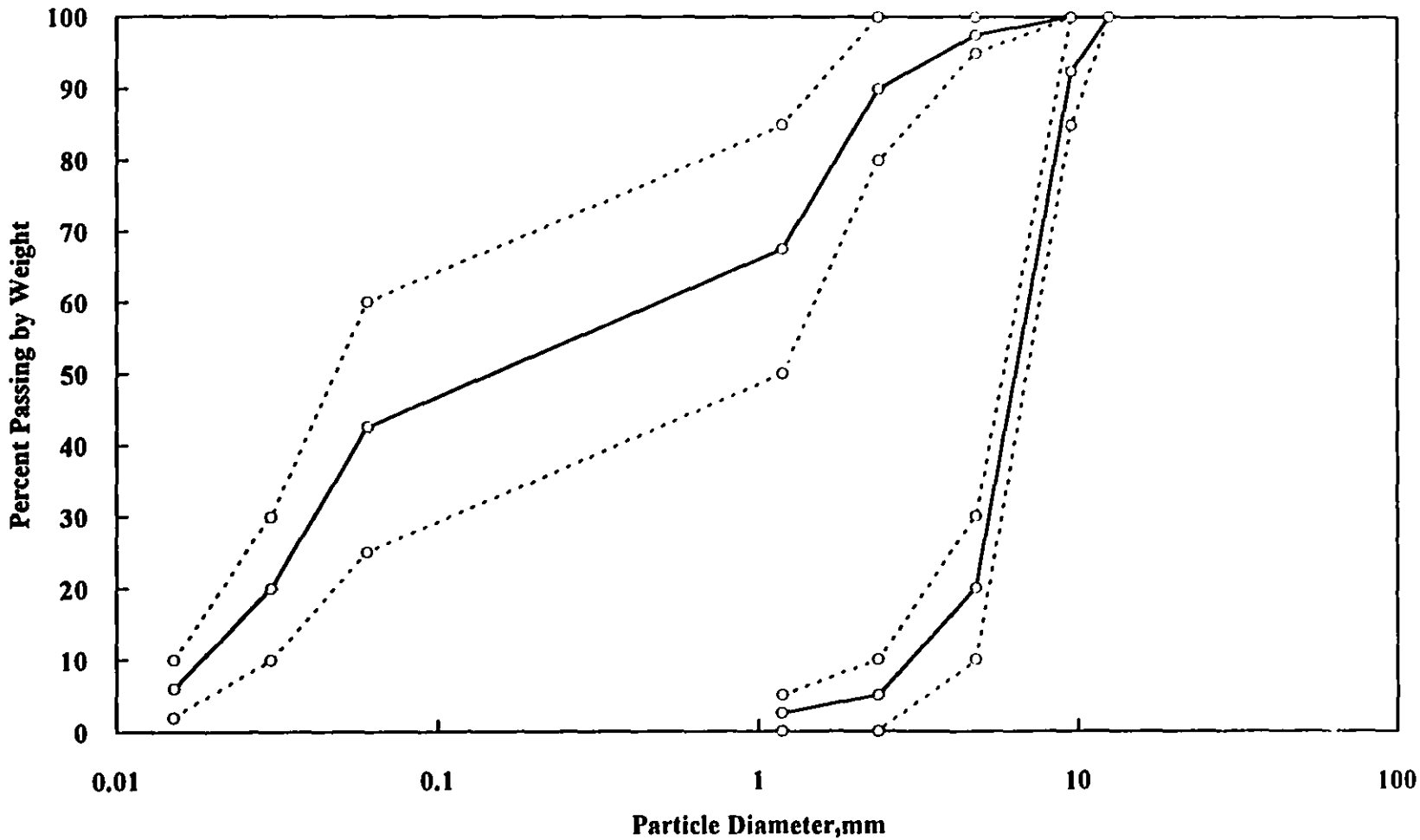

Figure 5.9 Graphical method for mix proportioning

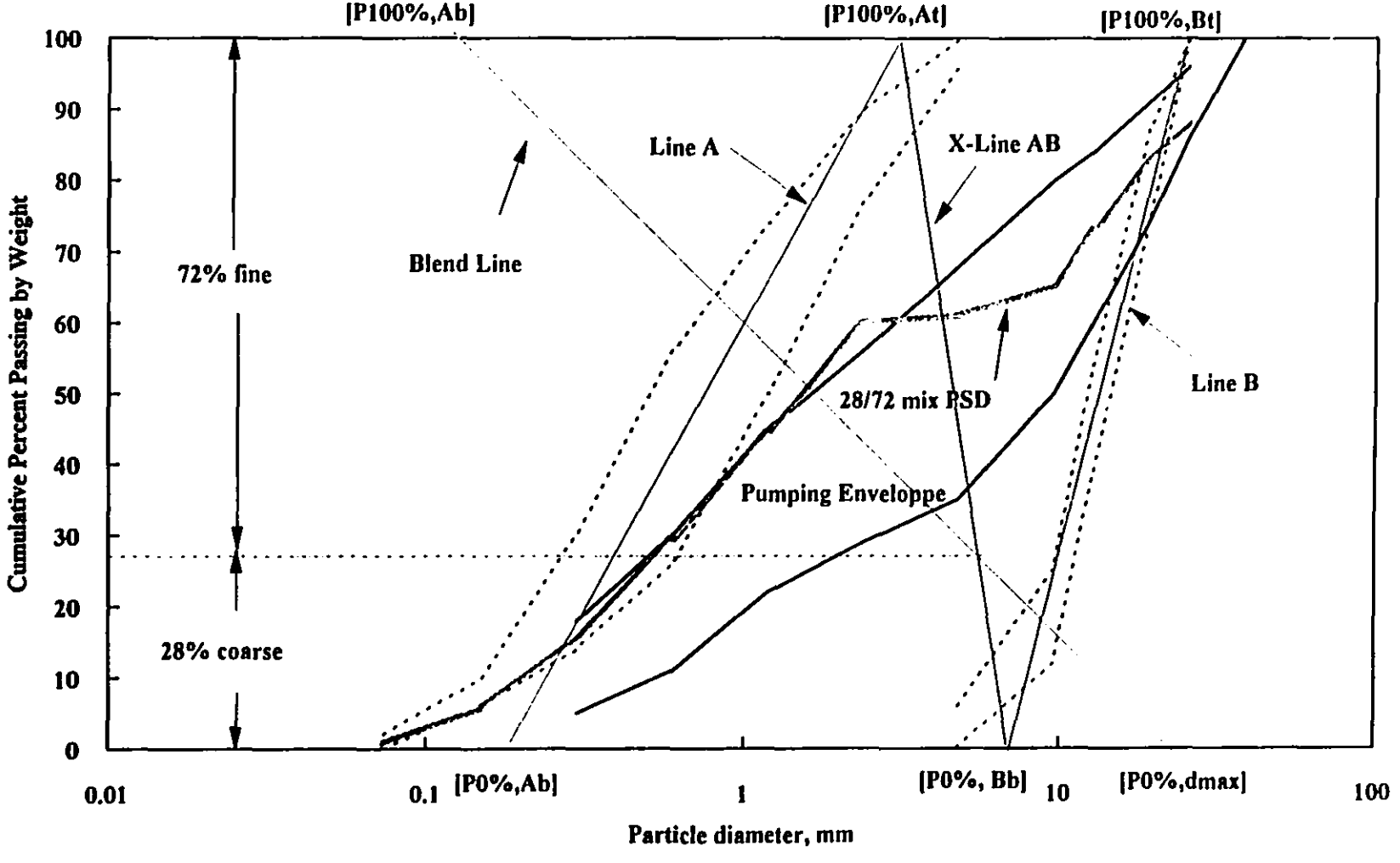

In addition to good workability, the above methods offer opportunities for substantial cement economy for cemented mine backfill.

Mostly empirical methods have dominated the field of mix proportioning. The use of combined grading envelopes for pumpability derived from experience has been widely used as illustrated above.

The following is a graphical method for proportioning coarse and fine aggregates giving optimum workability. This method allows the development of trial blend that is the most workable combination of given aggregates. This, however, does not guarantee that the proposed mixture will be suitable for pumping. Additional conditions are required as will be discussed further. Provisions are made in this graphical method to find the deficiencies if any in the aggregates, to indicate correction that may be desirable and to predict the influence of possible revisions. The procedure is outlined in the following steps and illustrated in Figure 5.9.

Step 1: Plot a histogram of the mixture to detect the presence of modes (components) of the mixture. If the components of the mixture are known, proceed to step 2.

Step 2: On a particle size distribution graph featuring percent undersize (passing) by weight versus particle size, it is recommended to plot the grading band of each component (mode) of the mixture. Coarse and fine aggregates in a bi-modal distribution, for example, should be represented by grading limits delineating the range of each component instead of single grading curves.

Step 3: Through each gradation line or band, draw a straight line in a median position (Line A and B). The points of intersections of these lines with top and bottom of the graph are noted (i.e. [P100%,At], [P0%,Ab], and [P100%,Bt], [P0%,Bb])

Step 4: Draw a line from the 100 percent passing line at the point [P100%, Ab] of the graph down to the intersection of the bottom (zero percent passing) line and the maximum aggregate size line at the point [P0%,dmax] , (dmax=38.1 mm in this example). Note that dmax is the actual maximum size in the aggregates, not the top

the top screen size with a percent retrained. The line drawn in this step is referred to as the Blend line.

Step 5: Draw cross lines from the 100 percent line intersection of the first aggregate component of step 2 to the bottom (zero percent line) intersection of the second aggregate component; then from the top of the second aggregate component to the bottom of the next component until the number of cross lines equals the total number of aggregate components minus one. In this example there is one cross line from point [P100%, At] to point [P0%,Bb].

Step 6: Intersections of the blend line obtained in step 4 with cross lines obtained in step 5 give the optimum percentages of each component for the mixture most likely to be the most workable (hence pumpable) combination of the materials graphed. Blend percentages should be recorded as the vertical percent increments, from the top down, of each intersection.

Step 7: Once the blend percentages are obtained, a graph of the resulting mixture should be plotted and compared with pumping/workability envelopes developed experimentally. Results obtained from this graphical method should come within close range of those obtained from reliable empirical mix proportioning methods for pumpability.

Proviso: For good pumpability, the combined blend should display a smooth curve in the middle of the grading curve. Horizontal part of the grading indicate deficiencies whereas vertical ones denote excesses, both of which can often be tolerated. If the combined line shows abrupt discontinuities that waver back and forth, then the mixture requires additional adjustments to become suitable for pumping.

5. 8 Void to Pipe Volume Ratio Measurement

In designing pumpable mixtures, careful grading of aggregates is required to minimize the void content in order to establish the so-called *blocked filter* effect which allows the fluid phase to transmit pressure without escaping from the mix. The objective of minimizing the void content is to produce maximum frictional resistance to the passage of the fluid phase within the mass of the mix and a

minimum frictional resistance to the walls of the pipe with a low surface area of aggregates.

In cemented fill, the cement paste occupies the interparticle voids. Minimizing these voids results in substantial saving of cement, however, this quantity of cement should be consistent with that required for the desired strength characteristics of the fill in place underground.

A void measuring apparatus, shown in Figure 5.10 was built similar to the one designed by Kempster (1969). A sample of aggregates are placed and compacted in a cylindrical container having the same diameter as the pipe to be used for conveying the mixture. The aggregates are compacted using a weight which also acts as a spacer used to determine when the container becomes filled with the required level. The air tight lid is then closed with the tap open. With the reservoir in position (A), the water level in the tube is brought to a predetermined level by adjusting the water level in the reservoir. The tap is closed and the apparatus is setup as shown in Figure 5.10. Void content in the sample is measured by lowering the reservoir to position (B) creating a pressure head in the measuring tube. After the water level settles to an equilibrium position , the void content of the sample can be read directly from a previously calibrated scale. Some typical values of void content for combined aggregate sand and cement are shown in Figure 5.11

The relative proportion of void and cement in a given mixture determines the pumpability as shown qualitatively and quantitatively in Figure 5.12.

According to Rumpf (1990), if samples of a given volume are taken from the random packing, then their porosity ε_{sa} will vary randomly from sample to sample. Their expected value is that of the porosity of the whole packing, i.e.:

$$E(\varepsilon_{sa}) = \varepsilon \qquad (5.28)$$

The variance of the porosity ε_{sa} of the samples can be calculated. If the packing consists of particles of equal size of volume υ_p, then it follows that:

Figure 5.10 Voidmeter

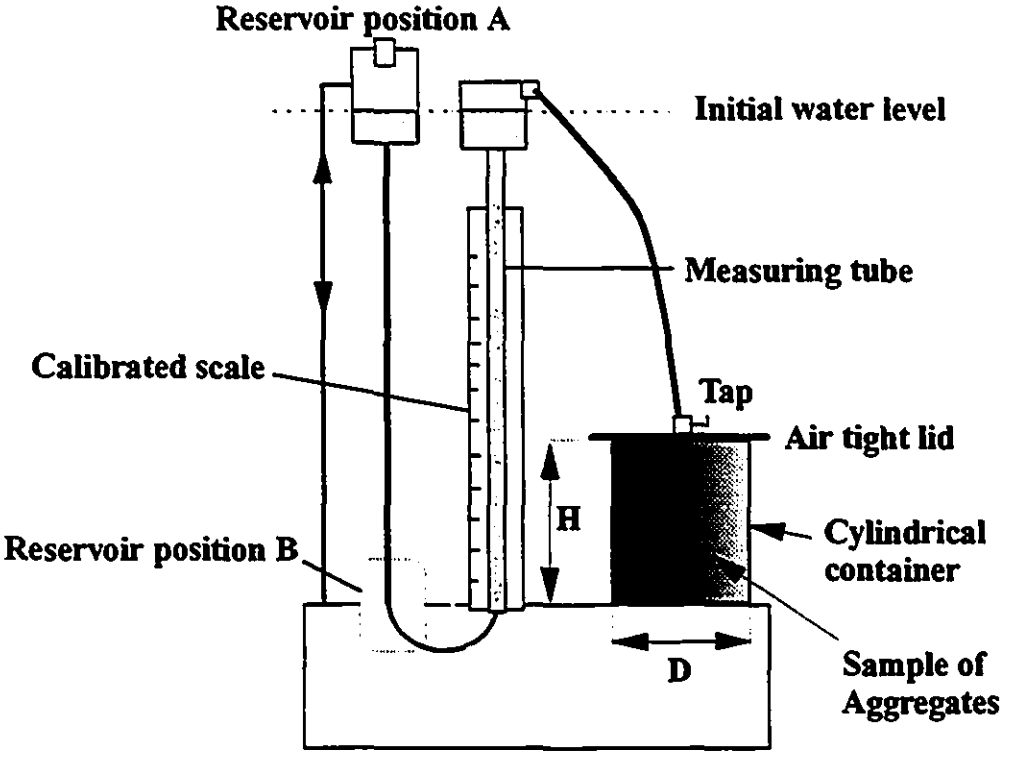

Figure 5.11 Void content of total volume as a function of cement and sand content (adapted from Cooke, 1990)

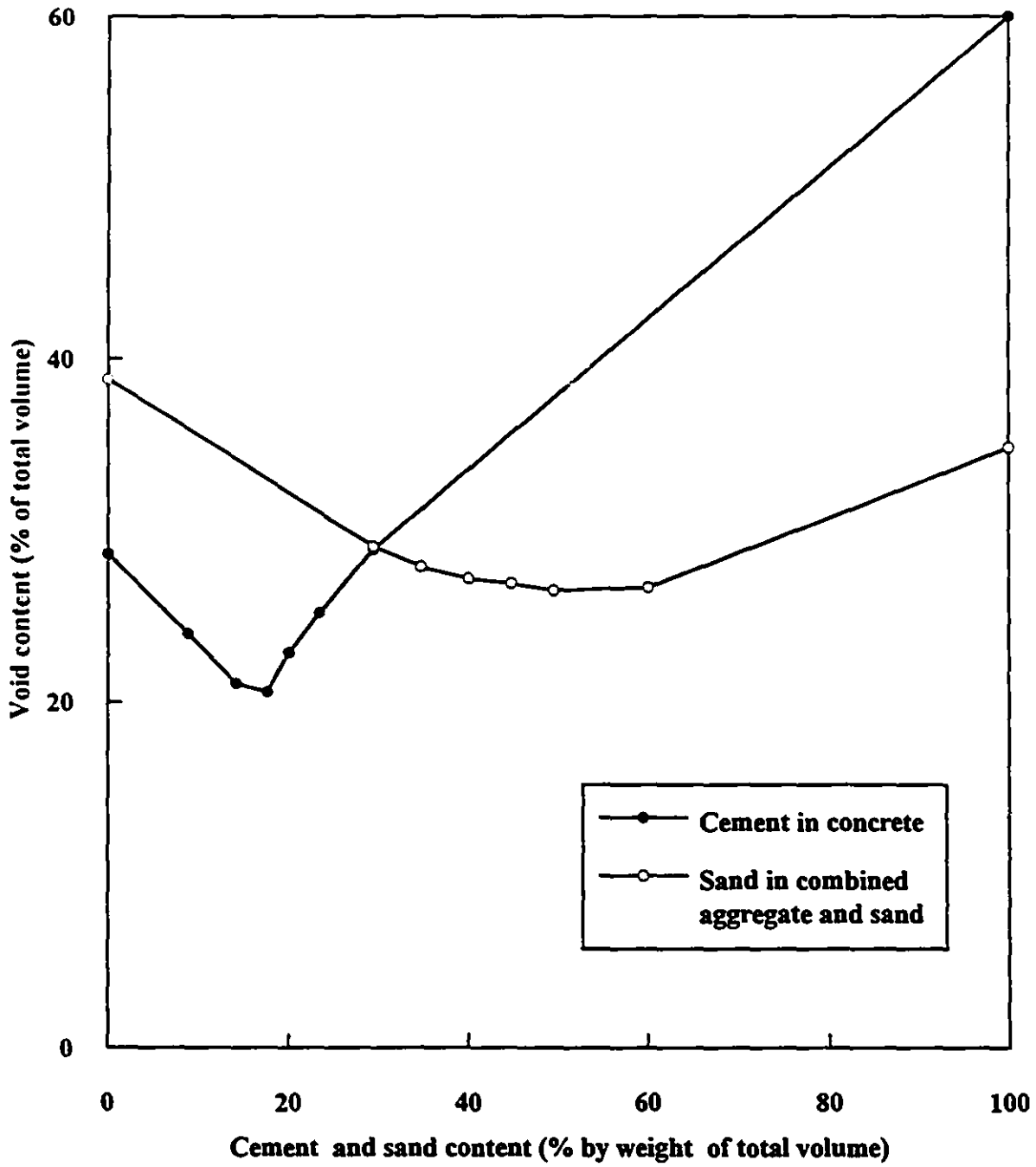

Figure 5.12 Effect of voids content in combined aggregates in relation to cement indicating pumpability (adapted from Kempster, 1969)

Cement content by volume	Void content volume 17% 1	20% 2	25% 3	28% 4
Z 15%	pumped	pumped but * blocked during experiment	did not * pump	did not pump
Y 20%	pumped	pumped	pumped *	did not pump
X 25%	pumped	pumped	pumped	did not * pump
W 30%	pumped with difficulty	pumped	pumped	did not * pump

* Mixes which became pumpable when cellulose ethers were added. Sand content 35%of combined aggregates in all mixes. Water content adjusted to give 75 mm slump

$$\sigma^2_{\varepsilon_{sa}} = \frac{\varepsilon(1-\varepsilon)\upsilon_p}{V_{sa}} \qquad (5.29)$$

where V_{sa} is the volume of the sample. This analysis is also applicable to packings of non-uniform particles.

5. 9 Comparison with Measured data of Duckworth et al. (1986)

The data of Duckworth et al.(1986) does not include the voids fraction values in the coarse aggregates therefore only the first method of predicting k will be used for comparison with experimental data.

The data presented by Duckworth et al. (1986) and summarized in Table 5.1 include the *actual* yield stress and *actual* viscosity of an initial suspension with no coarse particles, (i.e. data set #1, τ_y = 5.3 Pa, μ=0.13 Pa sec). The remaining data sets # 2,3,4, and 5 represent mixtures with increasing coarse solids content (with *apparent* viscosity and yield stress values) . Assuming that the composition of the annular layer remains unchanged and that the effect of adding coarse particles leads only to an increase in the core diameter; then it becomes possible to predict the parameter k (hence the annular layer thickness) by considering either the viscosity or the yield stress data. Theoretically either method should yield the same answer.

For the apparent viscosity data, Equation (5.18) offered values within 7% average deviation from the values given by Gandhi (1987). For the yield stress data, Gandhi (1987) observed that the reported increase in the yield stress values due to the addition of coarse particle (hence an increase in k) cannot be theoretically justified. Indeed our results show that an increase k should instead be coupled with a decrease in the values of apparent yield stresses.

The viscosity data was deemed more reliable than the yield stress data due to the better known techniques for measuring viscosity compared to those of measuring yield stress. Inference of yield stress from a rheogram is not recommended,

instead, direct determination as described by Nguyen and Boger (1992) is preferred.

Since the actual and apparent yield stress are within less than 15 % of each other as k is varied within a wide range (Figure 5.3), it is argued that the most likely valid value for the actual yield stress should be close to the measured ones rather than to that of the initial suspension (data set #1). This rationale is confirmed by the results obtained in Figure 5.13, where it was assumed that the actual yield stresses of the material at various concentration are those given in Table 1 for each data set , while the actual viscosity for all data sets is that of the paste suspension (data set #1).

If the actual yield stress of the suspension is taken to be that of the original one (i.e. data set #1) for all data sets, then the agreement between theoretical results and experimental data is not as good as in the previous case. Using values of k predicted from viscosity data and Equation (5.18), and taking the yield stress of data set #1 (i.e. τ_y = 5.3 Pa. sec.) to be the actual yield stress, it was possible to compute apparent yield stresses from Equation (5.19) which are consistent with k values obtained from Equation (5.18), as shown in Table 5.2 These calculated values however were not consistent with the ones reported by Duckworth et al. (1986).

From the above, it was found that only viscosity data could yield meaningful estimates for the annular layer thickness. Good prediction of pressure gradient as a function of flow velocity was possible only when apparent yield stresses (instead of the actual one) were used with the actual viscosity of the suspension.

For accurate results it is recommended to perform independent measurements of the magnitude of the annular layer thickness coupled with careful measurements of apparent and actual viscosity and yield stresses.

Figure 5.13 Model predictions with actual viscosity and apparent yield stress

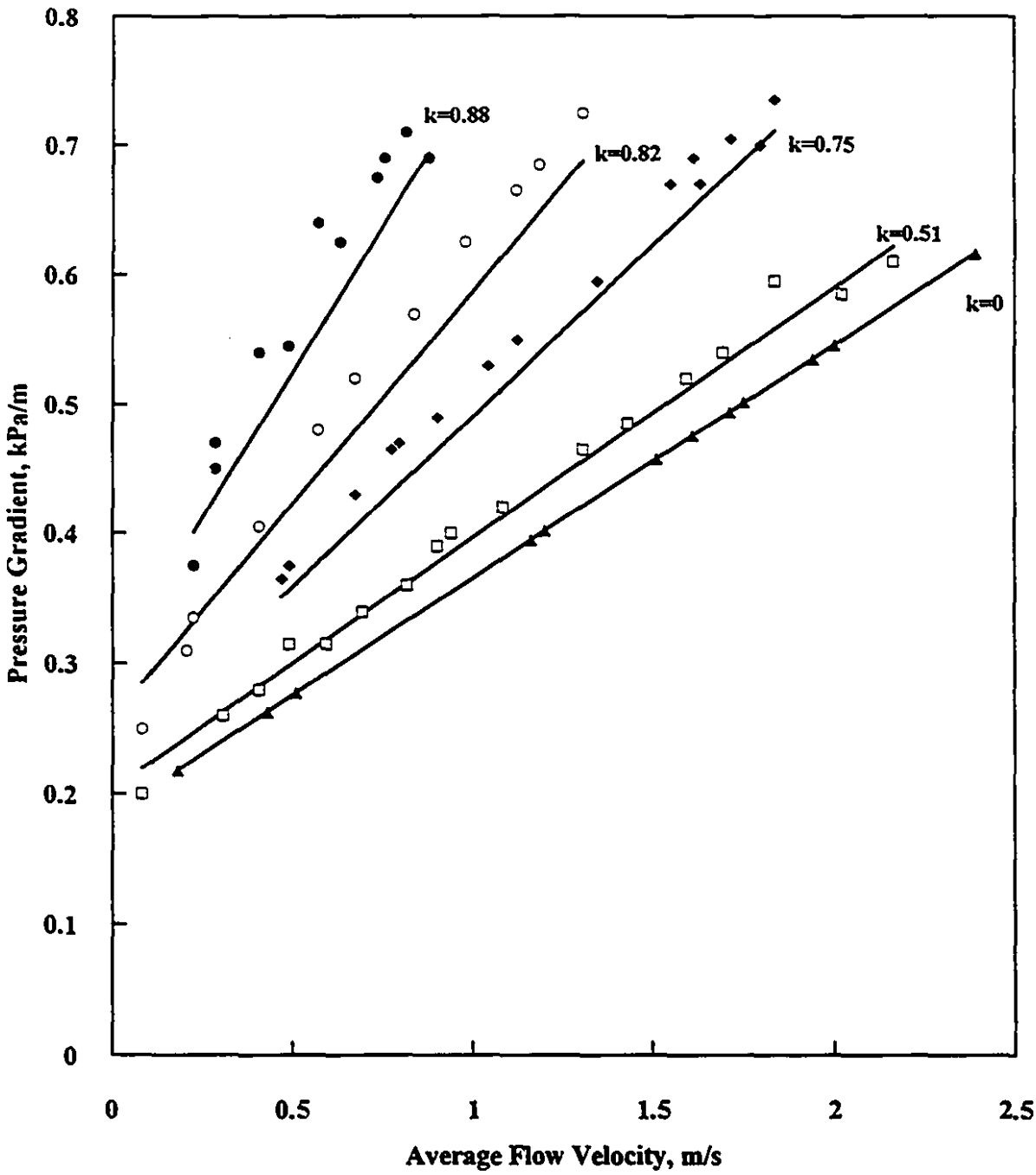

Table 5.1
Predicted k values based on Duckworth's et al (1986) data

Data set #	$\frac{W_c}{W_f}$	Cw, %	τ_y, Pa	μ, Pa.sec.	k from Eq. (18)	k from Gandhi (1987)
1	0	53.25	5.3	.13	-	-
2	.205	57.1	6.25	.14	.51	.6
3	.3	60.65	7.67	.19	.75	.79
4	.4	65.0	9.0	.24	.82	.87
5	.48	67.2	10.74	.32	.88	.93

Table 5.2
Calculated and reported (Duckworth et al. (1986))
apparent yield stress for different k values

k	.51	.75	.82	.88
τ_{y_a} (calculated)	4.93	4.48	4.34	4.22
τ_{y_a} (reported)	6.25	7.67	9.0	10.74

5.10 Slip Phenomena-The Classical Approach (Mooney (1931), Jastrzebski (1967), Heywood(1991))

The wall slip effect can be detected by using several pipe diameters to plot the wall shear stress τ_w versus nominal shear rate $\frac{8V}{D}$ diagram. If curves for different pipe diameter do not coincide, not because of turbulent , non-homogeneous or time dependent flow, then wall slip is the most likely source of discrepancy.

Assuming that slip is detected, it is necessary to correct the expression of the nominal shear rate used in the shear stress shear rate diagram. This is done by replacing the nominal shear rate $\frac{8V}{D}$ by $\frac{8(V-V_S)}{D}$, where V_S is the effective slip velocity , which can be determined from flow tests. This method indicates that slip results in a flow rate increase through the pipe compared to the non-slip condition.

The total flow rate derived from this method is given by :

$$Q = \frac{\pi D^2}{4} V_S + \frac{\pi}{8}\left(\frac{D}{\tau_w}\right)^3 \int_0^{\tau_w} \tau^2 f(\tau) d\tau \qquad (5.30)$$

And defining the effective slip coefficient by :

$$\beta = \frac{V_S}{\tau_w} \qquad (5.31)$$

In addition to being a function of τ_w, β was found to vary inversely with pipe diameter. Redefining the slip coefficient to make it depend only on shear stress:

$$\beta' = \beta D^q \qquad (5.32)$$

Substituting in equation (5.30) and rearranging, one obtains:

$$\frac{32Q}{\pi D^3 \tau_w} = \frac{8\beta'}{D^{q+1}} + \frac{4}{\tau_w^4} \int_0^{\tau_w} \tau^2 f(\tau) d\tau \qquad (5.33)$$

For a given value of wall shear stress τ_w, the slip coefficient β' can be determined as the slope of $\frac{32Q}{\pi D^3 \tau_w}$ versus $\frac{1}{D^{q+1}}$ for a range of pipe diameters.

The slip velocity is then given by:

$$V_s = \beta' \tau_w \qquad (5.34)$$

In many applications a value of q=1 resulted in a satisfactory linear fit of experimental data. It is also suggested that a value q should be selected to give a good linear fit of experimental data.

5.11 Assessment of the Suitability of the Classical Approach of Slip Analysis to Plug Flow

Although the empirical method proposed originally by Mooney (1931) to correct for slip effect may be applicable to a wide class of non-Newtonian fluids, it may not be suitable for suspensions for which apparent slip is defined in terms of Plug Flow with an annular lubricating layer (Dealy, (1994)). In Mooney's approach, slip is defined as a non-zero velocity boundary condition at the pipe wall, whereas in Plug Flow, no actual slip takes place at the pipe wall. Instead flow resistance is substantially reduced due to the presence of the annular layer.

Although this fluid layer has zero velocity at the wall, the bulk of the suspension moves relative to this layer. Regarded as one flowing medium, the suspension appears to have an *effective* slip velocity with respect to the wall.

From the expression of the total volumetric flow rate, the following expression is obtained:

$$\frac{Q}{\pi R_2^3 \tau_w} = \frac{1}{4\mu}\left(\left(1 - \left(\frac{R_1}{R_2}\right)^4\right) - \frac{4}{3}\frac{\tau_y}{\tau_w}\left(1 - \left(\frac{R_1}{R_2}\right)^3\right)\right) \qquad (5.35)$$

This equation clearly shows that no linearity exists between the left hand side of Equation (5.35) and $\frac{1}{R_2}$ or even $\left(\frac{1}{R_2}\right)^2$ as would be the case for Mooney's method. This significant result emphasizes that the annular lubricating layer effect in Plug Flow is indeed physically different from slip in the sense of Mooney's method. Thus the shear stress-shear rate dependence on pipe diameter could readily be explained in terms of the Plug Flow model by recalling that the shear stress-shear rate relationship is a function of k, which is inversely proportional to pipe diameter. Failure to realize this, may lead to using Mooney's method, where it is not applicable. This misinterpretation occurs whenever the dependence of the shear stress-shear rate curves on pipe diameter is erroneously understood as slip along the pipe wall instead of Plug Flow with an annular lubricating layer, which is a more likely flow mechanism for highly concentrated suspensions.

5.12 Maximum Pumping Distance

5.12.1 Saturated Flow with Annular Layer

Saturation of the mix is established when the pores of the aggregates are completely filled with a mixture of water and fine particles in the form of a paste. A tendency to squeeze out paste or water from the mixture under pressure was taken by Ede (1957) as an indication of saturation. The pressure loss in the pipeline for a saturated mixture was found to be linear with the distance pumped, and the pressure at any point in the line is given by:

$$P(x) = P_o - \frac{4 R_A x}{D} \qquad (5.36)$$

where:

$P(x)$	=	pressure in the pipeline at a distance x from the pump
P_o	=	pressure at the pump outlet
D	=	internal pipe diameter
R_A	=	flow resistance per unit area of pipe

The maximum distance pumpable in the saturated state is the distance where P(x) becomes zero, and is given by:

$$x_{max} = \frac{P_0 D}{4R_A} \qquad (5.37)$$

The forces to which an element of the plug is subjected, and the variation of concrete pressure down the pipeline in the case of a saturated mixture are shown in Figure 5.14 . Assuming steady flow conditions, the forces acting on the plug element are the pressure forces opposed by the friction forces resisting the flow. All shearing action is assumed to take place in the annular layer.

Figure 5.14 Saturated Mixture

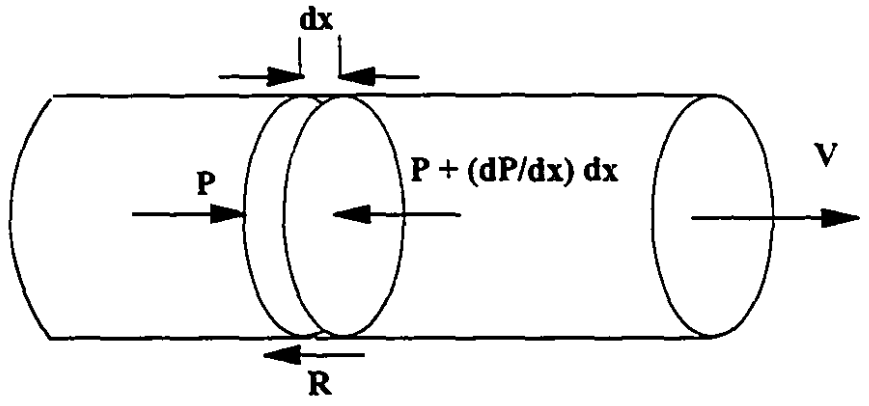

(a) Force balance

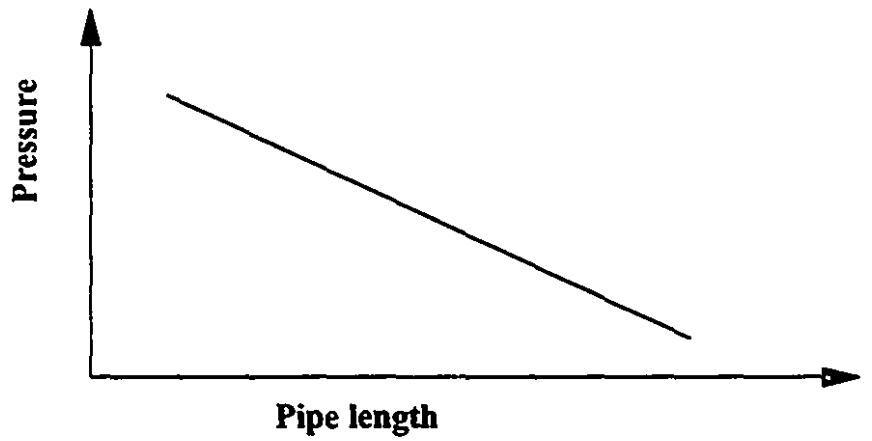

(b) Pressure variation with pipe length

5.12.2 Unsaturated Flow

In the absence of sufficient paste to fill aggregate voids and to form an annular lubricating layer, the mixture may be in the unsaturated state. In this case the pressure drop becomes exponential along the length of the pipeline . This resistance to flow is caused by the high sliding friction between solid particles and the pipe wall, which makes the radial pressure under unsaturated condition significantly less than the axial pressure. Ede (1957) showed that the axial pressure is given by:

$$P(x) = P_o \exp\left(\frac{-4\mu k\, x}{D}\right) - \frac{\left(1 - \exp\left(\frac{-4\mu k\, x}{D}\right)\right)A}{\mu k} \qquad (5.38)$$

from which the maximum pumpable distance for unsaturated flow is found as:

$$x_{max} = \frac{-D}{4\mu k} \ln\left(\frac{A}{P_o \mu k + A}\right) \qquad (5.39)$$

μ = coefficient of friction between the concrete and the pipe wall
A = adhesive resistance (similar in concept to the yield stress)
k = radial pressure-axial pressure ratio in the pipe

The forces to which an element of the plug is subjected, and the variation of concrete pressure down the pipeline in the case of a unsaturated mixture are shown in Figure 5.15. The effect of water-cement ratio on the axial pressure is summarized in Figure 5.16. It is clear that unsaturated flow should be avoided by making use of the mix proportioning and design methods described in this chapter.

Figure 5.15 Unsaturated Mixture

(a) Force balance

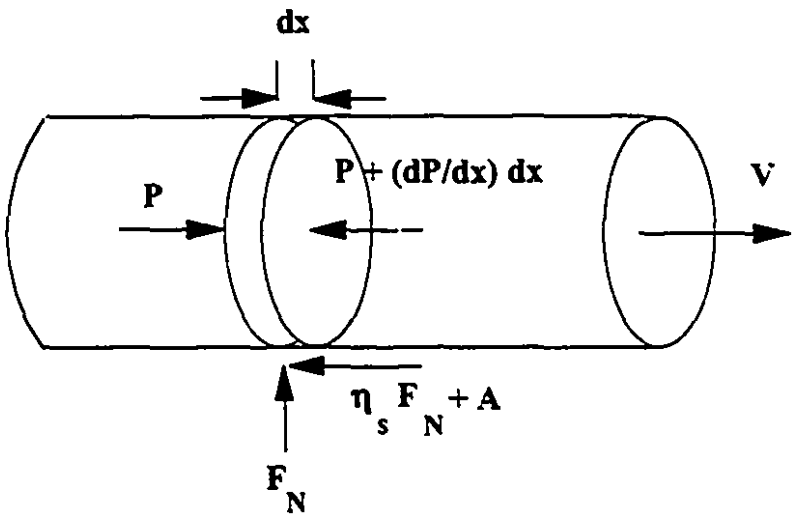

(b) Pressure variation with pipe length

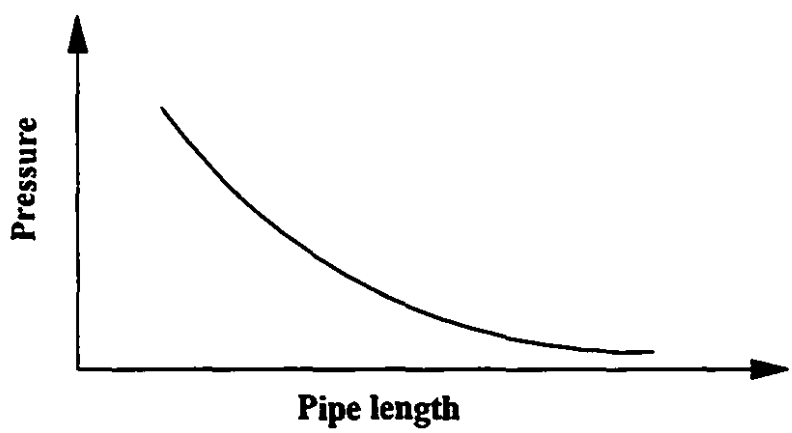

Figure 5.16 Effect of water-cement ratio on the pumping pressure
(adapted from Ede, 1957)

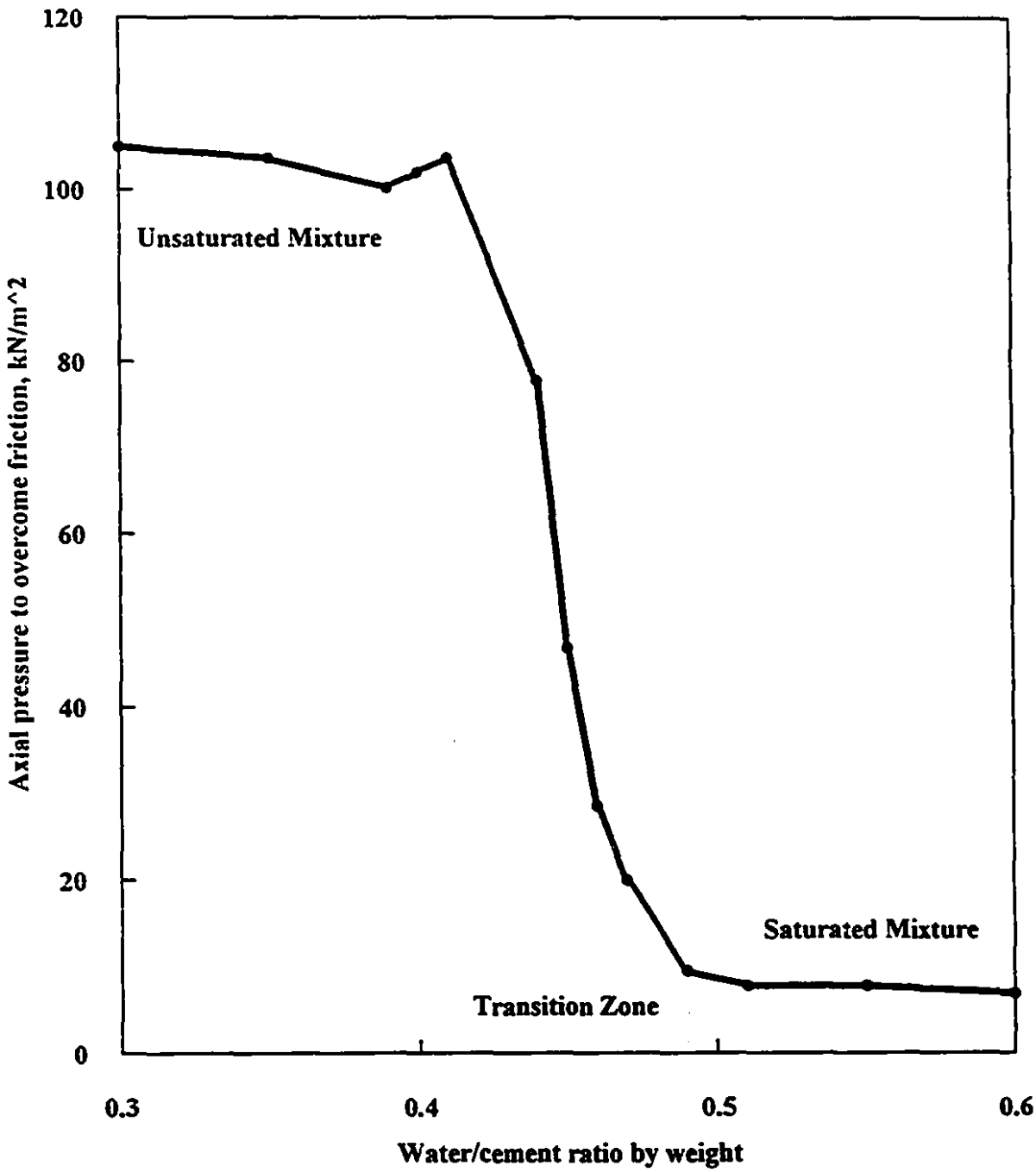

5.13 Conclusion

A general equation for the flow of a moving core of solid particles surrounded by a Bingham plastic annular layer was derived. This Plug Flow model depicts the flow behavior of a wide variety of highly concentrated suspensions whose motion through capillary viscometers or pipelines is made energy efficient owing to the existence of this annular layer.

Mooney's method for slip effect correction was shown to be inapplicable in case of Plug Flow where pipe diameter dependency of rheograms and the reduction in flow resistance are due to the existence of an annular lubricating layer.

Analytical predictive equations for estimating the thickness of the annular layer were proposed. This thickness controls the magnitude of the resulting pressure gradient measured.

Experimental data of Duckworth et al. (1986) was used to evaluate our theory. It was found that only viscosity data could yield meaningful estimates for the annular layer thickness. Good prediction of pressure gradient as a function of flow velocity was possible only when apparent yield stresses (instead of the actual one) were used along with the actual viscosity of the suspension.

CHAPTER SIX

TRANSORT OF MIXED REGIME SLURRIES: THE TWO-LAYER MODEL

6.1 Introduction

Since its publication, the two-layer model, proposed by Wilson et al.(1972), has been the focus of a great deal of attention due to its original approach in modeling the mechanism of solid-liquid transport in pipelines. The origins of this model go back to the work of Newitt et al. (1955) who investigated the flow of low concentration coarse particle mixtures in saltation or sliding bed, and developed pressure loss equations which could be applied for scale-up calculations. However, the derivation of Newitt's equation did not take the highly stratified nature of the flow into account. Wilson's model is also based on Streat & Bantin's (1972) work, where experiments were conducted with coarse slurries at high concentration to determine in-situ concentration and pressure losses.

Initially Wilson's model was restricted to very coarse particles and did not contain empirical parameters. A constant kinetic coefficient of friction was used, which could be determined from sliding friction tests using a ring shear cell or by tilting a section of a pipe and noting the point at which continuous sliding occurs. Later versions of the model extended the original concept to include finer particles and mixtures of coarse and fine solids. However, this required the use of flow derived coefficients to match the model with experimental data. This model is used to estimate pressure drop and to scale-up experimental data to larger pipe diameters for settling slurries.

The central feature of the two-layer model is the stratification of the flow , wherein the lower layer, made up of a contact (or bed) load, moves "en bloc" along the pipe wall; and an upper layer made up of the fluid medium in which a portion of solid particles may be suspended. The two-layer model is shown graphically in Figure 6.1

Figure 6.1 Definition of the two-layer model parameters

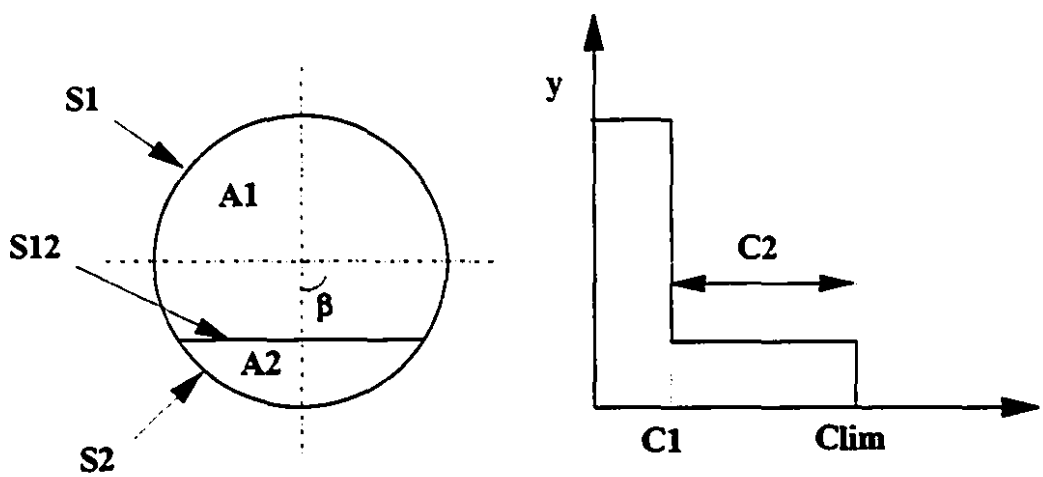

(a) Pipe cross section **(b) Concentration distribution**

The slurry flowing in a horizontal pipe is assumed to be divided into two layers separated by a horizontal surface. Each layer is assumed to have a constant solids concentration and velocity when computing boundary stresses and the stress at the interface. The mixture in the upper layer of volumetric concentration C1 is assumed to behave as a fluid as far as the stresses are concerned. The lower layer is assigned a concentration of loose-packed bed, C_{lim} , which could be determined from non-flow measurements . Head loss predictions for coarse particles is rather insensitive to the value of C_{lim} unless particle size distributions is very broad and the mean concentration is very high (Shook and Roco (1991)). Concentration increment C2 consists of particles whose immersed weight is transmitted to the pipe wall by interparticle contact. Coulombic sliding friction is assumed to occur at the contact between the wall and the lower layer

In the following, a statement of the two-layer model is presented with developments pertinent to the concentration distribution in the upper layer. The computational procedure for solving the problem and a discussion of some aspects of the model are also given.

Each layer will be represented by its average properties i.e. mean velocities and concentrations. It is assumed that slip (due to the higher flow velocity of the fluid phase with respect to the solids phase) does take place in the lower layer, therefore generating hydrodynamic forces that will be taken into account.

6.2 Model Development

Many versions of the two-layer model are found on the literature. The following is an updated version based on the work of Televantos et al. (1979), Doron et al. (1987), and Shook and Roco, (1991). The model uses momentum equations for each layer, expressed in terms of the boundary and interfacial stresses. For steady horizontal pipe flow, the momentum equation for the upper layer and lower layers are respectively given by:

$$\frac{dP}{dx} + \frac{\tau_1 S_1 + \tau_{12} S_{12}}{A_1} = 0 \qquad (6.1)$$

$$-\frac{dP}{dx}+\frac{\tau_{12}S_{12}-(\tau_{2f}S_2+\tau_{2s}S_2)}{A_2}=0 \qquad (6.2)$$

The shear stresses τ_1, τ_{2f} are given by:

$$\tau_1=\frac{f_1 V_1^2 \rho_1}{2} \qquad (6.3)$$

τ_{2f} is related to the fluid velocity near the wall of the lower layer. Using the mean fluid velocity V_{2f}, the friction factor f_2 and the density ρ_2:

$$\tau_{2f}=\frac{f_2 V_{2f}^2 \rho_2}{2} \qquad (6.4)$$

The friction factors in the above equations should be calculated from the viscosity and density of the mixtures in the upper and lower layer and the equivalent hydraulic diameters of the regions (Doron et al.1987) as given by:

$$f_1=\alpha_1\left(\frac{\rho_1 V_1 D_{eq1}}{\mu_1}\right)^{-\beta_1} \qquad (6.5)$$

$$f_2=\alpha_2\left(\frac{\rho_2 V_2 D_{eq2}}{\mu_2}\right)^{-\beta_2} \qquad (6.6)$$

$$\text{with } D_{eq1}=\frac{4A_1}{S_1+S_{12}} \qquad (6.7)$$

$$\text{and } D_{eq2}=\frac{4A_2}{S_2+S_{12}} \qquad (6.8)$$

The interfacial shear stress is assumed to result from the difference in velocity between the two layers. It is calculated using the density of the upper layer.

$$\tau_{12} = \frac{f_{12}(V_1-V_2)^2 \rho_1}{2} \qquad (6.9)$$

The roughness of the interface depends on the diameter of the particles. A modified version (Shook and Roco, 1991) of the Colebrook friction factor equation (independent of the equivalent hydraulic diameter of the upper layer) yields:

$$f_{12} = \frac{2(1+Y)}{(4\log_{10}(D/d) + 3.36)^2} \qquad (6.10)$$

Where Y=0 for d/D < 0.0015, and Y= 4+1.42 $\log_{10}$(d/D) in the range 0.0015< d/D < 0.15

for data taken at $Ar = \frac{4gd^3(s-1)\rho_f^2}{3\mu_f^2} < 3x10^5$

The contact load contribute the velocity independent resisting stress $\tau_{2s}S_2$ at the boundary S_2 as given by:

$$\tau_{2s}S_2 = \frac{0.5\, D^2\, \eta_s\, g\, (\rho_s-\rho_L)\, (\sin\beta - \beta\cos\beta)\, C2\, (1- C1 - C2)}{1 - C2} \qquad (6.11)$$

Ergun's equation for flow through a packed bed, may be used to relate the interfacial drag force $(f_s)_f$ to the relative velocity ΔV = V2f - V2s. This is expressed by:

$$(f_s)_f = \frac{C_{fb}\rho_f \Delta V\, |\Delta V|}{d_m} \qquad (6.12)$$

where:

$$\Delta V = V2f - V2s \tag{6.13}$$

$$C_{fb} = 1.75 + \frac{150\,\mu_f C_2}{d_m\,|\Delta V|\,\rho_f\,(1-C_2)} \tag{6.14}$$

Eliminating the pressure gradient term between the equations of the lower layer yields an expression for the hold-up velocity :

$$\Delta V|\Delta V| = \frac{d_m}{C_{fb}\rho_f A_2}\left(\frac{C_2(1-C_1-C_2)^2}{(1-C_2)(C_1+C_2)}\,0.5\,D^2\,\eta_s\,g\,(\rho_s-\rho_L)\,(\sin\beta - \beta\cos\beta) - \tau_{2f}S_2\right) \tag{6.15}$$

Eliminating the interfacial shear stress term between the equations of the upper and lower layer, the pressure loss equation for the two-layer model is obtained as:

$$-\frac{dP}{dx} = \frac{1}{A}(\tau_1 S_1 + \tau_{2f}S_2 + \tau_{2s}S_2) \tag{6.16}$$

which is equivalent to:

$$-\frac{dP}{dx} = \frac{1}{A}\left(\frac{f_1 V_1^2 \rho_1}{2}S_1 + \frac{f_2 V_{2f}^2 \rho_2}{2}S_2 + \frac{0.5\,D^2\,\eta_s\,g\,(\rho_s-\rho_L)\,(\sin\beta - \beta\cos\beta)\,C2\,(1-C1-C2)}{1-C2}\right) \tag{6.17}$$

6.3 Relations for solving the equations of the model:

$$S = S1 + S2 = \pi D \tag{6.18}$$

$$S1 = (\pi - \beta)\,D \tag{6.19}$$

$$S2 = \beta D \tag{6.20}$$

$$S12 = D\sin\beta \tag{6.21}$$

$$A = A1 + A2 = \frac{\pi D^2}{4} \tag{6.22}$$

$$A1 = \frac{D^2}{4}(\pi - (\beta - \sin\beta\cos\beta)) \tag{6.23}$$

$$A2 = \frac{D^2}{4}(\beta - \sin\beta\cos\beta) \tag{6.24}$$

$$y_b = \frac{D}{2}(\cos(\theta) - \cos(\beta)) \qquad (6.25)$$

$$-\frac{dP}{dx} = i\, g\, \rho_f \qquad (6.26)$$

6.4 The Regula Falsi Method For Estimating Angle β

A root searching algorithm known as the Regula Falsi method is used to determine the angle β defining the lower layer. Angle β is determined when the pressure drop in the upper layer (i1) equals that of the lower layer (i2) i.e. when the following condition is established:

$$F(\beta) = i1 - i2 = 0 \qquad (6.27)$$

It is sufficient to find two values $\beta 1$ and $\beta 2$, such that $F(\beta 1) \cdot F(\beta 2) < 0$, as an appropriate search interval for which a solution can be found by the proposed algorithm.

6.5 Estimation of the Mean Flow Velocities in the Upper V_1 and Lower V_2 Layers

Conservation laws for fluid and particles, assuming steady flow conditions and an incompressible fluid, require that:

$$A\,V = A_1\,V_1 + A_2\,V_2 \qquad (6.28)$$

where:

$$V_2 = C_2\,V_{2s} + (1\text{-}C_2)\,V_{2f} \qquad (6.29)$$

The volumetric flow rate balance of solids is given by:

$$C\,A\,V = C_1 A_1\,V_1 + C_2\,A_2\,V_{2s} \qquad (6.30)$$

However since V_{2s} cannot be known before all model equations are solved, another equation is used where a mean volumetric solids concentration in the lower layer,
C_b, is defined by :

$$C A V = C_1 A_1 V_1 + C_b A_2 V_2 \qquad (6.31)$$

C1 is estimated independently as will be shown below and C2 may be computed from:

$$C_2 = C_{lim} - C_1 \qquad (6.32)$$

where Clim is the concentration of the loose-packed bed , taken equal to 0.66 in our illustrative example. Solving Equations (6.28) and (6.31) for V1 and V2 yields:

$$V_1 = \frac{A}{A_1}\left(\frac{C_b - C}{C_b - C_1}\right) V \qquad (6.33)$$

$$V_2 = \frac{A}{A_2}\left(\frac{C - C_1}{C_b - C_1}\right) V \qquad (6.34)$$

Cb is initially estimated as C2. After Solving for the velocity differential from Equation (6.15):

$$\Delta V = V_{2f} - V_{2s} \qquad (6.35)$$

where:

$$V_{2s} = V_2 - (1 - C_2)\,\Delta V \qquad (6.36)$$

$$V_{2f} = V_2 + C_2\,\Delta V \qquad (6.37)$$

and from the mass balance equation:

$$C_b\ V_2 = C_2\ V_{2s} \tag{6.38}$$

a new mean concentration Cb may be computed as:

$$C_b = \frac{C_2}{V_2}(V_2 - (1 - C_2)\Delta V) \tag{6.39}$$

If the new Cb is not equal to the previous one, the equations of the model are recalculated with the new Cb, and the procedure is repeated until convergence is reached. The flowchart for the two-layer model calculations is shown in Figure 6.2

6.6 Concentration Distribution in the Upper Layer

Improvement in the two-layer model requires methods for predicting concentration distributions in the pipeline. The turbulent diffusion mechanism suggests that large scale eddies keep particles suspended in the upper layer and cause particle motion from the interface upward i.e. from the high concentration zone (lower layer) to the low concentration zone (upper layer). This tendency is balanced by the gravitational force which causes the particles to settle. This is expressed by the diffusion equation (Doron et al. 1987) :

$$\varepsilon \frac{\partial^2 C(y)}{\partial y^2} + w \frac{\partial C(y)}{\partial y} = 0 \tag{6.40}$$

With $C(y_b) = C_2$ as boundary condition.

C(y) is the local volumetric concentration in the upper layer, y is the vertical coordinate (perpendicular to the pipe axis), ε is the local diffusion coefficient, and w is the particles' local terminal settling velocity. Integrating the above equation twice yields the concentration distribution in the upper layer:

$$C(y) = C_2 \exp\left(-\frac{w}{\varepsilon}(y - y_b)\right) \tag{6.41}$$

Figure 6.2 Flow chart of the two-layer model simulation

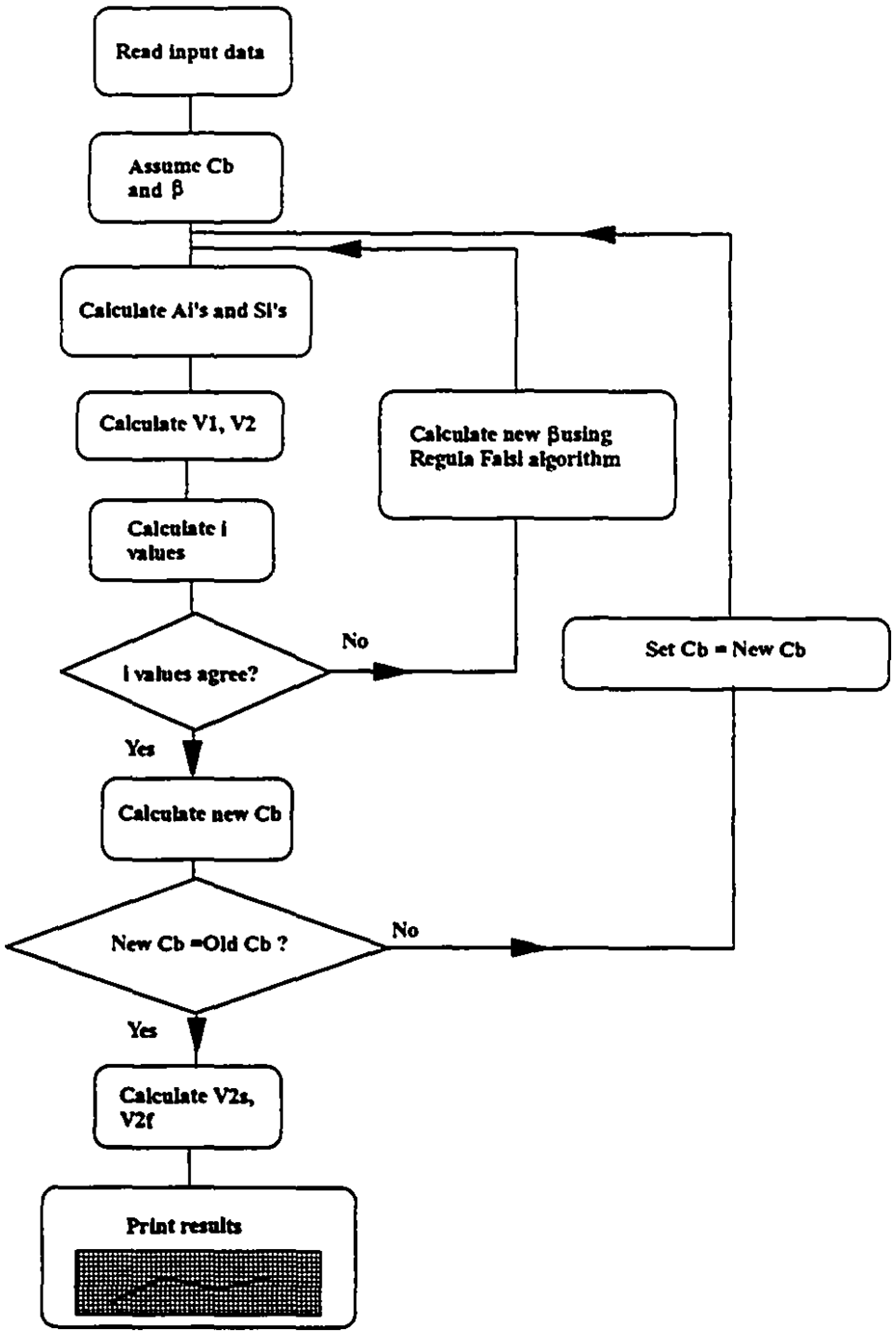

where y_b is the bed height, and the concentration at the interface is assumed to be that of lower layer C_2.

The mean cross-flow diffusion coefficient ε is evaluated according to Taylor (1954), assuming the mass-transfer coefficient and the momentum-transfer coefficient are nearly equal:

$$\varepsilon = 0.052\, V_* r \tag{6.42}$$

where V_* is the shear velocity given by:

$$V_* = V_1\sqrt{\frac{f_{12}}{2}} \tag{6.43}$$

and r is the hydraulic radius of the upper-layer cross section.

Where the terminal hindered settling velocity for a cluster of particles is estimated from the Richardson and Zaki (1954) correlation:

$$\frac{w}{w_o} = (1 - C)^m \tag{6.44}$$

where:

$m = 4.45\, Re_w^{-0.1}$ for $1 < Re_w < 500$ and 2.39 for $Re_w > 500$

Re_w is a particle Reynolds number based on w.

The mean concentration distribution equation in the upper layer is given in terms of β as:

$$C_1 = \frac{C_2 D^2}{2A_1}\int_{\beta}^{\pi} \exp\left(-x\frac{D}{2}(\cos\theta - \cos\beta)\right)\sin^2\theta\, d\theta \tag{6.45}$$

with $x = \frac{w}{\varepsilon}$

6.7 Case #1: Flow with a stationary bed

This flow regime is not recommended in practice. It will be used here as a limiting case to illustrate the applicability of the two-layer model.

For flow velocities below the critical deposit velocity, a stationary bed is expected to form. Flow takes place only in the upper layer . The dry frictional term $\tau_{2s}S_2$ can no longer be computed from Equation (6.14) since this equation applies only at the verge of motion. Since bed velocity $V_2 = 0$, and $C = C_1$, the velocity in the upper layer is given by:

$$V_1 = \frac{A}{A_1} V \qquad (6.46)$$

Since the mean concentration in the upper layer C_1 is known, the angle (β) and the bed height may be estimated from Equation (6.45) and (6.25) respectively. The shear stresses in the upper layer can be computed from Equation (6.3) and (6.9), and the pressure loss from Equation (6.1).

The static dry friction term $\tau_{2s}S_2$ can be computed from Equation (6.2) and compared to the minimum dry friction $(\tau_{2s}S_2)_{min}$ (estimated from Equation (6.11)) required to start the motion of the bed.

The bed is stationary as long as:

$$\tau_{2s}S_2 < (\tau_{2s}S_2)_{min} \qquad (6.47)$$

6.8 Case #2: Flow with a moving bed

As the mean flow velocity approaches the critical deposit velocity, the shear stresses increase while the bed height decreases until the condition

$$\tau_{2s}S_2 = (\tau_{2s}S_2)_{min} \qquad (6.48)$$

is reached, which indicates the transition from a stationary bed to a moving bed. In this case a solution for the pressure loss is obtained by an iterating procedure on all model equations as shown in Figure 6.3. The convergence criterion is satisfied when the pressure drop in the upper and lower layer are practically equal. This determines the angle (β), and the rest of model parameters.

6.9 Case #3: Fully suspended flow

As flow velocity increases further, bed height continues to diminish until it approaches zero. This is the onset of the fully suspended regime. In this case, the pressure drop is estimated from:

$$\frac{dP}{dx} = \frac{2f}{D}\rho_m V^2 \qquad (6.49)$$

where:

$$\rho_m = \rho_L(1-C_v) + \rho_s C_v \qquad (6.50)$$

and (f) is calculated from Equation(6.5) with $V_1=V$ and $D_{eq1}=D$.

The concentration profile is computed from Equation (6.41) with $y_2=0$ i.e.

$$C(y) = C_B \exp\left(-\frac{w}{\varepsilon}y\right) \qquad (6.51)$$

where C_B is the concentration at the bottom of the pipe, and is computed from:

$$C_B = \frac{\frac{\pi}{2}C_v}{\int_0^{\pi} \exp\left(-\frac{wD}{2\varepsilon}(\cos\theta)\right)\sin^2\theta \, d\theta} \qquad (6.52)$$

Similarly, the concentration at the top of the pipe C_T is computed using Equation (6.41) with y=D. As the slurry flow velocity increases, the mean cross-flow diffusion coefficient ε increases, and the concentration profile flattens making the ratio C_T/C_B approach unity. At $C_T/C_B \approx 0.95$, the concentration distribution is practically uniform, which indicates the transition from the heterogeneous to the pseudo-homogeneous flow regime. The pressure drop for pseudo-homogeneous flow is estimated from Equation (6.49).

6.10 Numerical Example: Flow With Slip Velocity in the Sliding Bed

INPUT PARAMETERS

Pipe internal diameter (m), D=0.0787
Mean flow velocity (m/sec), V=1
Mean particle diameter(m), dp=0.004
Mean delivered concentration, C=0.42
Density of base liquid (kg/m^3), ρ_f=1000
Density of solid particles (kg/m^3), ρ_s=2650
Base liquid viscosity (Pa sec)--Water at 20°C, μ_f=100.2*10^(-5)
Coefficient of particle-wall friction; η_s=0.40
Concentration of loose packed bed, clim=0.66
Mean concentration in the upper layer, C1=0.10

RESULTS

Mean velocity of the upper layer, (m/sec), V1= 1.850
Mean velocity of the lower layer, (m/sec), V2= 0.850
Mean fluid velocity in the lower layer, (m/sec),V2f= 0.883
Mean solids velocity in the lower layer, (m/sec),V2s= 0.824
Mean solids concentration in the lower layer, Cb= 0.543
Angle defining the lower layer,(degrees), β= 125.8
Lower layer (bed) height (m),yb= 0.0624
Ratio of bed height to pipe diameter, yb/D= 0.792
Concentration profile in the upper layer, C(y)=0.54 exp(-375.705(y-0.0624))
Total pressure drop,(m water/ m of pipe), i= 0.387

Figure 6.3 shows the concentration distribution in the upper layer. Figure 6.4 shows the convergence pattern of Cb. Figure 6.5 shows the convergence pattern of β by the Regula Falsi Algorithm. Figure 6.6 illustrates the principle of the Regula-Falsi root finding algorithm.

Figure 6.3 Concentration distribution in the upper layer

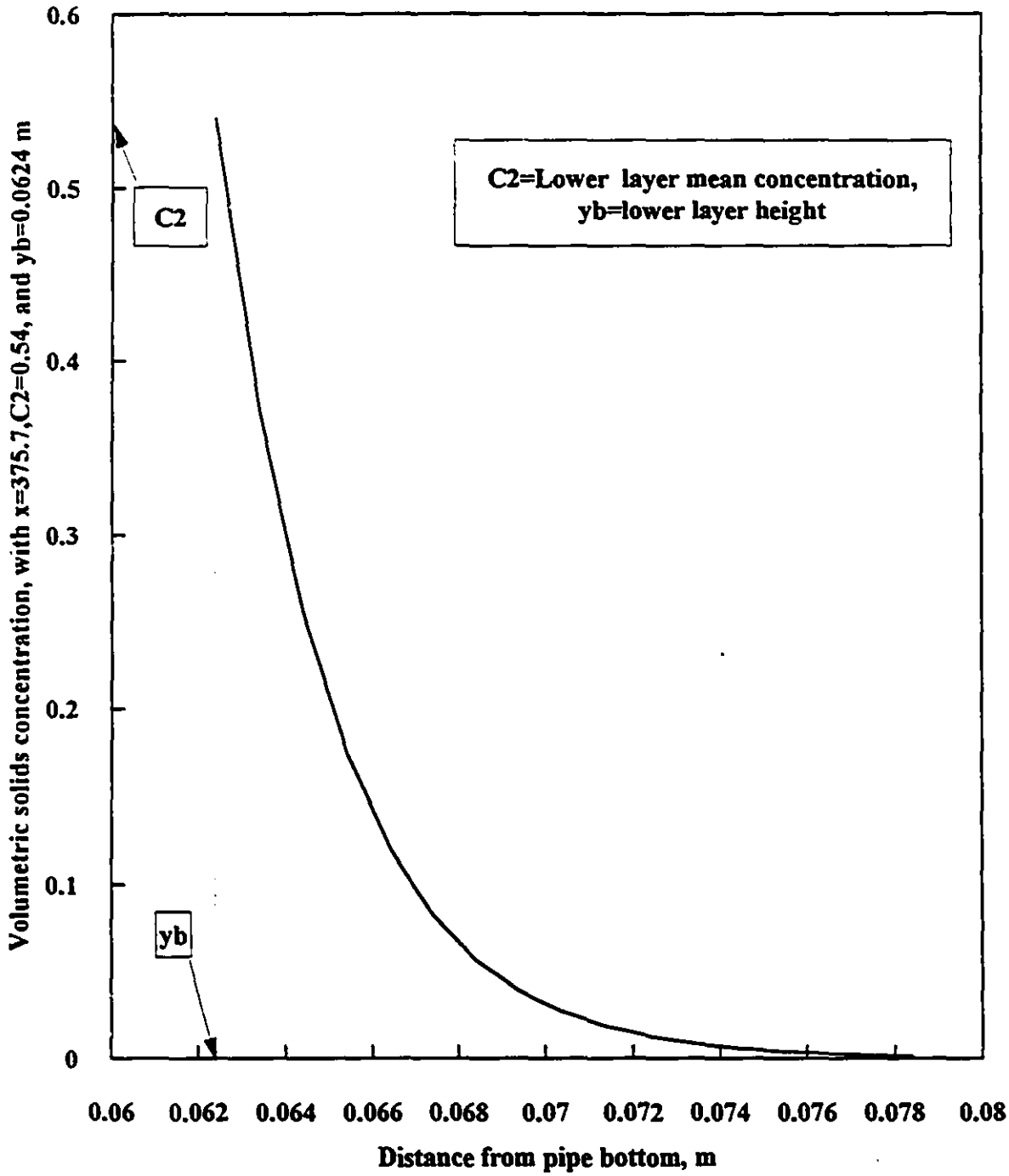

Figure 6.4 Convergence pattern of lower layer mean volumetric concentration Cb

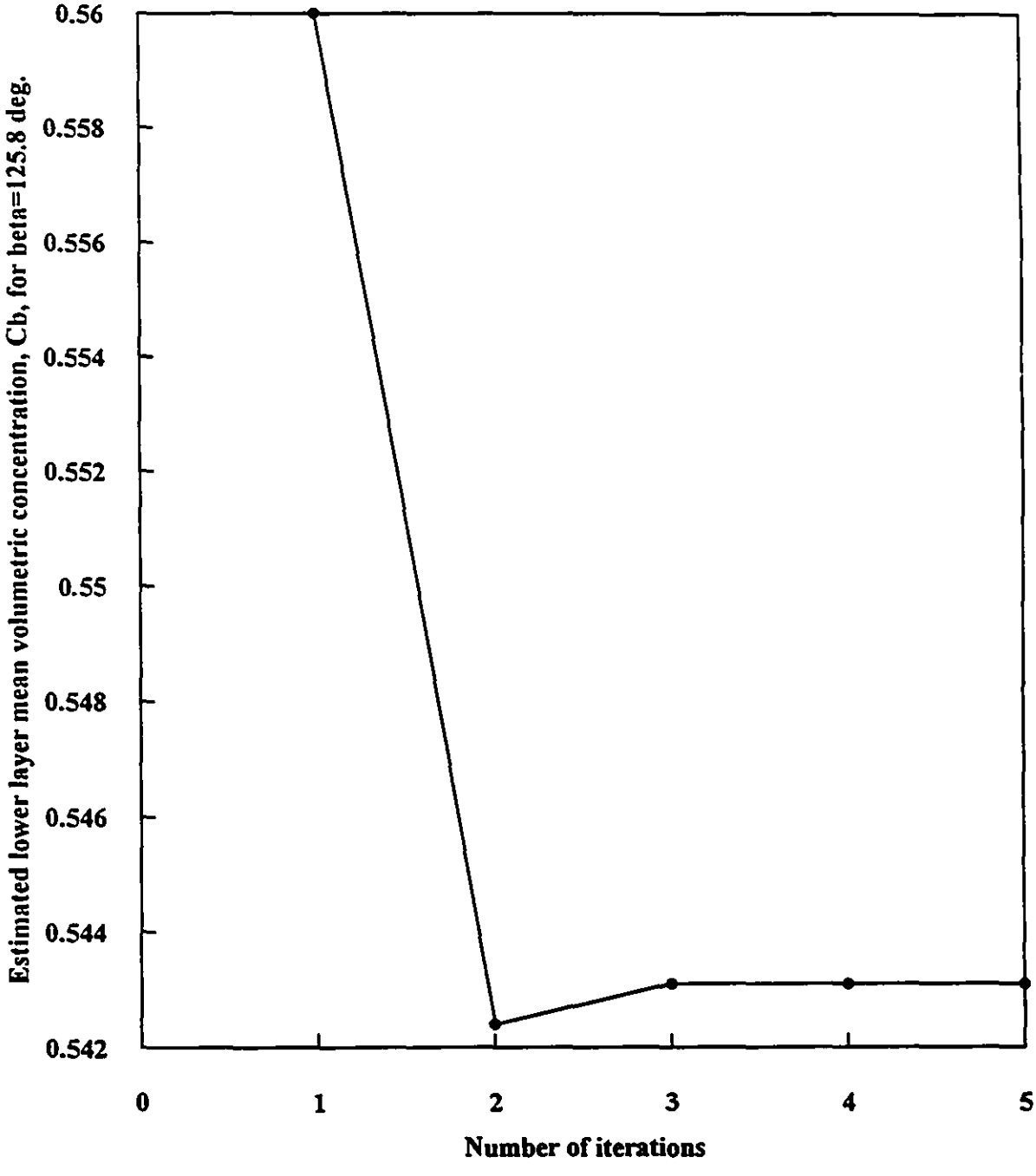

Figure 6.5 Convergence pattern of beta from Regula Falsi algorithm

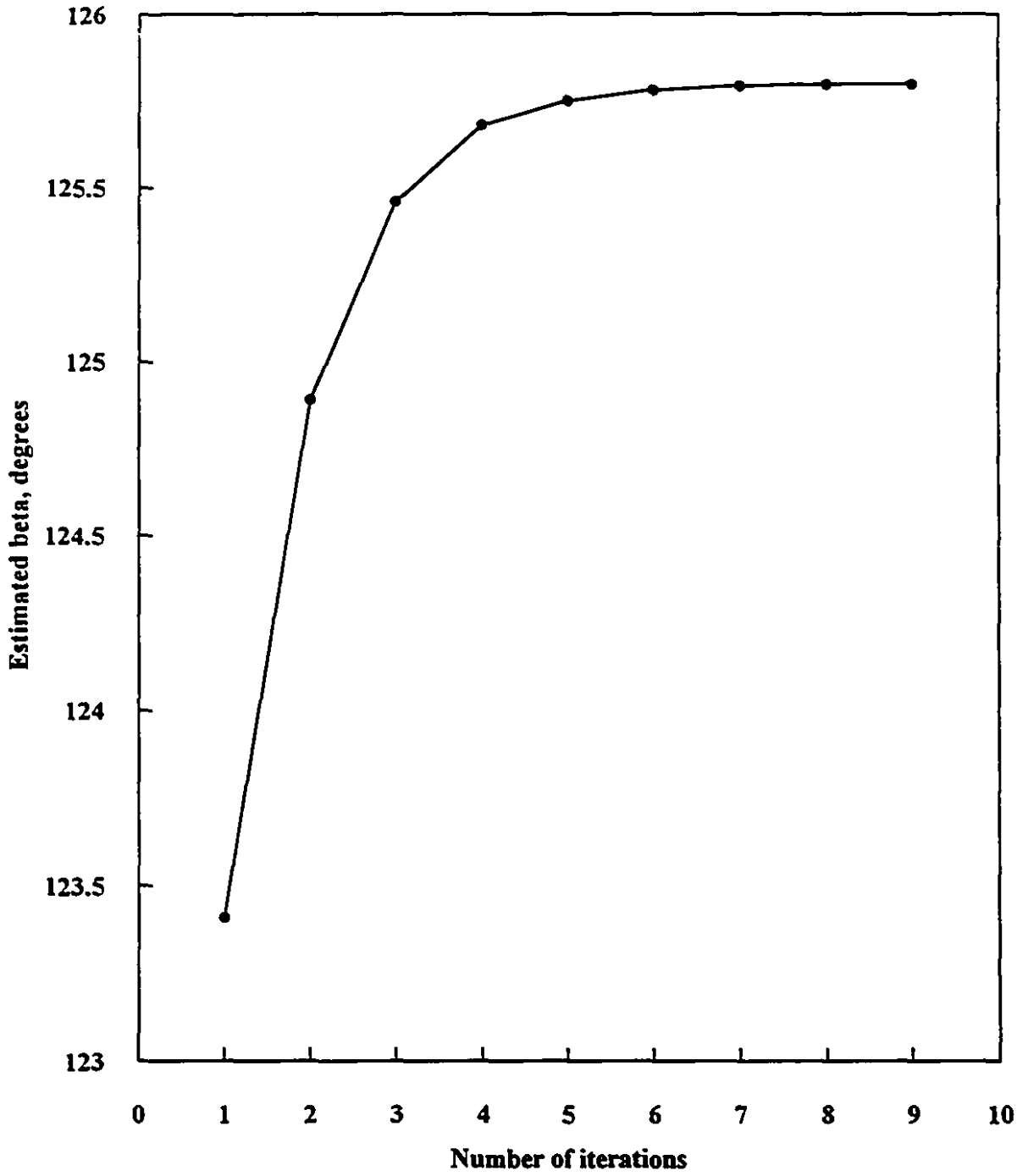

Figure 6.6 Regula falsi root finding method

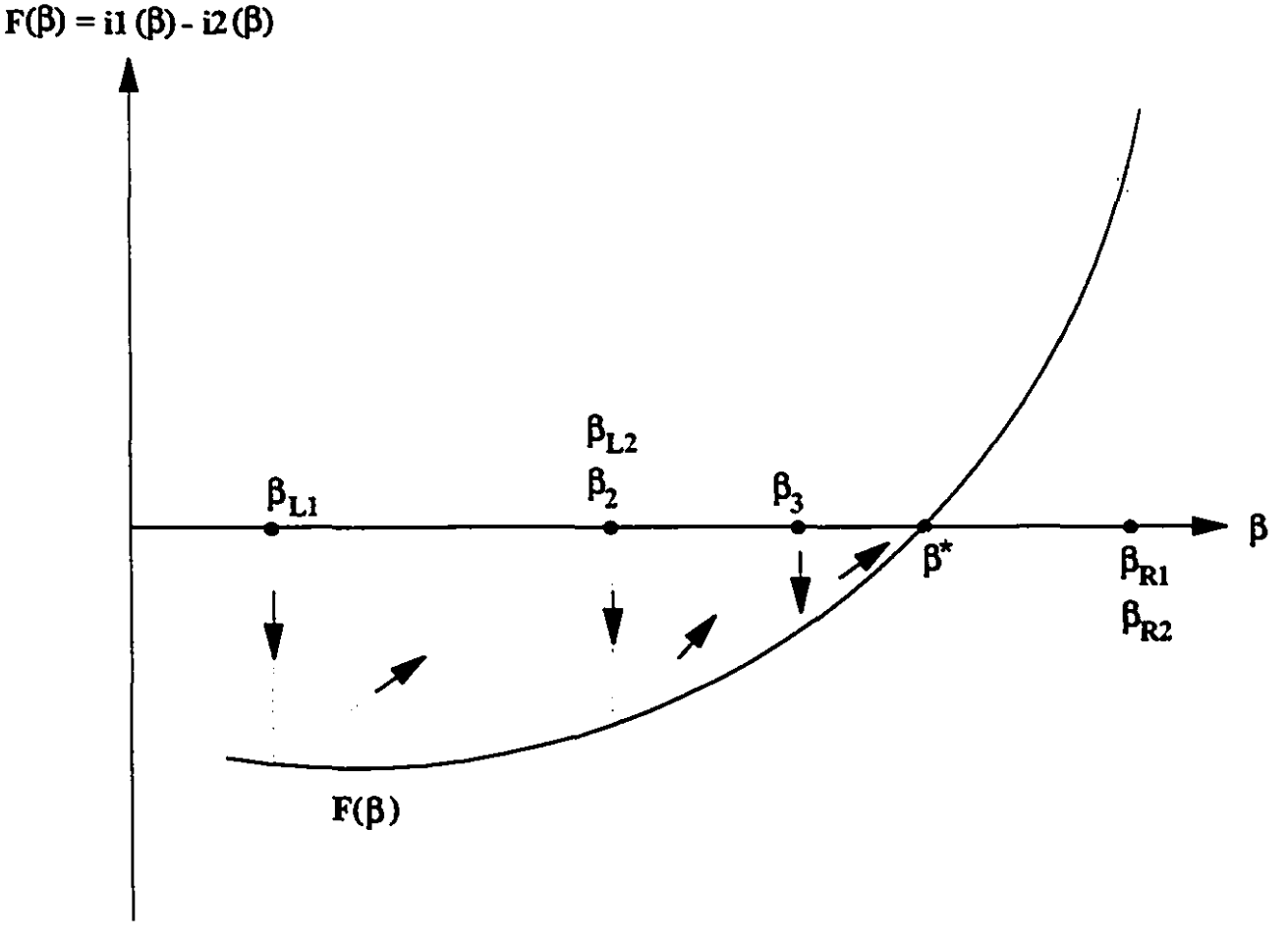

CHAPTER SEVEN

ASPECTS OF EXPERIMENTAL TESTING OF BACKFILL SLURRIES

The objective of this chapter is to describe some aspects of experimental testing of slurries, namely, viscometry and laboratory scale loop tests, a direct method for yield stress determination, empirical techniques for assessing workability (slump test), flowability (funnel test), dewatering (pressure bleed test), and stability (settling test). This chapter also contains a section on a novel sampling device designed to assess the concentration distribution in a settling column, and is shown to yield results that question the accuracy of the commonly used lateral ports sampling technique .

7.1 Viscometry Measurements

Non-settling slurries are usually characterized by rheological properties obtained by testing the slurry with varying shear rates and measuring the corresponding shear stresses. Such measurements could be done by a rotary viscometer which are used to cover the lower range of shear rates (up to 200 S^{-1}), or by capillary viscometer for a higher range.

Viscometry measurements are carried out in order to characterize the slurry by a selected rheological model. If the slurry exhibits non-Newtonian properties , the most common choice of rheological model is between Bingham plastic or Power law models ; although a three parameter model (yield pseudo-plastic) may also be used. Once a model is adopted and the corresponding parameters identified, standard graphs for friction coefficients may be used for calculating friction head losses. Scale-up studies of laboratory results could extend the model to apply to various pipe diameters and flow conditions.

Correct rheological characterization provides a sound basis for economic design in terms of pipe and energy cost. It also prevents under-provision or under-use of pump pressure (the former condition is more serious).

7.2 Laminar Flow Condition

Rheological models are usually determined with experimental data in the laminar flow regime. A practical method of guarding against "turbulent" data points is to carry out two sets of tests and to plot the results on the same curve. Data points on the high side of flow velocity axis for which the two curves do not coincide should not be used as they are probably in turbulent flow regime.

7.3 Capillary Tube Viscometer : Design Considerations

The basic configuration of a vertical capillary tube viscometer is shown in Figure 7.1 . The variables of interests are:

P = measured air pressure
Q = measured flow rate
D = Capillary diameter
L = capillary length (≥ 200 D)
h = fluid level
ρ_m = slurry density

V = flow rate = $\frac{4Q}{\pi D^2}$

$\frac{8V}{D}$ = nominal shear rate

τ_w = wall shear stress = $(P_A+\rho_m(h+L))\frac{D}{4L}$

In designing capillary tube viscometers, the following guidelines should be observed (Bain and Bonnington, 1970):

- The capillary viscometer should allow for changes in the length and diameter of the capillary.
- Driving pressure must be kept constant

Figure 7.1 Schematic of a vertical capillary tube viscometer

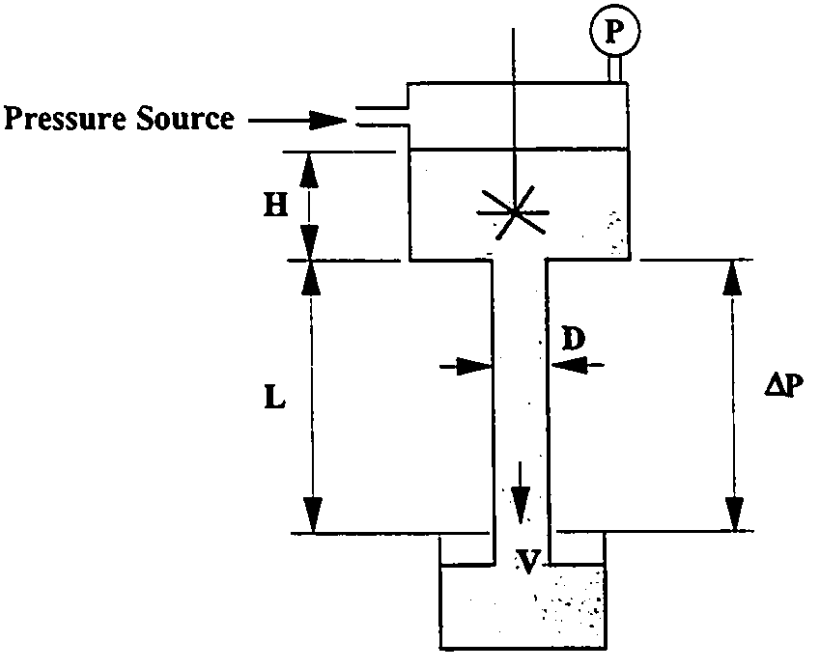

- Fluid level must be kept constant
- Thermal insulation or temperature control should be provided

For each selected slurry concentration, the primary measurements for a capillary viscometer over a range of flow rates, are: flow rate, liquid level, driving pressure.

7.4 Entrance Length

To make meaningful measurements on a capillary viscometer or test pipeline, the flow must be fully developed. To reach this state, the slurry must flow for a minimum distance called the entrance length x_e, which corresponds to 95% axial stabilization of the velocity profile. For laminar flow of a Newtonian fluid, Govier and Aziz(1987) suggest the relation:

$$\frac{x_c}{D} = 0.026\ Re \qquad (7.1)$$

where D is the pipe diameter and Re is the Reynolds number based on the mean flow velocity. Transition to turbulent flow is established for most fluids around Re≈3000 (conservative estimate) . This suggests an entrance value of at least $x_c \approx 78\ D$.

7.5 Selection of a Flow Model

A straight plot of shear stress $\tau = \frac{D\Delta P}{4L}$ versus nominal shear rate $\frac{8V}{D}$ on log coordinates indicates that the suspension may be described by a Power law. The slope of the line is the flow behaviour index n, and the fluid consistency index K is found from the intersection of the straight line on the shear stress axis for the value $\frac{8V}{D} = 1$ or estimated as outlined in Chapter Four.

If the logarithmic shear stress-shear rate is not a straight line, and more specifically if it is a concave upward curve, then the Bingham plastic model may be the appropriate one. Data should be plotted in a linear scale, which would give a straight line if the suspension was indeed of the Bingham plastic type. The slope of

of this line is the coefficient of rigidity. The yield stress for a Bingham plastic material is difficult to measure, because it is difficult to measure the pressure at the onset of flow.

7.6 Detection of Time-Dependent Behaviour

Time-dependent behaviour may be detected in a capillary viscometer by measuring the nominal shear rate at a given shear stress for various length and capillary diameter. An increase in shear rate as length increases, and a decrease in shear rate as diameter increases indicates a thixotropic behaviour. The opposite, indicates a rheopectic behaviour.

7.7 Yield Stress Determination

The yield stress is defined as the minimum shear stress corresponding to the first evidence of flow , i.e. the value of shear stress at zero velocity gradient (Nguyen & Boger (1983)). It is considered a material property denoting a transition between solid like and liquid like behaviour. It usually occurs in flocculated suspensions having a spatial structure where particle interaction results in mutual attraction. Yield stress is affected by particle concentration, size and size distribution, chemical additives, such as flocculents or dispersants, as well as pH modifying agents .

7.8 Indirect Method of Estimating Yield Stress

Yield stress can be determined by extrapolating the shear stress-shear rate data over the lowest measured shear rate range. Various viscoplastic models (i.e. models with a yield stress) are used to fit the low shear data and to estimate the yield stress. The constitutive equation of the most common models are:

Bingham plastic model $$\tau = \tau_B + \mu_p\left(-\frac{dV}{dr}\right) \qquad (7.2)$$

Herschel-Bulkley model $$\tau = \tau_h + k\left(-\frac{dV}{dr}\right)^m \qquad (7.3)$$

Casson model $$\sqrt{\tau} = \sqrt{\tau_c} + \sqrt{\eta_c\left(-\frac{dV}{dr}\right)} \qquad (7.4)$$

The values of yield stress derived from this indirect method are model-dependent. They represent model parameters, not an intrinsic material property as given by the direct method. The Bingham model for example is known to result in serious overestimate of the yield stress and in some cases prediction of non-zero value even for materials having no yield stress (Nguyen and Boger, (1983)). The uncertainty in using this indirect method is due to the lack of data at sufficiently low shear rates, the possibility of presence of slip effect, and goodness of fit of a particular rheological model to a given data set.

7.9 Direct Measurement of Yield Stress: The Vane Method

This method was originally described by Nguyen and Boger (1983) and was shown to be a simple and accurate method of determining the yield stress as an intrinsic property associated with the strength of a continuous network found in flocculated suspensions. A typical vane element used in the experimental set-up is shown in Figure 7.2a. The vane is made up of four thin rectangular blades at right angles to each other attached to a thin cylindrical shaft driven by a motor connected to an instrument console for recording the speed of rotation and torque.

It is assumed that the material between the blades is unstressed, therefore, for analysis purposes, the vane can be replaced by a cylinder of the same diameter.

The torque measured is equal to the torque due to shearing on the cylindrical walls and the two end surfaces. This torque balance is expressed as:

$$J = (\tau_R\, 2\pi RH)R + \int_0^{2\pi}\int_0^{R}(\tau(r)r)rdr\, d\theta + \int_0^{2\pi}\int_{r_s}^{r}(\tau(r)r)rdr\, d\theta \qquad (7.5)$$

where $R = \frac{D}{2}$ is the radius of the vane element, $r_s = \frac{D_s}{2}$ is the radius of the central shaft, and τ_R is the value of shear stress distribution along the vertical edge of the vane (i.e. the cylindrical surface).

The main assumption with this method is that the maximal torsion moment corresponds to yielding of the material along the cylindrical surface defined by the

Figure 7.2a A typical vane element

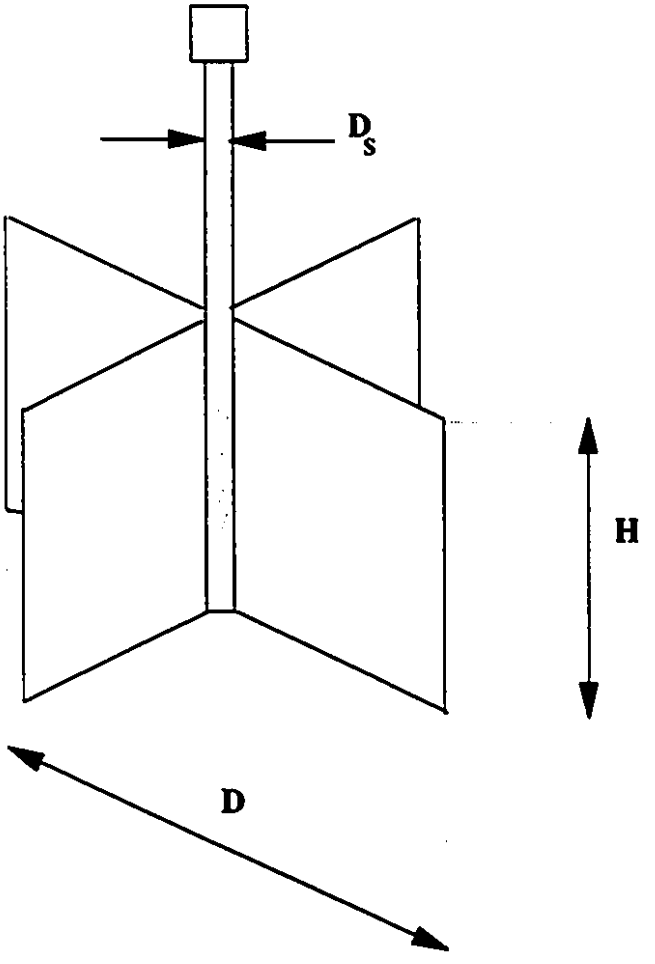

dimensions of the vane. According to Nguyen and Boger (1983), this assumption was supported by experimental evidence. Thus the yield stress can be calculated from the measured maximum torque at the known surface area of the cylindrical surface of yielding.

The stress distribution function $\tau(r)$ over the ends of the cylinder is unknown. At the point of yielding, it is assumed that $\tau(r) = \tau_y$. With these assumptions, the above equation becomes:

$$J_{max} = \frac{\tau_y \pi D^2 H}{2} + \frac{2\pi R^3 \tau_y}{3} + 2\pi\tau_y\left(\frac{R^3 - r_s^3}{3}\right) \qquad (7.6)$$

where J_{max} is the maximum torque measured corresponding to the yield stress of the material.

The assumption of uniform yield stress over the end surfaces was shown to be an acceptable approximation. By comparison with a hypothetical function describing a possible shear stress distribution function, Nguyen and Boger (1983) showed that for $\frac{H}{D} > 2$, the error associated with the uniform stress distribution assumption does not exceed 8%. The equation, above, can be written so that the terms inside the bracket are a function of the vane dimensions, as given by:

$$J_{max} = \tau_y\left(\frac{\pi D^2 H}{2} + \frac{\pi D^3}{6} - \frac{\pi D_s^3}{12}\right) \qquad (7.7)$$

From which the yield stress can be obtained as :

$$\tau_y = \frac{J_{max}}{K} \qquad (7.8)$$

where:

$$K = \frac{\pi D^2 H}{2} + \frac{\pi D^3}{6} - \frac{\pi D_s^3}{12} \qquad (7.9)$$

If the depth of immersion beyond the blade height, H, is not zero, the expression for K must be modified to account for this as given by:

$$K = \frac{\pi D^2 H}{2} + \frac{\pi D^3}{6} - \frac{\pi D_s^3}{12} + \frac{\pi D_s^2 L}{2} \qquad (7.10)$$

with L being the excess depth immersed beyond the blade height H. From the above, one obtains:

$$\frac{J_{max}(L)}{K} = \tau_y + \left(\frac{\pi}{2K} D_s^2 \tau_y\right) L \qquad (7.11)$$

A plot of $\frac{J_{max}(L)}{K}$ versus L yields τ_y as the intercept of a straight line. Figure 7.2b shows a typical torque-time response observed with the vane method.

7.10 Rotational Viscometer

Although useful for routine checks on slurry properties, rotational viscometers have serious limitations in characterizing the flow properties of suspensions. They are also less reliable in predicting pipe flow performance compared to capillary viscometers. This is due to the fact that the mode of shear in rotational instruments is not similar to that in pipe flow. Furthermore, rotational viscometers suffer from "end effects" in the sense that the torque on a rotating cylinder results from the shear stress at lateral cylindrical surface and the two circular end. Experience with a variety of suspensions shows the difficulty in maintaining slurries in a homogeneous state without stirring, which is a source of considerable errors when characterizing semi-stable slurries.

Rotational viscometers are better suited for studying time-dependent rheological behaviour. They provide quantitative measurements of the changes in properties with time, however such information may be not very relevant to the design of slurry flow pipeline systems.

Figure 7.2 b A typical torque/time plot observed with the vane method (adapted from Nguyen and Boger, 1983)

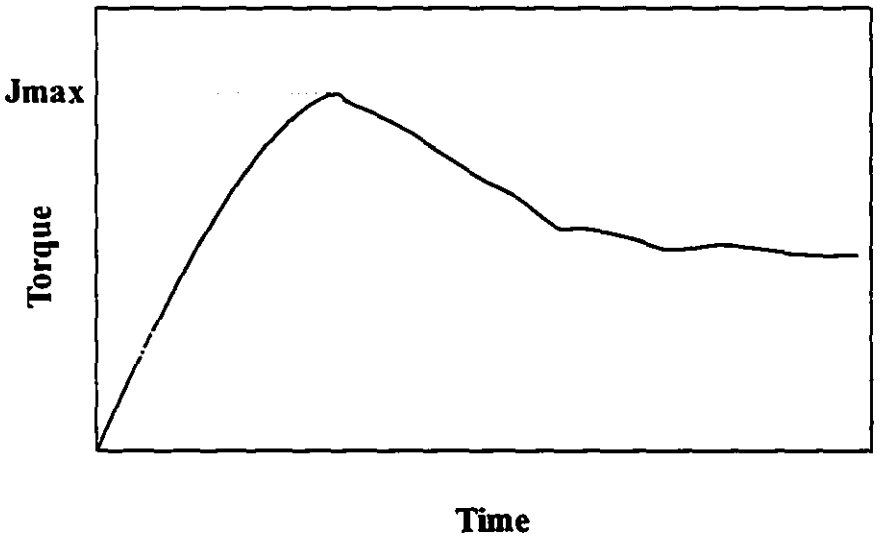

The widespread use of rotational viscometer, however warrants a brief review of their common mode of operation and the methods of correcting and using their data.

Rotational viscometers come in different designs depending on the manufacturer. Most of the commercial ones are provided with calibration and correction charts. For a given shear rate, a shear stress is obtained proportional to the resisting torque. If the fluid is known to be Newtonian, a calibrated chart may be provided to yield the viscosity in engineering units, otherwise, a shear stress-shear rate rheogram has to be drawn to establish an appropriate rheological model.

The principle of a rotational viscometer mode of operation is shown in Figure 7.3. The shear stress at the wall of the container is given by:

$$\tau_w = \frac{2M}{\pi D_o^2 L} \qquad (7.12)$$

The shear rate is a function of the ratio $S = \frac{D_o}{D_i}$. For small value of S, the shear rate may be approximated by:

$$\frac{-dV}{dr} = \frac{2\pi N}{(S-1)} \qquad (7.13)$$

For a very large value of S, i.e. when the bob is assumed to be rotating in an infinite container, the shear rate may be approximated by:

$$\frac{-dV}{dr} = \frac{4\pi N}{\alpha} \qquad (7.14)$$

where α is the slope of the logarithmic plot of torque versus rotational speed.

Figure 7.3 Basic configuration of a rotational viscometer

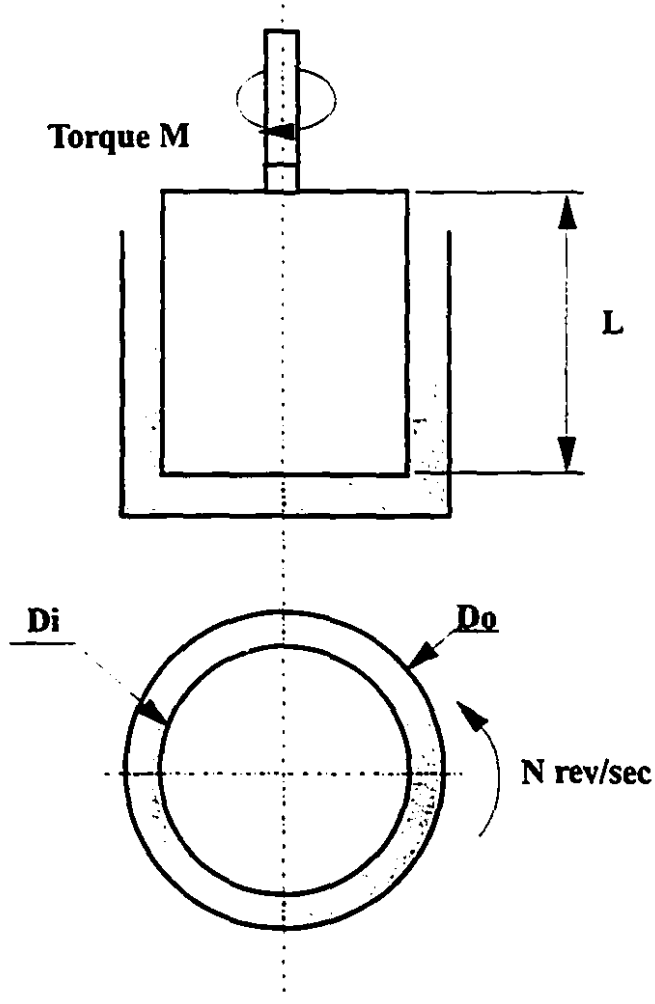

7.11 Laboratory Scale Loop-Test

Loop tests are usually conducted to collect data on the effect of the following parameters on the pressure loss:

- Flow velocity
- Solids concentration
- Particle size and distribution
- Particle density
- Pipe diameter
- Pipeline slope and orientation
- Bends and fittings

Loop tests are also used to visually inspect flow regimes and to determine critical flow velocities. For settling slurries, critical deposit velocity is the minimum transition velocity from moving bed flow to heterogeneous flow. It is identified as a point close to the minimum in the pressure loss-velocity curve and it is usually associated with minimum energy consumption The effect of the following parameters on the critical velocity is usually investigated:

- Particle size
- Particle density
- Solids concentration
- Pipe diameter

Laboratory test pipes may be equiped with various instuments to give on-line monitoring of pressure drop, flow velocity, mixture density, solids concentration, and temperature. A typical loop test configuration is shown in Figure 7.4.

7.12 Case of Non-Settling Slurries

Non-settling slurries must be prepared prior to conveying by combining and mixing the required amount of water with that of fine particles to yield a given concentration. Such mixtures are assumed to be stable and to form a homogeneous slurry. Once prepared, the slurry is injected into a progressive cavity pump and

Figure 7.4 Typical loop test configuration

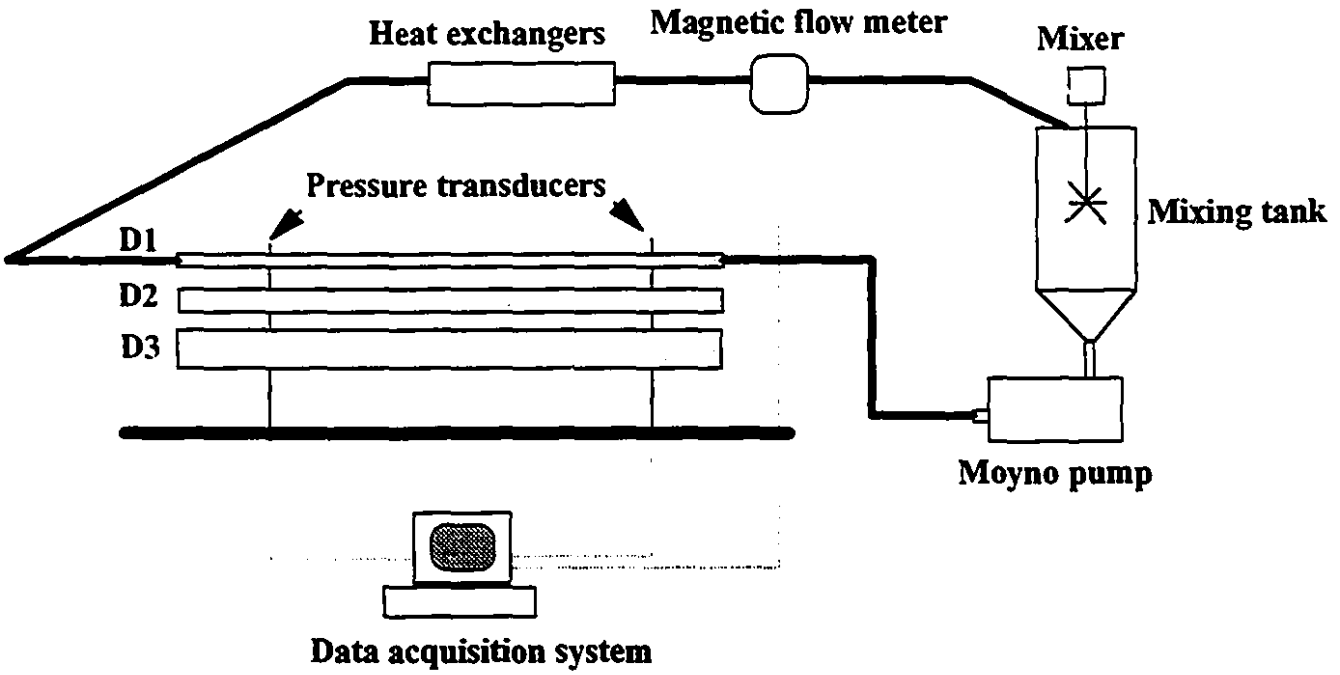

pumped through any desired pipeline diameter and profile (horizontal, inclined or vertical). The two main parameters of interest, while slurry is recirculated, are:

- The friction head loss
- The corresponding flow velocity

7.13 Pressure Loss Measurement

A survey was done on the possible instruments for differential pressure measurement; and it was concluded that a special purpose pressure sensor/isolator combination (Moyno RKL products) are best suited for this application. Such pressure sensors circumvent the shortcomings of the earlier methods of pressure measurements, which suffered from plugging , contamination etc. .

The advantage of the proposed pressure sensor is that it is isolated from the flowing fluid by a flexible elastomer element which transmits fluid pressure to either a pressure gauge or a transducer. A pair of such pressure sensors are required for measuring differential pressures along the pipeline. Figure 7.5 illustrates the design of such pressure sensors.

7.14 Flow Velocity Measurement

The simplest way of measuring flow velocity is to measure the volumetric flow rate and to deduce the mean flow velocity from knowledge of the pipe cross-sectional area. If on-line monitoring of the flow velocity is required, a magnetic flow meter is recommended.

7.15 Case of Settling Suspensions

The pressure loss and flow velocity measurement techniques used for non-settling slurries still apply to this case. Viscometry measurements are only needed for characterizing the suspending medium acting as a vehicle for the coarse particles.

Figure 7.5 Recommended pressure sensor/isolator design

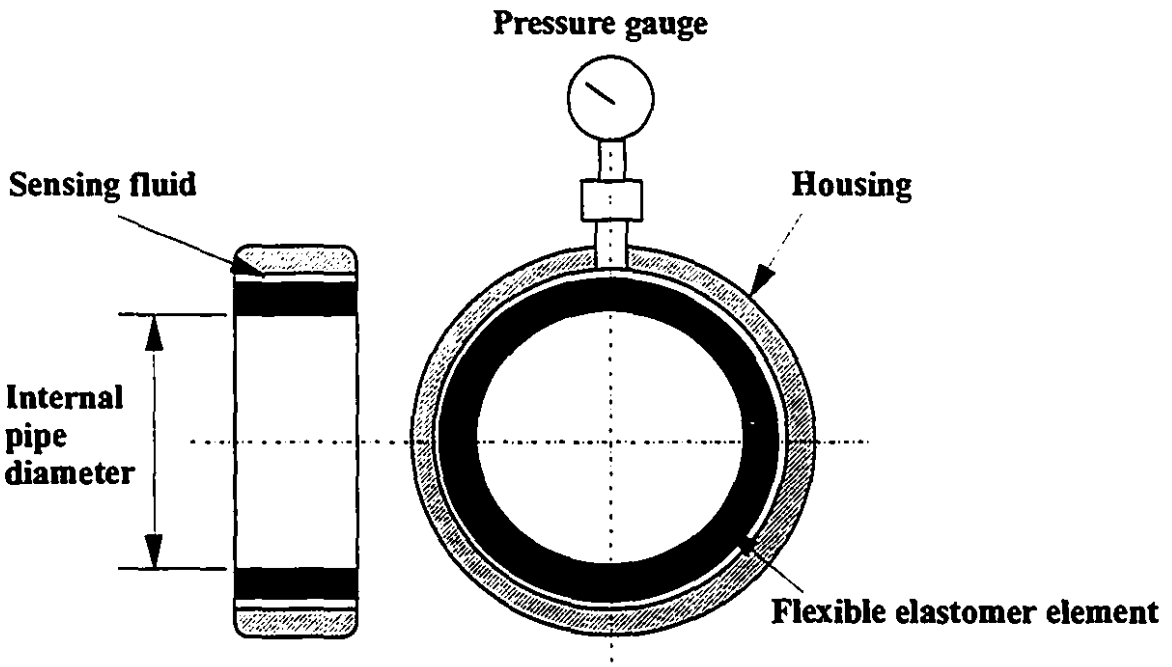

Pumps used in this case are of the centrifugal or positive displacement type. The former is usually used in small scale pilot plant and the latter is used for full scale applications.

When dealing with settling suspensions, it is recommended to experimentally determine drag coefficient versus a particle Reynolds number curve, and a representative coefficient of sliding friction between a bed of solid particles and the pipe wall. These parameters are needed as input to most equations predicting pressure losses and critical velocity in slurry flow.

Terminal settling velocity at different solids concentration, and the settling rate of suspensions are also important parameters characterizing a non-settling suspension.

7.16 Particle Size Analysis

Particle size distribution is determined using sieve analysis. This operation should be repeated periodically on the recirculated slurry to check for particle size degradation, which should be accounted for when predicting pressure losses. A modest reduction of mean particle size may result in a substantial increase in shear stress.

7.17 Empirical Methods for Assessing Pumpability

7.17.1 Slump Test

The principle of the slump test is shown in Figure 7.6. This is the most used test for measuring consistency of a backfill or concrete mix. It is also a measure of the workability which is an important property affecting pumpability. As described by Popovics (1982), the test consists of measuring the difference between the height of a specimen of fresh concrete or backfill material in a mold that has the shape of a truncated cone and its height after the mold was removed. The larger this difference called slump, the softer (wetter) is the consistency.

Figure 7.6 Schematic of the Slump Test

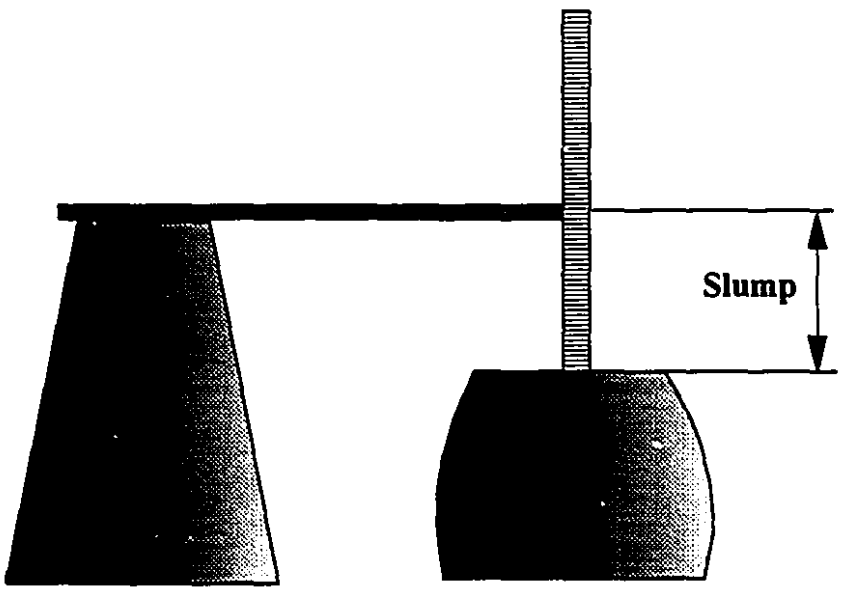

Many variations exist of this method differing mainly in the size of the cone. ASTM C143 has been the standard for carrying out this test in North America. A 12-in (30 cm)-high cone is used with a base diameter of 8-in (20 cm) and a top diameter of 4-in (10cm). When crumbling or collapsing occurs, which happens frequently with lean mixtures, it is difficult to relate the slump to the consistency of the mix. Nonetheless, a collapse indicates a low degree of cohesiveness and little ability for plastic deformation in the mixture.

Slump test is a simple and practical method of checking on a regular basis the consistency of a mixture. It is known to be sensitive to minor irregularities in testing procedure; thus care must be taken to ensure reliable and repeatable results. A frequently reported observation about the slump test is that variations of the results are too large , i.e. slump values obtained with mixtures of the same nominal composition fluctuate within wide limits. However, Popovics (1982) contends that variations of the slump results are much more a reflection of the sensitivity of the slump to variation in the composition of samples tested through changes in consistency of the mixture, than to the lack of reproducibility of the test method.

7.17.2 Funnel test

This is a comparative flow test applicable to stable non-settling slurries. It consists in filling a cone or a funnel with water and recording the time it takes for the water to drain from it. This time (T_0) is taken to be a reference. The test is repeated with various slurries at different concentrations. A flowability index (n) is then defined as:

$$n = \frac{T_s}{T_0} = \frac{\text{flow time of slurry}}{\text{flow time of water}} \qquad (7.15)$$

This index makes it possible to classify slurries from most to least flowable. The lower this index the more flowable the corresponding suspension.

Figure 7.7 Comparative funnel flow tests (adapted from Mining Research Associates, 1984)

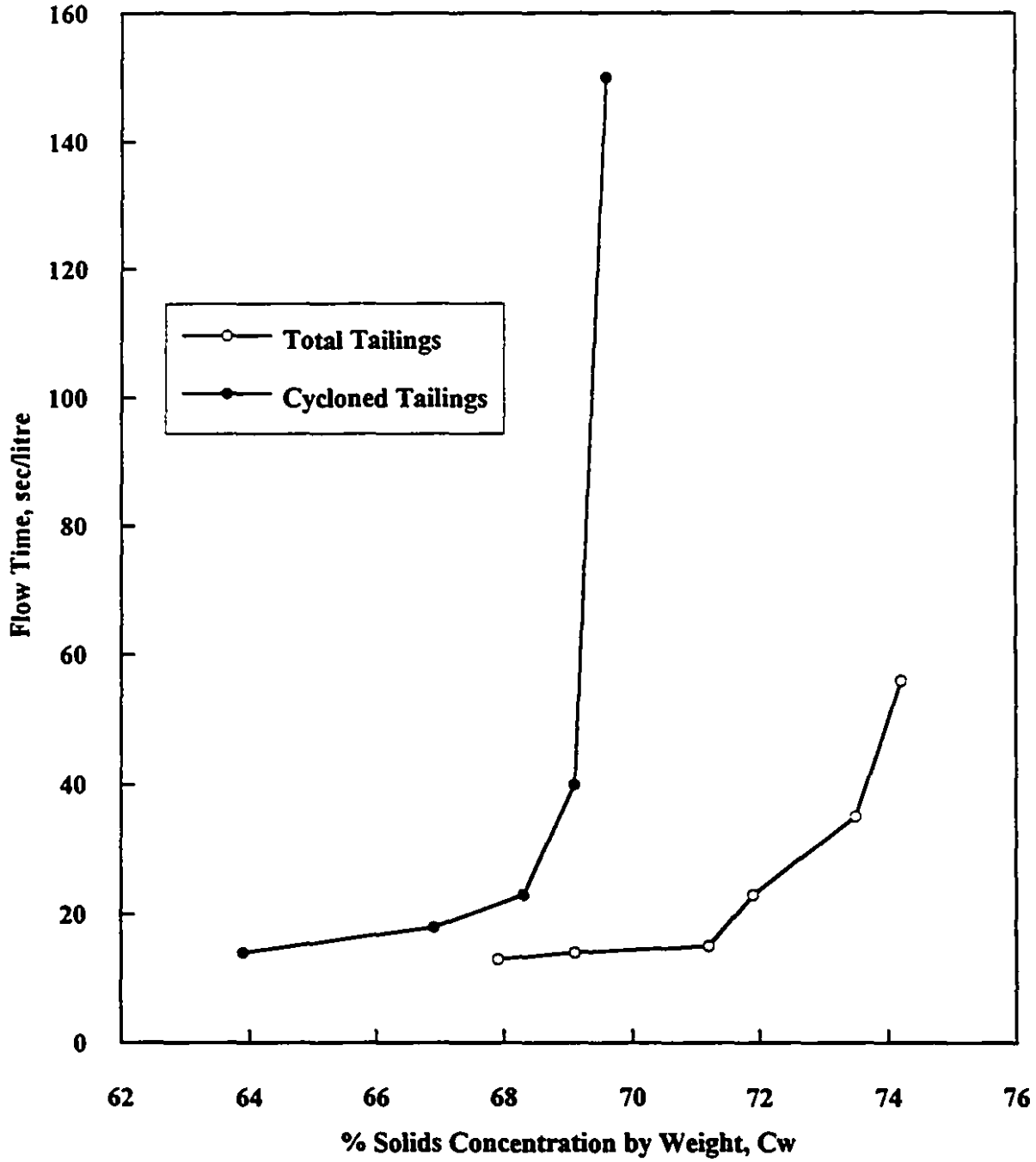

The test is repeated with slurries at increasing solids concentration. The concentration at which the flow time begins to increase sharply is taken to be the maximum solids concentration suitable for placement as a dense slurry.

At high solids concentration, a no-flow condition could arise. This is because the gravity head in the funnel is not sufficient to produce flow. However, such material may be pumpable with positive displacement pumps. Figure 7.7 shows an example of such comparative funnel flow tests.

7.17.3 Pressure Bleed Test

One measure of pumpability is the degree of dewatering to which a given solid-liquid mixture is susceptible under pressure. Dewatered slurry results in very high pressure losses leading eventually to pipeline blockage. A modified version of a pressure bleed test apparatus originally designed by Browne and Bamforth (1977) was used to simulate the state of fill material under pressure in a pipeline in which the dewatering characteristics of the fill are measured. A quantity of fill material is compressed in a cylinder and the quantity of water emitted under pressure and the corresponding time are measured.

The pressure is applied by a compressed-air driven piston and an electronic scale and timer are used to measure the quantity of fluid emitted and time elapsed respectively. Figure 7.8 shows the experimental set-up of the bleed test apparatus. Typical bleed test results are shown in Figure 7.9. Tests with Silica 325 at solids concentration Cw=67.3% , showed that for this particular suspension, most of the volume of fluid was emitted within 150 sec. However, the fluid volume emitted was different from one test to another due to variation in the degree of mixing of each sample and the time taken to set up each test.

The pressure bleed test for Mobrun tailings at solids concentration Cw=80% showed roughly the same trend as before except that most of the fluid was emitted within 350 sec, at which time a slight instability in the sample was recorded. This instability may be the result of variation in the solids concentration caused by the dewatering process.

Figure 7.8 Bleed test apparatus

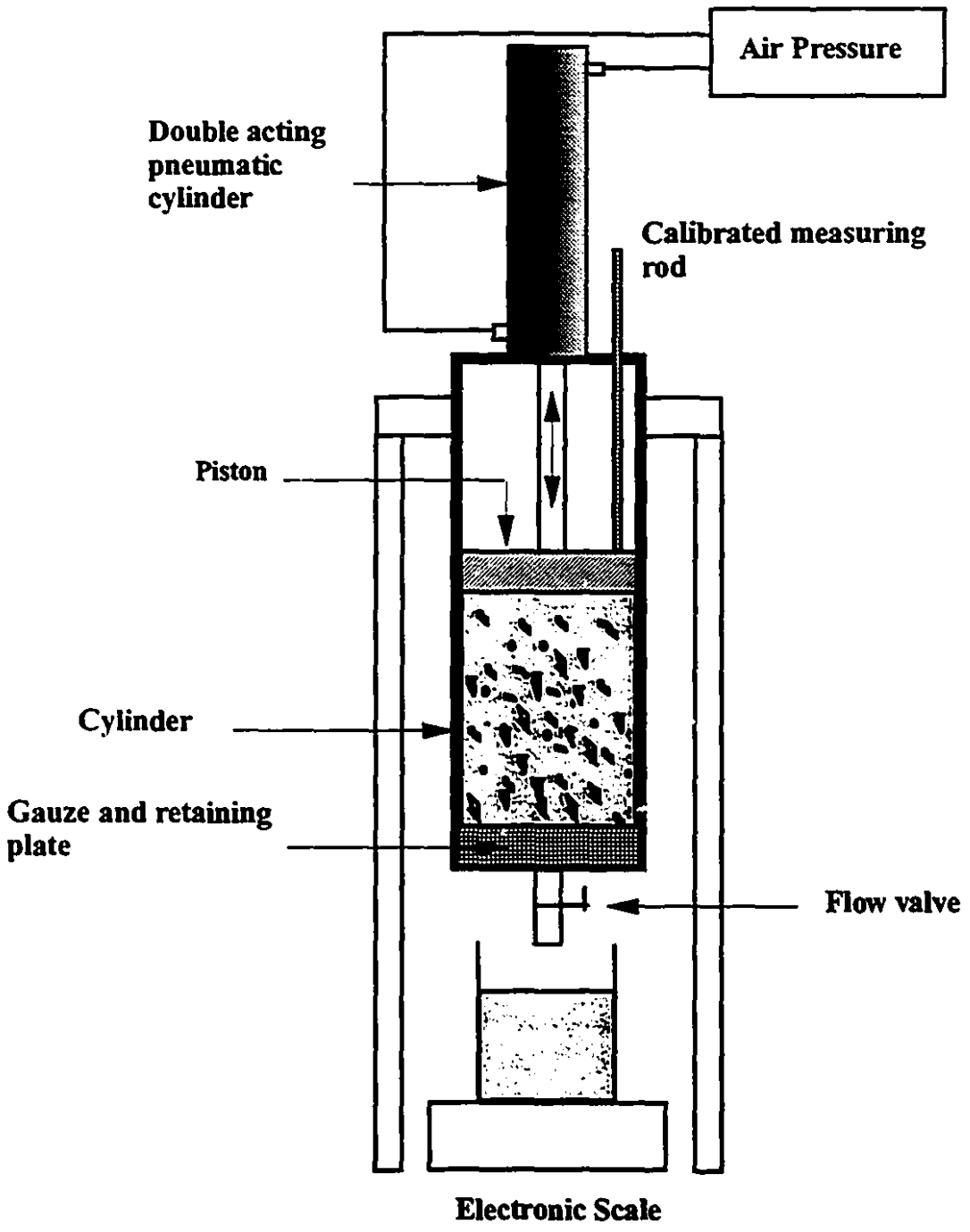

Figure 7.9 Bleed test results for Silica 325 at Cw=67.3%

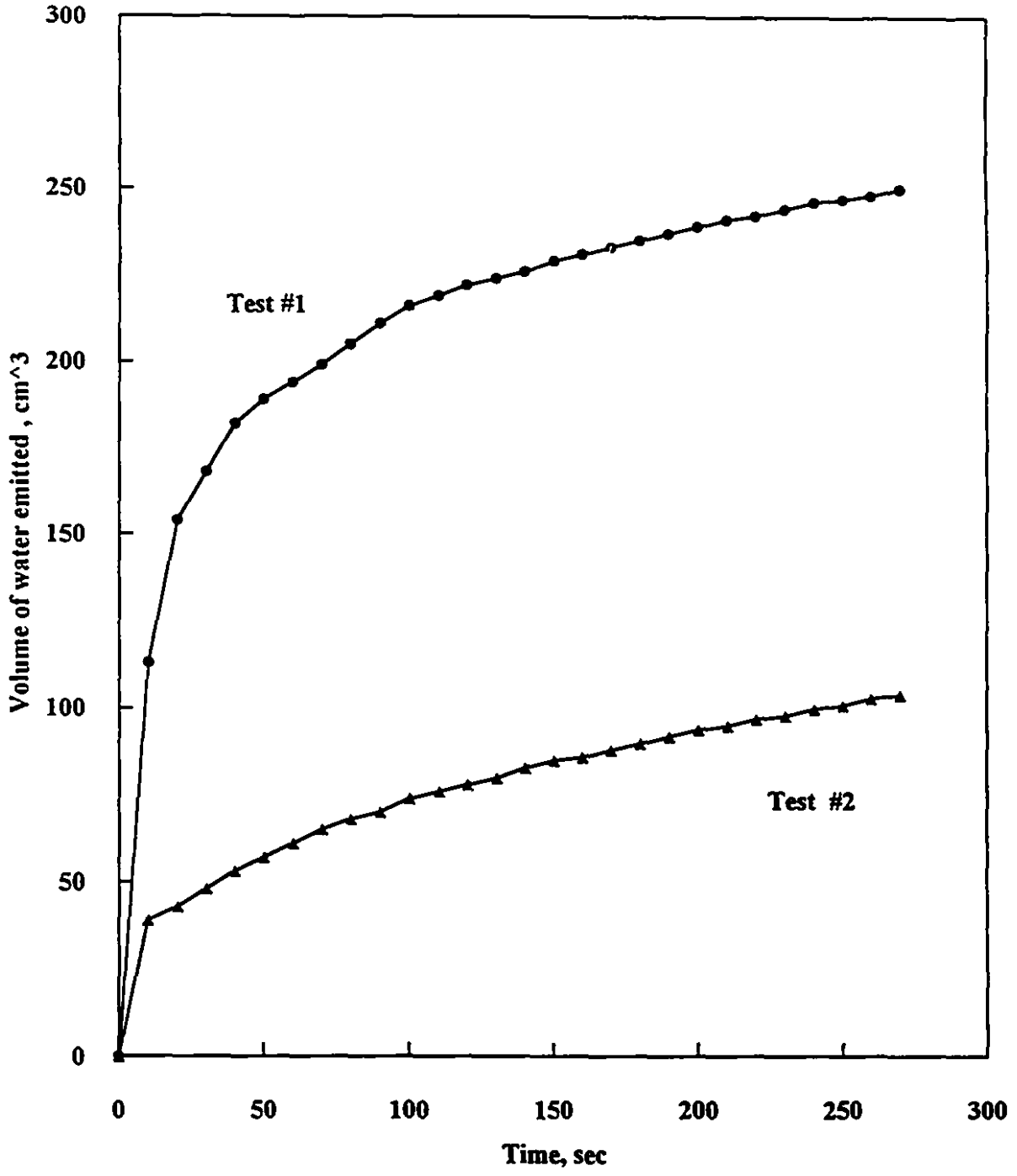

Figure 7.10 Pumpability as a function of slump and volume of water emitted (adapted from Browne and Bamforth, 1977)

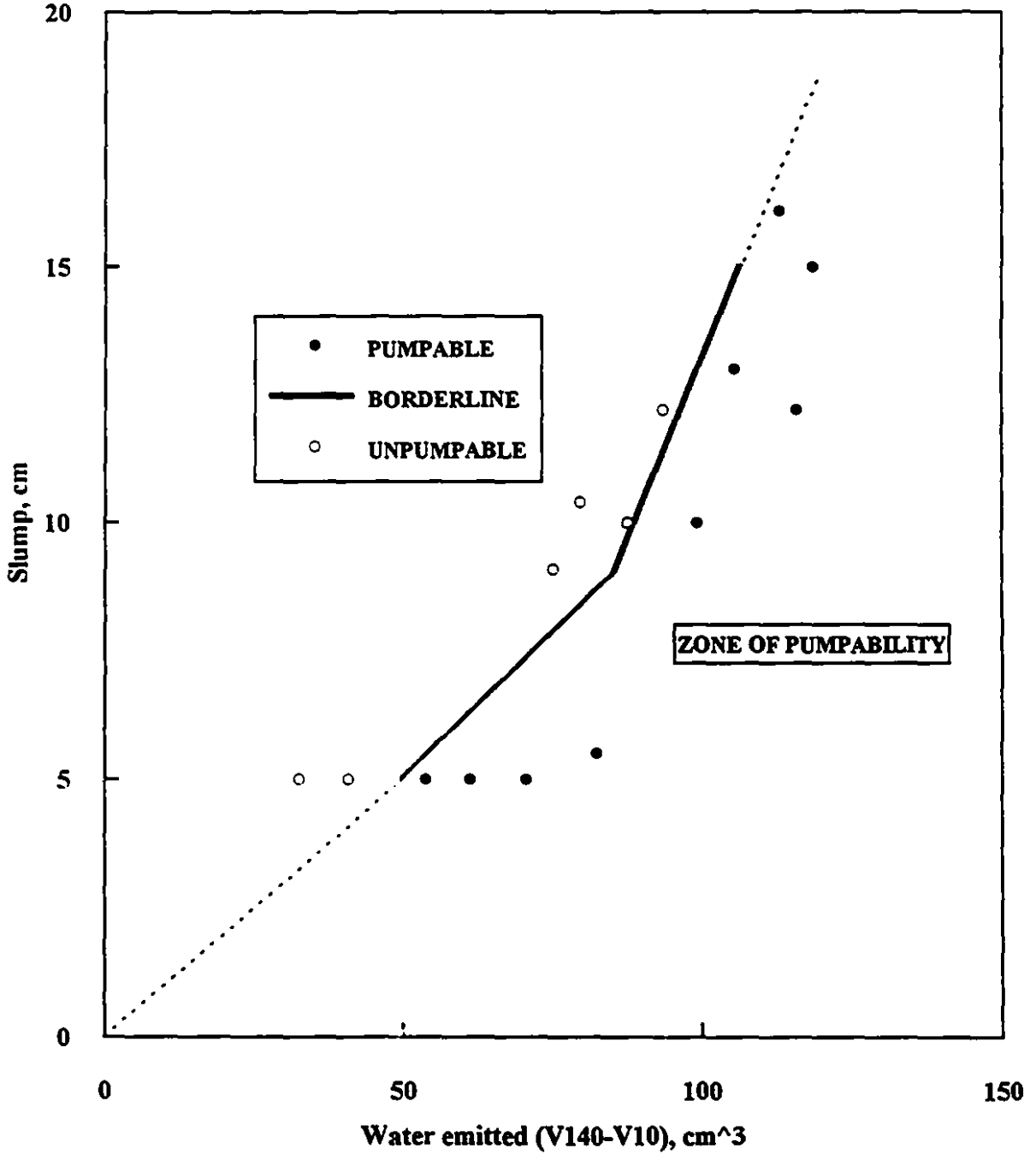

The time taken to emit most of the fluid phase may be taken as a measure of pumpability. The higher this time is, the less prone the mixture will be to dewatering. Browne and Bamforth (1977) applied this technique to concrete, and found a correlation between the pumpability of the mixture as a function of the volume of water emitted in the 10 sec-140 sec interval and the slump of the mixture. This is shown in Figure 7.16.

7.17.4 Settling Test

Settling tests are useful for assessing the degree of stability of a slurry, and its suitability to be transported in the laminar flow regime as if it were a single phase. A measure of the maximum tolerable settling velocity for a slurry to be considered pseudo-homogeneous may be obtained from the relationship (Govier and Aziz (1987)):

$$V_{sm} = \frac{4\,V\,x^2}{L\,D} \qquad (7.16)$$

where:

V_{sm} = the maximum tolerable settling velocity
V = the average pipe flow velocity
x = the average interpaticle distance
L and D = the pipe length and diameter respectively

This relation is derived on the assumption that a particle within a distance x from the bottom of the pipe wall finally settles by the time the fluid carrying it reaches the end of the pipe. More realistically, a certain amount of settling may be tolerated and the mixture may still be considered pseudo-homogeneous. A theoretical expression for the average interparticle distance (x) was derived by Bagnold(1956) for natural and rounded grains of diameter d_p at volumetric concentration C in the slurry as:

Figure 7.11 Variation of maximum settling velocity ratio, Vsm/V, with volumetric concentration C

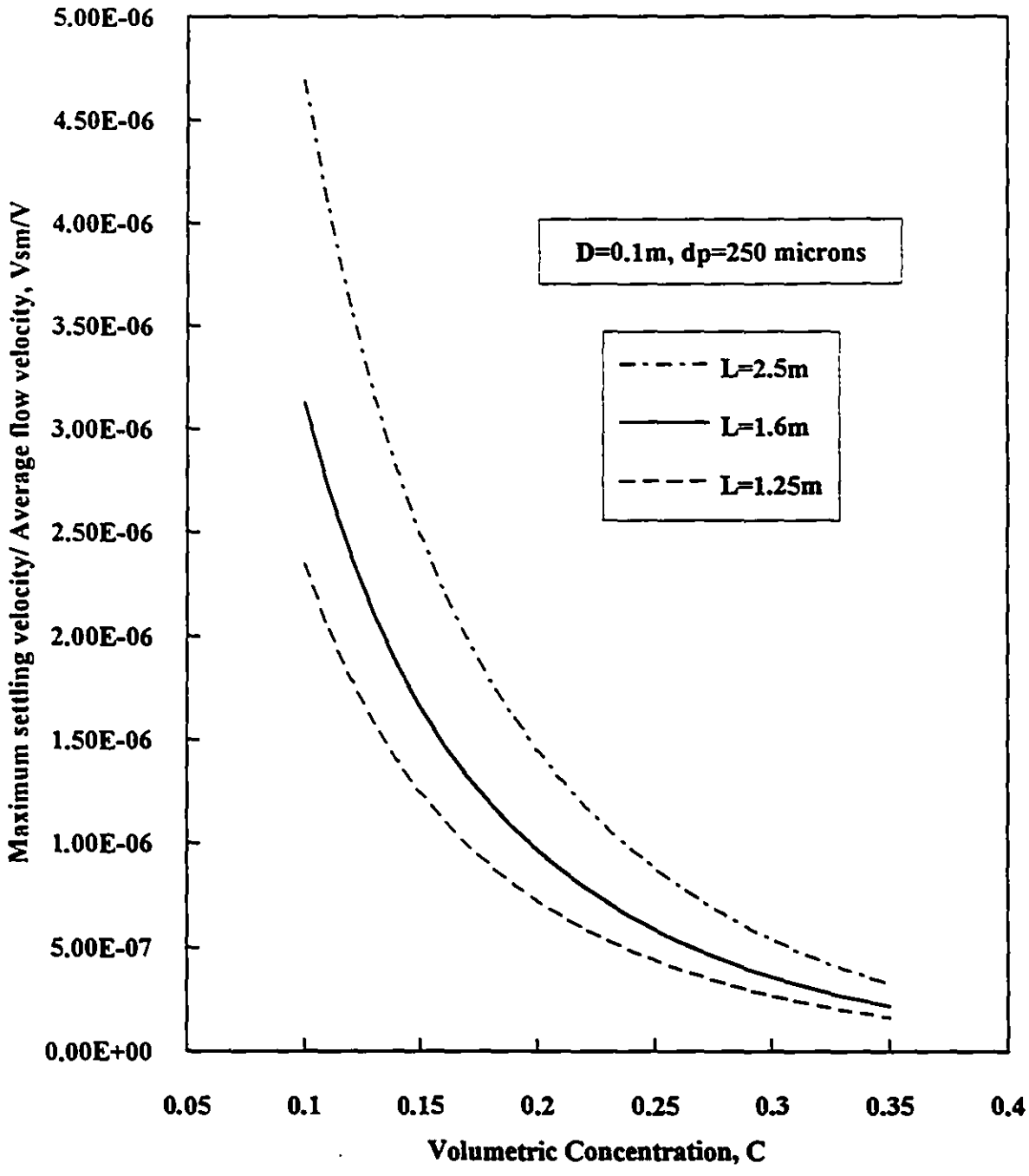

$$x = \left(\left(\frac{0.65}{C} \right)^{\frac{1}{3}} - 1 \right) d_p \qquad (7.17)$$

Substitution x in the above equation gives:

$$\frac{V_{sm}}{V} = \frac{4d_p^2}{DL} \left(\left(\frac{0.65}{C} \right)^{\frac{1}{3}} - 1 \right)^2 \qquad (7.18)$$

This equation gives an indications of the validity of treating a suspension as homogeneous when using a tube viscometer. Figure 7.11 shows the decrease of the ratio of maximum settling velocity to the average pipe flow velocity as volumetric concentration increases for different values of pipe lengths, with particle diameter d_p=250μm and pipe diameter D=0.1m. It also shows that the maximum tolerable settling velocity varies inversely with both pipe length and diameter.

7.17.5 A Novel Sampling Device for Measuring Concentration Distribution in a Settling Column

Concentration distribution in a settling column is the criterion for assessing the degree of heterogeneity in a suspension. Such criterion is useful in many applications. For example, it is required that suspensions of solid particles in agitated vessels be completely homogeneous for any further processing to take place. Rheological measurements of shear stress as a function of shear rate for a settling suspension in a rotational viscometer are valid only if provision is taken to maintain a uniformly distributed suspension during measurement. Pipelines, conveying backfill material, are known to become plugged because of inadequate mixing of the backfill in the agitator tanks. In batch settling experiments better methods of measuring concentration distribution are required. It is reported in Perry's Chemical Engineers Handbook that *virtually no experimental data are reported on concentration profiles of mixture of particle sizes even though practically all industrial applications have a mixture of particle sizes.*

Current practice for measuring concentration distribution makes use of visual or optical techniques which are not applicable to opaque suspensions. Sampling from lateral ports along the height of the container is a widely used technique. However this method suffers from a systematic error in the magnitude of the concentration measured due to non-isokinetic condition in the withdrawal of the suspension and due to solid particle migration from the high shear stress region near the wall to the lower shear stress region near the center of the column.

A novel sampling device of simple design was tested and proven to yield reliable reading for the concentration distribution in a settling column. This device is suitable for slowly settling suspensions at moderate concentrations (15 % to 40% by volume).

7.17.5.1 Design and Mode of Operation of the Sampler

The sampler is made up of a set of concentric tubes with hole openings that coincide only when the device is in the open position as shown in Figure 7.12. After a fixed settling time for the case of a settling experiment or for a given agitator speed in a mixing tank, the sampler is inserted (in the closed position) inside the tank to avoid unwanted sampling to take place. The position of the sampler with respect to a reference line should indicate the location of the sampling holes in the column thus correctly mapping the measurement.

Once in position inside the column, and after a predetermined time interval, the sampler is switched to the open position thus allowing adjacent layers of the suspension to seep into the hole openings. Hydrostatic pressure drives out any trapped air bubbles upward thus freeing the space to the suspended layers. To increase the rate of seepage inside hole openings, the sampler may be slowly rotated in reverse directions prior to being switched to the closed position. Samples are then collected in special receptacles. Each sample is then weighed in the wet and dry state and the difference indicates the corresponding amount of water contained. Thus solids concentrations can be determined. The number of data points is equal to the number of holes in the sampler. More data points may be obtained by using a second sampler in an off-set vertical position relative to the first one.

Figure 7.12 Design and mode of operation of the Sampler

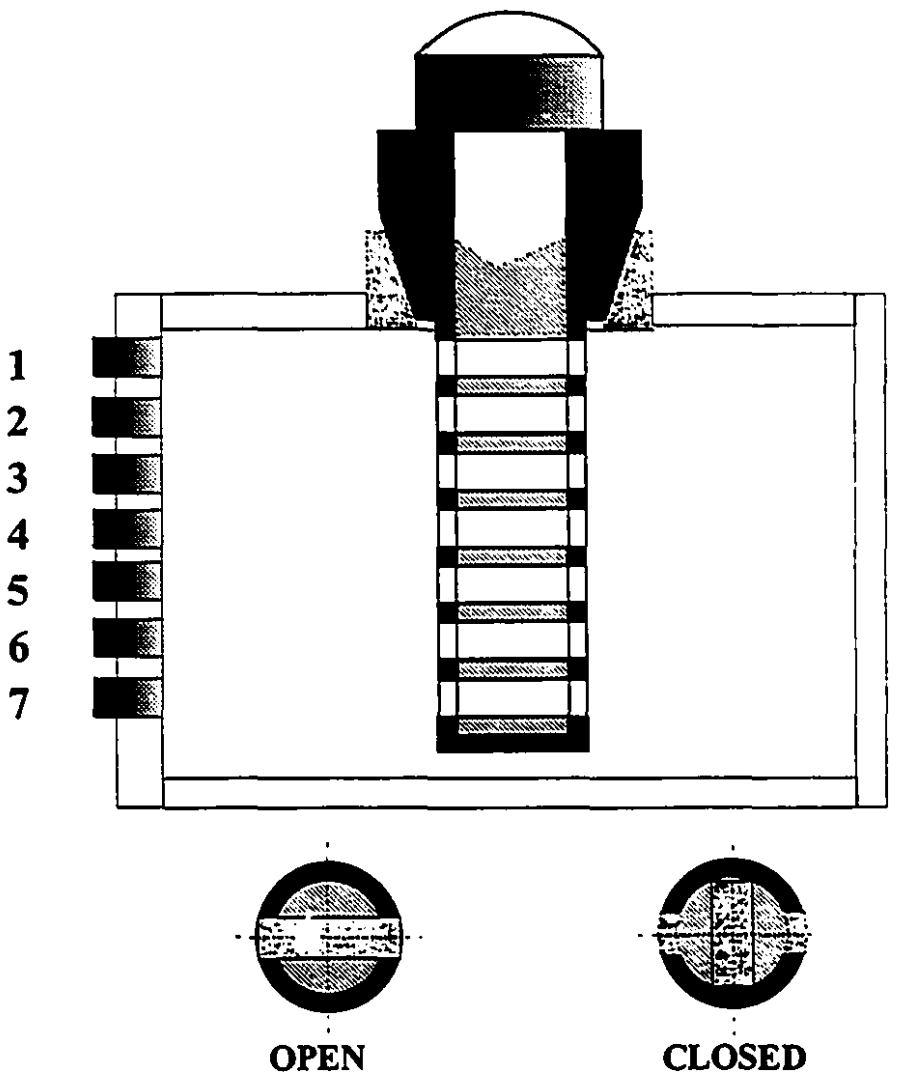

7.17.5.2 Results and Discussion

The results of two tests (#2 and #3) for measuring the concentration distribution in a settling column using the classical lateral ports method and the new sampling technique are shown in Figure 7.13 and 7.14. A suspension of -325 mesh (-44μm) silica powder with a specific gravity of 2.64 was used at solids concentration by weight C_w =32.2 % for test #2 and C_w=32.4 % for test #3. Mixing was done by shaking and rotating the column-sampler set-up to establish a uniform starting concentration distribution. After about one minute of settling time , samples were first withdrawn from lateral ports and then from the sampler. This sampling order was reversed in test #3.

Although sampling by the two methods were not performed simultaneously, in that one technique had to be used first, and even though the sampling order was changed in test #3, the results invariably showed that solids concentrations from sampling ports were lower than the corresponding ones measured by the sampler. This finding confirms the long held belief that lateral port sampling underestimates the actual solids concentration in the tank.

Error from lateral ports measurements increases linearly with the depth of the column as shown in Figure 7.15. This result is physically understandable since the flowability of the suspension at the lower part of the column decreases due to increase in solids concentration as particle settling progresses. Two empirical equations obtained by least square fitting of the linear variation of the difference between lateral ports and sampler measurements for test #2 and #3 are proposed:

For test #2:

$$\Delta C_w = 4.13\, N_h + 4.60 \qquad (7.19)$$

For test #3:

$$\Delta C_w = 5.18 N_h - 3.01 \qquad (7.20)$$

where N_h is the hole number which is a normalized distance for the depth of the cylinder (N_h=1 for the top hole and 7 for the bottom one).

Although equations above may be used to estimate actual concentrations in a settling column as measured by the cylindrical sampler for a bulk solids concentration in the vicinity of Cw= 30 % of fine silica powder, it is recommended to adjust the linear fit parameters when measuring concentration distributions for a suspension with a different specific gravity of solids, bulk concentration and particle size distribution. Our experimental set-up could easily be used for that purpose.

Figure 7.13 Comparison between results from Sampler, Empirical equation and Lateral ports for test #2

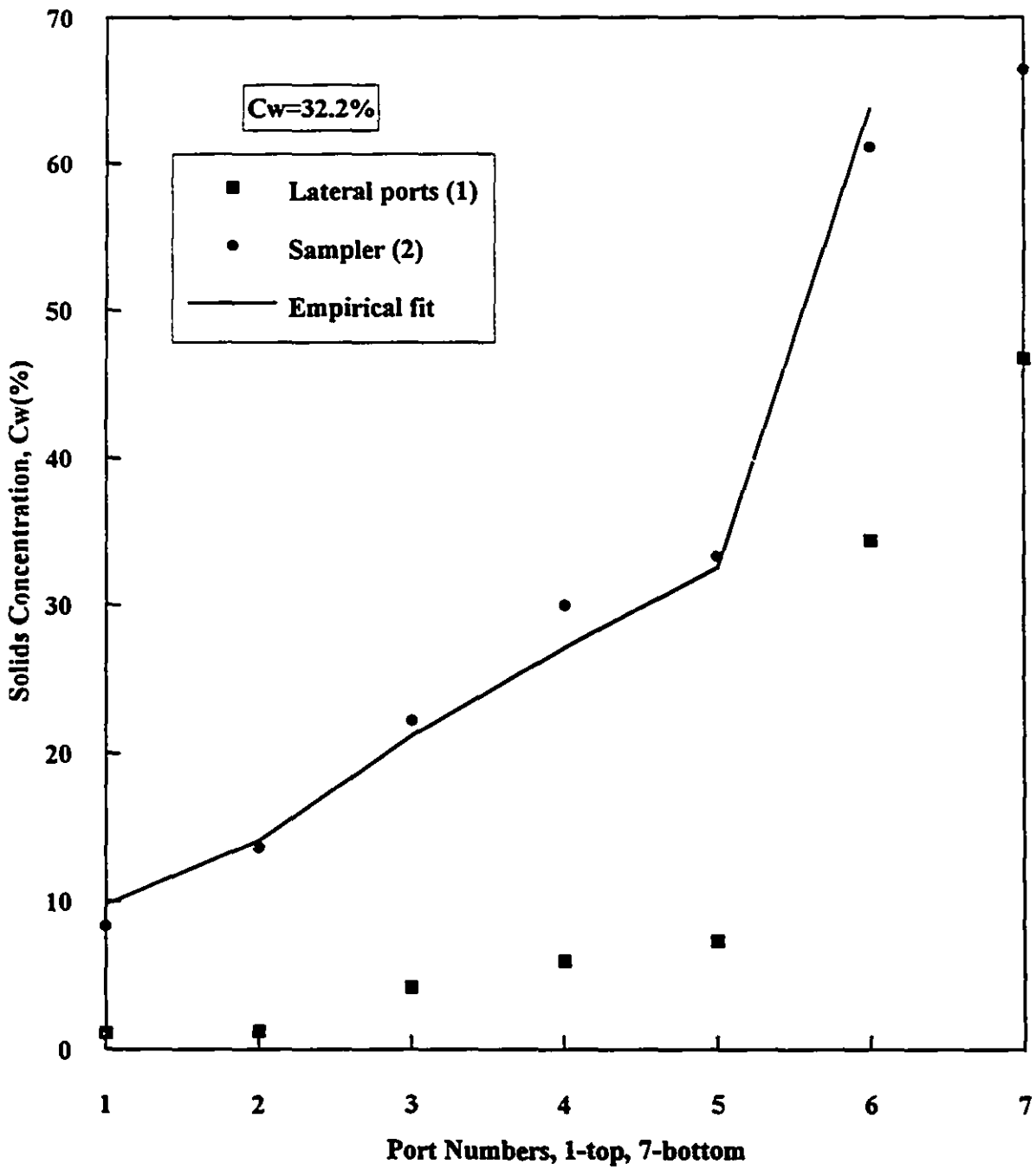

Figure 7.14 Comparison between Sampler, Empirical equation and Lateral ports results for test #3

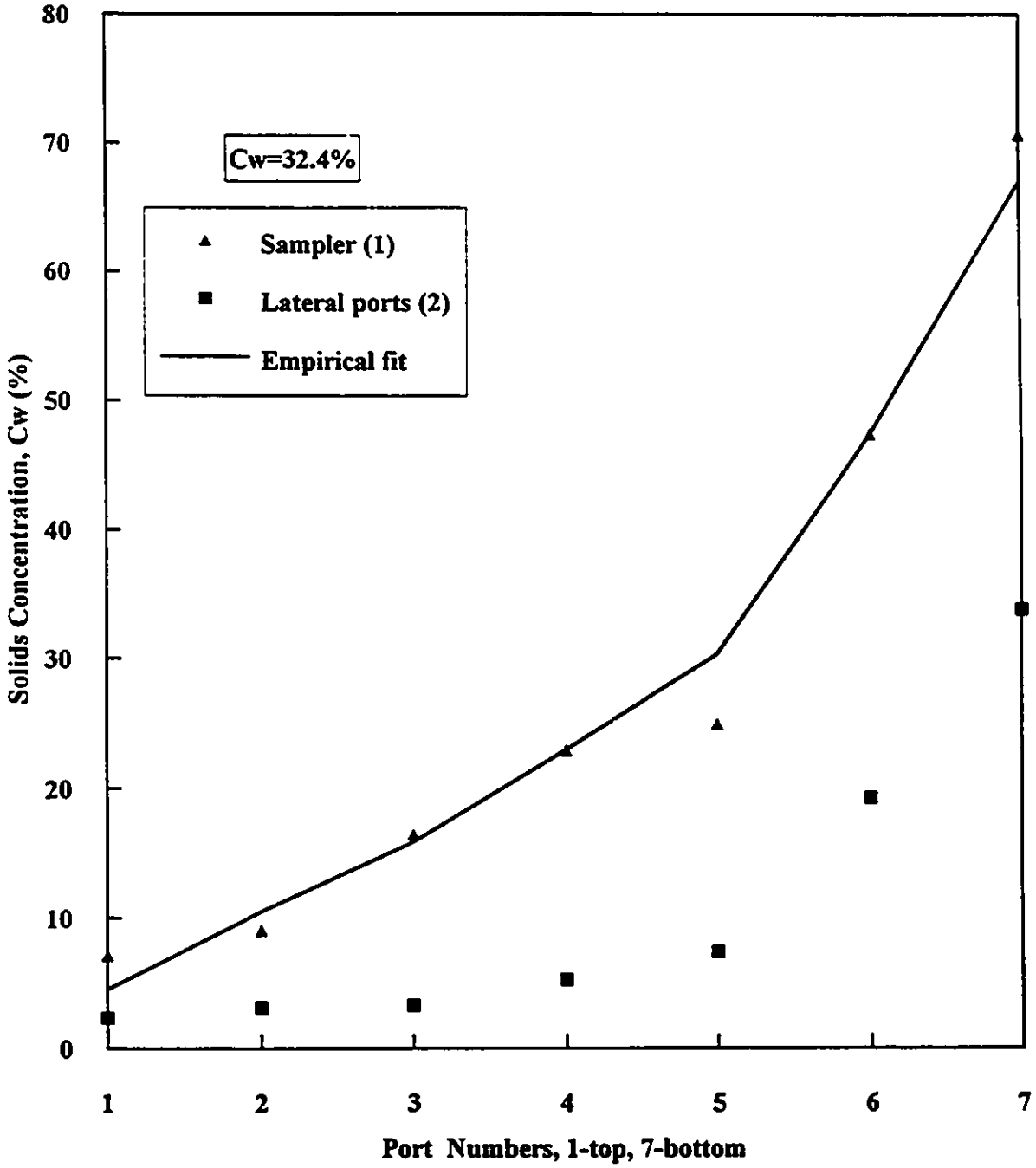

Figure 7.15 Difference between concentration results of sampler and lateral ports along depth of column for test #2 and #3

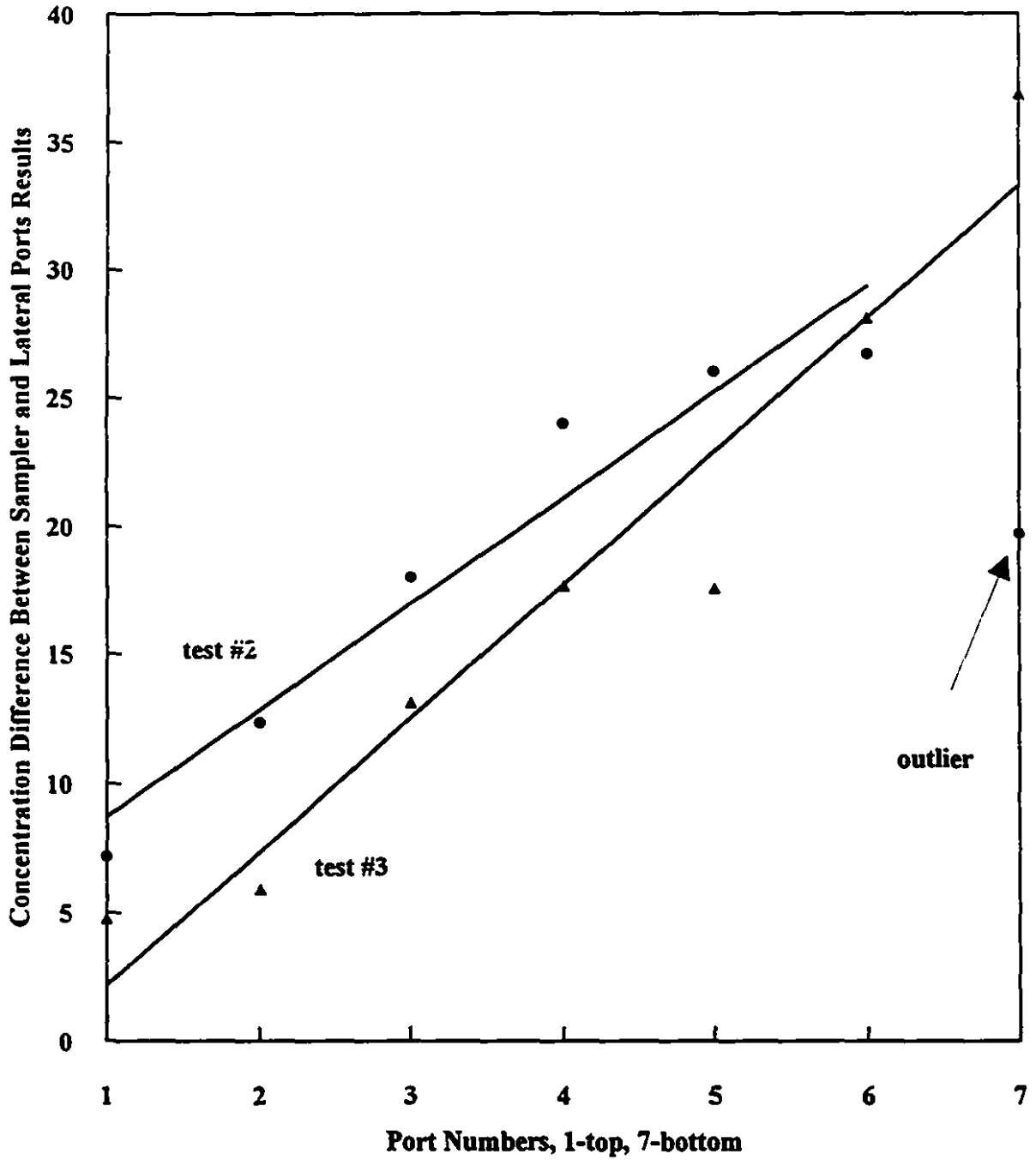

CHAPTER EIGHT

CONCLUSION AND RECOMMENDATIONS

8.1 Conclusion

The main contribution of this thesis is in the development of an analytical model to describe the flow and predict the pressure gradient of a class of high density backfill whose motion in pipelines follows the Plug Flow Model (PFM) as defined in Chapter Five. The development of this model called for investigating the conditions required for establishing this mode of flow. It was found that mix proportioning procedures, similar to those found in the concrete industry, are key factors in obtaining Plug Flow. Pressure drop was found to be a function of the thickness of the non-Newtonian annular layer surrounding the core of aggregates in Plug Flow. Analytical equations were proposed to solve for the magnitude of this layer by considering the rheology of the mixture. Alternatively, by considering the volume balance equation of the components of a Plug Flow mixture, it was possible to estimate the thickness of the annular layer provided the voids volume fraction relative to the total pipe volume is determined. This voids fraction could easily be measured by a making use of the voidmeter. The Plug Flow model for high density backfill was validated using experimental data from Duckworth et al. (1986).

An analytical interpretation of slip effects in pipelines is proposed, where the reduction in flow resistance and dependence of rheograms on pipe diameter are explained in terms of the annular effect. This is a new analytical interpretation of the annular layer effect, which may replace Mooney's method for slip effect correction, shown not to be applicable in this case.

Key concepts pertinent to the design and analysis of backfill slurry flow systems were clearly identified and defined. This served as a guiding reference throughout the course of this study, and could serve as such for further studies on this subject.

Empirical methods applicable to the flow of hydraulic fill were presented with emphasis on Wasp's and Turian's methods as the most likely reliable ways of predicting the flow characteristics of such slurries.

Considerations of the rheological methods of analyzing non-settling slurries showed the importance of model selection in reaching accurate results. The Power law model is found to be the simplest of rheological model to use for visco-plastic materials in the laminar flow regime because it gives a single correlation when the generalized Reynolds number of Metzner and Reed (1955) is used. However the Bingham plastic model has the advantage to take yield stress into account and offers a single correlation in the turbulent flow regime. The method of Metzner and Reed (1955) was found to be very useful for scaling up data without the need to assume a particular rheological model as illustrated in the KCM Case Study (Appendix I). However, this method is not very accurate in the presence of a yield stress. Direct numerical methods for calculating rheological parameters in the case of Bingham plastic and Power law fluids were proposed. This obviates the need for graphical methods for estimating rheological parameters.

For completeness and ease of reference, friction factors and wall shear stresses as a function of the nominal shear rate were given for Bingham plastic, Power law, Yield pseudo-plastic and Casson models, along with available friction factor design charts. Laminar-turbulent transition and non-Newtonian turbulent friction factor equations for Newtonian, Bingham plastic and Power law models were also included. Bowen's method for scaling-up flows in the turbulent regime as well as Mooney's method for correcting for slip effect in viscometers were also described.

An updated version of the two layer model was proposed with the possibility of taking the hold-up phenomena in the lower layer into account, and computing the concentration distribution in the upper layer. A computer program using the Regula-Falsi Algorithm (RFA) was developed to solve the equations of the model.

Some important aspects of testing slurry flow in pipelines such as capillary and rotational viscometry were presented with emphasis on the advantage of tube viscometers over rotational ones. The vane method was recommended as the preferred method for determining the yield stress of a visco-plastic suspension. A typical laboratory scale loop test was described with a recommended state-of-the-

art technique for pressure drop measurement. A test program was suggested for studying the effect of various flow parameters on the pressure gradient for both settling and non-settling slurries. Various experimental techniques for assessing pumpability were described. This includes slump, funnel, settling, and pressure bleed tests.

A novel sampling device for measuring the concentration distribution in a settling column was proposed, and experiments carried out to generate empirical equations for estimating concentration distribution.

Finally a case study of the Kidd Creek Mine backfill system is given to illustrate one of the proposed scale-up techniques.

8.2 Recommendation For Future Work

With respect to the Plug Flow Model, future efforts should be directed toward implementing the design methods obtained from this work. This could help generate experimental data to further assess the accuracy of the proposed model and may suggest ways of improving it, by taking the effect of eccentricity of the cylindrical core into account. This, however, may require numerical modeling methods which can handle the added complexity .

Furthermore, since the pressure gradient in Plug Flow depends on the thickness of the annular layer and its rheological properties, some efforts need to be focused on better ways of preparing such pastes to increase their lubricating effect (i.e. lower viscosity) and their ability to maintain coarser particles in suspension (i.e. higher yield stress). A study on additives serving this purpose may prove to be very useful.

Stability of Plug Flow and its capacity to resume after a down time as well as the corresponding pressure losses through bends and fittings need also to be investigated.

Air content in Plug Flow mixtures (such as fresh concrete) is known to improve flowability. The effect of this on the pumpability of high density mine backfill,

especially that the incompressibility assumption on the mixture may no longer be valid, calls for some analysis.

To add to the flexibility of backfill transportation and placement, safety margins to ensure Plug Flow in the event of possible variation in mix proportions should be estimated. The preferred approach, however, remains to keep proper control on mix proportioning to ensure uniformity and constancy.

With respect to the other flow models , experimental work via properly designed loop tests may prove to be the most reliable way of assessing the pressure drop and the flow behaviour of a given mixture. Scale-up equations could then be developed based on data specific to each backfill material.

APPENDIX ONE

Case Study: Pipeline Transport of High Density Fill at Kidd Creek Mine

Large amount of reject fines from rockfill preparation is available in surface at the Kidd Creek mine. By adding these reject fines to sand, it would be possible to use the mixture as filling material in addition to the rockfill currently used.

The high density fill is a mixture of sand, reject fines, cement (or fly ash/cement), and water. The flowability of the mixture is controlled by carefully proportioning the solids mixture and varying its water content as shown in Figure A1.1. Sand-fine rejects mixtures in ratios of 3:7 and 4:6 by weight blended with at least 20% by weight cement or (fly-ash/cement), and water were proposed by Hassani et al. (1992). The sand and reject fines physical characteristic are given in Table A1.1

Table A1.1
Sand and reject fines physical characteristics

Fill material	d10 (mm)	d50 (mm)	d60 (mm)	d90 (mm)	S.G. of fill sample	Porosity (%)
Sand	0.008	0.05	0.07	0.15	2.63	37
Reject fines	0.3	6.0	7.0	15.0	2.81	35
Sand:reject fines 3:7 (by weight)	0.065	2.1	3.0	9.0	2.76	25
Sand:reject fines 4:6 (by weight)	0.06	1.9	2.9	9.0	2.70	24

Pipeline layout for backfilling at the Kidd Creek mine is shown in Figure A1.2. At this stage of mining, ore production originates from levels 1600' and 2000', where fill is subsequently distributed.

Sand-reject fines fill is prepared in the form of slurry with solids concentration of 65-70% by weight, then delivered by gravity. The hydraulic parameters for sand-

reject fine slurry flow in 0.150 m diameter pipeline is shown in Table A1.2. This data show that pipeline geometry is favorable for flow by gravity due to the high potential energy available.

Table A1.2
Hydraulic parameters for sand-reject fine slurry
in a 0.150 m diameter pipe

Pipeline segment	Solids concentration by weight, Cw (%)	Specific gravity of slurry (T/m^3)	Maximum Flow velocity (m/sec)	Allowable pressure drop (kPa/m)	Safety factor K=V/Vc
A-F	65	1.7	12.97	7.4	4.10
A-F	70	1.83	13.77	8.0	4.10
A-N	65	1.7	9.77	5.1	3.01
A-N	70	1.83	10.13	5.5	3.01
A-O	65	1.7	3.95	2.7	1.03
A-O	70	1.83	3.47	2.9	1.03

Operating flow velocity (V) is selected equal to 1.3 times the critical flow velocity (Vc taken as 3.36m/sec).

Pressure drop is computed from the empirical equation (Hassani et al., (1992)) given by:

$$i = (-16.4\,\gamma_s + 58.7)\,V^2 + 2581.6\,\gamma_s - 2170.4 \quad [Pa/m] \qquad (A1.1)$$

where γ_s is the specific gravity of sand-reject fine slurry in T/m^3, and V is the operating flow velocity in m/sec.

This equation was used to generate shear stress data for a range of shear rates corresponding to a flow velocity range up to 1m /sec. The Scale-up technique of Metzner and Reed (1955) described in Chapter 4 was used to fit the data with a Power law model given by:

$$\frac{D\Delta P}{4L} = \frac{D\rho g}{4} i = K'\left(\frac{8V}{D}\right)^{n'} \qquad (A1.2)$$

with:

K' = 1.3612·10^(6)
n' = 0.007764

Comparison of pseudo-shear rate diagrams from Equations (A1.1) and (A1.2) is shown in Figure A1.3. Pressure drop predicted from Equations (A1.1) and (A1.2) is shown in Table A1.3

Table A1.3
Pressure loss predictions for D=0.150 m, V=4.37 m/sec

Pipeline segment	Cw (%)	S.G. of slurry (T/m^3)	i (kPa/m), from Eq.(A1.1)	i (kPa/m), from Eq.(A1.2)	Total pressure drop, (MPa), Eq. (A1.1)	Potential energy available (MPa)
A-O	65	1.7	2.80	2.27	4.49	8.63
A-O	60	1.62	2.62	2.07	4.20	8.23
A-N	65	1.7	2.80	2.27	3.45	6.91
A-N	70	1.83	3.10	2.60	3.84	7.44
A-F	65	1.7	2.80	2.27	2.44	6.91
A-F	70	1.83	3.10	2.60	2.70	7.44

Figure A1.1 High density fill system diagram

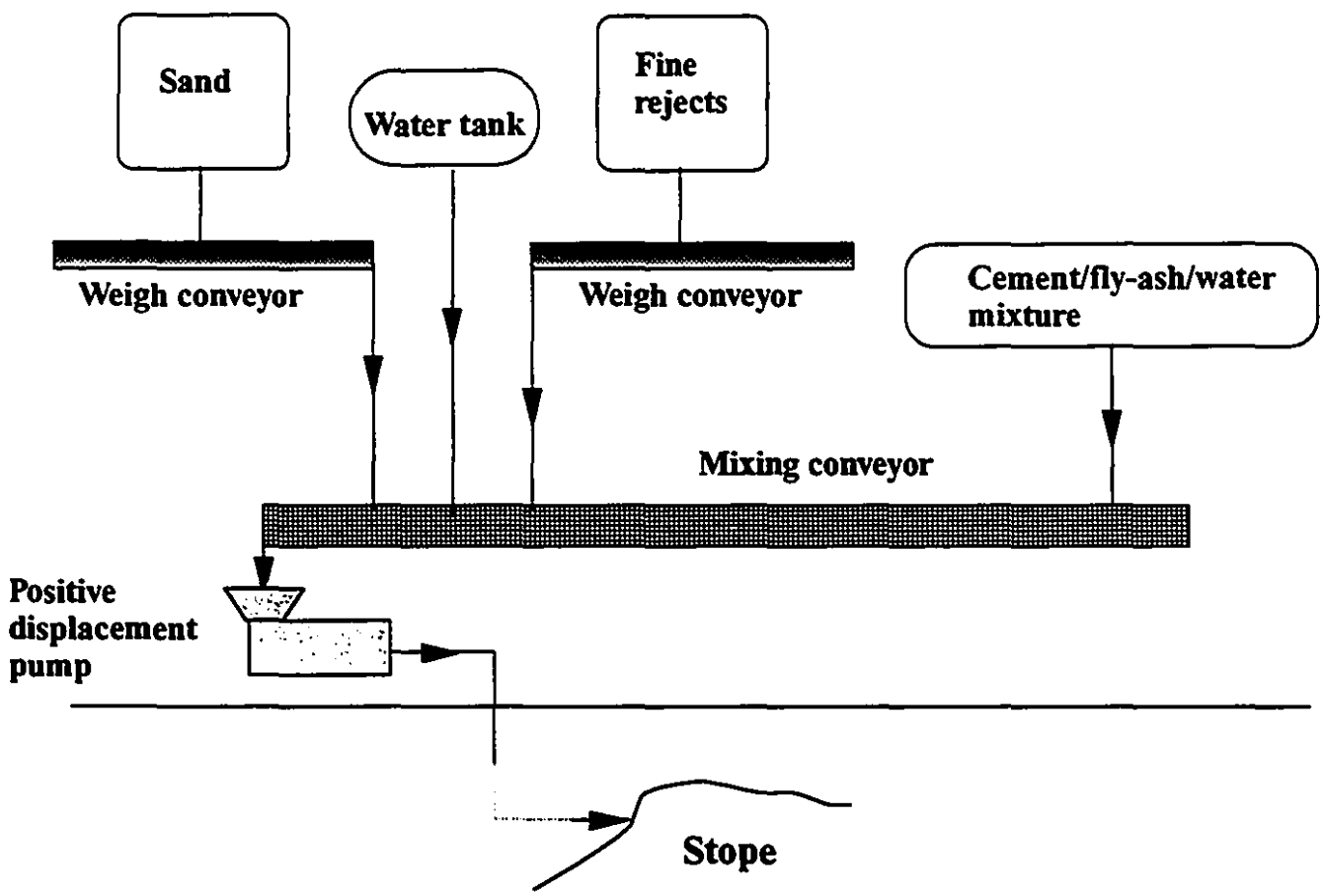

Figure A1.2 Fill distribution system at Kidd Creek Mine

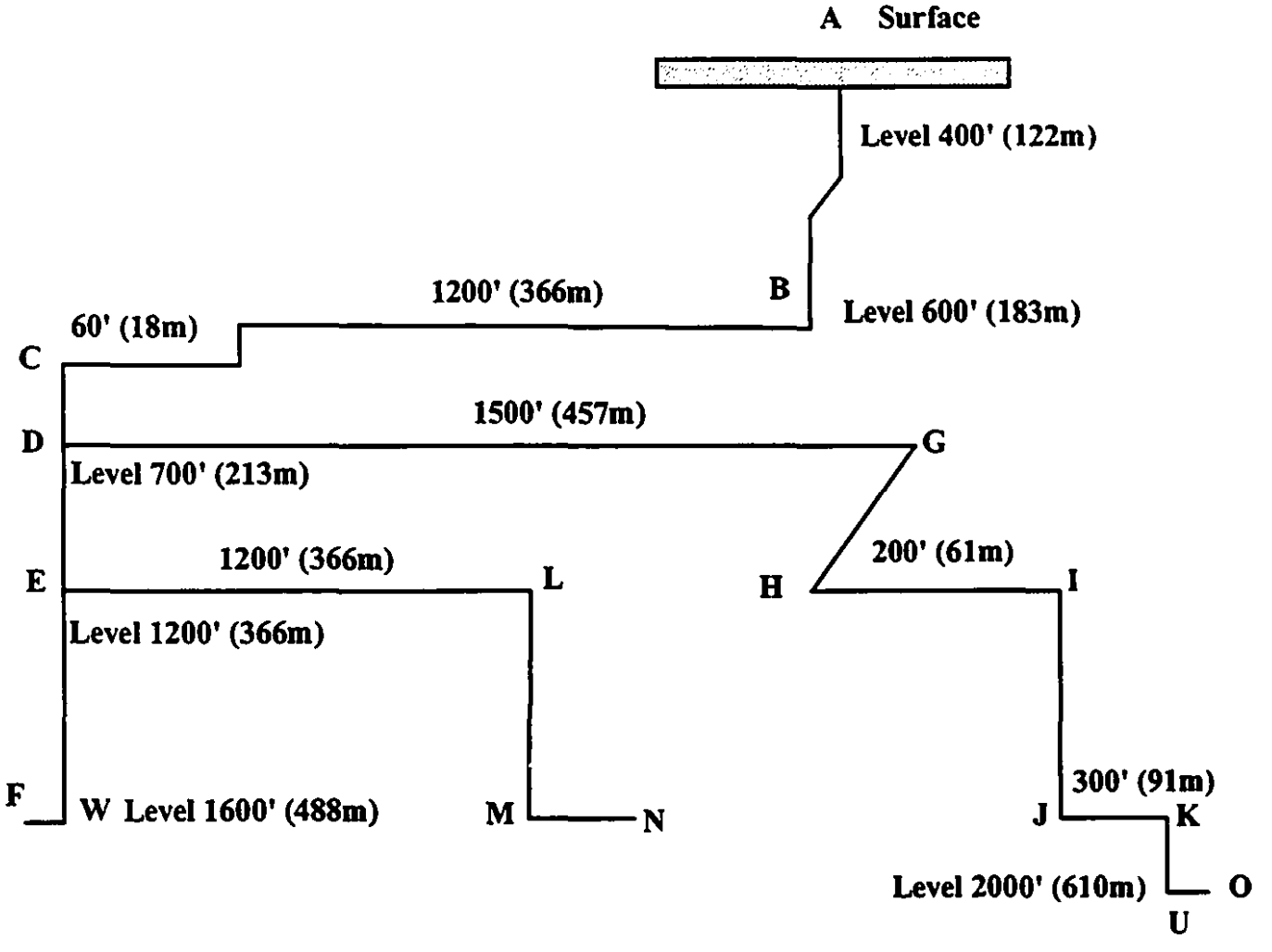

Figure A1.3 Comparison of Pseudo-shear diagrams from Eq.(A1.1) and Eq. (A1.2)

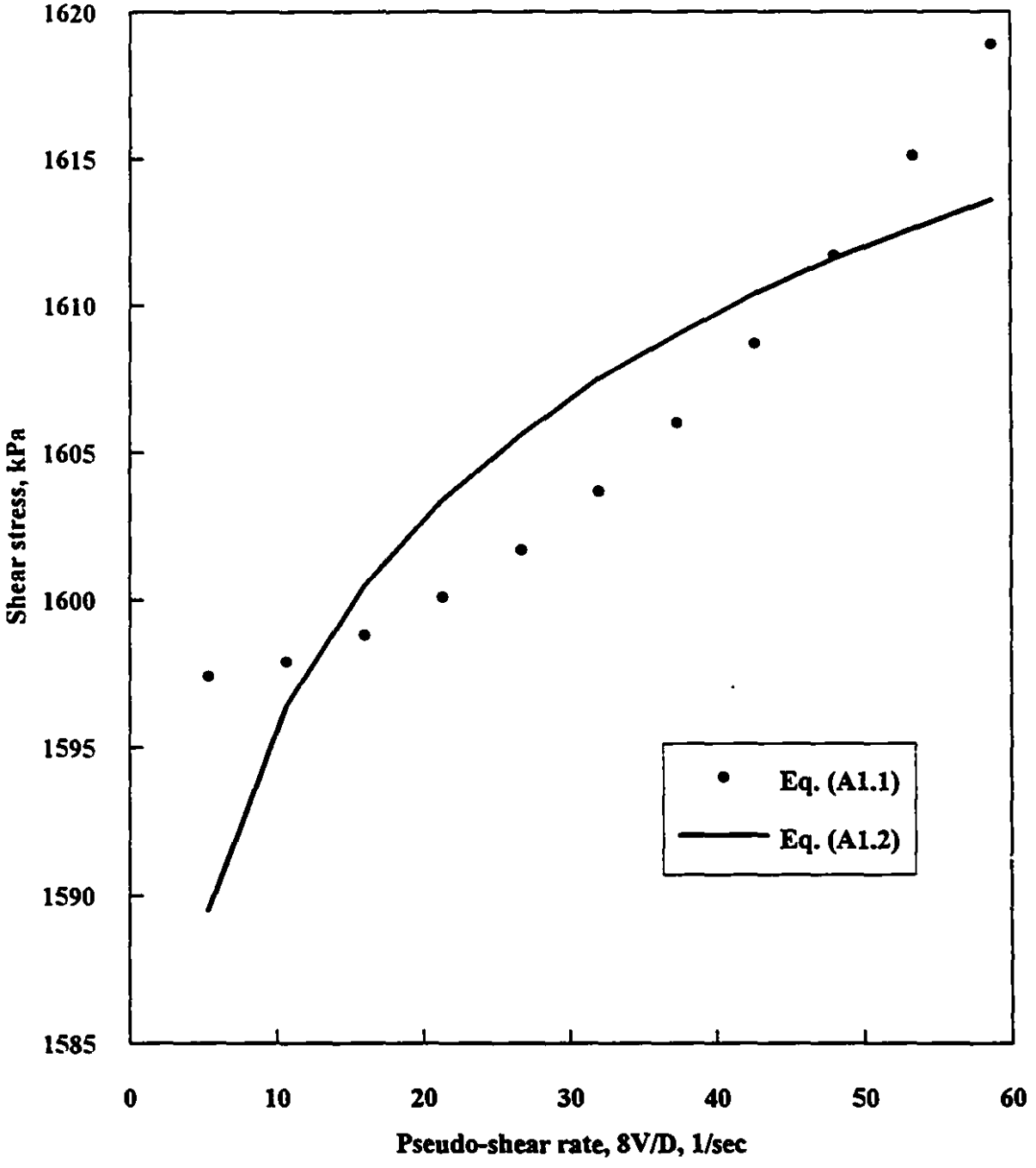

BIBLIOGRAPHY

Asszonyi, C., Kapolyi, L., Kantas, C., Meggyes,T., 1972, " An experimetal method to produce a size distribution ensuring maximum pipeline capacity" , The Second International Conference on the Hydraulic Transport of Solids in Pipes, University of Warwick.

Bagnold, R.A., 1954, "Experiments on a gravity free dispersions of large solid spheres in a Newtonian fluid under shear", Proc. R. Soc. A225, pp.49-63

Bagnold, R.A.,1956, "The flow of cohesionless grains in fluids", Phil. Trans. R. Soc. A249, pp.235-297

Bain, A.G. and Bonnington S.T., 1970, *"The Hydraulic Transport of Solids by Pipelines"*, Pergamon Press.

Barrett, A.J., Wrench, B.P. and Blair Hook, D. , 1988, "An overview of materials testing relevant to backfilling at Vaal Reefs Gold Mine," Backfill in South African Mines. Johannesburg, SAIMM, pp. 61-75

Berkowitz, N., Brown R. A. S., Jensen E., 1965, J., Can. J. Chem. Eng., 43, p.280

Best, J.F., Lane, R. O., 1980, " Testing for Optimum Pumpability of Concrete", Concrete International , pp. 9-17

Bouzaiene, R., Hassani, F., 1992, " A Selection of Pressure Loss Prediction Methods Based on Slurry/Backfill Characterization and Flow Conditions", CIM Bulletin, Vol.85, #959

Bowen, R.L.,1961,"Scale-up for non-Newtonian fluid flow", Chem. Engng. 68

Browne, R. D. , Bamforth , P., 1977," Tests to establish concrete pumpability", ACI Journal, Title No. 74-19, pp. 193-203

Chan,H.T., Johnston H.M.,Konecny,L., Hooton, R.D.,Dayal,R.,1989 " Use of a flue-gas desulphurization by-product for stabilizing hydraulic mine backfill", Innovations in Mining Backfill Technology, Hassani et al. (eds), Balkema, Rotterdam.

Charles, M.E., "The pipeline flow of capsules", Canadian Journal of Chemical Engineering Vol.41, 46, (1963).

Chen, L.J., Hassani, F.P., 1992, "Mining with high density tailing fill", Internal Report, McGill University, Department of Mining and Metallurgical Engineering.

Cheng, D. C.-H.,1975 " Pipeline design for non-Newtonian fluid", The Chemical Engineer

Cheng, D. C.-H., 1978 " Some observations on the rheological behaviour of dense suspensions", Rheologica Acta 17, 446-453

Churchill, W.,1977, " Friction Factor equation spans all fluid flow regimes, "Chemical Engineering. Vol. 84, Nov.7, pp91-2

Clark, I. H.,1988, "The properties of hydraulically placed backfill ", Backfill in South African Mines. Johannesburg, SAIMM, pp. 15-33

Clift, R., Grace, J.R., Weber M.E., 1978, "*Bubbles, Drops and Particles*", Academic Press, London, U.K.

Cooke, R., Lazarus, J.H., 1988" Isokinetic sampling probe for slurry flows", 11th International Conference on the Hydraulic Transport of Solids in Pipes, Stratford-upon-Avon, UK:19-21

Cooke, T.H., 1990, *Concrete Pumping and Spraying -A Practical Guide*

Darby, R.,1984, "Determination and utilization of rheological properties for prediction of flow behavior of pseudohomogeneous slurries", 9th International Technical Conference on Slurry Transportation, Lake Tahoe, Nevada, USA

Darby, R., 1986,"Hydrodynamics of slurries and suspensions", Chapter 2, in Encyclopedia of Fluid Mechanics Vol.5 Slurry Flow Technology, Gulf Publishing Company.

De Korompay, V.,1975, "Review of hydraulic transportation system for mine backfill", Department of Energy, Mines and Resources, Mine Branch, Mining Research Centre. Divisonal Report 74/118

Dealy, J.M., 1994, personal communication, McGill University

Dodge, D. W. and Metzner, A.B., 1959, " Turbulent flow of non-Newtonian systems", AIChE J. 5 (2), pp. 189-204

Doron, P., Granica, D., Barnea D.,1987,"Slurry flow in horizontal pipes-experimental and modeling", Int. J. Multiphase Flow, 13: pp.535-547

Duckworth, A. , Addie G. R., 1987 "Application of a Non-Newtonian Carrier to Transport Coarse Coal Refuse", Proc. of the 12th Int. Conf. on Slurry Technology, New Orleans, Louisiana, USA.

Duckworth, A. , Pullum, L., Addie G. R., Lockyear, C.F., 1986a "The Pipeline Transport of Coarse Materials in a Non-Newtonian Carrier Fluid", 10th International Conference on the Hydraulic Transport of Solids in Pipes, Hydrotransport 10, Austria. Paper C2

Duckworth, A. , Addie G. R., Maffett J.R., 1986b" Mine Waste Disposal by Pipeline Using a Fine Slurry Carrier", Proc. of the 11th Int. Conf. on Slurry Technology,pp. 187-194

Duckworth, A. , Pullum, Lockyear, C.F.,1983 " The Hydraulic Transport of Coarse Coal at High Concentration", Journal of Pipeline v. 3, Elsevier Science Publishers

Duffy, G. G., 1984, " A New Suspending Medium for the Pipeline Transport of Coarse, High Density and Dense Phase Particles and Capsules", Hydrotransport 9, 9th International Conference on Hydraulic Transport of Solids in Pipes, Rome, Italy, Paper E2

Duffy, G.G. ,1987,"New Uses for Wood Pulp Fiber", Tappi Journal, pp.107-112

Duffy G.G. , Walmsley, M.R., 1985," The Pipeline Transport of Solids Using a Novel Satbilizing Suspensing Medium", Proc. of the 10th International Conference on Slurry Technology, March 26-28, Lake Tahoe, Nevada, USA

Durand, R., and Condolios, E.,1952, "Hydraulic transport of coal and solid materials in pipes", Proceedings of a colloquium on the hydraulic transport of coal, pp.39-52, National Coal Board, London, England.

Ede, A. N., 1957, " The resistance of concrete pumped through pipelines", Magazine of Concrete Research , V.9, No. 27, pp.129-140.

Elliot ,D. E., Gliddon, B.J., " Hydraulic Transport of Coal at High Concentrations", Proc. 1st International Conference on Hydraulic Transport of Solids in Pipes, Hydrotransport 1, BHRA, , Paper G2, (1970).

Ellis,H.S. ,Kruyer J., 1970" The pipeline flow of capsules, Part10", 1st International Conference on the Hydraulic Transport of Solids in Pipes, BHRA.

Epstein, N, "Concentric laminar flows", The Canadian Journal of Chemical Engineering Vol.41, 181,(1963)

Gandhi, R., L., 1987 "Effect of the rheological properties of fines fraction on slurry hydraulics", Proc. of the 12th International Conference on Slurry Technology, , New Orleans, Louisiana, USA

German, R.M., *Particle Packing Characteristics*, Metal Powder Industries Federation, Princeton, New Jersey, (1989)

Gillies, R.G., Shook, C.A, 1991, "A deposition velocity correlation for water slurries" , Can. J. Chem. Eng

Govier, G. W., and Aziz, K.,1987, "*The Flow of Complex Mixtures in Pipes*", Krieger Publishing Company.

Graf, W.H.,1983, "*Hydraulics of Sediment Transport*," pp. 161-202, McGraw Hill Book Company, New York

Haaland, S.E.,1983, " Simple and explicit formulas for the friction factor in turbulent pipe flow', J. Fluids Engng 105, 89-90

Hanks , R.W.,Hanks K.W., 1982, " A new viscometer for determining the effect of particle size distributions and concentration on slurry rheology" Proceedings of the 7th International Technical Conference on Slurry Transportation., Lake Tahoe, Nevada, USA.

Hanks, R.W., 1981, " Course notes, Hydraulic Design for flow of complex fluids", Orem, Utah.

Hanks, R.W., 1981,"Laminar-turbulent transition in pipeflow of Casson model fluids", Journal of Energy Resources Technology, Vol.103 pp 319-321

Hartman, H. L., 1992, SME Mining Engineering Handbook

Hassani, F.P., 1992, *Etude Technique et Economique de la Technologie du Remblayage pour les Mine Souterraines du Quebec*, Entente Canada-Quebec pour le Developpement Mineral--Recherche et Developpement pour les Mines du Quebec

Hassani, F.P., Chen, L. J., Yu, T.R., 1992,"Potential use of fine rejects of rockfill at Kidd Creek Mine", Internal Report, McGill University, Department of Mining and Metallurgical Engineering

Heywood, N. I., 1991"Pipeline design for non-settling slurries", *Chapter 7 in Slurry Handling*, Brown N.P and Heywood N.I, Editors, Elsevier Applied Science

Heywood, H., 1962, "Uniform and non-uniform motion of particles in fluids". In *Interaction between fluids and particles*, Institution of Chemical Engineers, London, U.K.

Hou, H. C., 1986, " Investigation of optimal grain-distribution for transport with high concentration", 10th International Conference on the Hydraulic Transport of Solids in Pipes, Innsbruck, Austria, paper E3.

Hsu, S. T., Beken, A. V., Landweber, L. and Kennedy, J.F., 1971, " The distribution of suspended sediment in turbulent flows in circular pipes", Reprint of paper presented at Atlantic City AIChE meeting on Solids Transport in Slurries.

Ismail ,H.M., 1952, "Turbulent transfer mechanism and suspended sediment in closed channels," Trans. ASCE, V.117, pp. 409-447.

Jastrzebski, Z.D., "Entrance effects and wall effects in an extrusion rheometer during flow of concentrated suspensions", Ind. Eng. Chem. Fundam., 6, 445, (1967)

Kalyon, D. M., Yaras, P., Aral, B., Yilmazer, U. ,1993,"Rheological Behaviour of a Concentrated Suspension: a Solid Rocket Fuel Simulant", Jour. of Rheology 37(1), pp. 35-53

Kao, D.T., Kazanskij , I.,1979 " On Slurry flow velocity and solid concentration measuring techniques", 4th International Technical Conference on Slurry Transportation, Las Vegas, Nevada, USA

Kramers, C. P., Russell, P.M., Billingsley, I.,1989 , " Hydraulic transportation of high density backfill," Innovations in Mining Backfill Technology,Hassani et al. (eds), Balkema, Rotterdam, pp. 387-394.

Laird, W. M., 1957, " Slurry and Suspension Transport", Industrial and Engineering Chemistry, Vol. 49, No1

Lazarus, J. H., Slatter, P.T., 1988," A method for the rheological characterization of tube viscometer data", Journal of Pipelines, 7(1988)

Lazarus, J. H., 1989, " Mixed-regime slurries in pipelines. I : Mechanistic model", Jour. of Hydraulic Engineering, Vol. 115, #11.

Metzner, A.B., Reed, J.C., 1955 " Flow of non-Newtonian fluids correlation of laminar transition and turbulent flow", AIChE, December.

Mooney,M., " Explicit Formulations for Slip and Fluidity", J. Rheol., 2, p.210, (1931).

Nasr-El-Din, H, Shook, C.A., Esmail, M.N.,1984 " Isokinetic probe sampling from slurry pipelines", The Canadian Journal of Chemical engineering, Vol.62,

Newitt, D. M., Richardson, J. F., and Shook C. A.,1962, " Hydraulic conveying of solids in pipes, Part II: Distribution of particles and slip velocities", Symposium on Interaction Between Fluids and Particles, London, Proc., pp. 87-100

Newitt, D. M.; Richardson, J. F.; Abbott, M.; Turtle, R. B.,1955, "Hydraulic conveying of solids in horizontal pipes", Trans. Inst. Chem. Engrs., Vol.33.

Nguyen, Q. D., Boger, D.V.,1983, " Yield stress measurement for concentrated suspensions" Journal of Rheology 27(4), 321-349.

Nguyen, Q. D., Boger, D.V.,1992 " Measuring the flow properties of yield stress fluids", Annu. Rev. Fluid Mech., 24:47-88.

Nienow A.W., 1985, " The suspension of Solid Particles", Chap. 16 in *Mixing in The Process Industries*, Editors: Harnby, N. et al., Butterworths 1985

Oroskar, A. R., Turian, R.M., 1980," The critical velocity in pipeline flow of slurries", AIChE Journal, Vol. 26, No4

Paterson, A.J.C., 1991 *The Hydraulic Transport of High Concentration Stabilized Flow Full Plant Mineral Tailings*, PhD Thesis, University of CapeTown, South Africa, Dept. of Civil Engineering

Paterson, A.J.C., Lazarus, J.H., , " Analysis of high concentration stabilized mineral tailings", International Conference on Bulk Materials Handling and Transportation; Symposium on Freight Pipelines, Wollongong, Australia, (1992).

Paterson,A.J.C., Lazarus, J.H., " The 'anomalous' flow behaviour of highly concentrated full plant tailings used as backfill"; Minefill 93, Johannesburg SAIMM pp. 205-208, (1993).

Perry's Chemical Engineers' Handbook, 5th Edition, McGraw-Hill Book Company, p. 19-10

Raudkivi, A.J.,1990,"*Loose Boundary Hydraulics*", Pergamon Press, 3rd Edition

Richardson, J. F. and Zaki, W. N., , 1954, " The sedimentation of a suspension of uniform spheres under conditions of viscous flow," Chem. Eng, Sci., v3, p65.

Rumpf, H., 1990 *Particle Technology*, Chapman and Hall

Sakuta, M., Yamane, S., Kasami, H., and Sakamoto, A., "Pumpability and rheological properties of fresh concrete", Takenoka Technical Research Laboratory", Tokyo, Japan, 1979. Published by the Swedish Cement and Concrete Research Institute, Stockholm, Sweden.

Savage, S.B., 1978, "Experiments on Shear Flows of Cohesionless Granular Materials", Proc. U.S.-Japan Seminar Continuum Mechanical and Statistical Approaches on the Mechanics of Granular materials, Tokyo, Japan, 1978.

Scoble, M. J., Piciaccha, L., 1991, *Ingénieries des Remblais Souterrains*, Centre de Recherches Minérales, Ministère de l'Energie et des Ressources, Gouvernement du Québec

Sellgren A.,1989, " A simulation model for efficient hydraulic fill transport," Innovations in Mining Backfill Technology, Hassani et al. (eds), Balkema, Rotterdam, pp. 395-401.

Shah, S.N, Lord, D., 1991,"Critical velocity correlations for slurry transport with non-Newtonian fluids", AIChE, Vol. 37, No6

Shook C.A., Roco, M.C.,1991, *"Slurry Flow: Principles and Practice"*, Butterworth-Heinemann

Sive, A.W.; Lazarus, J. H., 1989, " Mixed-regime slurries in pipelines. II : Experimental Evaluation", Jour. of Hydraulic Engineering, Vol. 115, #11.

Skelland, A. H. P., *Non-Newtonian flow and heat transfer*, John Wiley and Sons, Inc., New York, 1967

Slatter P.T.; Lazarus, J.H.,1988, " The application of viscometry to the hydraulic transport of backfill material", Backfill in South African Mines, Johannesburg, SAIMM,pp.263-285

Smith L.G., Husband W.H.W., Schriek W., Haas D.B., 1973, "'Slurry Pipeline Research Facilities at the Saskatchewan Research Council" , S.R.C. Report #1.

Soszynski, R. M., 1991, " The Plug Flow of Fiber Suspensions in Pipes " Nordic Pulp and Paper Research Journal No3, pp.110-117

Stewart, R.M.,1959, "Hydraulic fill slurries", in 'The handling and placement of hydraulic backfill underground', Transaction CIM, Vol. LXIII, pp.462-476

Takaoka,T.; Hisamitsu, N.; Ise,T.; Takeishi, Y,1980, "Blockage of slurry pipeline" Hydrotransport 7; BHRA Fluid Engineering, Cranfield, England; Paper B4 pp. 71-89.

Tatsis, A. Jacobs, B. E. A., Osborne, B., Astle, R. D., 1988, " A Comparative Study of Pipe Flow Prediction for High Concentration Slurries Containing Coarse Particles", Proc. 13th International Conference on Coal and Slurry Technology

Tatsis, A. Jacobs, B. E. A., Lewis S., Culbert, B., 1988, " Phase Change Boundary Detection Project-A New Method", Hydrotransport 11, 11th International Conference on the Hydraulic Transport of Solids in Pipes, paper G4

Tatsis, A.,1990 "An investgation of the pipe flow regime for high concentration slurries with coarse particles", Proc. of the 15th International Conference on Coal and Slurry Technologies, Clearwater, Florida, USA

Tattersall G. H., Banfill, P.F.G., *The Rheology of Fresh Concrete*, Pitman Advanced Publishing Program, (1983).

Taylor, G., 1954,"The dispersion of matter in turbulent flow though a pipe", Proc. R. Soc. A223, 446-468

Televantos, Y., Shook,C, Carleton, A., Streat, M.,1979,"Flow of slurries of coarse particles at high solids concentrations", The Canadian Journal of Chemical Engineering, Vol.57.

Thomas E.G.,Nantel, J.H, Notley, K.R. 1979, "Fill Technology In Underground Metalliferous Mines", International Academic Services Limited, Kingston, Ontario, Canada .

Turian, R. M.; Yuan, T.,1977," Flow of slurries in pipelines"; AIChE Journal, Vol. 23, #3

Udd, J.E.,1989, " Backfill research in Canadian Mines," Innovations in Mining Backfill Technology, Hassani et al. (eds), Balkema, Rotterdam, pp. 3-13

Van Waser, J.R.; Lyons, J.W.; Kim, K.Y.; Colwell, R.E., 1963, " Viscosity and flow measurement- A laboratory handbook for rheology", J. Wiley, interscience, NY

Verkerk,C.G., Marcus, R.D., 1988, "The pumping characteristics and rheology of paste fills". Backfill in South African Mines. Johannesburg, SAIMM, pp.221-233.

Vocadlo, J.,J.,Charles, M.E., 1972," Prediction of pressure gradient for the horizontal turbulent flow of slurries", The 2nd International Conference on the Hydraulic Transport of Solids in Pipes.

Wani, G. A.,1986, "Critical velocity in multizise particle transport through pipes", Chapter4 in Encyclopedia of Fluid Mechanics, Volume 5-Slurry Flow Technology. Gulf Publishing Company.

Wasp, E. J.; Kenny, J.P., Gandhi, R. L., 1977, " Solid-liquid flow- slurry pipeline transportation" , Trans Tech Publications

Wayment W.R., Wilhelm G.L.,1962, " Factors Influencing the Design of Hydraulic Backfill Systems", USBM Report # 6065.

Weber, M, 1976" Critical velocity as optimum operating velocity in solids pipelining", 4th International Conference on the Hydraulic Transport of Solids in Pipes, 18-21 Wilson, K.C., Streat, M., Bantin, R.A., 1972, "Slip-model correlation of Dense two-phase flow", Proc. Hydrotransport 2 Conf., BHRA, Cramfield, UK, Paper B1, pp.1-10.

Wilson, K. C.; Brown N.P.,1982, "Analysis of fluid friction in dense-phase pipeline flow", Canadian Jour. chem. Engineering, Vol.60.

Wilson, K.C.,1976, " A unified physically based analysis of solid-liquid flow" Proc. Hydrotransport 4; BHRA Fluid Engineering, Cranfield, England; Paper A1 pp. 1-16.

Wilson, K.C., 1982, " The Dense-phase option for coarse coal pipelining", Journal of pipelines, Vol.2, pp.95-101

Wilson K. C., 1979, " Deposition-limit nomograms for particles of various densities in pipeline flow ", Hydrotransport 6, BHRA Fluid Engineering, Cranfield, England; Paper A1, pp.1-12.

Woodcock, C.R., Mason, J.S., 1987, "*Bulk Solids Handling*", Leonard Hill, New York

Worster, R.C., Denny, D.F., 1955,"Hydraulic transport of solid material in pipes", Inst. Mech. Engrs. London

Zandi, I ; Govatos, G, 1967, Proc. A.S.C.E (hyd. divn.).

Zigrang, D.J., N.D. Sylvester, 1982, AIChE J., 28 (3).